Raman amplification and performance altering effects

Tim John Ellingham

Doctor of Philosophy

Aston University

May 2006

Aston University

Raman amplification and performance altering effects

Tim Ellingham
Doctor of Philosophy

May 2006

Summary

This thesis presents an experimental investigation into several applications of the Raman scattering effect in communication optical fibres as well as how some of these applications can be modified to enhance the resulting performance. The majority of the work contained within is based on laboratory results using many commercially available components. The results can be divided into and presented in three main parts:

Firstly, a novel application of a known effect is used to broaden Raman pump light in order to achieve a more continuous distribution of gain with respect to wavelength. Multiple experimental results are presented, all based around the prior spreading of the pump spectrum before being used in the desired transmission fibre. Gathered results show that a notable improvement can be obtained from applying such a technique along with the scope for further optimisation work.

Secondly, an investigation into the interaction between the well known effect of Four Wave Mixing (FWM) and Raman scattering is provided. The work provides an introduction to the effect as well commenting on previous literature regarding the effect and its mitigation. In response to existing research experimental results are provided detailing some limitations of proposed schemes along with concepts of how further alleviation from the deleterious effects maybe obtained.

Lastly, the distributed nature of the Raman gain process is explored. A novel technique on how a near constant distribution of gain can be employed is implemented practically. The application of distributed gain is then applied to the generation of optical pulses with special mathematical properties within a laboratory setting and finally the effect of pump noise upon distributed gain techniques is acknowledged.

Keywords: Nonlinear optics, Optical amplification, Four wave mixing, Modulation instability, Quasi lossless

This thesis is dedicated

to the memory of

James F. G. Hamley

Acknowledgements

Firstly, I would like to say that in no form or way would have this thesis been possible without the help and input of fellow friends and colleagues. Sincere thanks and gratitude goes to the photonic teams at Aston University, Birmingham, and at the former Marconi communications

First and greatest thanks go to my friend, colleague and co-author on many works: Dr Juan-Diego Ania-Castañón, for without whom the pace of research would have been much less energetic and productive. Special appreciation goes to Prof. Sergei Turitsyn whose infectious enthusiasm was always a revelation and highly inspirational especially when I have been feeling despondent about the telecoms industry.

I would like to thank my other co-authors and collaborators of my papers whose contributions have helped create many successful publications and conference papers, especially those from the Russian Federation who I met only a few times when on visits to England, including Dr. Alexei Pustovskikh, Dr. Serguei Kobtsev, Prof. Mikhail. P. Fedoruk and Dr. Olga Shtyrina. In addition I would naturally like to thank my colleagues here in the UK from the Photonics Research Group members including Mr Mykhaylo Dubov, Mr. Xianfeng Chen, Prof. Lin Zhang, Dr. Paul Harper, Prof. Keith Blow, Prof. Ian Bennion, Dr David Birkin and Mr Richard Reeves.

Gratitude goes to all my former colleagues at Marconi who helped introduce me into the world of photonics during those memorable days of the Solstis project. A special mention goes to Dr. Liam Gleeson for aiding in my first research paper and Prof. Nick Doran for employing me after my first degree. Appreciation goes to my external supervisor Dr. Steven Alleston for providing the path to continue research using the Marconi labs after departing from the company and for providing a van load of Raman pump lasers.

Thanks goes to all the other research students at Aston, including Dr. Ashley Gray, Dr. Rachel Won, Dr. Amos Martinez, Miss Helen Dobb, my long term friends since my first degree Dr. Robin Ibbotson and Dr. James Harrison; all of whom have tirelessly listened to my repeated rantings about the telecoms industry. I'd like to acknowledge members from the mechanical engineering research group who became good friends and my training partners in the gym, Mr. Paul Slack and Mr Robin Taylor, you provided an often needed mental lift after a day losing my sanity in a windowless laser lab.

I'd like to thank my family and especially my grandparents who have always believed in me throughout my education and taken an active interest in my progression through ascending qualifications.

Last but certainly not least, to my beloved Sue Tong, I thank you for always being supportive, suffering many practice presentations even after a night shift and for providing a stable home life that allowed me to concentrate on my research.

Contents

Chapter 1 12
1.1 Historical Perspective 12
1.2 Thesis Outline 15
Chapter 2 17
2.1 Introduction 17
2.1.1 Fibre construction 17
2.1.2 Fibre losses 19
2.1.3 Dispersion 21
2.1.4 Polarisation Mode Dispersion (PMD) 23
2.1.5 Fibre nonlinearities 25
2.2 Conclusions 31
Chapter 3 32
3.1 Introduction 32
3.2 History of the Raman Effect 34
3.3 Source of Raman Scattering 35
3.4 Amplification by Raman in optical fibres 38
3.5 Noise processes in Raman amplified systems 45
3.6 Pump configurations 49
3.7 Conclusions 53
Chapter 4 54
4.1 Introduction 54
4.2 Spectral broadening mechanisms 55
4.3 Experimental Pump Broadening 58
4.4 Gain Flattening and Spectral Broadening 70
4.5 Conclusions 88
Chapter 5 90
5.1 Introduction 90
5.2 Four-Wave-Mixing processes 90
5.3 Four-Wave Mixing between pumps 93
5.4 Four-wave mixing between pumps and signals 105
5.5 Mitigation of FWM between pumps and signals 111
5.6 Effect of FWM mitigation techniques with data transmission 128
5.7 Conclusions 139
Chapter 6 141
6.1 Introduction 141
6.2 Advantage of distributed gain 142
6.3 Experimental Measurements 145
6.4 Single wavelength pumped quasi-lossless system 152
6.5 Transmission over quasi-lossless system 160
6.6 Relative Intensity Noise RIN 166
6.7 Distributed gain medium for pulse generation 170
6.8 Conclusions 176
Chapter 7 Conclusions 178
Publications 182
Bibliography 184

List of Figures

Figure 2.1 Step index fibre construction 18
Figure 2.2 Step index fibre side profile 18
Figure 2.3 Sample of loss spectrum form a single mode step index fibre 21
Figure 2.4 Measured dispersion for three fibre types 23
Figure 2.5 Time domain effect of PMD in a short length of birefringent fibre 24
Figure 3.1 Effect of Raman gain upon signal strength 33
Figure 3.2 Scattering diagrams for Stokes and anti-Stokes Raman scattering 36
Figure 3.3 Depiction of the quantum mechanical process taking place during Raman scattering 37
Figure 3.4 Comparison of gain shape for a DCF fibre and a standard SMF fibre 39
Figure 3.5 WDM Raman pump gain 40
Figure 3.6 Individual pump wavelengths after 25km LEAF 42
Figure 3.7 All pump wavelengths together after 25km LEAF 42
Figure 3.8 Schematic of simple Raman amplifier scheme employing co and counter pumping 43
Figure 3.9 DRBS Illustration 46
Figure 3.10 Counter pumping 49
Figure 3.11 Co pumping 50
Figure 3.12 Co and Counter pumping 50
Figure 3.13 Simplified illustration of energy transfer in a second order pumping scheme 51
Figure 3.14 Two abstract configurations A and B where a loss element αL is placed either before or after a discrete amplifier. Noise figure expressions are for linear units 52
Figure 4.1 Differing pump wavelengths after propagation through TW-RS span 58
Figure 4.2 Fibre type and power level broadening experiment 59
Figure 4.3 Result on pump spectra for varying fibre type and input pump power 59
Figure 4.4 and 10dB bandwidths for measured power levels over each fibre type used 60
Figure 4.5 Fibre span dispersion 61
Figure 4.6 Power level on MI experiment 62
Figure 4.7 Evolution of MI in a 2.2km reel of TW-Classic fibre with increasing power 62
Figure 4.8 Effect of pump wavelength on MI spectra experiment 63
Figure 4.9 Gain from 1365nm pump laser for MI sweep experiment 64
Figure 4.10 Selected steps from the MI sweep experiment 64
Figure 4.11 Spectral evolutions (left – time domain, middle – spectral domain) of the pump wave power along a modelled TW fibre. Pump power is 800mW at 1455nm. Right – pump spectrum after 25km propagation in anomalous and normal dispersion regimes. Pump power 500mW at 1455nm 65
Figure 4.12 Left - Period of temporal modulation [ps] due to MI for varying dispersions [ps/nm/km] and nonlinear coefficient [1/W/km]. Pump power is 1W at 1455nm. Right – Dependence of the oscillation period on pump power (at 1455nm) after 5km TW fibre, Solid line – Numerical simulation, Dashed line – Theory 65
Figure 4.13 Processes in later stages of broadening 66
Figure 4.14 Broadening of a 1455nm Raman fibre laser in 25.5km TW-RS 66

Figure 4.15 800mW 1455.14nm pump after propagation through TW-RS reels with varying dispersion values 68
Figure 4.16 TW-RS dispersion 68
Figure 4.17 3 and 10dB pump bandwidths vs. dispersion at pump wavelength 68
Figure 4.18 Effect of pump direction on broadening 69
Figure 4.19 Illustration of a broad pump as a collection of narrow pumps and the associated gain spectra 70
Figure 4.20 Initial gain variation result for broader pump, left - 1424nm, right - 1457nm 71
Figure 4.21 Counter propagating pre-fibre experimental set-up 72
Figure 4.22 Gain comparison for varying pre-fibres 72
Figure 4.23 comparison of bandwidths for a 1 and 10% reduction from peak value 73
Figure 4.24 Gain comparison for with/without pre-fibre 73
Figure 4.25 Effect of increasing pump power on pump and gain spectra 75
Figure 4.26 Pump and gain shape evolution 76
Figure 4.27 Dual pump WDM Raman experimental set-up 77
Figure 4.28 Pump spectra at the input (blue lines) and output (red lines) of the broadening pre-fibres Left - 1480nm. Right - 1480 nm. 78
Figure 4.29 Fig. 4 Gain spectra of the amplifier on its different configurations: 79
Figure 4.30 Measured HNLF dispersion with inset effect on three semiconductor lasers, Blue traces - before fibre, Red traces - after fibre 82
Figure 4.31 HNLF experimental layout 83
Figure 4.32 Evolution of 1480nm pump in HNLF for varying input powers and effect of the WDM on the 561mW spectrum 84
Figure 4.33 Comparison of gain spectra for the cases with and without HNLF pre-fibre 85
Figure 4.34 Gain comparison between using 86
Figure 4.35 Experiment for investigation of pre-fibre gain on data transmission 87
Figure 4.36 Pre-fibre/no pre-fibre transmission results 88
Figure 5.1 Non-degenerate Four-Wave-Mixing 91
Figure 5.2 Degenerate Four-Wave-Mixing 91
Figure 5.3 Pump-Pump FWM Experiment 94
Figure 5.4 Individual pump wavelengths after 25km SMF 96
Figure 5.5 All pump wavelengths together after 25km SMF 96
Figure 5.6 Individual pump wavelengths after 25km LEAF 96
Figure 5.7 All pump wavelengths together after 25km LEAF 97
Figure 5.8 Individual pump wavelengths after 25km TW-RS 98
Figure 5.9 All pump wavelengths together after 25km TW-RS 98
Figure 5.10 1438 and 1466nm pumps after propagation through TW-RS 99
Figure 5.11 1424 and 1496nm pumps after propagation through TW-RS 100
Figure 5.12 1438 and 1452nm pumps after propagation through TW-RS 101
Figure 5.13 1452 and 1466nm pumps after propagation through TW-RS 102
Figure 5.14 1452 and 1466nm pumps after propagation through TW-RS 102
Figure 5.15 Effect of pump spacing from ZDW and 1496nm pump point in LEAF. 103
Figure 5.16 Mixing between pump pairs towards ZDW 104
Figure 5.17 Fibre dispersions (solid - measured, dashed - linear fit) 105
Figure 5.18 Experimental set-up for co-propagating FWM investigations 106
Figure 5.19 Pump modes onto signal (green - I/P signal, blue - O/P signal) 107
Figure 5.20 Overlay of signal and pump spectra in the frequency domain 107
Figure 5.21 ECL swept through FWM region 108

Figure 5.22 Adjacent channels in FWM region 109
Figure 5.23 Effect on 50 GHz grid 110
Figure 5.24 Swept gain vs. BBLS gain 111
Figure 5.25 Experiment for investigation of FWM mitigation techniques 112
Figure 5.26 1455nm Raman pump after different FWM mitigation techniques 113
Figure 5.27 Effect on counter propagating signal OSNR 114
Figure 5.28 Inherent pump broadening 114
Figure 5.29 Counter pumped spectra with no pre SMF for 10, 12.5, 15 and 20dB gain 116
Figure 5.30 Counter pumped spectra with pre SMF for 10, 12.5, 15 and 20dB gain 117
Figure 5.31 OSNR for each gain level and with/without the SMF pre fibre 117
Figure 5.32 Counter pumped spontaneous/FWM spectra for the 10, 12.5, 15 and 20dB gain pump powers used when signal present. No pre SMF – left, With pre SMF – right 118
Figure 5.33 Co pump experiment for investigation of SMF pre fibre FWM suppression technique 118
Figure 5.34 Investigation of Co pump in LEAF with no SMF pre fibre 119
Figure 5.35 Investigation of Co pump in LEAF – output without Raman 120
Figure 5.36 Pump spectrum for varying applied signal wavelength as in Fig. 5.34 .. 120
Figure 5.37 Signal stepped in 0.2nm steps with effect on mixing products in pump region 121
Figure 5.38 Investigation of Co pump in LEAF with SMF pre fibre 122
Figure 5.39 OSNR comparison for 122
Figure 5.40 Investigation of Co pump in LEAF with SMF pre fibre spontaneous (left) and with increasing pump power (right) 123
Figure 5.41 Signal stepped in 0.2nm steps with effect on mixing products in pump region with SMF 124
Figure 5.42 Output from 10km TW with increasing I/P power (left) and effect of pumping direction on 500mW I/P power (right) 125
Figure 5.43 Co pump with TW pre fibre, A to B direction 126
Figure 5.44 Co pump with TW pre fibre, B to A direction 126
Figure 5.45 OSNR comparison for co pump FWM reduction techniques 127
Figure 5.46 Gain comparison with BBLS used as signal source 127
Figure 5.47 Experiment for investigation of degenerate and non-degenerate FWM and pump shape 129
Figure 5.48 Pump spectra for with TW scenario (left) and without TW (right) 130
Figure 5.49 Results of wavelength sweep through FWM region under each operating condition 131
Figure 5.50 No signal mixing product (left) and minimum OSNR (right) 132
Figure 5.51 OSNR comparison for each experimental variation 133
Figure 5.52 Transmission experiment for FWM degradation investigation 134
Figure 5.53 OSNRs and gain for Degenerate case (1452+1496nm pumps) and Non-degenerate (1452nm pump only) 136
Figure 5.54 BER for each experiment variation 136
Figure 5.55 Spectra and Eye diagrams for the no pre/TW experiment 138
Figure 5.56 Spectra and Eye diagrams for the with pre/TW experiment 138
Figure 6.1 Actual and 'Effective' system for Raman counter pumping. Shows the fictitious pre-amplifier with gain G_{on-off} and noise figure NF_{eff} that follows the unpumped span with length L 142

Figure 6.2 Two abstract configurations A and B where a loss element αL is placed either before or after a discrete amplifier. Noise figure expressions are for linear units 144
Figure 6.3 System for measurement of distributed Raman gain 146
Figure 6.4 Experimental signal evolution with counter pump 147
Figure 6.5 Experimental signal evolution with co pump 148
Figure 6.6 Experimental signal evolution with co and counter pump 148
Figure 6.7 Basic illustration of the dual gain transfer in second order pumping 149
Figure 6.8 Dual order co-pump configuration 150
Figure 6.9 Comparison between single and dual order co-propagating pump 151
Figure 6.10 Bi direction second order pumping 1550nm signal variation 152
Figure 6.11 Second order quasi-lossless span using single wavelength pumps 153
Figure 6.12 Pump laser spectrum for each laser at similar power 154
Figure 6.13 Spontaneous spectrum formed from bi directional 1365nm pumping of a 75km SMF span 155
Figure 6.14 Profiles for FBGs used in quasi-lossless system 155
Figure 6.15 Spontaneous spectrum formed from bi directional 1365nm pumping of a 75km SMF span with FBGs at either end and for 25km TW-RS inset 156
Figure 6.16 Simplified OTDR measurement system 157
Figure 6.17 Results for three different span lengths using single wavelength quasi-lossless system 157
Figure 6.18 Simulation result of signal variation versus span length and grating reflectivity 159
Figure 6.19 Comparisons between the high (~99%) and low (~33%) FBG in 20 and 52km SMF spans 160
Figure 6.20 Gain spectrum for 75km quasi-lossless system 161
Figure 6.21 Individual gain spectra from 1365 and 1455nm pumps 161
Figure 6.22 Signal variations along a 75km SMF span at different wavelengths 162
Figure 6.23 QL transmission configuration 163
Figure 6.24 OSNR comparison at point D 165
Figure 6.25 Optical eye diagram comparison 165
Figure 6.26 Investigation of noise transfer from pump to signal 168
Figure 6.27 Electrically converted measured noise from 1452nm semiconductor laser (left) and a 1455nm Raman fibre laser (right) 169
Figure 6.28 Attempt to compare the transfer of noise from pump to signal for two fibre types 170
Figure 6.29 Parabolic pulse generation experiment 171
Figure 6.30 TWC dispersion 172
Figure 6.31 Temporal results for parabolic pulse generation 172
Figure 6.32 Input pulse to TWC fibre without booster EDFA 173
Figure 6.33 Input and output pulses, temporal and spectral results from using no booster EDFA 174
Figure 6.34 Compression of the generated parabolic pulse using various lengths of SMF 175
Figure 6.35 Comparison of pulse widths and amplitudes for compression of the direct Pritel pulse and generated parabolic pulse 175

List of Tables

Table 3.1 Pump powers at each wavelength for WDM Raman 40
Table 4.1 HNLF parameters 81
Table 6.1 QL transmission results 164

Abbreviations

ASE	Amplified Spontaneous Emission
BER	Bit Error Rate
BW	Bandwidth
CW	Continuous Wave
DCF	Dispersion Compensating Fibre
DFB	Distributed Feedback
DFF	Dispersion Flattened Fibre
DGD	Differential Group Delay
DM	Dispersion Managed
DRBS	Double Rayleigh Backscattering
DSF	Dispersion Shifted Fibre
DWDM	Dense Wavelength Division Multiplexing
ECL	External Cavity Laser
EDFA	Erbium Doped Fibre Amplifier
FBG	Fibre Bragg Grating
FP	Fabry Perot
FWHM	Full Width Half Maximum
FWM	Four Wave Mixing
GVD	Group Velocity Delay
HNLF	Highly Non-Linear Fibre
LEAF	Large Effective Area Fibre
MI	Modulation Instability
NF	Noise Figure
NLSE	Non-Linear Schrödinger Equation
NZ-DSF	Non-Zero Dispersion Shifted Fibre
OSA	Optical Spectrum Analyser
OSNR	Optical Signal to Noise Ratio
PMD	Polarisation Mode Dispersion
RBS	Rayleigh Backscatter
RIN	Relative Intensity Noise
RZ	Return to Zero
SBS	Stimulated/Spontaneous Brillouin Scattering
SMF	Single Mode Fibre
SOA	Semiconductor Optical Amplifier
SPM	Self Phase Modulation
SRS	Stimulated/Spontaneous Raman Scattering
SSMF	Standard Single Mode Fibre
TW	True Wave
TW-RS	True Wave Reduced Slope
VOA	Variable Optical Amplifier
WDM	Wavelength Division Multiplexing/Multiplexer
XPM	Cross Phase Modulation
ZDW	Zero Dispersion Wavelength
ZMD	Zero Material Dispersion

Chapter 1

Introduction

1.1 Historical Perspective

The ability to communicate has always been an obvious essential requirement for people but the challenge has always been the ability to communicate over long distances, quickly and efficiently. The use of light as a signal has been used for many hundreds of years, one example being the signalling fires in the UK to warn of foreign attack, such basic techniques allowed information to travel faster than say a horseback messenger but were extremely limited in the amount of detail that could be sent. It was not until the discovery of electricity that communications started to really move forward and 'telecommunication' was born. The following list gives the dates of some important steps in telecommunication development:

- 1809 S. Von Sömmering: Electric telegraph 3.5km
- 1840 S. Morse: Morse code
- 1876 A. Graham Bell: Telephone patent
- 1896 G. Marconi: Wireless telegraph system
- 1923 John Logie Baird: Television
- 1962 TELSTAR Commercial television satellite
- 1966 Optical fibre for telephone demonstrated
- 1972 Demonstration of ARPANET early INTERNET
- 1977 Cellular phone system by Bell Labs

Turning our attention to back to optics it is interesting to note that four years after patenting the telephone Bell published his work on a light communication system known as a photophone [1]. It used sunlight reflected from a thin voice modulated

mirror to carry conversation. At the receiver the modulated sunlight fell on a photo conducting selenium cell, which converted the message to electrical current; the system could operate over a distance of 200m. . It was not until 1960's that interest was seriously renewed in optical communications with the invention of the laser. The device could provide powerful coherent light capable of being modulated at high frequency and with low beam divergence. The last point helped enhance free space communication but this was limited by the need to be line of sight and by interference from foreign bodies. What was required was a waveguide to channel the light securely over distance. In 1966 the first optical fibres debuted, however these had extremely high attenuation figures around the 1000dB/km mark. Over the next ten years losses had been reduced to around 5dB/km and in 1979 the attenuation at the lowest loss wavelengths was down to just over 0.2dB/km. Since then fibre loss has only decreased slightly due to the limitation imposed by Rayleigh scattering. Optical fibres generated much interest due to the advantages that could be obtained over co-axial electrical systems; put simply these included [2]:

- Enormous potential bandwidth
- Small size and weight
- Electrically isolated
- Secure, meaning that it is hard to access the data without being intrusive/detected
- Low transmission loss

At the same time as development of the fibre, other components were evolving. Lasers sources were experimented with and semiconductor lasers were formed, photodiodes for signal detection were improved upon and all were developed to be compatible in size to the fibres. For many years commercial systems used short fibre spans followed

by regenerators which were optical-electrical-optical devices where the signal was received, converted back to an electrical signal, reshaped, retimed and then retransmitted optically again. This method was adopted from the 1970s into the early 1990s when optical amplifiers became popular. The advantages of an optical system included: less complexity, lower cost and greater reliability due to a single optical amp replacing many delicate electrical components.

Optical amplification in fibres had been looked at many years before it was deployed in commercial systems, for example Roger Stolen and his team published work [3] regarding optical amplification using the Raman effect in 1973. However when optical amplification was deployed it was Erbium Doped Fibre Amplifiers (EDFA) that found favour despite having just been a research area in late 1980s. The main reason for this was concerned with the high power lasers required for Raman amplifiers in comparison to EDFAs. Towards the end of the twentieth century high power semiconductor lasers were emerging that could enable practical Raman amplifiers within commercial systems.

As the need for faster data rates grew systems with multiple channels were developed where each channel was assigned a different wavelength which, when multiplexed together, could be sent simultaneously down the same fibre, this technique is commonly referred to as Wavelength Division Multiplexing or WDM. Along with advances in optical amplification and many other components by the beginning of the twenty-first century optical systems were commercially available which offered multi Tera-Bit per second performance over thousands of kilometres, e.g. the Marconi MultiHaul platform which offers 6.4 TBit/s over 4000km [4]. Not only has the distance and speed of optical systems increased dramatically but also so has the flexibility whereby the use of add/drop multiplexers channels can be taken out or

added into a transmission line. This technology has allowed metropolitan ring systems to be deployed, increasing cross-city communications.

1.2 Thesis Outline

As stated in the previous section, optical amplification is essential for modern optical fibre systems, whether it be EDFA, Raman or Semiconductor Optical Amplifiers (SOA). With the current availability of high power laser sources much attention has been turned to Raman amplification in the last ~10 years [5] and it is this form of amplification that is explored in this thesis. The work presented tackles existing ideas and explores new ones from an experimental, physically realisable point of view, and aims to provide the reader with inspiration for further research. An abstract overview of the chapter contents is as follows:

- Chapter 1. A brief history of telecommunications and optical fibre development.
- Chapter 2. An introduction to modern optical fibres, illustrating the physical make up and the main effects and phenomena that can be encountered during optical data transmission.
- Chapter 3. Introduces the Raman effect and its application to amplification in optical fibres. Commonly observed effects that serve to benefit and detriment the effectiveness of the process are discussed.
- Chapter 4. Explores what happens when Raman pump light is subject to conditions that cause spectral domain broadening and how the resulting light can provide an advantage to the amplification process.
- Chapter 5. Investigates the distributed nature of Raman gain and how it can be improved further still.

- Chapter 6. Looks at the effect of the four wave mixing phenomena on the Raman amplification process and how it maybe possible to reduce the impairments produced by it.
- Chapter 7. Finally conclusions for the thesis are presented along with suggestions for future work.

Chapter 2

Introduction to Communication Optical Fibres

2.1 Introduction

Fibre optic cables are now the most common technology for sending large volumes of information around the world quickly. By using the basic principle of total internal reflection, today's ultra low loss fibres can allow light signals to propagate for hundreds of kilometres before requiring some from of amplification. When amplification is applied periodically any planetary distance can be achieved, including the largest ocean crossings.

This chapter aims to provide an initial insight into the primary principles, main characteristics and effects that can be found in telecommunication optical fibres.

2.1.1 Fibre construction

The most common style of fibre used in optical communications for any substantial distance is known as the step-index fibre, which refers to the step change in refractive index between the core and the cladding. The fibre is usually constructed from silicon dioxide and consists of a central core with refractive index n_1 that is surrounded by a cladding with refractive index n_2, see figure 2.1 [6]

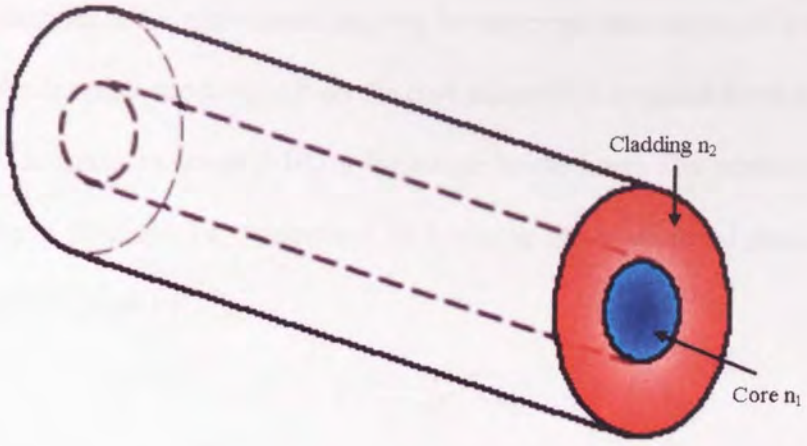

Figure 2.1 Step index fibre construction

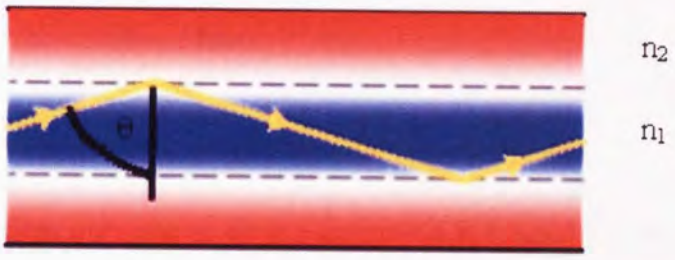

Figure 2.2 Step index fibre side profile

Complete lightwave guidance requires that the reflection angle θ be equal to or greater than the critical angle θ_c, which is given by:

$$\sin\theta_c = \frac{n_2}{n_1} \tag{2.1}$$

The fractional index change Δ is an important fibre parameter given by:

$$\Delta = \frac{n_1 - n_2}{n_1} \tag{2.2}$$

And it is always positive, because for the critical angle to exist the n_1 must be larger than n_2. Not only are modern communications fibres step index, but they are also single mode at the signal wavelength. This means that only one guided electromagnetic mode (generally the HE_{11} mode) is allowed in the waveguide, as opposed to multi mode fibres where multiple paths exist, which leads to intermodal dispersion due to the

different transit times for each mode, causing the temporal broadening of a transmitted pulse. To obtain single mode operation the core diameter is reduced from about 50μm for multimode fibres to about 2-10μm for single mode fibre. The number of modes supported by a fibre can be determined by knowing the *normalised frequency* or V number which is given by:

$$V = \frac{2\pi a}{\lambda}\sqrt{n_1^2 - n_2^2} \tag{2.3}$$

Where a is the core radius and λ is the free space wavelength. By using V a single chart can be drawn that applies to any combination of values of a, λ, n_1 and n_2. The number of modes can then be calculated from:

$$N = \frac{V^2}{2} \tag{2.4}$$

For a step index fibre only one mode is supported if $V < 2.405$ [2]. As mentioned, the glass is made from silica (silicon dioxide, SiO_2) but has dopants added to change the refractive indices. One of these dopants is germanium, which raises the refractive index of the core, allowing guiding to occur.

2.1.2 Fibre losses

There are three main processes that combine to generate the fibre loss:

1. Absorption

Even though modern optical fibres are extremely pure, intrinsic absorption will still be heavy at certain wavelengths. This absorption is strongest in the ultraviolet region, due to electronic and molecular transitions, and between 7-12μm in the infra red region, due to vibrations of chemical bonds [6]. Absorption is also caused from impurities. The two most problematic impurities are:

- Transition metal ions
- Hydroxyl ion (OH)

The metal impurities absorb strongly at telecom wavelengths [1300-1600nm] and should not exceed a few parts per billion. The OH ion is the most important impurity to reduce as one of the most harmonic loss peaks (commonly known as the water peak) occurs around the 1390nm region, with the largest peak occurring at 2.73μm. The OH impurity must be kept to a few parts per million, and in the case of some modern fibres the water peak is reduced to an extremely low level, for example in Sumitomo Pure-band fibre [7].

2. Scattering

Scattering occurs from local variations in refractive index throughout the glass. A beam passing through such a structure will have some of its energy scattered by these variations as if they were small object embedded in the glass. This type of Scattering is called Rayleigh scattering and is inversely proportional to the wavelength raised to the power four; therefore it dominates at short wavelengths.

3. Geometric effects

Bending in a fibre causes attenuation. Bends are categorised into two types; macro and micro. Macro bends are greater than 25mm in radii of curvature and give rise to small losses. Micro bends, less than 25mm radii, can give rise to significant losses as the incident angle between the propagating light and the cladding does not satisfy the conditions for total internal reflection.

There are other sources of losses that are primarily to do with the cabling process which include splice loss, connector loss and mode field diameter mismatch. Figure

2.3 gives the loss profile of a single mode step index fibre which clearly shows the OH absorption peak (first overtone of the main OH peak) around 1380nm and a minimum loss of 0.2dB/km which is a typical figure, but values as low as 0.168dB/km are available as in Sumitomo Z-plus fibre [8].

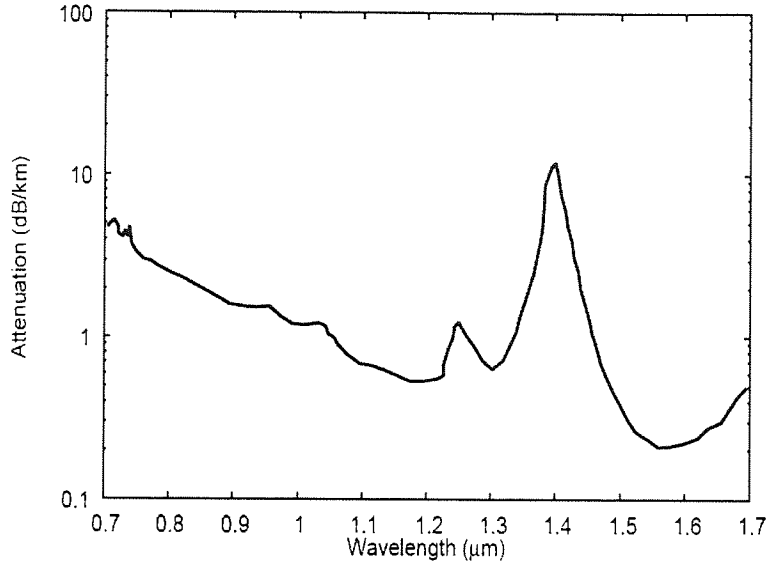

Figure 2.3 Sample of loss spectrum form a single mode step index fibre

2.1.3 Dispersion

When a signal pulse propagates along a single mode fibre it will broaden temporally due to chromatic dispersion or intra-modal dispersion, meaning that different wavelengths that go together to form a pulse spectrally, propagate at differing speeds. The variation of propagation time τ with wavelength λ is known as dispersion D.

$$D = \frac{d\tau}{d\lambda} \tag{2.5}$$

A multi mode fibre will experience inter-modal dispersion from the propagation time difference of each mode that was created when the pulse was launched as well as any extra spreading due to intra-modal dispersion. Chromatic dispersion in a single mode

fibre can be attributed to the dispersive properties of the material and effects from the waveguide structure, known as material and waveguide dispersion. The material dispersion can be given by [2]

$$D_m = \frac{\lambda}{c}\left|\frac{d^2 n_1}{d\lambda^2}\right| \tag{2.6}$$

Where n_1 is the core refractive index and c is the speed of light in a vacuum. The waveguide dispersion can be given by

$$D_w = -\left[\frac{n_1 - n_2}{\lambda c}\right]\frac{Vd^2(Vb)}{dV^2} \tag{2.7}$$

Where n_2 is the cladding refractive index, V is the normalised frequency for the fibre and b is the normalised propagation constant for the fibre.

The total dispersion is a combination of the material and the waveguide dispersions. At wavelengths longer than the zero material dispersion (ZMD) point in most common fibre designs, the D_m and D_w components are of opposite sign and can therefore be made to cancel each other at some longer wavelength. This means that the wavelength of the zero first order chromatic dispersion can be shifted to various wavelengths in the low loss 1300 and 1500nm regions. This can be achieved by changing the core diameter and relative or fractional index difference. Resulting fibres generally fit into one of three categories depending on their zero dispersion wavelengths (ZDW):

1. Standard Single Mode Fibre (SSMF or more commonly referred to as SMF), ZDW ≈ 1300nm
2. Dispersion Shifted Fibre (DSF), ZDW ≈ 1550nm
3. Non-Zero Dispersion Shifted Fibre (NZ-DSF), ZDW ≈ 1400-1500nm

There is another type of fibre called Dispersion Flattened Fibre (DFF) which maintains a similar dispersion value over a large wavelength range, say less than 2ps/nm/km over 1300 to 1600nm [1]. In such fibres, the dispersion shape is actually a shallow curve,

which results in the fibre possessing two zero dispersion wavelengths. These fibres require complex refractive index profiles to achieve the flattened dispersion profile and are not as easily obtainable as the three types listed. Figure 2.4 shows the measured and extrapolated dispersion values for three fibres, two of which are NZ-DSF (Corning LEAF and OFS TrueWave) and one is SSMF (OFS SMF).

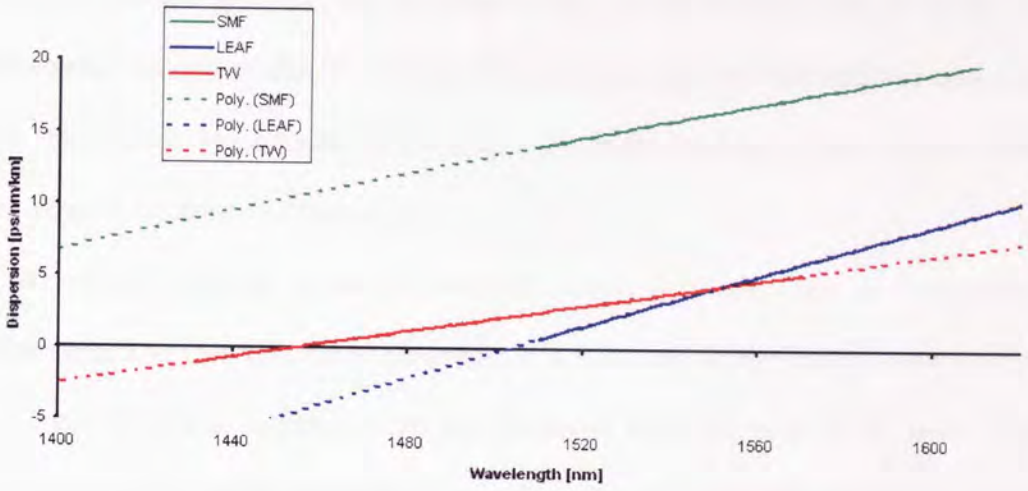

Figure 2.4 Measured dispersion for three fibre types

Note how although both LEAF and TW are considered NZ-DSF their zero dispersion wavelengths and dispersion slopes are notably different owing to the different index profiles used by each fibre manufacturer.

2.1.4 Polarisation Mode Dispersion (PMD)

When considering pulse propagation, polarisation mode dispersion must also be taken into account, in addition to chromatic dispersion. Even though the term single mode is used, referring to the HE_{11} electromagnetic mode supported by the fibre, this mode can itself be represented as the superposition of two orthogonally polarised HE_{11} modes [9]. In the ideal symmetrical cylindrical fibre these modes will propagate together at

the same velocity. However, a real fibre is not perfectly cylindrical, which makes it birefringent and gives rise to two HE_{11} modes, with distinct propagation characteristics.. PMD arises as a consequence of the birefringence as the two modes create a special case of the general problem of inter-modal dispersion as experienced in multi-mode fibres. As a pulse propagates, each polarisation mode will see a slightly different refractive index and therefore arrive at the receiver will a small time differential known as the Differential Group Delay (DGD). The received pulse will then be perceived as broader, in the temporal domain, than the original pulse even in the absence of chromatic dispersion.

PMD effects resemble those of chromatic dispersion, but there is a significant difference. The total chromatic dispersion is a relatively stable phenomenon [10] and the total chromatic dispersion can be calculated from the sum of its parts. PMD however is not a stable parameter at any given signal wavelength due to the random birefringence that is encountered in fibres. This results in PMD being a statistical value and making periodic compensation extremely complex. The effect of PMD can be visualized graphically in figure 2.5 below.

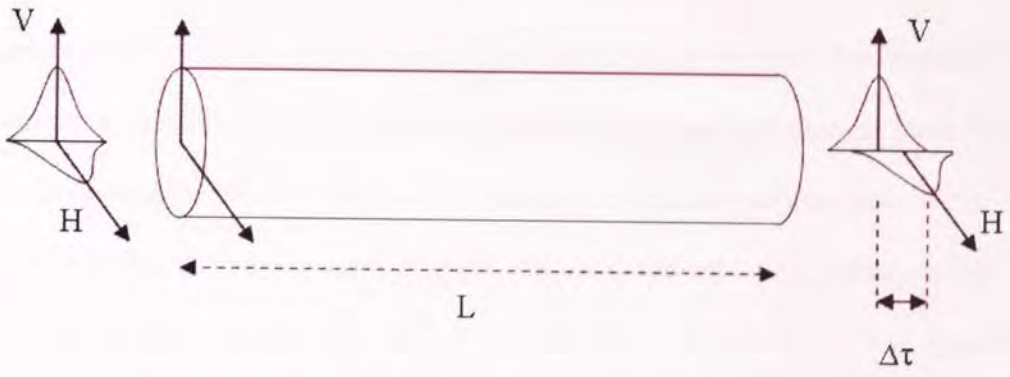

Figure 2.5 Time domain effect of PMD in a short length of birefringent fibre

Here a pulse is launched at 45° to the horizontal, where it can be interpreted as the vector addition of the horizontal (**H**) and the vertical (**V**) modes and the pulse can then

be resolved into two individual pulses, one in the horizontal plane and the other in the vertical. Due to the birefringence these two linearly polarized modes will encounter different refractive indices and will therefore propagate at different velocities. This results in the **H** and **V** components of the original pulse arriving at the fibre end at slightly different times. The DGD between the pulses can then be denoted by $\Delta\tau$. The two pulses will be seen as a broadened single pulse by a polarisation insensitive receiver, leading to errors in the received data if the DGD is large enough. The value of $\Delta\tau/L$ is known as the intrinsic or short length PMD and has the units ps/km, and for a transmission fibre a value of 1 ps/km is typical [9]. However, when quantifying the PMD of transmission link the units of ps/$\sqrt{}$km are used as a result of the PMD not accumulating in a simple additive fashion [9].

2.1.5 Fibre nonlinearities

At low powers, a single mode fibre can be regarded as a linear medium, as the output power spectrum follows a linear relationship with the input power. However at higher powers and/or in the presence of multiple light channels a fibre exhibits a non-linear relationship between the input power and the output power, whereby the output power, at the same wavelength, as the input fails to grow linearly with increasing input power. In today's modern WDM long distance systems the presence of nonlinear effects is a major problem, as to achieve the required distances and data rates, signal powers are high and multiple signals are present simultaneously in the fibre. The generated nonlinear effects add to the previously mentioned impairments, contributing to limit the achievable bit error rates. The main nonlinear effects can be classified into one of two groups:

- Stimulated inelastic scattering effects

- Intensity dependant refractive index effects

The first results in the part transfer of optical field energy to the nonlinear medium, the fibre, in the form of vibrational excitation modes of silica. The second is a result of the nonlinear electric polarisation of bound electrons in silica. The intense light interacts with the dielectric medium, whose response results in a change of the refractive index with the light intensity. These two categories can then be extended further still to detail the main related phenomena.

- Spontaneous inelastic scattering effects
    - Spontaneous Raman Scattering (SRS)
    - Spontaneous Brillouin Scattering (SBS)
- Intensity dependant refractive index effects (optical Kerr effect):
    - Light induced birefringence
    - Self-induced polarization changes
    - Self-Phase Modulation (SPM)
    - Cross-Phase Modulation (XPM)
    - Soliton propagation
    - Parametric processes

Quantum mechanically, spontaneous Raman scattering occurs from the scattering, by the fibre lattice, of an incident optical photon such that the scattered photon possesses less energy and therefore a lower frequency then the incident photon. The energy given up by the incident photon causes the fibre lattice to vibrate to a higher energy state; this is known as generation of an optical phonon [11], in this case where the emitted photon is at a lower wavelength, the wave is known as the Stokes wave. It is possible for an incident wave to receive energy from the vibrations and actually emit a photon of higher energy and frequency known as the anti-Stokes wave, but the efficiency in

this much less than for the Stokes generation due to the phase matching requirement between the incident photon and the present optical phonon. SRS is explored more in-depth in chapter 3. Similarly, SBS can be viewed as the annihilation of a pump photon that creates a scattered Stokes photon and an acoustic phonon simultaneously. The pump field generates an acoustic wave through the process of electrostriction (an electric field induced strain). The acoustic wave in turn modulates the refractive index of the medium. This pump-induced grating scatters the pump light through Bragg diffraction and the scattered light is down shifted in frequency because of the Doppler shift associated with a grating moving at the acoustic velocity in silica. The frequency shift of the Stokes wave depends on the scattering angle, being maximum in the backwards direction and virtually vanishing in the forward direction. By contrast, the frequency shift due to SRS can occur in both the forward and reverse directions. It should be noted that the frequency involved with SBS phonons is much lower than for SRS phonons. Also an abstract distinction between the two is that; an SBS phonon is a longitudinal acoustic wave and the SRS phonon is a transverse wave.

The optical Kerr effect or light induced birefringence is an interpretation of the original effect seen by John Kerr where a DC electric field could induce birefringence in an initially isotropic dielectric medium. In the presence of an intense, linearly polarized light beam, an isotropic medium will become birefringent. A weaker probe beam will then see a refractive index change that differs whether the probe is polarized parallel or normal to the strong pump [12].

Self-induced polarization changes occur as a result of the Kerr effect. If the intense light beam is not linearly polarized but is elliptically polarized, then the interaction with the nonlinear medium results in changes in the polarization state by the beam itself. If the medium is isotropic, the polarization ellipse only rotates with propagation

distance (and intensity) without changing shape. If the nonlinear medium is anisotropic, as in a birefringent optical fibre, both the shape and orientation of the polarization ellipse will change with propagation distance and intensity.

The nonlinear refractive index, generally referred to as n_2, is added to the linear refractive index, n, to create a total refractive index for a given optical intensity. From [11],

$$\tilde{n}(\omega,|E|^2) = n(\omega) + n_2|E|^2 \tag{2.8}$$

Where $|E|^2$ is the optical intensity inside the fibre and $n(\omega)$ is the linear part that can be approximated from the Sellmeier equation,

$$n^2(\omega) = 1 + \sum_{j=1}^{m} \frac{B_j \omega_j^2}{\omega_j^2 - \omega^2} \tag{2.9}$$

where ω_j is the resonance frequency and B_j is the strength of the jth resonance. The intensity dependence of the refractive index leads to a large number of interesting nonlinear effects including self-phase modulation and cross-phase modulation.

Self-phase modulation is the self-induced phase shift experienced by an optical field during propagation in a fibre due to its own intensity when the intensity is at a high enough level. SPM has many consequences including the spectral broadening of ultra short pulses and the formation of optical solitons in the anomalous dispersion regime of fibres.

A similar effect to SPM that occurs when two or more wave/signals propagate along the same fibre is cross-phase modulation (XPM). If each signal experiences SPM then the refractive index change induced by each channel will be experienced by the other signal resulting in phase modulation of the signal by the other. The XPM induced coupling between waves gives rise to a multitude of nonlinear effects in fibre, including [11]:

- XPM induced nonlinear birefringence
- Polarization instability
- XPM induced pulse compression
- XPM induced optical switching

As previously mentioned SPM can be utilised in a positive manner in the formation of optical solitons. Optical solitons can be considered as a special case of nonlinear dispersion compensation, where the nonlinear chirp, from SPM, postpones the temporal broadening, from anomalous dispersion, of a pulse. This is a very basic view of solitons and there are many texts which look into this phenomenon including the renowned Nonlinear Fibre Optics, by G.P. Agrawal [11]. Solitons can be used to improve the performance of dispersion limited communication systems by balancing the fibre dispersion as mentioned. In order to achieve this, the peak power should be kept fairly constant to avoid dropping out of the nonlinear regime and therefore losing the balancing effect of SPM. To maintain the soliton in presence of fibre losses the launch power maybe increased further still, and/or periodic amplification maybe invoked. The use of periodic amplification is already utilised in optical communication systems with the use of EDFAs and Raman amplification. The amplifier boosts the soliton energy back to its original input level, the soliton then readjusts its width to the input level. Systems which employ periodic amplification often utilise periodic dispersion compensation for linear systems. If a true soliton was sent through such a system it is likely to become unstable due to the normal dispersion element it will encounter. Research using periodic dispersion compensation systems led to discovery of another class of soliton known as the Dispersion Managed (DM) Soliton.

A DM soliton is a nonlinear pulse which varies in its shape during propagation in a "breathing" fashion and which can propagate through a dispersion managed span

which was originally intended to suppress nonlinear effects. The DM soliton can recover its shape through the system elements periodically and can be regarded as a quasi-stationary pulse [13].

Final nonlinear effects to outline in this chapter are parametric processes, namely four wave mixing (a subject which is covered in more detail in chapter 5). In stimulated processes, like Raman and Brillouin scattering, the fibre plays an active role through the participation of lattice vibrations (Raman) or acoustic phonons (Brillouin). In parametric processes the fibre plays a passive role apart from facilitating the interaction among optical waves through the nonlinear response of bound electrons. Parametric processes arise from modulation of a fibre parameter, such as the refractive index. These processes include harmonic generation, four wave mixing and parametric amplification. Parametric effects can be grouped into either second-order or third order depending whether their existence originates from the second order $\chi^{(2)}$ susceptibility or the third-order $\chi^{(3)}$. The second-order susceptibility should not exist for an isotropic medium such as silica and therefore second-harmonic generation should not be possible in fibres, however, second harmonic generation has been reported due to imperfections in the fibre geometry/construction, see reference [11]. Third-order processes in general involve the interaction between four optical waves and include phenomena such as third-order harmonic generation, FWM and parametric amplification. Four wave mixing can be a problematic effect where several different wavelength signals essentially exchange power to create a new wavelength, this wavelength may impinge upon an existing data signal therefore reducing its optical signal to noise ratio. However, FWM can be used positively in the efficient generation of new wavelengths.

With so many effects bought into play during light propagation it would be important to obtain a single equation which could account for all of them. Fortunately such and equation has already been devised and is known as the Non-linear Schrödinger Equation or NLSE. The equation in its general form is given below (for derivation please refer to reference [11]):

$$i\frac{\partial A}{\partial z}+\frac{i}{2}\alpha A-\frac{1}{2}\beta^2\frac{\partial^2 A}{\partial T^2}-\frac{i}{6}\beta^3\frac{\partial^3 A}{\partial T^3}+\frac{2\pi}{\lambda_0}\frac{n_2}{A_{eff}}|A|^2 A=0 \qquad (2.10)$$

Where A is the pulse amplitude (with respect to z,t), $T=t-\beta_1 z$, α is the linear attenuation coefficient, $|A|^2$ is the pulse power, β is the propagation constant, λ_0 is the carrier wavelength, n_2 is the fibre nonlinear refractive index and A_{eff} is the fibre effective area.

2.2 Conclusions

This chapter has looked at the main characteristics of optical fibres. It has abstractly looked at the physical construction of a fibre and illustrated the way in which a beam of light travels through it. Fundamental parameters such as fibre loss and dispersion are introduced, two parameters that affect all light waves whether they be data signals or quasi-CW (non-monochromatic with noise component). Nonlinear effects such as Raman scattering and four wave mixing have been presented, displaying that optical waves can, through these processes, generate radiation at new wavelengths not originally present in the fibre. These terms will be seen extensively within later chapters.

Chapter 3

Introduction to Raman Scattering in Optical Fibres

3.1 Introduction

For modern telecommunications to exist, vast distances must be covered in order to connect cities, countries and continents. In addition to the vast distance, enormous amounts of data must be moved reliably and there is only one cost effective way to do this, which is the use of optical fibres. To operate over these distances, optical systems must employ periodic amplification, which can be facilitated by the use of Erbium Doped Fibre Amplifiers (EDFAs) or Raman amplifiers. Even though Raman amplifiers were existent in the 1970s and 1980s, it was EDFAs that became the amplifier of choice in the 1990s due to the high power lasers that were required for Raman. More recently interest in Raman has been greatly revived by the advent of high power semiconductor pump lasers by companies such as Fitel Inc. This allows fibre pump modules to be created that are of no greater footprint than EDFAs and have acceptable power and heat dissipation requirements. However this is not the only driving force behind the increasing popularity of the Raman amplifier; the ever-increasing demand for data capacity, which in turn requires an optical system with more useable bandwidth, can also be attributed. To obtain multi tera-bit transmission rates it is necessary to use many channels at different wavelengths and EDFAs can only provide gain at certain wavelengths, determined by the dopants used, so therefore the number of channels that can fit within a given band is limited. To counteract this, Dense Wavelength Division Multiplexing (DWDM) is used, whereby channels are closely spaced together, typically 100 and 50GHz spacing for 10GBit/s systems, though as close as 25 and 12.5GHz has been demonstrated. Even if DWDM is used,

the use of faster channel data rates 40Gbit/s and beyond limits how close channel spacing can be and thus new wavelength regions must be sought. This is where Raman can provide solutions. By offsetting the pump wavelength from the signal wavelength by the appropriate amount, gain can be provided at the wavelength required. EDFAs, on the other hand, need special dopants to achieve alternative wavelength ranges, which can be hard to produce and therefore expensive. By the use of multiple pumps and correctly chosen wavelengths, Raman amplification can provide flat gain over continuous bands, something that is not possible within a single EDFA.

Gain wavelength flexibility is major benefit of Raman amplification, though possibly not the number one benefit. That honour goes to the distributed nature of the generated gain. If the transmission span fibre is the medium to be used for the Raman process then the signal starts to receive gain long before the end of the fibre. This outcome has multiple benefits including improving the effective noise figure of the amplifier by distributing the gain and keeping the signal away from the noise floor. This can be quickly illustrated by studying figure 3.1 below where the two traces depict the signal power without Raman gain, in blue and with gain, in red.

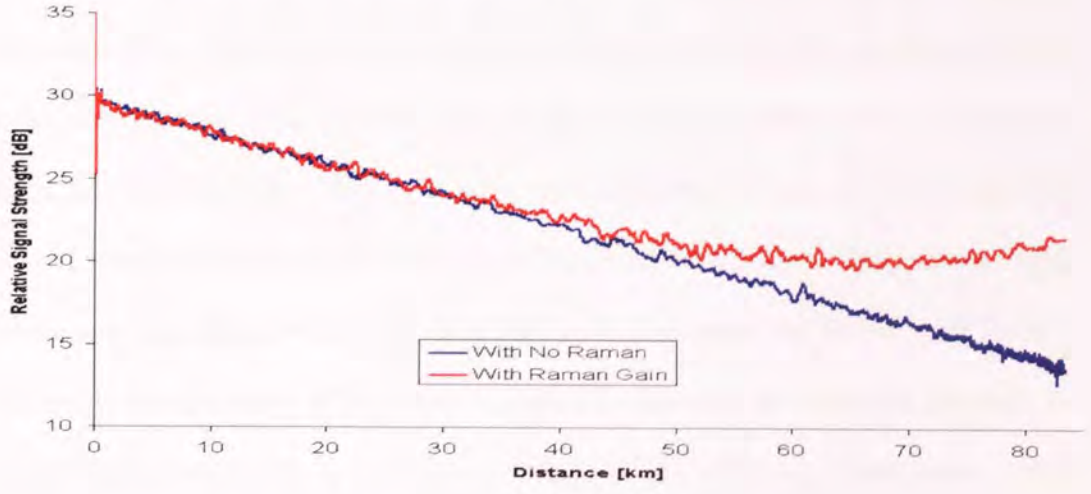

Figure 3.1 Effect of Raman gain upon signal strength

For this result an 85km span of fibre was pumped in the counter signal direction; the result of which is the signal receiving noticeable gain from the 40km onwards point. Using such a scheme would improve the received signal to noise ratio at the end of the span.

This chapter aims to cover the main concepts, advantages and disadvantages of Raman amplification in telecommunications systems.

3.2 History of the Raman Effect

In the early 1920s Sir Chandrasekhra Venkata Raman felt that his research into vibrations and the properties of sound had run its course and he began to look towards other fields. Raman began to study light scattering in liquids in the last months of 1921 [14]. Some of this work established that the blue colour of the sea is due to scattering by molecules [15], but the rest of the work left little mark on the science world. However, in the course of the experiments Raman noticed that scattering from transparent liquids always included some radiation of a frequency lower than that of the incident light. Initial experiments were carried out by using sunlight confined by a filter to a fairly narrow wavelength band, the results of which were summarised in a letter to the journal Nature in 1928 [16]. The sun was soon replaced with a mercury arc lamp, which enabled the effect to be seen more clearly and it was also noted that that not only lower frequencies are created (the Stokes wave) but higher frequencies could be formed (anti-Stokes wave). In 1930 Raman was awarded the Nobel prize for his discovery. Raman stated in [17] that '...makes it clear that the scattered spectrum is practically a description in spectroscopic form of the chemical constitution of the molecule'. This fact forms the basis for Raman spectroscopy used extensively in chemistry for the identification of materials.

Moving along to 1962, Stimulated Raman Scattering was reported, whereby the Stokes wave grows rapidly inside a medium such that most of the power of the pump beam is transferred to it [18]. In 1972 Roger Stolen *et. al.* published the observation of stimulated Raman emission in a single mode silica fibre [19] and suggested the possible use as a means of light amplification, and in 1973 the first Raman amplifier for fibre was demonstrated [20]. Although interest in Raman amplification remained, it was not until the 1990s when high power solid state lasers became available that the technology became mature for commercial long haul systems. However, during this time commercial systems were not employing Raman technology but generally sticking with tried and tested EDFA techniques and it was only into the 21st century that research papers were extensively reporting the use of Raman amplification [5].

3.3 Source of Raman Scattering

The Raman scattering process is a nonlinear process and nonlinearity can be interpreted by considering a simple spring. If a small force pulls the spring, then the spring extends in a directly proportional way. However if a large force is applied then the extension of the spring becomes nonlinearly proportional to the force applied. Similarly, the response of a dielectric medium, such as an optical fibre, is linear for low input optical powers but becomes nonlinear in response to strong incident optical power and Raman scattering is one of several responses to this power.

When an optical field is incident on a molecule its bound electrons oscillate at the frequency of the incident wave. The induced dipole moment produces optical radiation at the same frequency as the wave that caused it, but with a phase difference. This leads to the material's refractive index. At the same time the material molecular structure is oscillating at frequencies determined by various molecular vibrations [5].

So, now present in the material are the range of indigenous frequencies and the frequency/frequencies induced by the incident optical wave, this leads to the aforementioned dipole moment having sum and difference frequencies between the optical and vibrational frequencies. It is these products that give rise to Raman scattered light in the re-radiated field.

Looking towards the quantum mechanical description, the process can be interpreted as optical photons that are inelastically scattered by quantized molecular vibrations called optical phonons. Here the energy of the incident photon is either lost in heating the molecular lattice of gained by cooling of the lattice. Where energy is lost, the re-radiated wave is shifted to a longer wavelength and is referred to as the Stokes wave or line. Where energy is gained, the wave re-radiated is now at a higher frequency and is labelled the anti-Stokes wave or line. The frequency shift that occurs is equal to the oscillation frequency of the lattice optical phonon that is created or destroyed. Figure 3.2 displays this is a simplistic form.

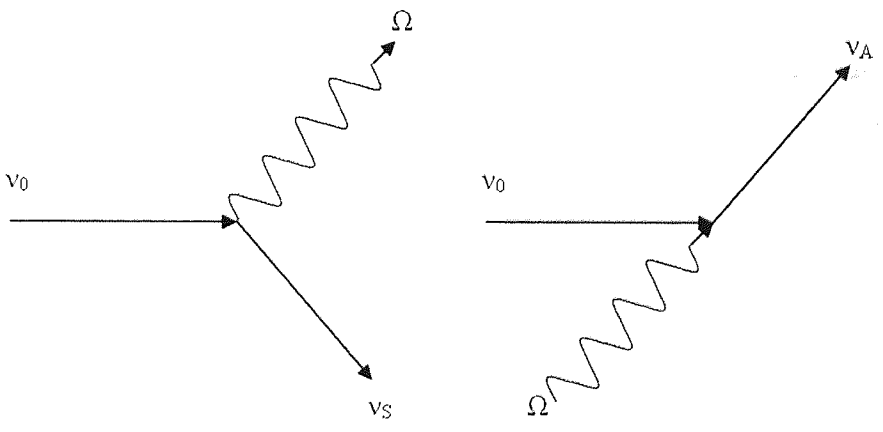

Figure 3.2 Scattering diagrams for Stokes and anti-Stokes Raman scattering

Here ν_0 is the frequency of an incident photon, Ω is a quantum of vibrational energy, ν_S is a resulting photon at the Stokes frequency and ν_A is a resulting photon at the anti-Stokes frequency. Therefore, $\nu_S = \nu_0 - \Omega$ and $\nu_A = \nu_0 + \Omega$ [21].

Raman scattering can also be stimulated by signal light at the appropriate frequency shift from a pump, leading to what is commonly referred to as Stimulated Raman Scattering (SRS). Here the pump light and signal light are coherently coupled by the Raman process [5]. This process can be illustrated by use of an energy level diagram as in Fig. 3.3.

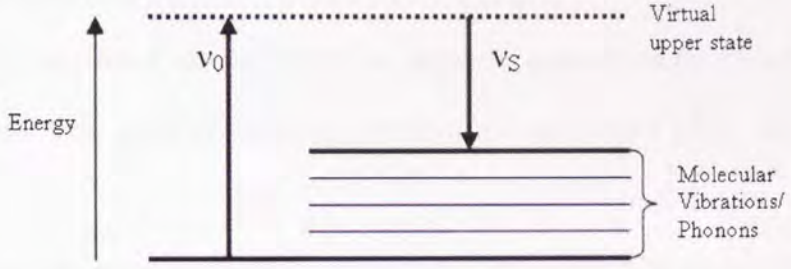

Figure 3.3 Depiction of the quantum mechanical process taking place during Raman scattering

Here ν_0 can be considered as a pump photon and ν_S can be considered as the emitted spontaneous photon. A pump photon excites a molecule up to a virtual level (nonresonant state), if another optical wave is present at the same frequency as ν_S it will stimulate the photon, from the decay of the excited molecule, to have the same frequency and phase as itself. Hence the emitted photon, ν_S, is no longer generated in a spontaneous fashion but is stimulated and adds coherently with the incoming optical wave and therefore amplification is achieved. The difference in energy between the pump and signal photons is dissipated by molecular vibration within the incident material. It is the vibrational levels which define the frequency shift and the distribution of the generated Stokes lines and within an amplifier the gain curve/shape, in a typical Ge-doped core optical fibre the peak of this frequency is ~13.2THz. With increasing pump power this peak can grow rapidly, greater than surrounding wavelengths, to the point where the majority of pump power is transferred to the Stokes peak wavelength. This can happen even when there is no discrete signal input

into the fibre and the spontaneous emission acts as a signal, this phenomenon can be utilised in the creation of Raman fibre lasers.

3.4 Amplification by Raman in optical fibres

When considering Raman for amplification of lightwave signals, it is useful to acknowledge the following fundamental properties [5]:

- Raman gain has a spectral shape that primarily depends on the frequency offset and not their absolute frequency, though the latter does affect absolute gain [22]
- Raman gain does not depend on the relative direction of the pump and signal
- Raman is a fast process (sub-picosecond [23] there are no long upper state lifetimes to buffer pump fluctuations)
- Raman gain is polarization dependent [24], with coupling strength between co-polarized pump and signal being an order of magnitude greater than if they are orthogonal

As mentioned in the previous section, the distribution of Raman gain is dependent upon the vibrational levels supported within a fibre. This distribution changes when the chemical make up of a fibre changes. This can be seen clearly in the next figure, Fig. 3.4, where two distinctively different fibres were used to amplify the same broad band signal in the counter propagating direction.

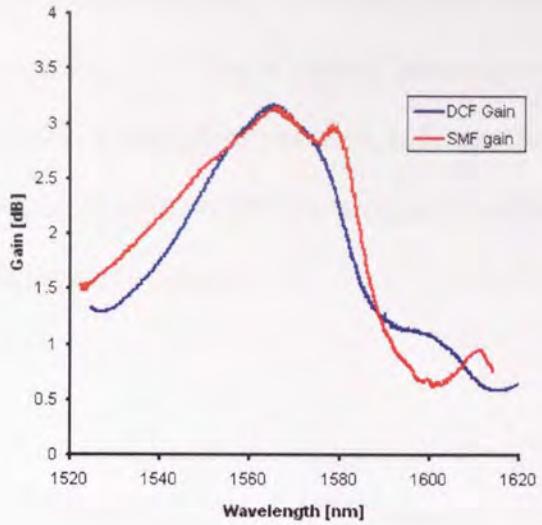

Figure 3.4 Comparison of gain shape for a DCF fibre and a standard SMF fibre

Here a length of standard SMF and a length of DCF were used to obtain the same level of gain. The differences in the profile is clear and can be attributed to the composition of each fibre, the addition of GeO_2 in the DCF not only creates a single peak gain profile but also increases Raman gain efficiency [25]. It is important to note that the above gain spectra are obtained by utilising cross polarised pump lasers at a single wavelength, essentially providing gain regardless of the signal polarisation. If the signal was at an orthogonal polarisation to the pump laser then the resulting gain is far less, see [26].

Figure 3.4 shows the gain for a single wavelength pump which, although covers a considerable bandwidth, is still not wide and flat enough for modern DWDM communication systems. To create a gain profile that covers a greater wavelength range, multiple pumps at different wavelengths can be used which results in multiple gain spectra that overlap. The pumps are combined by use of Wavelength Division Multiplexers (WDMs) which allow low loss combining into the transmission fibre of about 0.5 dB per WDM. Any number of pumps can be used simultaneously, with some cases reporting up to 12 wavelengths combined [27] to produce the desired gain

continuity, but a more typical number is around five. The gain from such a configuration is shown in Fig. 3.5. Here a counter pumping semiconductor Raman pump module from the Fitel Corporation was used, with wavelengths at 1425, 1437, 1452, 1467 and 1495nm, along with two EDFAs acting as broadband light sources and a 75km span of SMF as the gain medium.

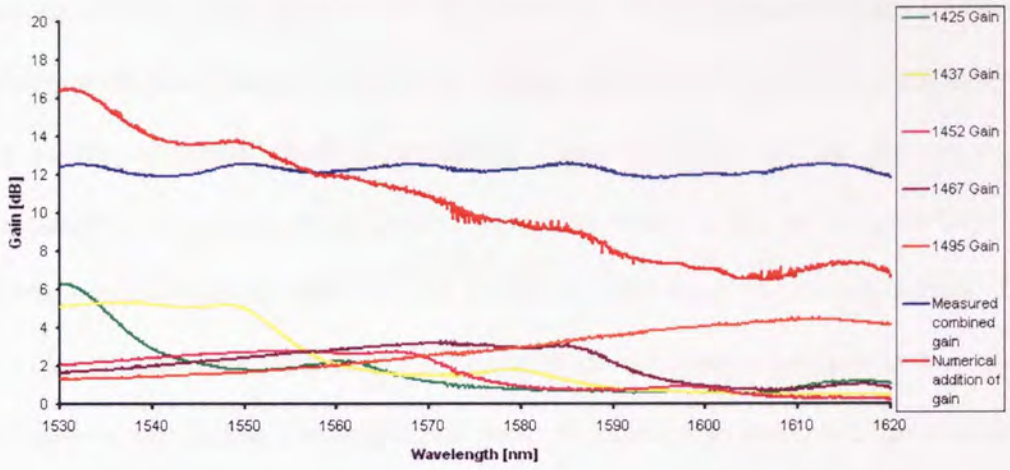

Figure 3.5 WDM Raman pump gain

Here the blue trace is the combined gain created by having all pump wavelengths operating at a specific level to produce a flat gain. The individual pump powers (per wavelength cross polarised pair) were:

Wavelength	Power [mW]
1425	400.6
1437	311.3
1452	160.1
1467	176.6
1495	247.7

Table 3.1 Pump powers at each wavelength for WDM Raman

Referring back to Fig. 3.5, the combined gain is subject to the effect of inter-pump gain, whereby the gain from the shortest wavelength not only provides gain to the shorter signal wavelengths but also to longer wavelength pumps. This gives rise to pump depletion of the shorter wavelengths and its effect on power can be seen in table 3.1 where the highest pump power is at the shortest wavelength. The gain in the absence of other pump wavelengths can be seen in the lower traces of Fig. 3.5 for the pump powers stated above. Performing a linear addition of the individual traces gives rise to the red trace which is noticeably sloped in favour of the shorter signal wavelengths. As already seen, the true combined effect is flat as the gain from the shorter pump eventually increases the gain from the longer wavelength pumps. This interplay of gain makes the choice of pump diode wavelength and power less trivial then maybe anticipated. The transfer of power from pump to pump and the overlap of respective gain spectra must be evaluated to ensure optimum variation with respect to wavelength of the desired operating gain level. A further issue that affects the use of WDM Raman pumping in modern transmission fibre is the generation of four-wave mixing components. The subject is dealt with more thoroughly in chapter 5, but in essence concerns the formation of noise products that can appear within the signal region lowering optical signal to noise ratio (OSNR) performance. This is more noticeable when fibres with a zero dispersion wavelength in between the pump and signal bands are used due to efficient phase matching of involved photons. Fibres such as Corning LEAF employed in the experiment for figures 3.6 and 3.7 can be used to illustrate the phenomena.

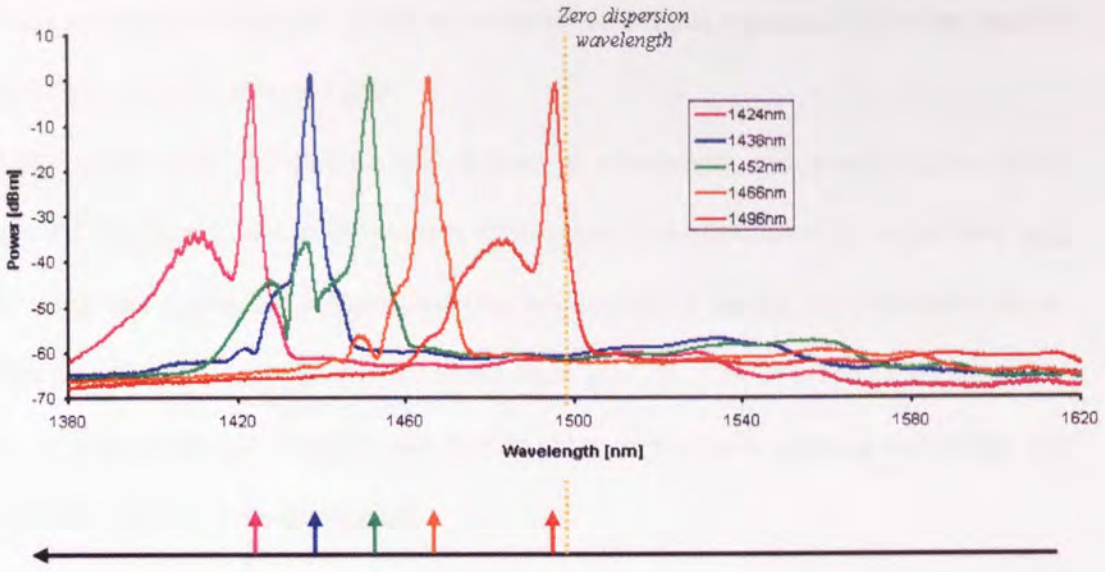

Figure 3.6 Individual pump wavelengths after 25km LEAF

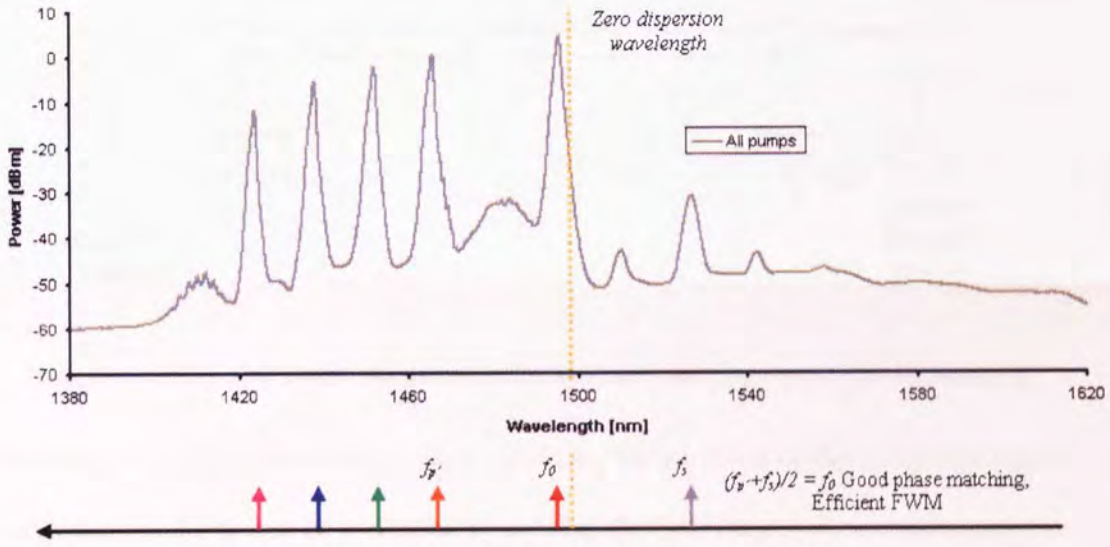

Figure 3.7 All pump wavelengths together after 25km LEAF

Comparing these two figures it can be recognised that there are peaks present in the 1500 to 1600nm region (the signal band in this example) when all pumps are present that were not there when only one pump wavelength was propagating. These peaks are formed through the four-wave mixing between pump wavelengths and that of spontaneous noise within the signal band. It can be appreciated that such formations

could drastically reduce the OSNR of one or several signal channels within the locality leading to errors in received data.

Better signal gain distribution with respect to wavelength can also be achieved by spectral broadening of a lower number of wavelengths as discussed in chapter four and by using time dependent pumping where a single pump is rapidly and repeatedly swept over the necessary range to provide broad-band gain, see [28, 29]. The predicted result of the latter technique is impressive, but as yet no cost effective pump technology for this technique has been developed.

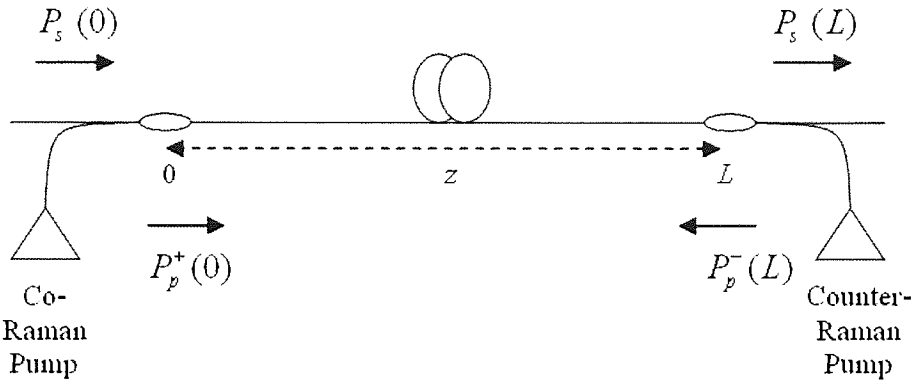

Figure 3.8 Schematic of simple Raman amplifier scheme employing co and counter pumping

Returning to a single wavelength pump amplifier, the variation of the pump and signal in the above scheme can be modelled by solving the following two coupled equations [30] where only fibre attenuation and interaction between one pump and one signal are considered.

$$\frac{dP_p^{\pm}}{dz} = \mp\alpha_p P_p^{\pm} \mp \frac{\nu_p}{\nu_s}\frac{g}{A_{eff}} P_s P_p^{\pm} \tag{2.11}$$

$$\frac{dP_s}{dz} = -\alpha_s P_s + \frac{g}{A_{eff}} P_p^{\pm} P_s \tag{2.12}$$

Where $P_p^{\pm}$ and P_s are the powers for a forwards/co (+) or backwards/counter (-) propagating pump and the signal respectively. The fibre attenuation at the pump and signal wavelengths is given by α_p and α_s respectively, g is the Raman gain coefficient and A_{eff} is the effective core area of the fibre at the pump frequency. If only small signal amplification with no pump depletion is considered then the pump power term in (2.12) can be substituted for (in the case of a forward propagating pump):

$$P_p(z) = P_p(0)\exp[-\alpha_p z] \tag{2.13}$$

and (in the case of a backwards propagating pump):

$$P_p(z) = P_p(L)\exp[-\alpha_p(L-z)] \tag{2.14}$$

This provides an analytical solution for the power at the end of the fibre span used as the amplifying medium in the form of:

$$P_s(L) = P_s(0)\exp\left(\frac{g}{A_{eff}}P_0 L_{eff} - \alpha_s L\right) \tag{2.15}$$

With P_0 being either $P_p(0)$ or $P_p(L)$ depending on the launching point of the pump, and L_{eff} being the effective length within which most of the Raman gain occurs, given by:

$$L_{eff} = \frac{[1-\exp(-\alpha_p L)]}{\alpha_p} \tag{2.16}$$

It must be noted that these equations make no allowance for the existence of amplified spontaneous noise and Rayleigh backscattering. In the presence of high signal powers, multiple signals, and multiple pumps much more involved equations are required to take into account the depletion suffered by the pump laser.

3.5 Noise processes in Raman amplified systems

It has been seen that the Raman process can provide gain to a signal but they also provide a source of noise in addition. The main sources of noise are:

- Spontaneous Raman Scattering/Emission generating Amplified Spontaneous Emission (ASE)
- Double Rayleigh Back Scattering (DRBS)
- Pump-noise transfer, also known as RIN transfer
- FWM between pumps/signals as previously mentioned, also see chapter 5

The most problematic is ASE, which is an unavoidable by-product of gain in all amplifiers and appears as a noise because of the random phases associated with all spontaneously generated photons. The mechanism is similar to the spontaneous emission that affects EDFAs, but in the Raman case it depends on the phonon population in the vibrational state, which itself is dependant on the temperature of the Raman amplifier. The generation and amplification obeys, from [5]

$$\pm\frac{dP_A^{\pm}}{dz} = -\alpha_a P_A^{\pm} + \frac{g}{A_{eff}}(\lambda_A.\lambda_p)P_p P_A^{\pm} + \frac{g}{A_{eff}}(\lambda_A.\lambda_p)[1+\eta(T)]h\nu_A B_{ref} P_p \qquad (2.17)$$

Where $P_A^{\pm}$ is the ASE power in one polarisation component in a bandwidth B_{ref}, propagating in the $\pm z$ direction, P_p equals the total depolarized pump power at position z, travelling in both directions. $\eta(T)$ is a phonon occupancy factor given by

$$\eta(T) = \frac{1}{\exp\left[\frac{h\Delta\nu}{k_B T}\right] - 1} \qquad (2.18)$$

Where h is Planck's constant, k_B is Boltzmann's constant, T is the temperature of the fibre in Kelvins, and $\Delta\nu$ is the frequency separation between the pump and the signal.

At 25°C, $\eta \approx 0.11$ at the peak Raman gain $(\Delta\nu = 13THz)$, and can be considered a small correction factor.

ASE becomes most problematic when it is co polarised with signal light propagating in the same direction, leading to intensity fluctuations known as 'signal-spontaneous beat noise'. These fluctuations can cause voltage/current fluctuations within the system receiver that may lead to errors due to bits being wrongly interpreted.

It has been shown that the use of Raman to provide gain has a large advantage concerned with noise figure improvement [5], but this advantage suffers from the threat of being reduced by the effect of Double Rayleigh Back Scattering (DBRS or DRS). DRS can be interpreted as a Multiple Path Interference (MPI) process whereby the original signal is delayed in some way and then continues thus creating out of sync data which can be interpreted as noise. The delay mechanism in DRS, is the Rayleigh Backscattering of the signal into a counter propagating direction and the subsequent scattering back into the co propagating direction, see Fig. 3.9.

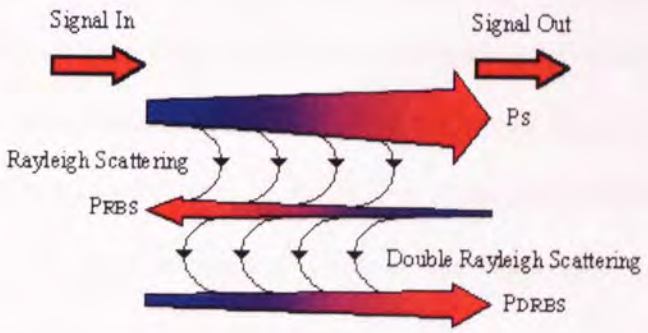

Figure 3.9 DRBS Illustration

DRBS is derogatory within passive and discrete amplified systems but the effect in distributed amplifiers can be more severe [26]. For example consider a backward pumped span and the shape of the arrows as shown in Fig. 3.9, as the initial signal (P_s) propagates towards the end of the span it grows in magnitude, as it grows a larger

quantity of photons are scattered into the reverse direction. These initially scattered photons create a reverse propagating signal (P_{RBS}), which also receives gain from the Raman pump, a proportion of P_{RBS} is then once again reflected back into the original signal direction. This doubly reflected signal, P_{DRBS}, receives Raman gain yet again as it travels towards the span end and the pump laser. The distributed Raman amplifier also adds spontaneous emission to the signal; thus, in addition to the Rayleigh reflected signal the Rayleigh reflection process also causes an extra contribution to the spontaneous emission. The most severe contribution occurs from the backward propagating noise and needs only to be reflected once, in the simplest interpretation, to mix with the forward propagating noise. It has been shown that for on-off gains of less than 20dB the contribution is less than the normal forward propagating ASE [31].

As previously stated the Raman process is an inherently fast process and therefore, pump power fluctuations can be transferred to signals as noise. This said, in the case of fibre amplifiers, the pumps and signals interact over relative time scales that are considerably longer because they propagate over many kilometres of fibre. This produces an averaging effect that limits the bandwidth over which pump noise is transferred. This phenomena is described in the frequency domain as a transfer of Relative Intensity Noise (RIN) from a pump to a signal [5]. Equation (2.19) is the fundamental RIN definition from [26], given as the fluctuation power in 1Hz of bandwidth relative to the average power squared

$$RIN(f) = \frac{S_{\Delta P}(f) \cdot \Delta f_0 (\equiv 1Hz)}{P_0^2} \tag{2.19}$$

where $S_{\Delta P}$ is the power spectral density of the fluctuation [W^2/Hz], f is the frequency, P_0 is the average power and $\Delta f_0 \equiv 1Hz$ is the bandwidth. If the fluctuation is

bandwidth limited to a small bandwidth Δf, over which the spectral density is constant, the RIN definition can be expressed as [26]

$$RIN = \frac{\left\langle \Delta P^2(t) \right\rangle}{P_0^2} \cdot \frac{\Delta f_0}{\Delta f} \tag{2.20}$$

Where $\left\langle \Delta P^2(t) \right\rangle$ is the time averaged mean square fluctuation of the laser. The pump-noise transfer function represents the enhancement in the signal noise at a specific frequency f and is defined as

$$H(f) = \frac{RIN_s(f)}{RIN_p(f)} \tag{2.21}$$

For a given amplifier, the value of $H(f)$ depends on the pumping direction, the pump and signal wavelengths, and the amount of on-off gain. In the fibre the Raman gain builds up as the signal propagates inside the fibre, for a small dispersion value in the co-pumping regime the pump and signal travel at similar speeds. Therefore, any pump fluctuation stays in the same temporal window as that of the signal. When the dispersion value is large the pump and signal travel at different velocities and the signal moves out of the temporal window associated with that fluctuation. Because of this walk-off the signal sees a more averaged gain; the same applies to the counter pumping configuration. The effect is far more pronounced in the counter pumping direction because the relative speed is extremely large (twice that of the signal group velocity). In this configuration, the fluctuations are smoothed out to a degree that almost no RIN enhancement occurs this is also true to a certain extent in the forward pumping direction with large values of fibre dispersion [32]. As well as dispersion the following gain fibre characteristics are relevant to the transfer efficiency: fibre length, pump loss coefficient and dispersion slope. It's due to these reasons that counter/backwards pumping is used and forward pumping is only utilised when very

low RIN lasers are operated along with a careful selection of fibre, chapter six looks again at this issue.

3.6 Pump configurations

It is worth clarifying graphically the main pumping configurations used in distributed Raman amplification work, i.e. where the spanning transmission fibre is used as the gain medium, and to mention a few more novel set-ups. The three main conventional pumping layouts are:

- Counter pumping: the Raman pump is launched into the transmission fibre at the opposite end to the signal
- Co pumping: the Raman pump is launched into the transmission fibre at the same end to the signal
- Co and Counter: a combination of the previous two where the pump is launched from both ends

The following Figs. 3.10, 3.11 and 3.12 depict the above and give an idea of the simplicity of Raman amplification and the resulting effect upon a real signal.

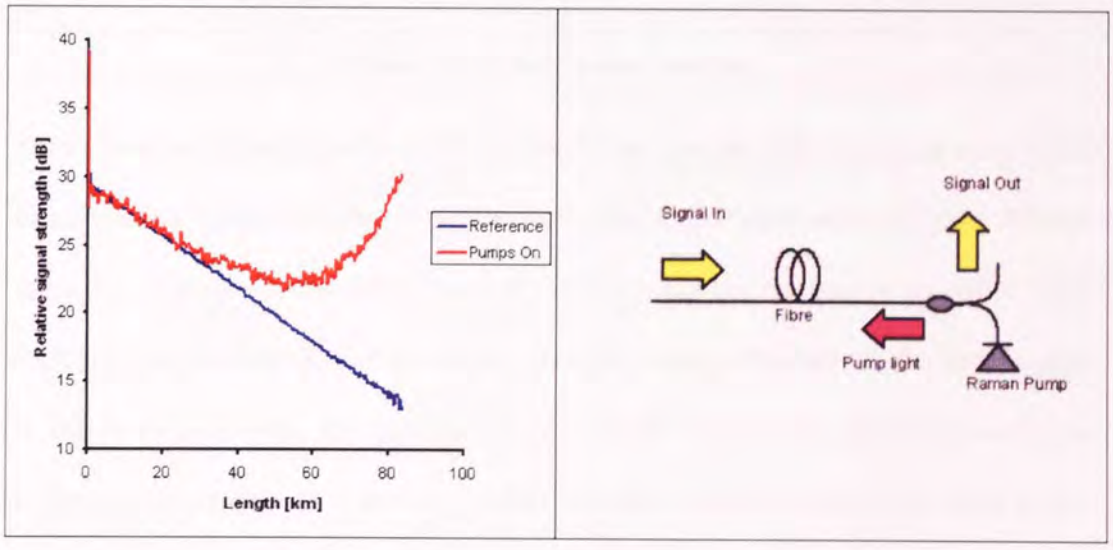

Figure 3.10 Counter pumping

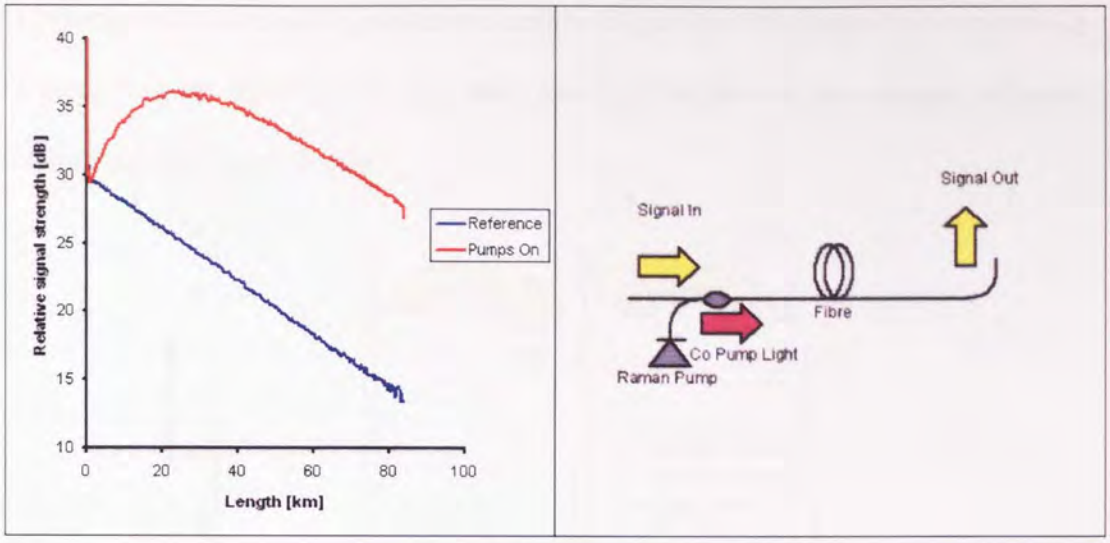

Figure 3.11 Co pumping

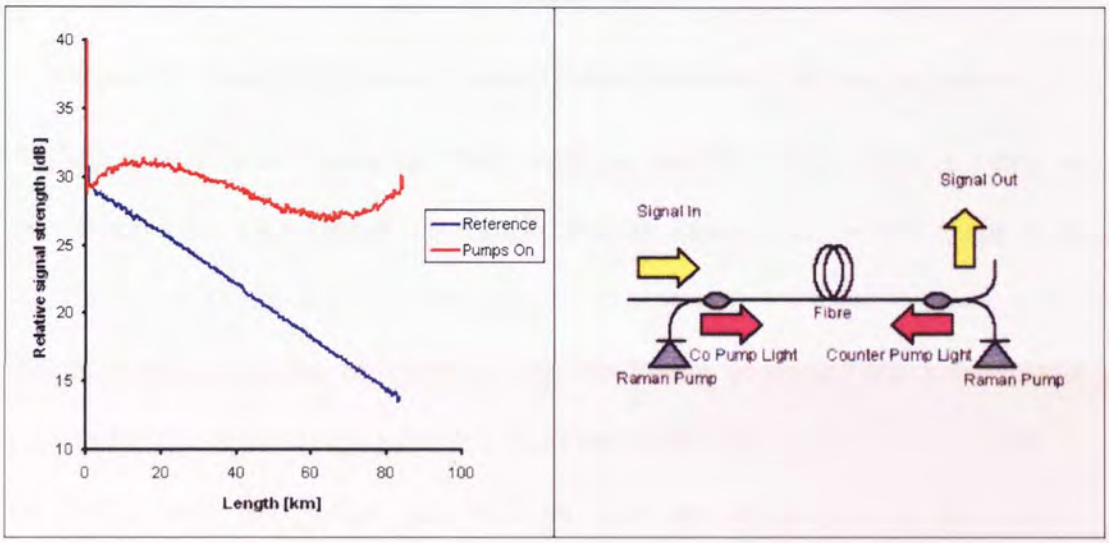

Figure 3.12 Co and Counter pumping

These basic configurations can be built upon by the use of WDM pumping as covered in section 3.4, and by the use of higher order pumping. Higher order pumping utilises more than one pump wavelength as in WDM pumping but the pumps are offset from each other by the Raman shift frequency; thus one pump effectively looks like a signal to the other one. With this arrangement the longer wavelength pump receives gain from the other pump as it travels through the fibre, which in turn gives gain to the signal; a simple depiction is given below in Fig. 3.13 for the energy transfer. The

advantage of this method is greater penetration of gain into the fibre which can provide a more constant signal power especially when applied in a co and counter style, see chapter six for further details

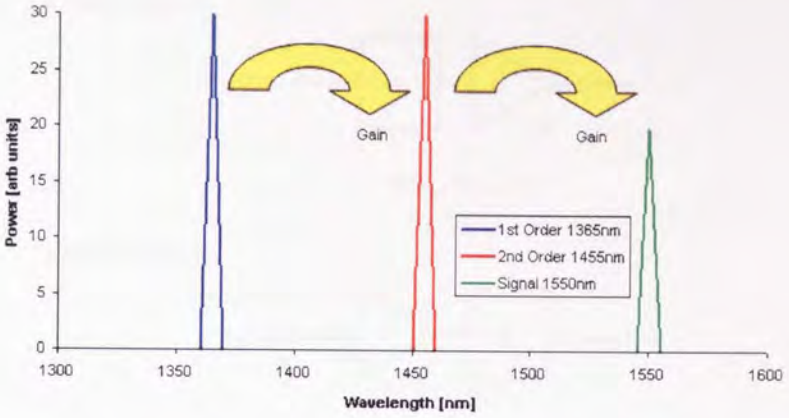

Figure 3.13 Simplified illustration of energy transfer in a second order pumping scheme

Beyond second order pumping third order is possible where another pump is introduced at an even shorter wavelength. For the example above this could be at ~1270nm, see [33] for third order pumping.

All these techniques can be applied to discrete Raman pumping, where the gain is provided by a dedicated high gain fibre at the end of the span much in the same way as an EDFA. Here the Raman gain medium does not act as part of the 'useful' transmission span but provides gain at the end of the span in a lumped fashion, the result is an amplifier which can offer some of the advantages of distributed gain without the concerns of high power pump light exiting the communications cubicle/room.

By distributing the gain throughout a fibre a vast improvement in noise figure can be obtained resulting in a value that a discrete amplifier, such as an EDFA could not match. In essence the improvement stems from the fact that when lumped amplification is used at the end of a span the signal has approached the noise floor then

both noise and signal receive similar amounts of gain. With distributed amplification, by introducing gain earlier, the signal is kept away from the noise floor. Understanding can be aided by considering the following figure.

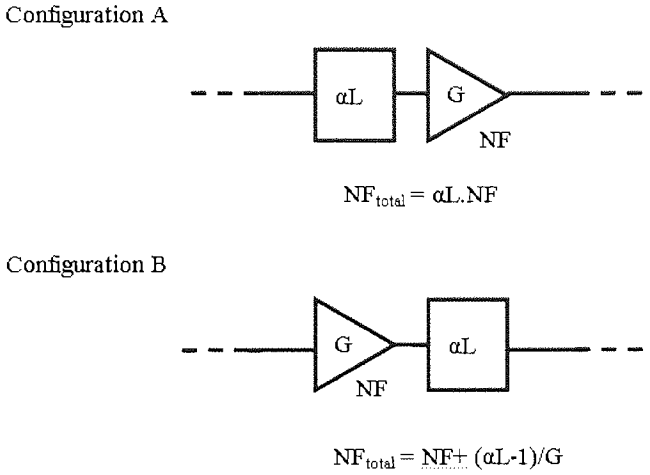

Figure 3.14 Two abstract configurations A and B where a loss element αL is placed either before or after a discrete amplifier. Noise figure expressions are for linear units

Here a loss element (αL), typically a fibre, is inserted before (configuration A) or after (configuration B) an amplifier (G, NF). The total noise figures shown are in linear units. Entering some numbers for illustration, NF = 3dB and G = αL = 20dB, configuration A has a total NF of 23dB and configuration B has 4.8dB. In configuration B the signal and ASE are attenuated equally together but in configuration A only the signal is attenuated therefore resulting in a reduced OSNR. Distributed gain acts as the amplifier G in configuration B, but rather than being a single lumped amplifier it can be interpreted as a chain of multiple amplifiers in immediate succession. Chapter six provides further discussion and illustration of this process.

3.7 Conclusions

With the advent of high power semiconductor lasers Raman has become a viable commercial alternative to Erbium doped fibre amplifiers, allowing a similar physical footprint and power consumption. This chapter aimed to present the important characteristics of implementing the Raman effect as an optical amplification technique. Advantages over EDFAs include the possibility of gain at any wavelength, essential in today's broadband DWDM systems, without the need for speciality fibres and dopants, achieved by selection of the pump wavelength. The range of useable gain bandwidth can also be extended and flattened by the addition and combination of other wavelength pumps. These are important features but possibly the most interesting and unique feature is the distributed nature of the gain process and how this can be obtained throughout the transmission span. By distributing gain the optical signal to noise achieved can be lower than for even the best EDFA placed at the end of the span. Despite the numerous advantages provided by Raman there are some challenging negative effects. These include the enhancements of double reflected Rayleigh backscattering -which serves to create multipath interference-, as well as amplitude noise transfer from the pump to the signals due to the fast response of Raman, especially in the co pump configuration. In addition, the mixing between pumps, signals and noise can produce signal degrading noise components that can be considerable if certain fibre types are employed. However, even with these complications, Raman amplification offers many positive possibilities for optical communication systems in industry and in research.

Chapter 4

Pump Spectral Broadening for Enhancing Raman Amplification

4.1 Introduction

The use of distributed Raman amplification has the ability to extend the span lengths and/or the number of WDM channels in an optical transmission system requiring high data capacity and long distances to be covered [34]. Raman amplification can provide a wide gain bandwidth of ~100nm by utilising multiple wavelength pump lasers offset from the respective channels by around 100nm, to provide gain to the shorter wavelength, as demonstrated in Chapter 3. As shown in Chapter 3 the Raman gain profile is not flat with respect to wavelength and to achieve a flat gain profile over the desired signal region many pumps have to be employed [35]. To further complicate matters, pumps interact with each other through the Raman effect, so to obtain a gain profile with the required level of flatness for WDM transmission is not a trivial issue. Hence, it is of interest to improve the gain flatness and possibly reduce the number of pumps. One method to try and achieve this is by using a wavelength swept Raman pump [36] whereby a high power laser has its frequency changed at a rate so that a large bandwidth can be amplified with minimal disruption to data being carried. The downside to this is the complexity of the system; another gain profile improvement method is based around spectral broadening of the pump wavelength therefore broadening the gain profile. This can be achieved by generating a broad pump source as in [37] or by broadening existing pump lasers as first demonstrated in [38]. This chapter explores this latter technique as applied to single and dual pump Raman amplifiers.

4.2 Spectral broadening mechanisms

In this chapter we are very much concerned with the spectral broadening of CW or quasi-CW that can be considered partially coherent. If we consider the beam to be coherent then the early stages of spectral broadening in a fibre can be attributed to Modulation Instability (MI). MI is the result of an interaction between nonlinear and dispersive effects [9], which creates an instability that leads to a modulation of the steady state. For this to occur in optical fibres MI requires that the CW or quasi-CW beam is propagating in the anomalous dispersion region and manifests itself as the break-up of the beam into a train of ultra-short pulses whose duration is dependant on several parameters including initial CW power, fibre nonlinear coefficient and β_2.

During these initial stages where MI is the dominating effect, the frequency-dependent gain coefficient, under the assumption of a coherent pump (which is enough for the purpose of this explanation), is given by the well-known expression

$$g(\Omega) = \left|\beta_2 \Omega\right| [\Omega_c^2 - \Omega^2]^{1/2} \tag{4.1}$$

Gain exists only if

$$\Omega^2 < \Omega_c^2 = \frac{4\gamma P_{in} e^{-\alpha z}}{\left|\beta_2\right|} \tag{4.2}$$

Where γ is fibre nonlinear coefficient, β_2 is dispersion, α is the fibre loss, and P_{in} is the pump input power. The MI causes power transfer from the CW pump and generates two bands symmetrically positioned at both sides of the initial pump, with a maximum at

$$\omega_0 \pm \Omega_{MAX}, \Omega_{MAX} = \left[\frac{2\gamma P_{in} \exp(-\alpha Z)}{\left|\beta_2\right|}\right]^{1/2} \tag{4.3}$$

In the time domain, the CW beam is converted into a sinusoid with the period $T = 2\pi / \Omega_{MAX}$. The separation of the side peaks depends on the characteristics of the fibre and the distance Z. A low (but anomalous) dispersion leads to a more substantial broadening. Therefore, a simple design rule for initiating MI is to choose pump/fibre parameters using the expression for Ω_{MAX} in order to shift the side peaks to the required positions in the spectral domain, however it is important to note that the MI broadening process is just the start of a series of processes that cause the overall broadening seen experimentally. The dependence of MI characteristics on input power, dispersion and nonlinear coefficient can be used to select the best combination of pump/fibres parameters in order to achieve optimal pump broadening at any given frequency. Please note that although the simple analytical approximation used in equations (4.1) to (4.3) is perfectly sufficient for our purpose of illustrating the initial break-up mechanism of the continuous wave beam, a precise analysis of the MI process in realistic conditions would have to account both for the fibre loss in a non-phenomenological way [39] and for the partial coherence of the pump sources, as illustrated in [40, 41]. MI can also be viewed in terms of Four Wave Mixing that is phase matched by the nonlinear refractive index n_2 [11]. If a probe signal at $\omega_1 = \omega_0 + \Omega$ co-propagates with the CW beam at ω_0, it would experience a power gain given by (4.1). Physically, the energy of two photons from the intense CW pump beam is used to create two different photons at the probe signal frequency ω_1 and at the idler frequency $2\omega_0 - \omega_1$. When the probe signal is launched together with the intense CW wave the case is called 'induced' MI. As previously mentioned when the pump propagates by itself MI initiates a sin wave which coupled with the full Nonlinear Schrödinger Equation can lead to a spontaneous break-up into a periodic pulse train. Noise photons/spontaneously emitted photons act as a probe in this case and are

amplified by the gain provided by the MI. The largest gain occurs at frequencies given by (4.3). Evidence of 'spontaneous' MI at the fibre output is provided by two spectral sidebands located symmetrically at $\pm\Omega_{MAX}$ on each side of the central line ω_0. With generation of a pulse train that generally consists of short pulses e.g. 2ps for a 100mW Raman Fibre Laser [42], non-linear phenomena associated with such pulses can come into play. MI, and the subsequent interplay between nonlinear effects in the fibre (primarily FWM, SPM and SRS) can give rise to a Raman pulse that experiences intra-pulse Stimulated Raman Scattering (SRS), where shorter wavelengths of the propagating pulse continuously undergo SRS to generate longer wavelengths. As the spectrum of the Raman pulse broadens further with high launch powers, the fibre can support a Raman soliton. These pulses are not stable under the presence of higher order dispersion, particularly third-order dispersion [38]. These Raman solitons undergo fission into stable red-shifted fundamental solitons and blue-shifted dispersive waves. These 'non-solitonic radiations (NSR) are produced at certain frequencies, for which a precise phase matching condition is satisfied with fundamental solitons. The radiation frequency and detuning depends on both the dispersion coefficients and on the CW power and can be written as [41]

$$\delta\omega = -3\frac{\beta_2}{\beta_3} + \frac{4\beta_3\gamma P_{in}}{3\beta_2^2} \tag{4.4}$$

These components can be observed experimentally and are illustrated later in this chapter.

4.3 Experimental Pump Broadening

To obtain spectral broadening of a high power pump laser is fairly straight forward and only requires a high power laser and a length of fibre exhibiting the desired dispersion and nonlinear characteristics, and originally was noticed by this author as part of an investigation into pump-pump depletion when using different Raman pump modules manufactured by Corning, Fitel and JDS Uniphase. It was observed that one of the wavelengths had a much greater spectral width than the others after propagation; the initial pump width was verified by the use of an attenuator (in place of the fibre with similar loss value) and was seen that it started propagation with the same width as the other pumps. The components used were a 100km span of OFS (then Lucent) TrueWave-Reduced Slope TW-RS fibre and a Raman semiconductor pump module from one of the previously mentioned suppliers; the result of this initial experiment is shown in Fig. 4.1. At this stage it was unclear what was happening so further investigations were devised to look at the effect of fibre type and power on the pump spectrum of the 1457nm wavelength from the Corning two-wavelength pump module. The experiment as simply depicted in Fig 4.2 utilised one of three 100km fibre spans, constructed using Corning SMF, Corning LEAF or TW-RS fibre along with the Corning Raman pump module. In addition the fibre spans were replaced with 3x10dB attenuators (10dB at 1550nm) to give a reference for any inherent increase in

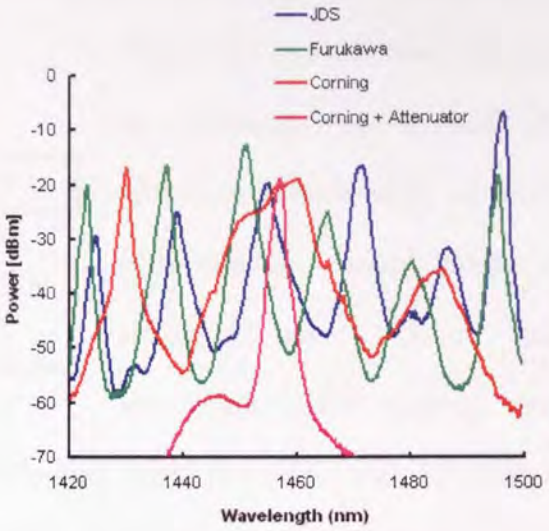

Figure 4.1 Differing pump wavelengths after propagation through TW-RS span

pump spectral width directly from the module output. Use of the three fibre types, provided three notably different dispersion characteristics to be explored as well as three different core sizes and hence three non-linear coefficients to be considered.

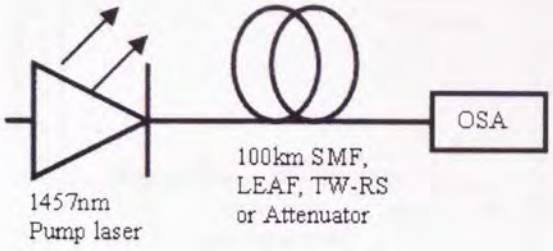

Figure 4.2 Fibre type and power level broadening experiment

The power into the fibre was raised by increasing the applied drive current in 100mA steps to the two cross-polarised pump lasers that constitute the 1457nm pump wavelength. Drive current ranged from 100 to 500mA, which gave the following output powers for 100, 200, 300, 400 and 500mA respectively: 35, 82, 128, 174 and 218mW. The results for the effect on pump spectra for fibre type and power level are grouped together in Fig. 4.3.

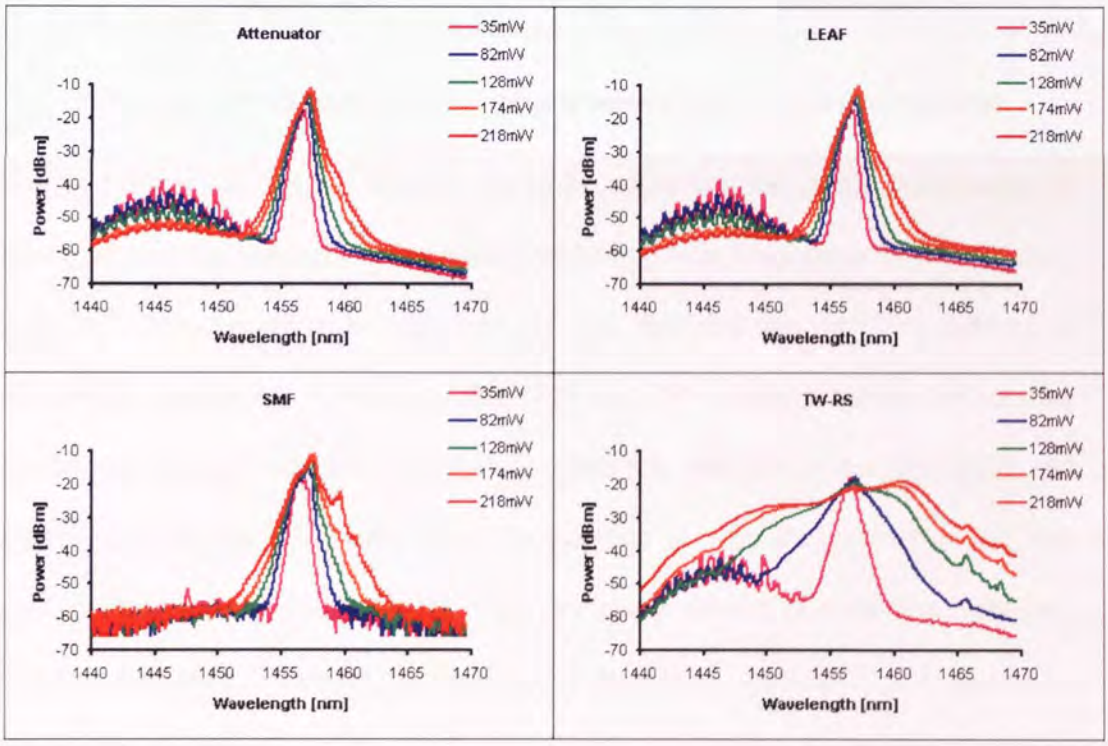

Figure 4.3 Result on pump spectra for varying fibre type and input pump power

It is useful to interpret Fig. 4.3 along with measurements of the 3 and 10dB bandwidths for the increasing power and fibre type as shown in Fig 4.4.

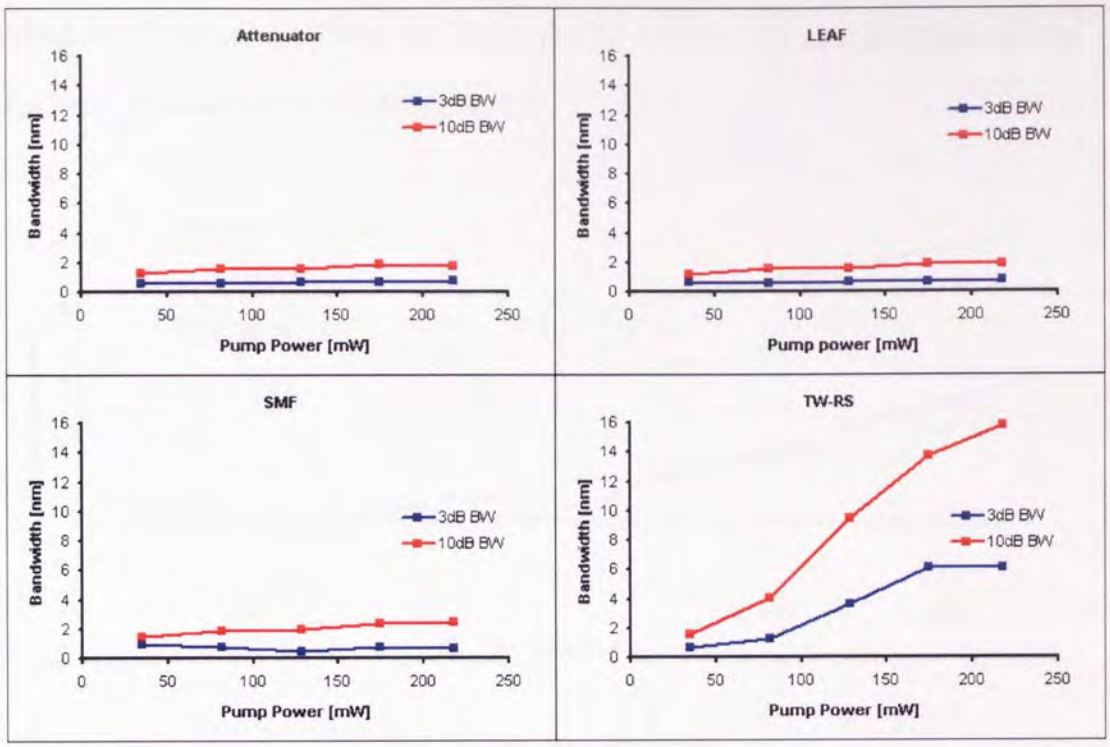

Figure 4.4 and 10dB bandwidths for measured power levels over each fibre type used

Taking Figures 4.3 and 4.4 together it can be noted that the pump undergoes only minor inherent spectral broadening with increasing power when the attenuator is used. This is also the case when the LEAF span is used, implying that such fibre induces no broadening phenomena. Turning to the SMF and TW implementations, broadening above and beyond the inherent level is observed, marginally for the SMF and enormously for the TW. This raised the question of why the difference and was quickly answered by considering the dispersion characteristics of each fibre type/span. The big difference is between having normal dispersion, the LEAF, and anomalous dispersion, the TW-RS and the SMF, at the pump wavelength. Anomalous dispersion would allow phenomena such as modulation instability to take place whereas normal dispersion would not. Further still if we consider the proximity of the pump to zero

dispersion wavelength it is possible to see that the nearer to it the greater the broadening, e.g. the SMF has a zero dispersion wavelength, in this case, near 1300nm whilst the TW used has a ZDW on average around 1455nm. The average dispersion for the fibre spans used is illustrated in Fig. 4.5.

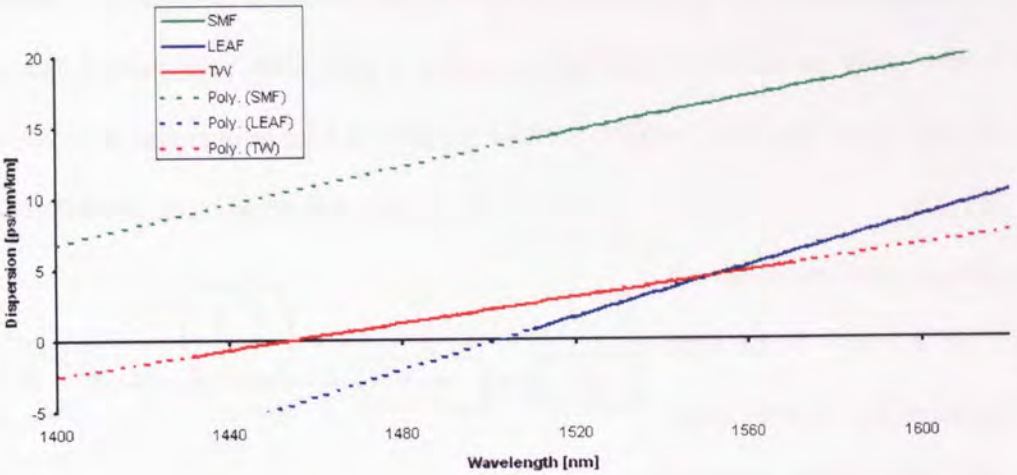

Figure 4.5 Fibre span dispersion

This effective broadening near the ZDW in the anomalous region can be understood, as mentioned earlier, in terms of MI or four wave mixing phase matched by self-phase modulation [9]. Consider the phase matching condition, $\kappa=0$, can be written:

$$\kappa = \Delta k_M + \Delta k_W + \Delta k_{NL} = 0 \tag{4.5}$$

Where Δk_M, Δk_W, and Δk_{NL} represent the mismatch occurring due to the material dispersion, waveguide dispersion and the nonlinear effects, respectively. When the pump wavelength lies in the anomalous-GVD regime, Δk_M exceeds Δk_W and it becomes difficult to achieve phase matching. However, because $\Delta k_M+\Delta k_W$ is negative it is possible to compensate it by using the nonlinear contribution Δk_{NL}. Therefore a pump propagating in the anomalous-GVD would develop side bands at frequencies given by equation (4.1) in the explanation of MI. As mentioned in the previous section it is MI that is dominant in the initial stages of the broadening process, so before

moving onto looking at greater broadening in later stages it is interesting to observe this MI stage. Two experiments were devised to observe the MI effect, one to see the effect with increasing power and the other to see the effect of wavelength. Each experiment used different components to generate the pump wave and the MI spectrum. The power experiment, as simply depicted in Fig. 4.6, used a 1480nm 1.5W Calmar Raman fibre laser with a 2.2km reel of TrueWave Classic fibre, whilst the wavelength experiment used a tuneable 1400 to 1500nm laser and a 25.5km reel of TW-RS fibre, as set out in Fig. 4.8.

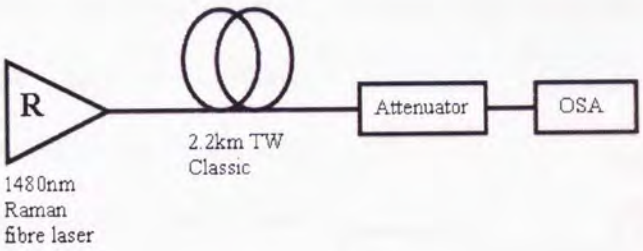

Figure 4.6 Power level on MI experiment

For the power level experiment depicted in Fig. 4.6 the fibre lasers' output was increased in arbitrary steps from 105 to 848mW. The output from the fibre was attenuated before entry into the OSA to prevent damage. The recorded result is shown in figure 4.7.

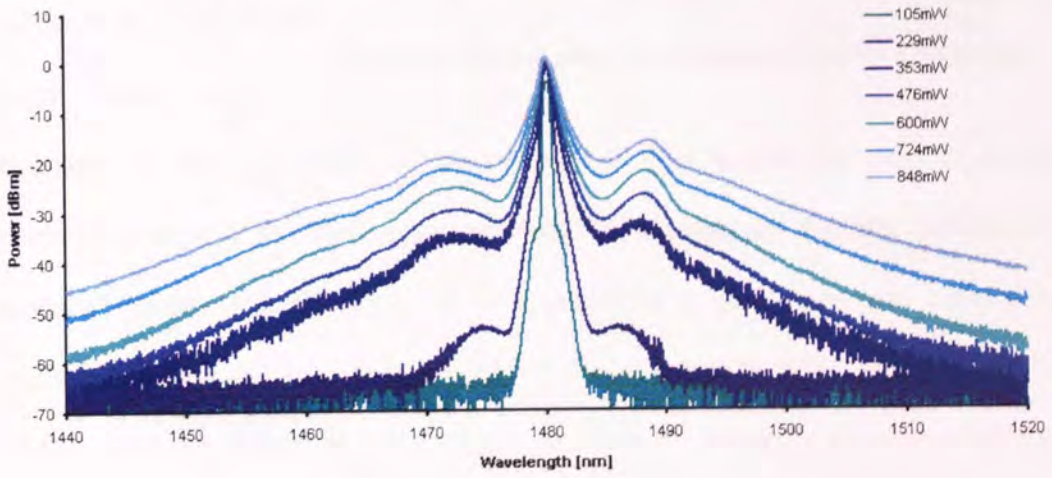

Figure 4.7 Evolution of MI in a 2.2km reel of TW-Classic fibre with increasing power

The MI peaks either side of the pump central wavelength can clearly be seen evolving and becoming more pronounced with increasing power. Such side bands are indicative

of some form of modulation and it has been proposed that the resultant temporal pulse train can be viewed with the aid of an autocorrelator as seen in [41]. This was attempted and resulted in a trace that resembled the one given in the aforementioned reference but was found to be present even without the fibre and further attempts to obtain a temporal domain picture were unsuccessful. The wavelength sweep experiment, Fig 4.8, was successful but required a combination of components to generate the desired result.

Studying Fig. 4.8 the inclusion of a 1365nm Raman fibre laser can be seen which is not immediately intuitive as to why. The reason for this pump laser is to add gain to the 1400 to 1500nm tuneable laser because, on its own, the tuneable laser did not have enough output power to give rise to the MI effect. The gain spectrum of the 1365nm pump laser can be evaluated in Fig. 4.9, where it can be seen it falls around the zero dispersion wavelength value of the fibre under consideration, allowing the tuneable laser to now produce spectra with MI signature components. The gain trace was created by sweeping the tuneable laser with a very low output power to avoid generation of MI artefacts but with enough power to act as signal for the 1365nm pump, approximately -11dBm. The pump power was set to ~574mW.

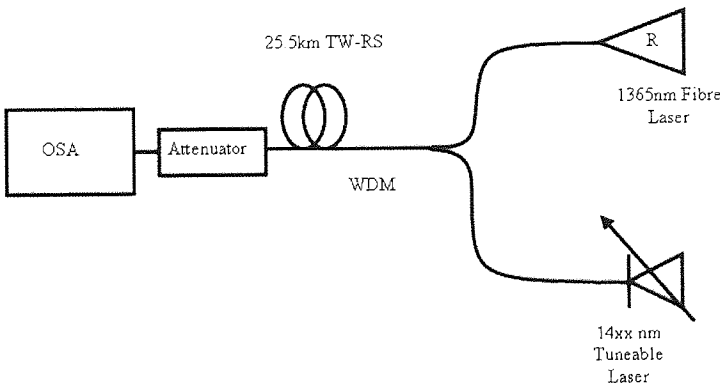

Figure 4.8 Effect of pump wavelength on MI spectra experiment

This gain allowed the other laser to sweep from 1445 to around 1465nm with roughly constant power. For the actual sweep through the ZDW region (the term region is used

as the ZDW varies with fibre length and this will be seen later on) the tuneable laser was set with an output power of 11dBm and the fibre loss in this wavelength range was ~8dB. The laser was stepped in 0.5nm steps from 1449 to 1469nm from which a selection of resultant traces can be seen in Fig.4.10. OSA resolution bandwidth was 0.07nm.

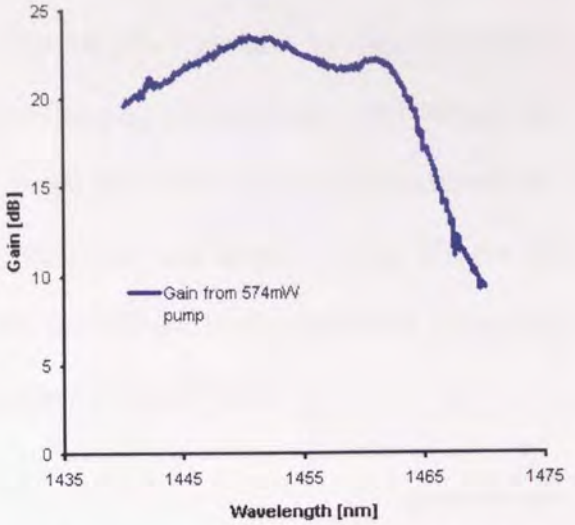

Figure 4.9 Gain from 1365nm pump laser for MI sweep experiment

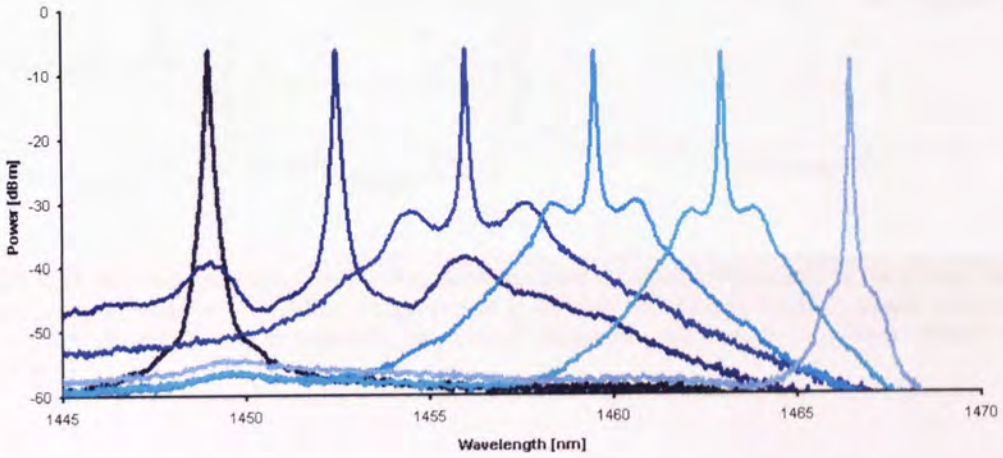

Figure 4.10 Selected steps from the MI sweep experiment

From the results in Fig. 4.10 we can once again see MI components being formed, but here it is interesting to note the separation of the peaks as the swept wavelength passes through the ZDW region of ~1452nm of the fibre used. Below the ZDW, the leftmost trace, there are no clearly identifiable MI peaks to be seen, but as the laser passes beyond the ZDW very pronounced peaks are formed far from the central wavelength. These peaks move in towards the central wavelength as the laser is swept away from the ZDW and further into the anomalous dispersion region until they virtually

disappear in the furthest right trace, though it must be remembered that the gain/signal power has fallen off at this wavelength. The MI effect can also be seen in modelled results, which allow us to see the effect of changing the non-linear coefficient of the fibre, average dispersion value and fibre length that is not easy to do experimentally. Figure 4.11 shows the effect of fibre dispersion and length on the MI process numerically and figure 4.12 illustrates the dependence of the generated pulse train period on fibre dispersion, nonlinear coefficient and power [43].

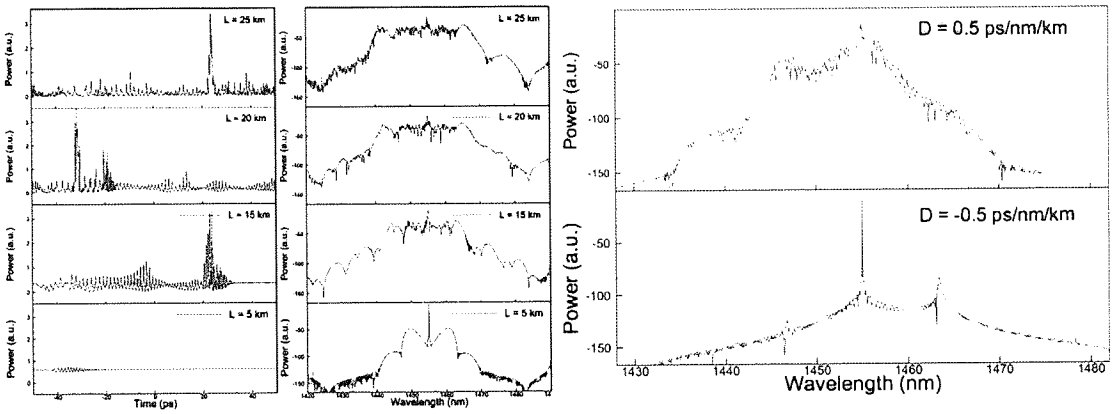

Figure 4.11 Spectral evolutions (left – time domain, middle – spectral domain) of the pump wave power along a modelled TW fibre. Pump power is 800mW at 1455nm. Right – pump spectrum after 25km propagation in anomalous and normal dispersion regimes. Pump power 500mW at 1455nm

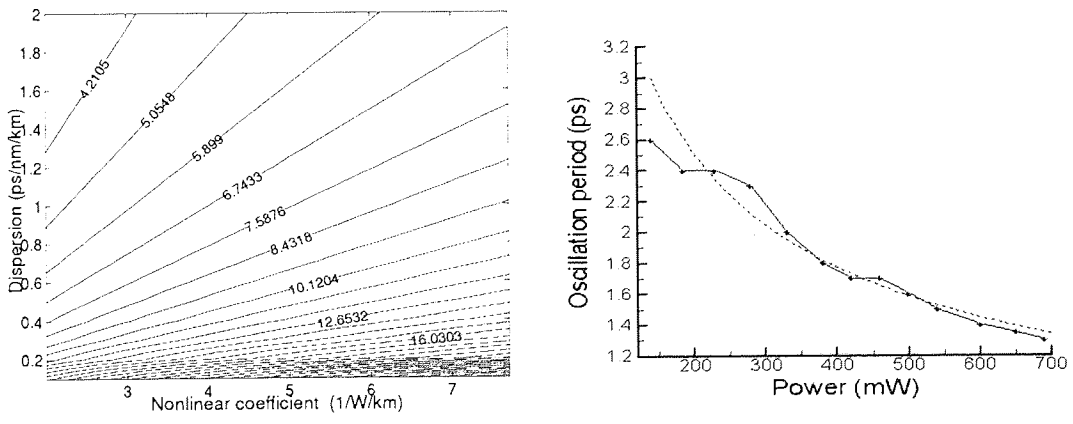

Figure 4.12 Left - Period of temporal modulation [ps] due to MI for varying dispersions [ps/nm/km] and nonlinear coefficient [1/W/km]. Pump power is 1W at 1455nm. Right – Dependence of the oscillation period on pump power (at 1455nm) after 5km TW fibre, Solid line – Numerical simulation, Dashed line – Theory

It has now been seen that MI does indeed play a role in the broadening process, but as mentioned earlier other processes come into operation during broadening such as Raman soliton generation. If the measurement span for the previous experiment is opened up to 1435-1475nm evidence of these processes can be seen, refer to Fig. 4.13. The components illustrated with red arrows in Fig.4.13 are similar to those illustrated and attributed to generation of solitons and dispersive waves as demonstrated in [44]. These effects can be seen more clearly, as well as later effects, if a higher power laser is used as the pump laser than the one used in Fig. 4.9. This is achieved by using a Raman fibre laser, like in Fig. 4.7, at 1455nm with the 25.5km TW fibre, from Fig. 4.9, the result of which is in Fig. 4.14. Listed powers are power into the fibre and all traces except that labelled 'direct' were measured after the TW-RS fibre.

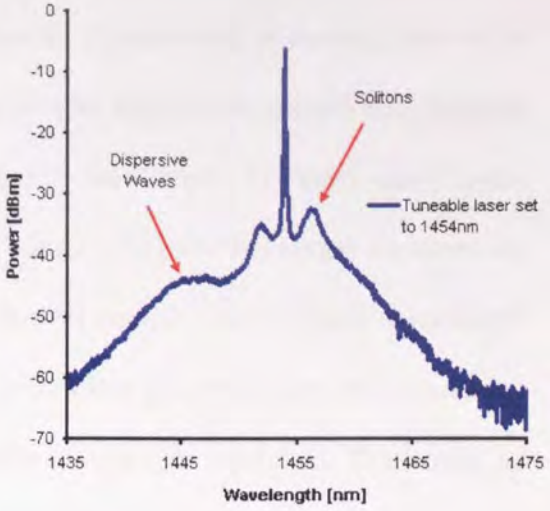

Figure 4.13 Processes in later stages of broadening

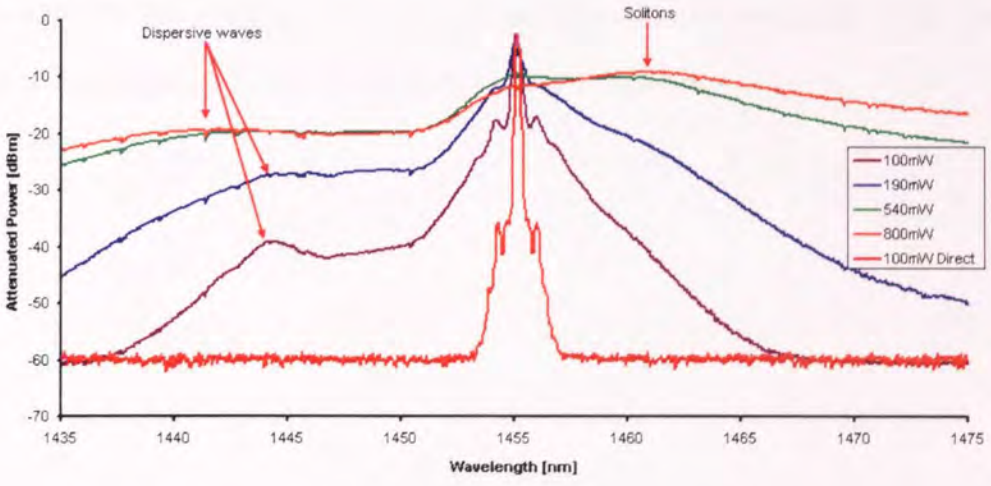

Figure 4.14 Broadening of a 1455nm Raman fibre laser in 25.5km TW-RS

Once again the generation of components that are characteristic of those mentioned in reference [44] can be seen. It is important to note for later on the migration of the peak wavelength, and certainly the mean pump centre wavelength, to longer wavelengths caused, in part, by soliton formation and the Raman effect towards longer wavelengths. From the result in Fig. 4.10 it is clear that the MI contribution is clearly wavelength dependent, as is expected from theory, it is therefore presumed that the broadening with inclusion of other nonlinear effects is also wavelength dependant. This would be simple to verify if access to a tuneable Raman laser was possible, alas in the context of this work no such device was available. As an alternative method of researching this concept other TW-RS reels were obtained with very similar lengths but with varying dispersion zero wavelengths, in addition it was found that by changing the temperature of the fibre the ZDW moved. Temperature tuning, and hence dispersion tuning, was achieved on the TW reel used in Fig. 4.12 by placing the entire reel inside an environmental chamber at a set temperature for 24 hours and then measuring the dispersion. This allowed a finer variation in dispersion, about 1.3nm from temperature range 21 to 70°C, which was not possible by selection of fibre reels. The lengths of the reels were ~25.5km and Fig. 4.15 shows the resultant effect of sending the 1455.14nm pump laser through each reel with an output power of 800mW.

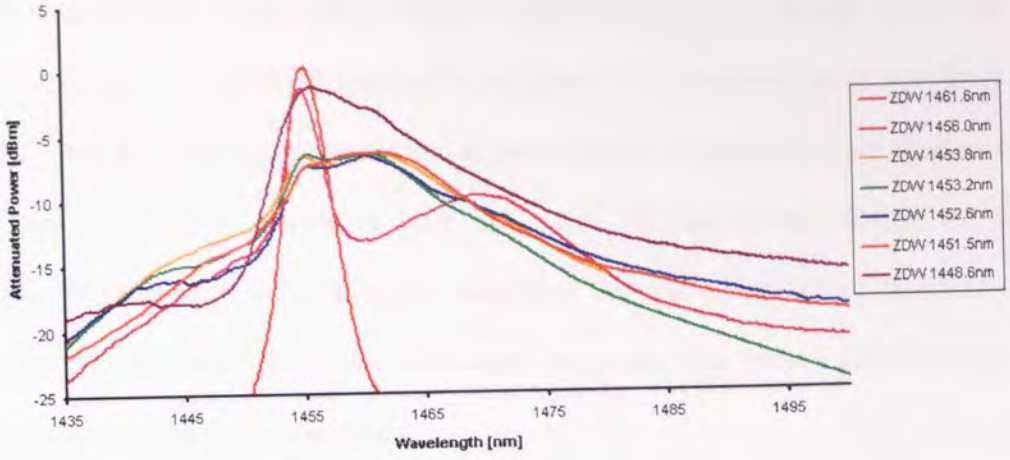

Figure 4.15 800mW 1455.14nm pump after propagation through TW-RS reels with varying dispersion values

As with the MI experiment results, the broadening increases, as we pass the zero dispersion wavelength and then decreases as we move further into the anomalous region. It is important to point out the fibre with ZDW 1456nm displays broadening,

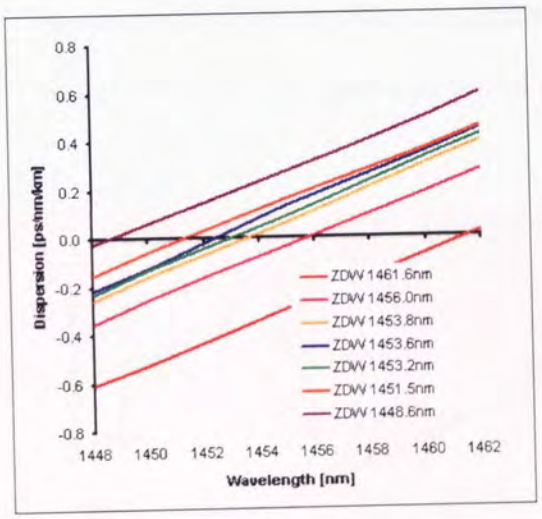

Figure 4.16 TW-RS dispersion

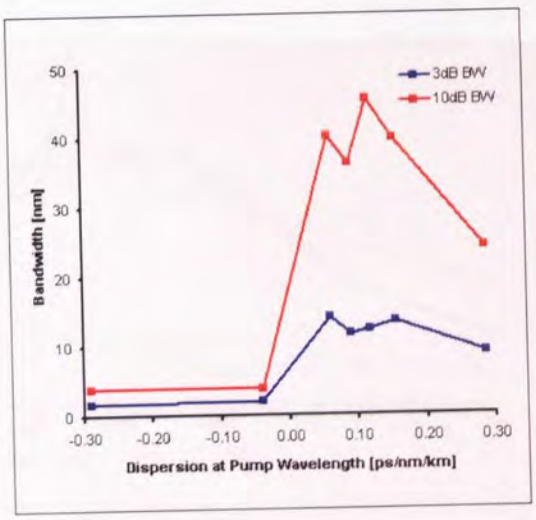

Figure 4.17 3 and 10dB pump bandwidths vs. dispersion at pump wavelength

which in the given theory here, it shouldn't – this can be explained by highlighting that the ZDW given is the average value over the fibre and that sections of the fibre may well have a localised ZDW below 1455.14nm. This can be seen if the fibre is pumped from the opposite end

as is shown later. For a clearer understanding of Fig. 4.15 it is worth referring to Fig. 4.17 where the 3 and 10dB bandwidths are given for the resultant pump spectra in Fig. 4.15, and Fig. 4.16 where the dispersion measurements for each fibre are displayed.

From Fig. 4.17 it is evident once again that for notable broadening the pump wavelength must reside within the anomalous dispersion region and therefore some portion of the fibre being used to broaden the pump must have a ZDW at a shorter wavelength than that of the pump.

As mentioned above, it is necessary to acknowledge that the dispersion varies with respect to length along the fibre, as this explains why different degrees of broadening can be obtained from pumping the same length of fibre from the alternate ends. This is confirmed in figure 4.18, where the same 1455nm Raman fibre laser as used above was propagated with a power of 300mW through a 10.4km TW-RS fibre who's ZDW was at 1453.8nm. The fibre ends were arbitrarily labelled end 'A' and end 'B'.

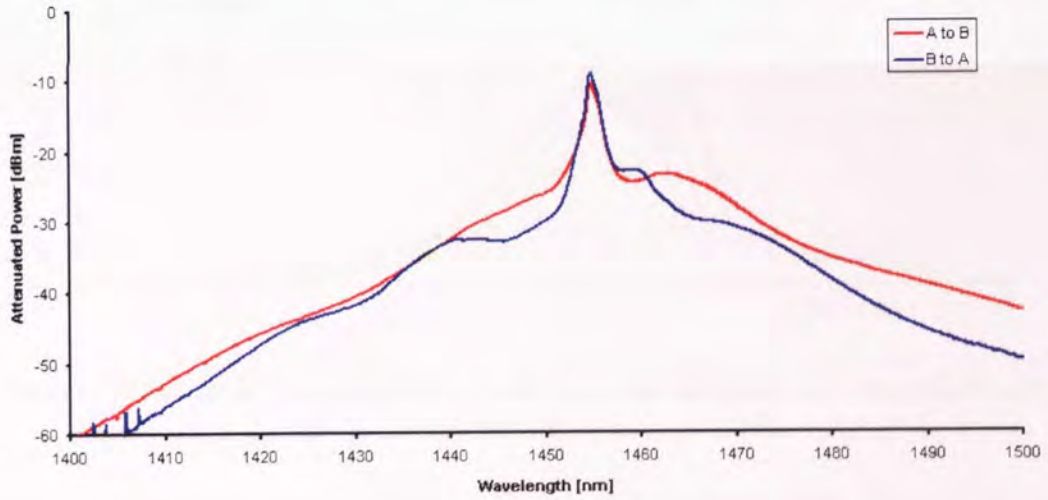

Figure 4.18 Effect of pump direction on broadening

Here it can be observed that the pump spectrum alters quite significantly depending on the pump direction and this result gives indication that the pumping direction is important when undertaking broadening work such as discussed in this chapter. Note

that, since dispersion varies locally, by changing the pump direction we are also varying the interplay between local dispersion and pump power, which explains the different nonlinear broadenings. Thus so far we have looked at the pump spectrum, it is then logical to proceed to investigate the associated gain spectrum and this is now undertaken in the next section.

4.4 Gain Flattening and Spectral Broadening

The objective of pump spectral broadening is to generate a gain spectrum, which is flatter and more uniform with respect to wavelength. This can be understood by considering a broad pump as a collection of narrow pumps closely spaced, see Fig. 4.17, creating multiple 'conventional' gain spectra that can be summed together to generate a more uniform/broad gain spectrum.

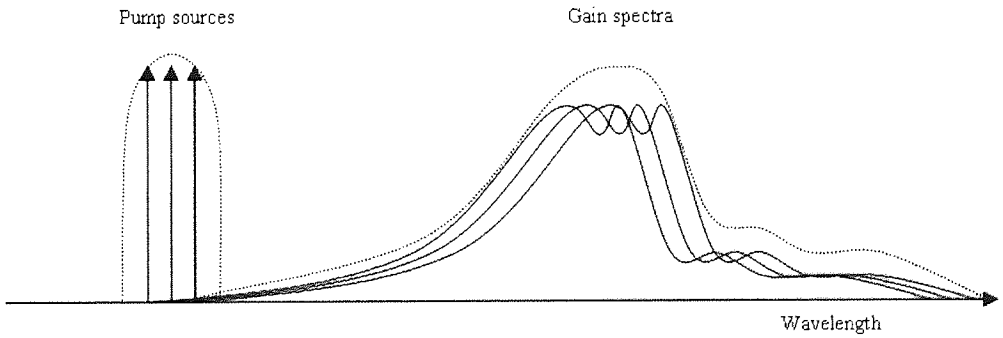

Figure 4.19 Illustration of a broad pump as a collection of narrow pumps and the associated gain spectra

The change in gain shape was noticed at the time the change in pump shape in Fig. 4.2 was observed. What was seen was a variation in gain shape in the same fibre that was brought about by using different pump wavelengths; this original result is shown in Fig. 4.20 where the same 100km fibre spans were used with two differing pump lasers

at 1424nm and 1457nm driven at a level to produce a similar gain for all cases. The signal source used was a tuneable laser in the counter propagating direction.

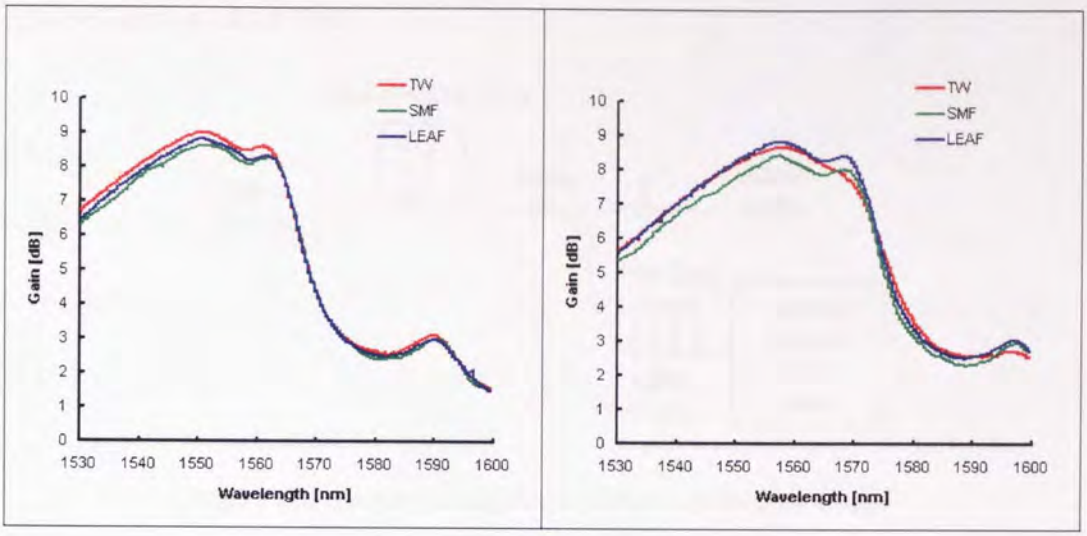

Figure 4.20 Initial gain variation result for broader pump, left - 1424nm, right - 1457nm

The significant difference is in the gain shape for the TW fibre, using the 1424nm pump the gain shape is similar to the other fibres in that the high gain region comprises of two peaks whilst with the 1457nm pump it has been reduced to a single high gain peak. Now this single gain peak trace is no wider than when the pump had suffered no broadening, although it was considered that further broadening may produce a gain spectrum which encapsulates that of the non-broad pump gain. The problem with the above example is that the pump broadens during the transmission fibre, meaning that for some distance it is not much wider than the unbroadened case and therefore the gain spectrum is no wider. It was proposed that to obtain this broader gain spectrum the pump should be broadened before the main transmission fibre thus allowing the pump to be wide from the initial launch. To implement this, a pump broadening fibre, which is referred to as a 'pre-fibre', was placed after the pump unit but before the transmission span and coupled via a suitable WDM. This pre-fibre, of course, induces an extra loss to the pump wavelength (about 0.3dB/km for TW-RS) so many of the

following experiments use high power fibre lasers to compensate this loss. This pre-fibre arrangement is shown in Fig. 4.21 below where the transmission fibre was 75km span of Corning LEAF fibre.

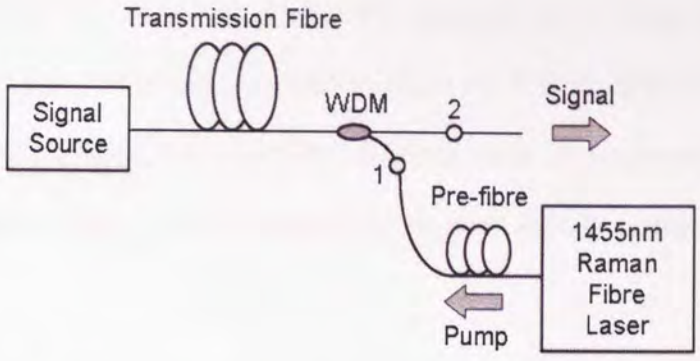

Figure 4.21 Counter propagating pre-fibre experimental set-up

Having settled on the above configuration it was then required to find a pre-fibre capable of broadening the pump spectrum to produce a gain that would be broader than the conventional counter propagated pump set-up using the same laser. This work was essentially undertaken in production of the results for Figs. 4.15 and 4.17, and all that was required was to adjust the pump powers slightly so that a nominal gain value was achieved with each pre-fibre. The following figure compares the normalised gain, to ease evaluation, for each pre-fibre.

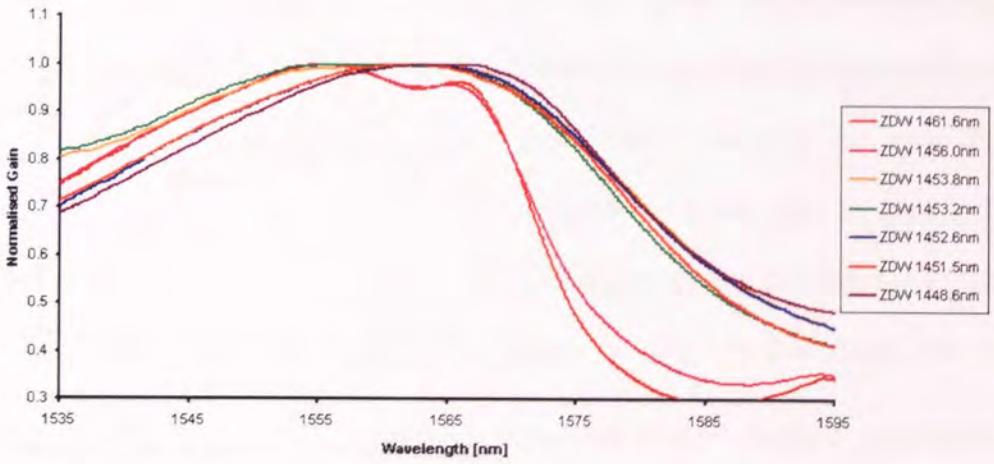

Figure 4.22 Gain comparison for varying pre-fibres

The variation in gain can be appreciated more easily by comparing 1 and 10% reduction from peak gain bandwidths, as done so in Fig. 4.23. One aspect that can be noticed is the movement of the peak gain wavelength/region towards longer wavelengths when a broader pump is used, this can easily be attributed to migration of the mean centre pump wavelength as seen in Fig. 4.14. If a pre-fibre set-up was to be used for pump broadening in an amplifier, then care must be employed to choose the fibre/wavelength to cater for this generated offset over and above the typical Raman shift.

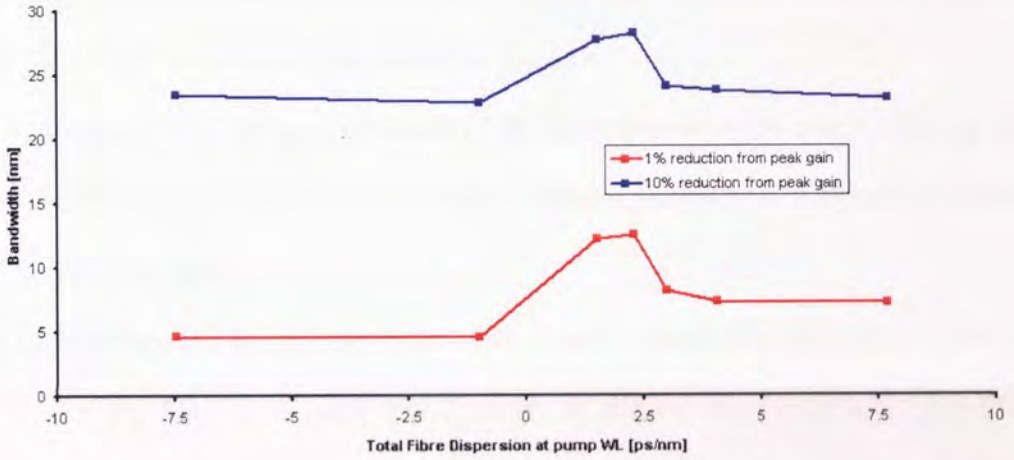

Figure 4.23 comparison of bandwidths for a 1 and 10% reduction from peak value

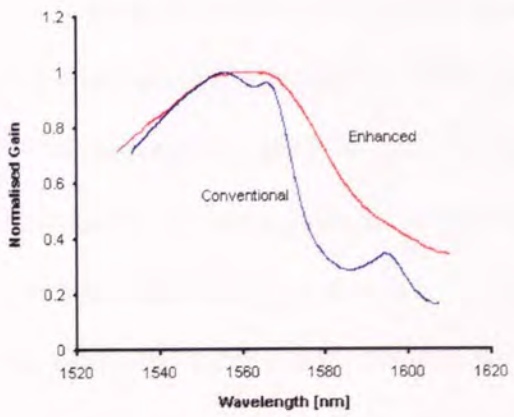

Figure 4.24 Gain comparison for with/without pre-fibre

To further gauge the improvement in gain bandwidth it is useful to compare the best gain from above with the case of an unbroadened pump gain, as done in Fig. 4.24 and originally presented in [38] and again in [26]. In this figure the gain spectrum of the 'enhanced' case has been moved, due to the aforementioned

wavelength offset, to enable a clearer comparison.

Considering a 1% reduction from peak gain value the continuous bandwidth has increased from 4.25nm with out any pre-fibre to 12.57nm with the pre-fibre and as it can be seen that at all other reduction levels the gain bandwidth is increased. This was a successful result but which was limited by the available gain level that could be created, which for Figure 4.24 was actually about 2.8dB. It may be asked that with such a powerful pump laser being used, why not just increase the pump power to increase the gain? Increasing the pump power, as we have seen previously, increases the broadening and initially the gain level will increase but after a certain point the gain then begins to decrease, this can be attributed to:

1. Reduction of the spectral density: the pump broadens too much reducing the effective peak power and creating a supercontinuum that is below the power level for SRS
2. Reaching the Raman threshold: after a certain power the Stokes wave within the pre-fibre is so great that it serves to deplete the pump laser [11] (this happens even before nonlinear broadening via MI can lower the effective peak power) and hence when entered into the transmission fibre, the pump is not of great enough power to produce meaningful gain

It is worth clarifying in relation to the points above that without the use of dedicated WDM between the pre-fibre and the transmission fibre then pump and/or Stokes components will occupy the same wavelength range as data signals – thus degrading them; this topic is looked at with data transmission later. Also, not only can increasing the power too much reduce the gain level, but also it can affect its shape. As with increasing gain with a conventional Raman amplifier, the peaks grow at a non-constant rate so when a broad pump is used the optimum gain flatness maybe obtained before

the peak gain level is achieved. This point can be illustrated using the similar components that produced figure 4.24 and increasing the pump power so that the gain level increases. This figure demonstrates that the higher gain level has lost the 'flatness' of the lower level, but if we consider the pump spectra also shown it can be seen that the higher gain level has a broader pump (FWHM) and that the flatter gain level has a narrower pump. Put simply, the broadest pump does not necessarily provide the flattest gain.

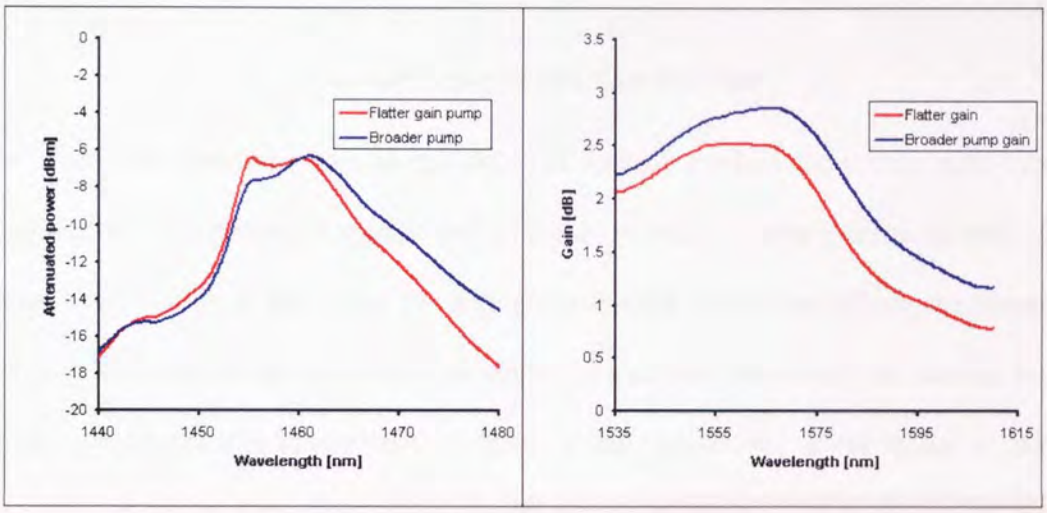

Figure 4.25 Effect of increasing pump power on pump and gain spectra

Fig. 4.26 presents essentially the same result but for a greater range of pump and gain values, here the pre-fibre was a 10.4km reel of TW-RS and demonstrates how the gain shape evolves with increasing power. The power levels listed here are actually the powers out of the pre-fibre and into the transmission fibre.

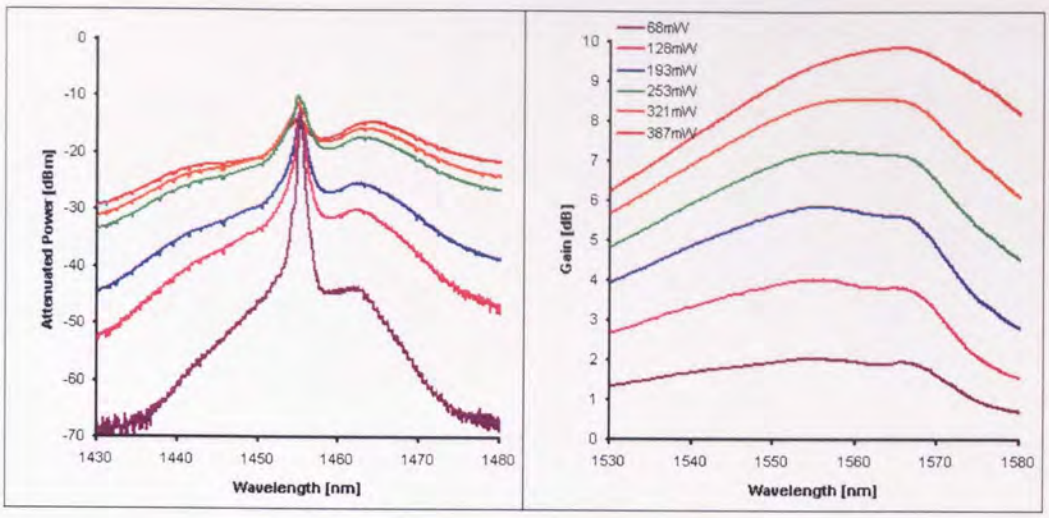

Figure 4.26 Pump and gain shape evolution

As before, the broadest pump, in red, does not actually produce the flattest gain - the slightly narrower pumps, in orange and green, do produce a more continuous gain. A point worth noting is that when the gain starts to drop due to the effects mentioned above it will drop to the same level as where the gain was previously the flattest, but from experiments it is known that this gain on the 'way-down' is not as flat as that produced on the 'way-up' despite the broader associated pump.

Despite the improvement in gain bandwidth it may still be desirable to have gain over a greater wavelength range and to accomplish this it is possible to apply conventional pump wavelength division multiplexing coupled with the spectral broadening technique. The aim now is to broaden all pumps to the desired degree, either in the same pre-fibre or in separate dedicated fibres, then couple them together and launch them into the transmission fibre. For broadening in the same fibre it would be necessary to obtain a fibre that could present the same dispersion value to each pump wavelength. Such a fibre would need a slightly anomalous dispersion value over the pump wavelength range and hence be dispersion flattened. DFF fibres do exist but are highly specialised and difficult to obtain, so in the context of this work the second

proposal of a separate pre-fibre for each pump wavelength will be investigated. As proposed in [38, 45] a dual broadened pump configuration would provide superior gain ripple variation over a conventional WDM pump configuration. Such a configuration is shown in Fig. 4.27, which is also the experimental set-up for investigation of this concept [45, 46, 47].

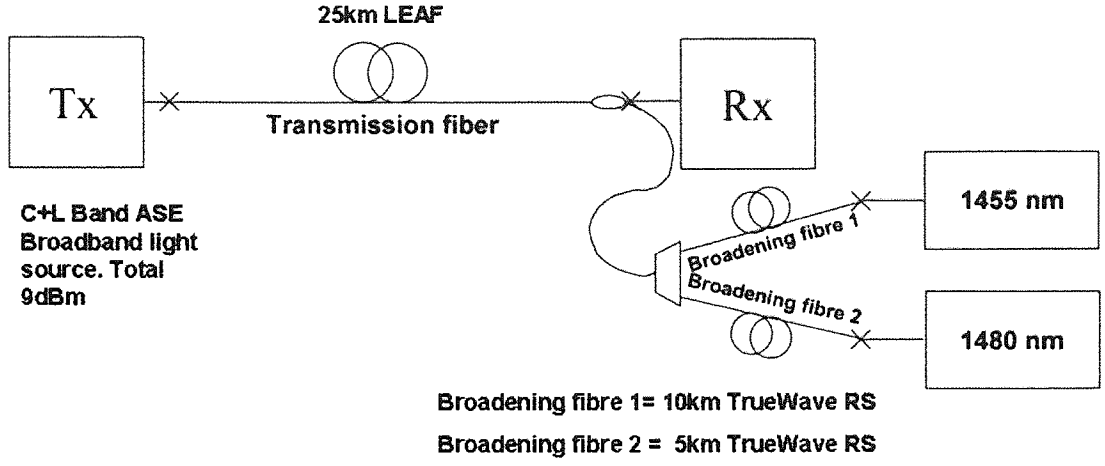

Figure 4.27 Dual pump WDM Raman experimental set-up

The system is a traditional transmission line backward pumped with two conventional Raman laser pumps, centred at 1455 and 1480 nm. Each of the pumps propagates through a different broadening pre-fibre before being combined together by a 3dB coupler and then injected into the transmission/amplification medium, in our case comprised of 25.26km E-LEAF fibre, via a Wavelength Division Multiplexer (WDM). The WDM does not only couple the pump light into the transmission line but also removes any spontaneous component that may otherwise occupy the signal band. Two TW-RS fibres were used for the broadening of the pumping waves. For the 1455 nm pump, a 10.390 km reel with a zero-dispersion wavelength of approximately 1454 nm and a dispersion slope of 0.046ps/nm^2/km was used, this fibre is different to the one used for Fig. 4.25 and was used due to its shorter length and therefore its ability to enable a higher gain level in the transmission fibre. The 1480 nm pump was broadened

in a 5.077km piece of fibre with a zero dispersion wavelength at approximately 1475nm with a dispersion slope of 0.049ps/nm^2/km. The non-linear coefficient of TrueWave (given at 1550nm) is 1.84W^{-1}km^{-1}. Note that the zero dispersion wavelengths given are an average value and must be considered approximate due to their variation along the fibre length. Pump powers at the input and the output of the pre-broadening fibres were monitored using a power meter, which integrates over the whole pump bandwidth. Figure 4.28 shows the pump spectra at the input and output of the broadening fibres, in order to obtain broadened pump powers of 250mW (1455nm) and 416mW (1480nm), from input powers of 448mW and 628mW respectively. Further losses in the coupler between the broadening fibres and the transmission fibre bring the pump powers down to 108mW (1455nm) and 164mW (1480nm).

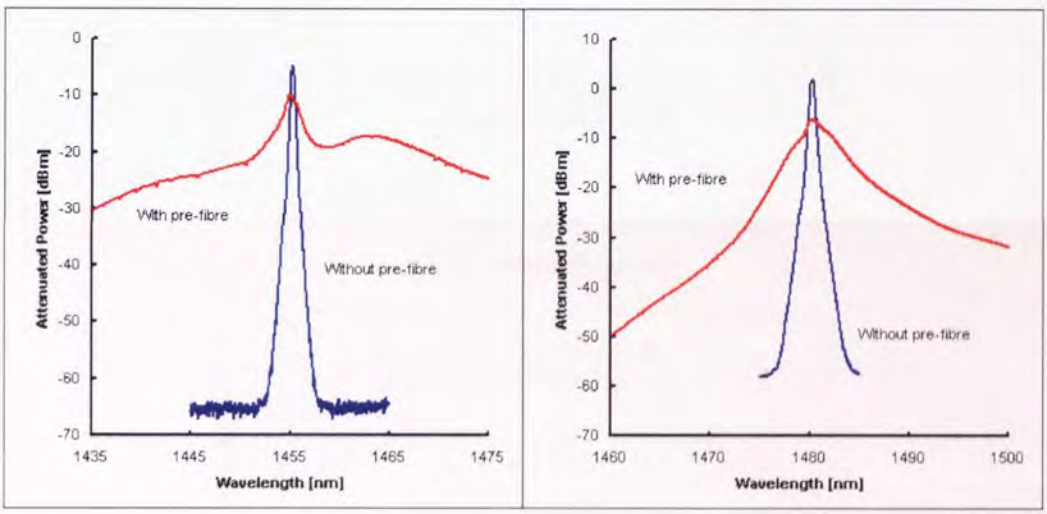

Figure 4.28 Pump spectra at the input (blue lines) and output (red lines) of the broadening pre-fibres Left - 1480nm. Right - 1480 nm.

Even though the available pre-broadening fibres are not ideal, Stokes generation at high input powers limits the range of possible outputs, we can see that thanks to the proximity of the zero-dispersion wavelength, the broadening in the 1455 nm pump is excellent. The main limitation to its applicability being the asymmetry of the broadened spectrum that, at high input pump powers, causes a noticeable offset of the

effective central wavelength of the pump. Both the broadening and the offset are less evident for the 1480 nm pump, which is more than 5 nm apart from the zero-dispersion wavelength of its broadening fibre and has a shorter length for the MI process to operate over.

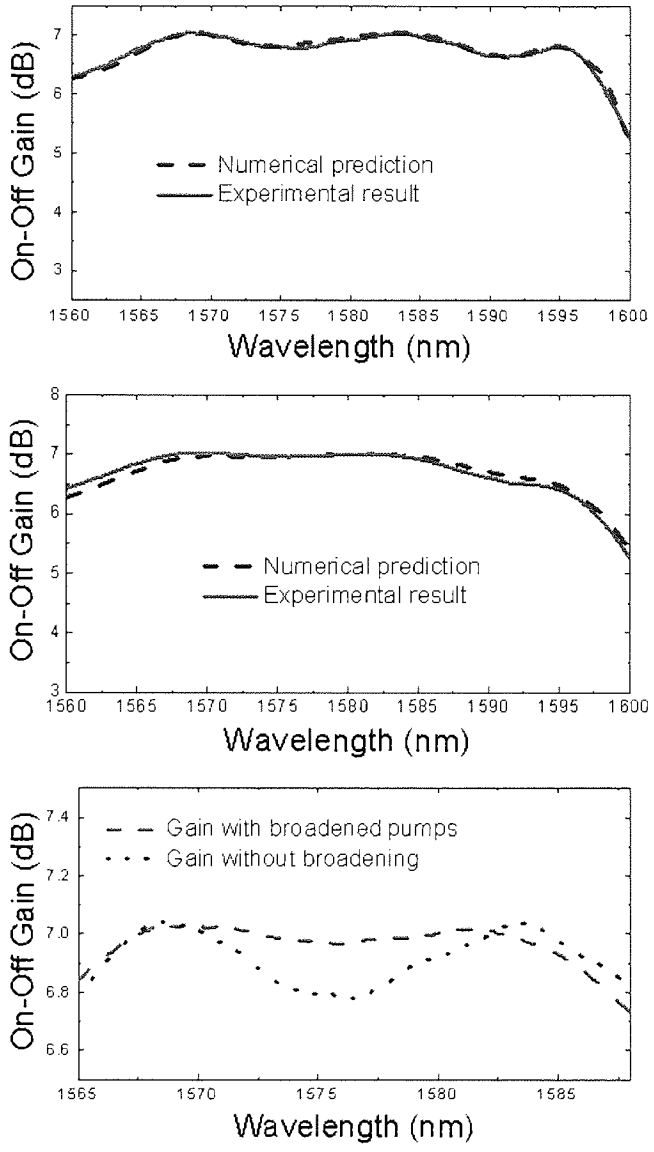

Figure 4.29 Fig. 4 Gain spectra of the amplifier on its different configurations:

Top - With unbroadened pumps. The solid line corresponds to the experimental result, while the dashed line shows the numerical prediction.

Centre - With nonlinearly-broadened pumps. The solid line corresponds to the experimental result, while the dashed line shows the numerical prediction.

Bottom - Comparison between the gain ripples with and without pump broadening.

Figure 4.29 (top) compares the numerically obtained low-power signal (-10 dBm/channel, 170 GHz channel spacing) on-off amplifier gain for the case of non-broadened pumps (considered monochromatic for the simulation), and the measured experimental gain curve, for pump powers of 80mW (1455 nm) and 206mW (1480 nm) after the coupler. The transmission/amplification fibre is composed of 25.26 km of E-LEAF with a Raman gain co-efficient of $0.5(W/km)^{-1}$. The numerical model considered, based on the integration of the well-know Raman amplifier average power equations [48], and superior to that used in [38] where gain profiles were overlaid. The model used here estimates the gain spectrum for the discretised frequency space using experimental broadened pump profiles as the initial pump light and takes into account all important effects, including pump-to-pump interaction, Rayleigh backscattering and pump depletion. The agreement between numerics and experiment is excellent.

The equivalent gain curve obtained with the broadened pumps shown on Fig. 3 is depicted on Fig. 4.29 (centre), which compares again the numerical prediction and experimental result. In this case, a dense series of experimental broadened pump spectra were sampled for their use in the numerical simulations, so that the spectral profile of a broadened pump in our simulations could be approximated by the measured broadened spectra of a pump of similar power. Please note that the optimal pump powers that lead to a flattened gain response of the amplifier differ from the case of monochromatic pumps. The main reason can be found in the wavelength offset of the broadened pumps, which are not centred at 1455 and 1480 nm anymore.

Even though the limitations imposed by the available pre-broadening fibres, especially by that of the 1480 pump, led to a drop in the gain at about 1590 nm for the broadened pump amplifier, the improvements in gain ripple performance are evident, as shown in Fig. 4.29 (bottom). In particular, the continuous bandwidth corresponding to a gain

ripple of 0.1 dB is increased from 5 nm to 19 nm, and the total gain variation over a 20 nm window is halved from 0.26 dB to 0.13 dB. A more appropriate 'pre-fibre' (more effective broadening for less pump attenuation) would allow for encapsulation and extension of the gain bandwidth over that of the case without broadening. One contender for such a fibre is Highly Non-Linear Fibre (HNLF), which will be investigated next. It is also worth pointing out that the performance of the system could be improved greatly if the 3dB coupler was replaced with a more suitable and lower loss, WDM device.

So as mentioned and shown up to now using TW as a pre-fibre can work but has limitations due to the long lengths required to create satisfactory broadening namely power loss at the pump wavelength. This length can be reduced if a the nonlinear coefficient is increased, application of a Highly Non-Linear Fibre (HNLF) is of interest to reduce the required fibre length and pump losses. Fortunately a suitable fibre was made available allowing various experiments to be carried out to see if this fibre type could do the same job as the TW fibre, see [49]. The fibre made available was a prototype Sumitomo HNLF with the following specifications:

Length	1.1km
Loss at 1550nm	0.57dB/km
Dispersion slope(1450-1550nm)	~0.04ps/nm/km^2
Zero Dispersion Wavelength	1466nm
Effective area	11μm^2

Table 4.1 HNLF parameters

As previously mentioned, a low anomalous dispersion value and a high non-linear coefficient are desirable for efficient broadening of a pump wavelength. The HNLF

used here exhibits such qualities. A low slope enables the low dispersion value to extend across a longer wavelength range thus allowing the efficient broadening of multiple wavelengths within a single fibre, as discussed in [46]. Fig. 4.30 shows the measured dispersion for the HNLF, along with its before/after effect on the propagation of three Fabry-Perot semiconductor pump lasers at 1466, 1490 and 1496nm, each injecting ~220mW into the fibre.

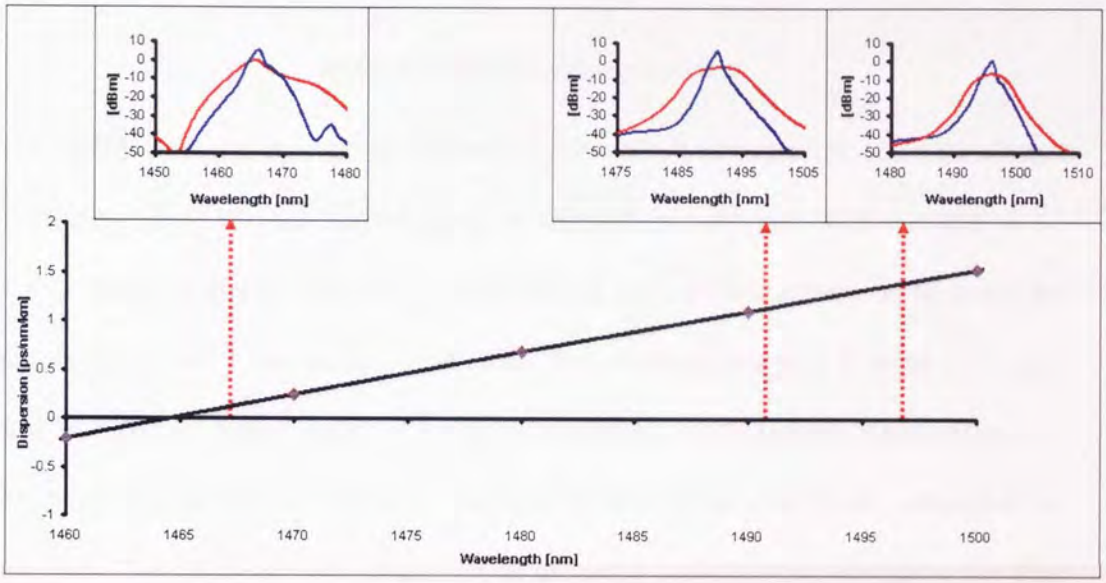

Figure 4.30 Measured HNLF dispersion with inset effect on three semiconductor lasers, Blue traces - before fibre, Red traces - after fibre

In order to achieve greater gain levels in the transmission fibre a high power (1.5W) 1480nm Raman fibre laser was used as the pump source for the experiment laid out in Fig. 4.31.

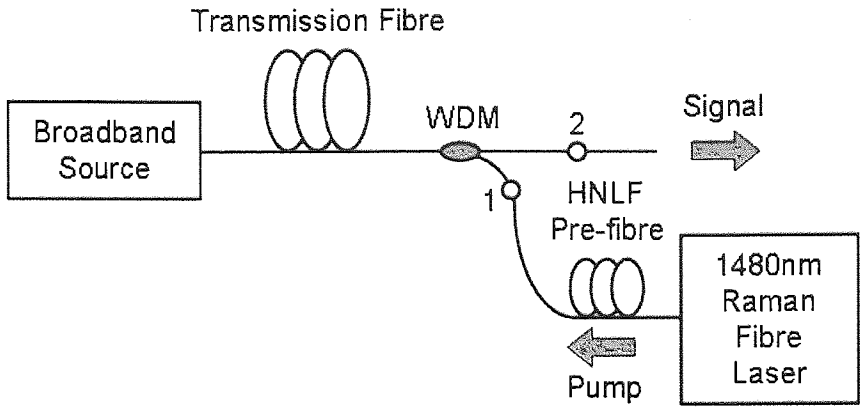

Figure 4.31 HNLF experimental layout

The HNLF presents an average dispersion value of ~0.69ps/nm/km and a non-linear coefficient of 18 W-1km-1 at the pump wavelength of 1480 nm. With a length of 1.1 km in length, coupled with loss at 1480 nm of ~0.5 dB/km, allows us to avoid the problems derived from using a long fibre. The signal source is a L-band ASE light source with total output power of 9.6 mW, equivalent to 32 channels transmitting a -5 dBm average power per channel. 25km of LEAF fibre is used as the amplification medium. The initial step was to investigate the pump evolution for varying power after propagation through the HNLF. The spectrum was monitored before the WDM, at point 1 in Fig. 4.31, in order to explore the degree of broadening available in the HNLF. Figure 4.32 illustrates the pump spectra after propagation for pump powers varying between 58 and 1152mW.

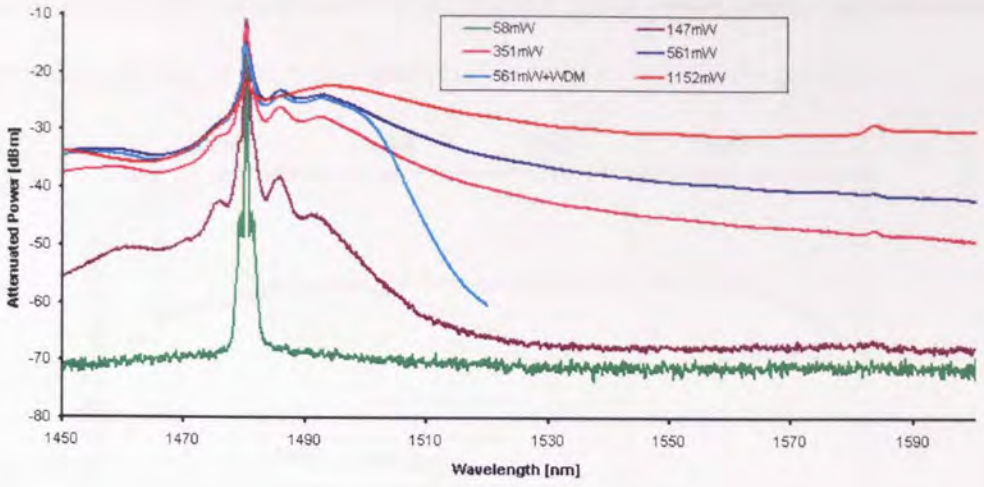

Figure 4.32 Evolution of 1480nm pump in HNLF for varying input powers and effect of the WDM on the 561mW spectrum

Broadening can be achieved from modest powers onwards. At powers above ~350mW, generation of a Stokes component could be seen towards 1600nm, with the highest power (1152mW) showing generation of a supercontinuum. Such a broad spectrum is of no use for Raman pumping application, since radiation is both spread beyond the bandwidth of interest for signal amplification and presents too low a spectral density for efficient Raman conversion. The peak Raman gain and optimal flatness (as we will show below) were reached for pump powers far below this maximum power value. These Stokes components – although present to some degree at lower powers – do not impede signal wavelengths, since a Wavelength Division Multiplexer (WDM), which limits pump wavelengths to below 1500 nm, is included. The WDM also limits the maximum bandwidth of the broadened pump, and its effect of can be appreciated in Fig. 4.32 in the 561mW + WDM trace.

In order to study the effect of the broadening on the gain spectra in the transmission fibre, signal power was measured at point 2 in Fig. 4.31. The maximum gain obtained with a broadened pump in this case was ~11 dB, with a near optimal gain flatness obtained at 9.2 dB for a pump power of 561mW. As expected, the optimal broadening

for gain flattening is not obtained for the highest pump power, since this leads to an excessive broadening of the pump spectrum.

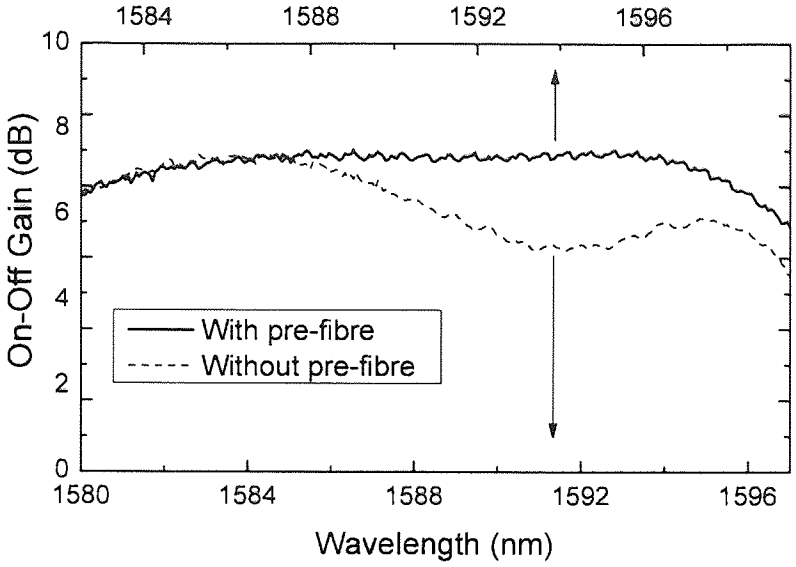

Figure 4.33 Comparison of gain spectra for the cases with and without HNLF pre-fibre

The gain spectra for the "without HNLF" and "with HNLF" cases, both obtained for the same peak gain value, are compared in Fig. 4.33. Please note that although the figure superimposes both gain spectra for a clearer comparison, there is an offset of approximately 1.5 nm for the "with" case due to the migration of the centre pump wavelength with increasing pump power in the HNLF, which can attributed to the Raman gain and other non-linear effects. The top x-axis in the figure corresponds to the "with" case, whereas the bottom one corresponds to the case without broadening. From previous work, it was expected that the resulting gain spectra with HNLF would encompass that of the case without broadening fibre. This effect is even more pronounced here, the peak gain for the case with HNLF being nearly continuous for over 10nm. If we compare the continuous bandwidths (the continuous wavelength range for which then gain varies by only a specified amount) for a 0.1 dB, 0.5 dB and 3 dB reduction from the peak gain value we obtain 3.38, 11.31 and 41.795 nm for the

case without HNLF, and 11.895, 18.85 and 51.61 nm respectively for the one with HNLF. From these results it can clearly be seen that the continuous bandwidth for each condition is greatly improved by the use of the HNLF, and that this improvement is more important as our requirements for gain flatness become stricter (bandwidth is tripled for a 0.1 dB gain ripple requirement).

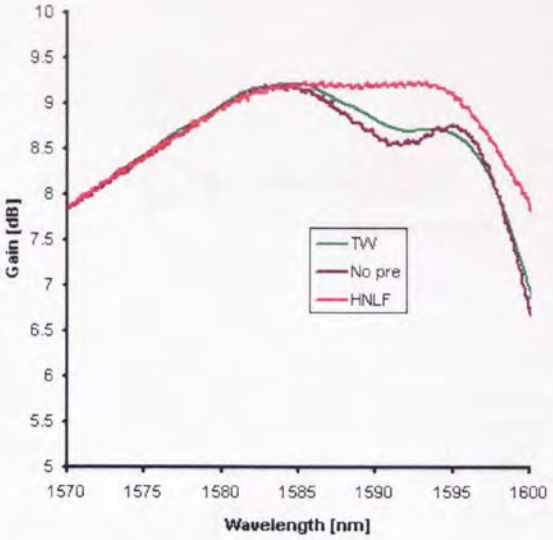

Figure 4.34 Gain comparison between using HNLF or TW as pre-fibre and no pre-fibre

Finally it is useful to compare the HNLF gain to that produced by using the TW 10.4km fibre used in the dual pump example, of course neither fibre is 100% tailored for the broadening application but it is interesting to see if the HNLF has provided a better result than what we have used previously, Fig. 4.34 shows the outcome.

As a final note to this section is brief exploration of the effect of spectral broadening on signal transmission. Two questions regularly appear in regards to using this technique for data transmission, which are:

1. Does the broad pump spectrum interfere with the signal band in regards to increase noise floor and therefore reduced OSNR?
2. If the broadening is initiated by the MI effect which can be viewed as a train of pulses, does this not essentially create a pulsed Raman system which may create a pulsating gain level and therefore interfere with data?

To answer these questions a simple transmission experiment was setup as given in Fig. 4.35.

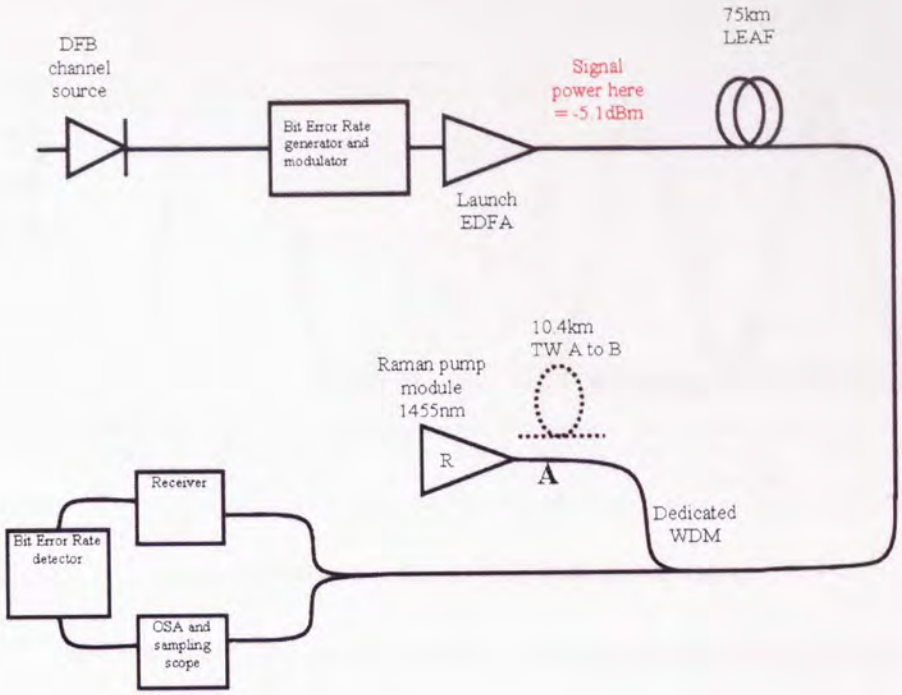

Figure 4.35 Experiment for investigation of pre-fibre gain on data transmission

In answer to question 1, the use of a suitable WDM will eliminate unwanted spectral components venturing into the signal band, but it is true at very high powers some element can find its way across. A higher specification/extinction ratio WDM would be required if these components were causing problems. The shown experiment aims to explore this and any pulse gain issues, though the latter is doubtful due to the fast repetition rate of any MI pulse coupled with the counter propagating pump scheme. The system was configured to be reliant upon Raman amplification i.e. not to work without Raman and therefore a low launch signal power was used which without Raman gain resulted in a received error rate of 1.5×10^{-2}. This configuration would make the system sensitive to any noise components added by the Raman amplification. The system was set with two Raman 'on' schemes, either the 10.4km TW pre-fibre at point A in Fig. 4.35 or no pre-fibre at all. The gain was set to 7dB for a 10Gbit/s signal

at 1555nm for both Raman schemes. The received eye diagram and spectra is given in figure 4.36 below.

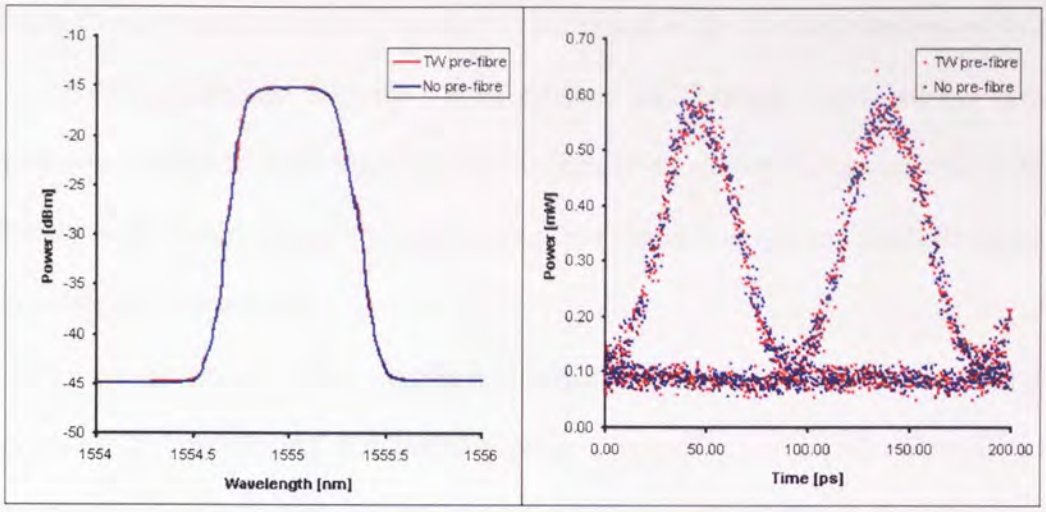

Figure 4.36 Pre-fibre/no pre-fibre transmission results

The associated error rates for the no pre-fibre case and the pre-fibre case are $1x10^{-12}$ and $7x10^{-11}$, respectively. Looking at Fig. 4.36 there is no apparent difference in the performance between the pre-fibre case and without, the only difference is given by the error rates. This difference is attributed to pump stability which for the fibre laser used is dependant on the output power level and which was less stable at the power level required when the pre-fibre was present, this could be suppressed by use of a more advance current control circuit. In essence there is no performance degradation due to the use of the pre-fibre in this experiment.

4.5 Conclusions

This chapter has provided an introduction into CW or Quasi-CW laser spectral broadening with reference to Raman amplifier pumps and originally for the first time shown how such broad pumps can then provide a broader, flatter gain spectrum than is conventionally available [38] which has since been repeated in [50, 51, 52]. This

concept has then been extended to the case of a dual pump WDM Raman unit to provide a gain with a noticeable reduction in ripple over a specified bandwidth. Related issues were discussed in relation to pump loss in the fibre and the sensitivity to pre-fibre dispersion, the need for a more efficient pre-fibre was expressed and novel work was carried out on a highly nonlinear fibre in an attempt to address this desire. Finally work to explore any degradation to a data signal from using a pre-fibre Raman amplifier was carried out.

From the work shown in this chapter it is possible to state that use of a pre-fibre for pump spectral broadening can indeed provide a smoother and broader Raman gain spectrum from a standard Raman pump laser. The result of this is that the power variation between channels in a WDM system, utilising repeated similar spans, can be reduced. This can lead to all channels remaining away form the noise floor as well as narrowing the dynamic power range an optical receiver is required to work over, thus reducing cost and complexity. Also the wider gain region could also allow more channels to be used, therefore increasing the total data capacity of a transmission system.

It is also possible to note that if such a broadening technique was to be used then very careful consideration must be applied to selection of the pre-fibre with regards to its length, nonlinear coefficient, and dispersion characteristic and to the required gain level in the transmission span to be amplified. This work provides a basis for much future work including the continuing need for an accurate numerical model of the broadening process, which truly resembles the measured broadened pump profiles, in order to determine these characteristics for an ideal pre-fibre for any amplification requirement.

Chapter 5

Four Wave Mixing and Raman

5.1 Introduction

As shown in chapter 3, to obtain a flatter and broader Raman gain spectrum multiple pump lasers of different wavelengths can be multiplexed together before being launched into a fibre. It has also been possible to extend the gain bandwidth by interleaving the pump laser within the signals [54]. Although there are the benefits, as mentioned, by the utilisation of WDM Raman pumps, there are also problems that arise, for example; pump-to-pump interactions – causing depletion of shorter wavelength pumps, and Four-Wave Mixing (FWM) – between pumps and pumps/signals.

This chapter aims to explore some of the effects resulting from FWM, the factors affecting them, and their impact on a communications system, along with investigations on previously proposed mitigation techniques.

5.2 Four-Wave-Mixing processes

Four-Wave-Mixing is a nonlinear process that arises from a third-order susceptibility parametric process, with second-order susceptibility very small in an isotropic silica fibre. In FWM two photons at frequencies f_1 and f_2 are destroyed while two new photons are created at frequencies f_3 and f_4. Significant FWM occurs only if there is conservation of the photon momentum and energy between the four guided waves involved. With energy conserved $f_1+ f_2= f_3+ f_4$ and phase matching of the wave vectors $k_1+k_2=k_3+k_4$ FWM can develop efficiently [21]. Looking now in terms of Pump and Signal [54], consider the mixing between two pump photons $hf_{p'}$, hf_p and a

signal photon hf_s to generate a forth photon at $hf_{s'}$. To conserve energy this generated photon has its optical frequency as:

$$f_{s'} = f_{p'} - f_p + f_s \tag{5.1}$$

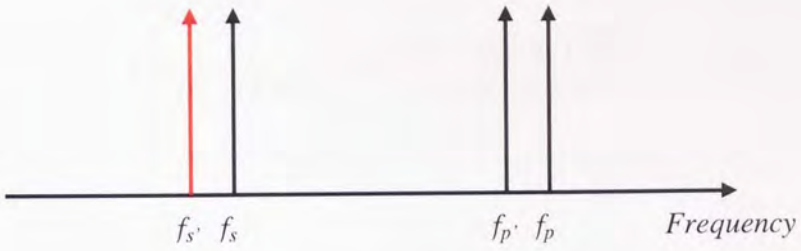

Figure 5.1 Non-degenerate Four-Wave-Mixing

This can be written as $\Delta f = f_{s'} - f_s = f_{p'} - f_p$, this is the non-degenerate case where the difference in the pump frequency equals that of the signal frequencies. In a degenerate case two photons from the same frequency are destroyed i.e. in our notation $f_{p'} = f_s$.

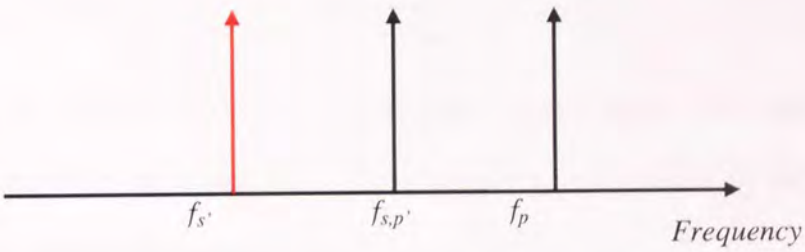

Figure 5.2 Degenerate Four-Wave-Mixing

From [54, 55] it is possible to obtain an expression approximating the power at the generated frequency as a function of fibre length L (km). If the two pump waves $f_{p'}$ and f_p have identical attenuation α_p and mix with a signal wave f_s with attenuation α_s the FWM generated power at the frequency $f_{s'}$ is

$$p_{s'}(L) = \frac{\eta}{9} d^2 \gamma^2 P_p P_{p'} P_s \exp(-\alpha_s L)(L_{eff}^p)^2 \tag{5.2}$$

Where the pump effective length is given by

$$L_{eff}^p = \frac{1-\exp(-\alpha_p L)}{\alpha_p} \tag{5.3}$$

The FWM efficiency can be given by

$$\eta = \frac{\alpha_p^2}{\alpha_p^2 + (\Delta\beta)^2}\left\{1 + \frac{4\exp(-\alpha L)\sin^2(\frac{\Delta\beta L}{2})}{[1-\exp(-\alpha_p L)]^2}\right\} \tag{5.4}$$

$$\cong \frac{1}{1+\left(\frac{\Delta k}{\alpha_p}\right)^2} \tag{5.5}$$

Where P_p, $P_{p'}$, and P_s in (5.2) are the input powers at their respective frequencies of f_p, $f_{p'}$ and f_s. If $\alpha_p L >> 1$ then the approximation (5.5) is valid. The variable d in (5.2) is known as the degeneracy factor and is equal to three for degenerate and six for non-degenerate four wave mixing [55]. γ is the non-linear coefficient of the fibre given by

$$\gamma = \frac{2\pi n_2}{\lambda_s A_{eff}} \tag{5.6}$$

Where A_{eff} is the effective mode field area, λ_s is the vacuum signal wavelength and n_2 is the nonlinear-index coefficient [11]. The efficiency η, is dependent on the amount of propagation constant mismatch $\Delta\beta$ [54]

$$\Delta\beta = (\beta_{p'} - \beta_p) - (\beta_{s'} - \beta_s) = \Delta\beta_1 + \Delta\beta_2 + \Delta\beta_3 \tag{5.7}$$

Where

$$\Delta\beta_1 = \frac{2\pi}{c}\Delta f(N_p - N_s) \tag{5.8}$$

$$\Delta\beta_2 = \frac{\pi}{c}(\Delta f)^2(\lambda_s^2 D_s - \lambda_p^2 D_p) \tag{5.9}$$

$$\Delta\beta_3 = \frac{\pi}{3c^2}(\Delta f)^3\left[(2\lambda_p^3 D_p - 2\lambda_s^3 D_s) + \left(\lambda_p^4 \frac{dD_p}{d\lambda_p} - \lambda_s^4 \frac{dD_s}{d\lambda_s}\right)\right] \tag{5.10}$$

The notations $\Delta\beta_1$, $\Delta\beta_2$ and $\Delta\beta_3$ are the first, second and third order terms from the Taylor expansion of $\Delta\beta$ in terms of Δf. N_p and N_s are the group indexes for pump and signal respectively. D is the fibre chromatic dispersion and is given by

$$D = \left(\frac{1}{c}\right)\left(\frac{dN}{d\lambda}\right) \tag{5.11}$$

And the dispersion slope is given by

$$\frac{dD}{d\lambda} = \frac{1}{c}\frac{d^2N}{d\lambda^2} \tag{5.12}$$

When the first order mismatch (5.8) has been minimised the second order term from (5.9) dominates. In this chapter we are interested in dealing with pump and signal interactions, which means we are dealing with broad bandwidths in the region of 100nm. The presence of third order dispersion in the fibre implies that β_2 is a wavelength dependent quantity [56]. It is therefore important to note that, for efficient FWM, it is required to have $|\Delta\beta| \approx 0$, which holds true when β_2 at $f = (f_{p'} + f_s)/2$ is approximately equal to zero, i.e. when $(f_{p'} + f_s)/2 = f_0 =$ zero dispersion frequency. Hence, efficient, phase-matched FWM takes place at $f_{s'} = f_{p'} - f_p + f_s$ when λ_0, the zero dispersion wavelength, falls symmetrically between the pump and signals. In other words, from [57] third order phase matching is achieved when two pumps are symmetrical with regard to the zero dispersion frequency. In the degenerate case this means the pump is exactly at the zero dispersion wavelength λ_0.

5.3 Four-Wave Mixing between pumps

The previous section sought to look at FWM from a Pump-Signal interaction angle, but mixing products can be formed between different pumps in a system employing WDM Raman pumping if the dispersion characteristics of the fibre used satisfy the required phase matching condition, in this case noise and/or another pump acts as the signal in the previous section. There are multiple combinations of products that can be formed depending on where the zero dispersion wavelength sits in the pump band and whether it falls at a pump wavelength; giving rise to a degenerate FWM case. The products that are created can lead to multiple problems, for example:

- Products may fall within the signal band diminishing OSNR
- Products may fall at longer wavelengths within the pump band serving to deplete the pump sources
- The formation of products may interfere with techniques aimed at achieving optimum gain shape

Construction of an experiment to investigate the location and magnitude of such products is relatively simple and is depicted in figure 5.3.

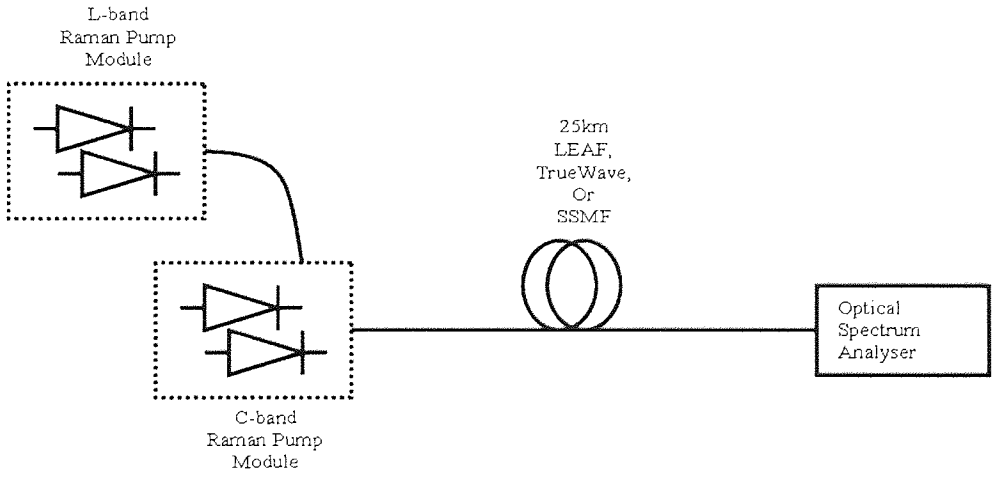

Figure 5.3 Pump-Pump FWM Experiment

The Raman pump modules consisted of two primary units:

C-Band pump module

L-Band pump module

The construction of the two units was:

C-band unit:

Three wavelengths, 1424, 1437 and 1452nm

Six pumps diodes

Two at each wavelength cross-polarised

L-Band unit:

Two wavelengths, 1466 and 1496nm

Four pump diodes

Two at each wavelength cross-polarised

Fibre was varied between 25km lengths of Corning LEAF, OFS TrueWave RS and OFS SSMF to provide a variation in dispersion characteristics, namely the dispersion zero wavelength (ZDW). The dispersion zero wavelengths for the three fibres were approximately, 1498, 1452 and 1310nm respectively. From using various combinations of pumps it is possible to observe clearly the mixed components, following figures 5.4 to 5.16 display the results of this.

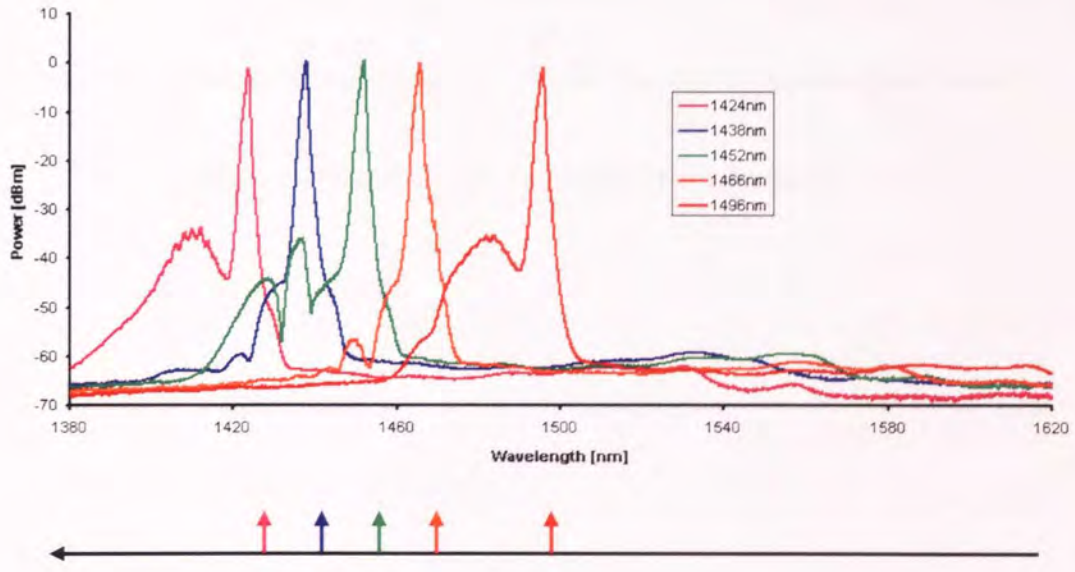

Figure 5.4 Individual pump wavelengths after 25km SMF

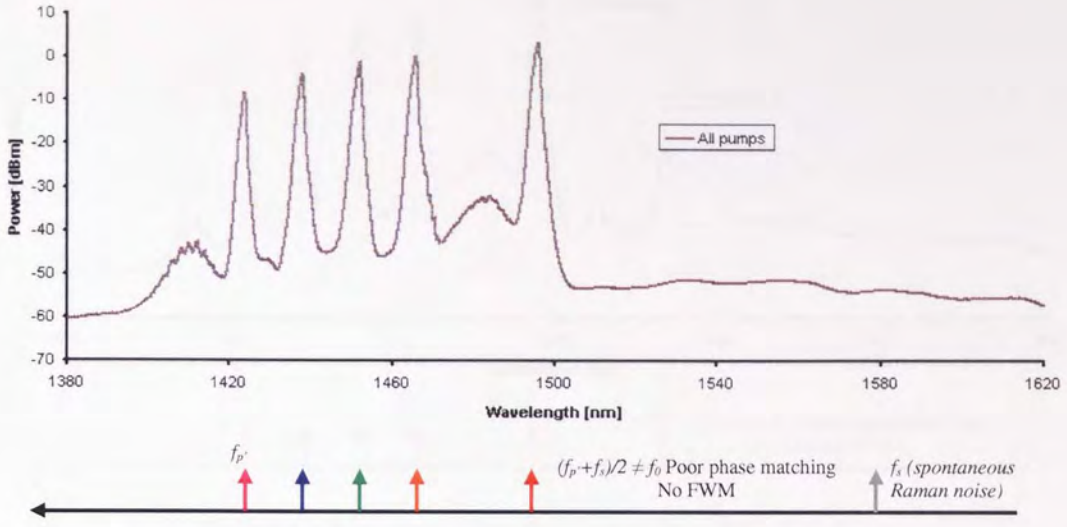

Figure 5.5 All pump wavelengths together after 25km SMF

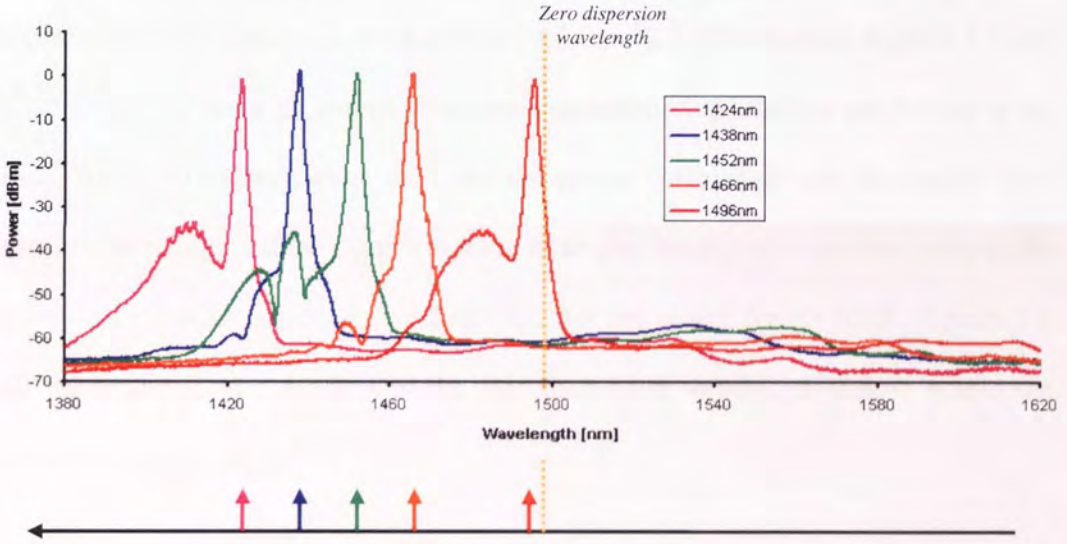

Figure 5.6 Individual pump wavelengths after 25km LEAF

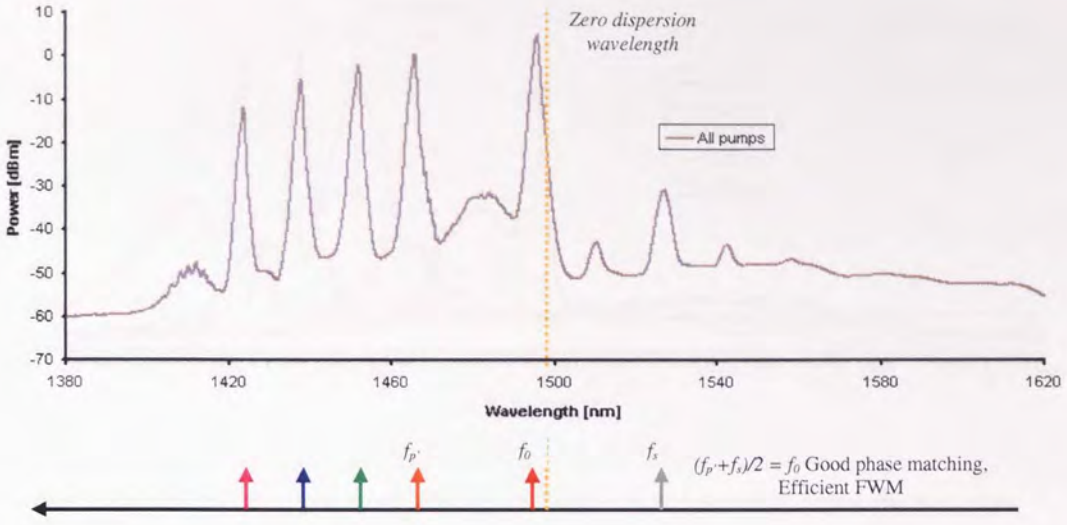

Figure 5.7 All pump wavelengths together after 25km LEAF

From figures 5.4 and 5.6 it can be noted that individual pumps propagating by themselves do not induce, or not notably in this case, a FWM product. Figures 5.5 and 5.7 illustrate that when all pumps propagate together mixing products are formed in the signal band (>1500nm) when the zero dispersion wavelength (or frequency) falls between the pumps and the signal (in these examples the signal should be taken as the spontaneous Raman noise) as the LEAF case but not in that for the SMF. Figures 5.8 and 5.9 below show the effect of the zero dispersion wavelength falling within the pump wavelength range.

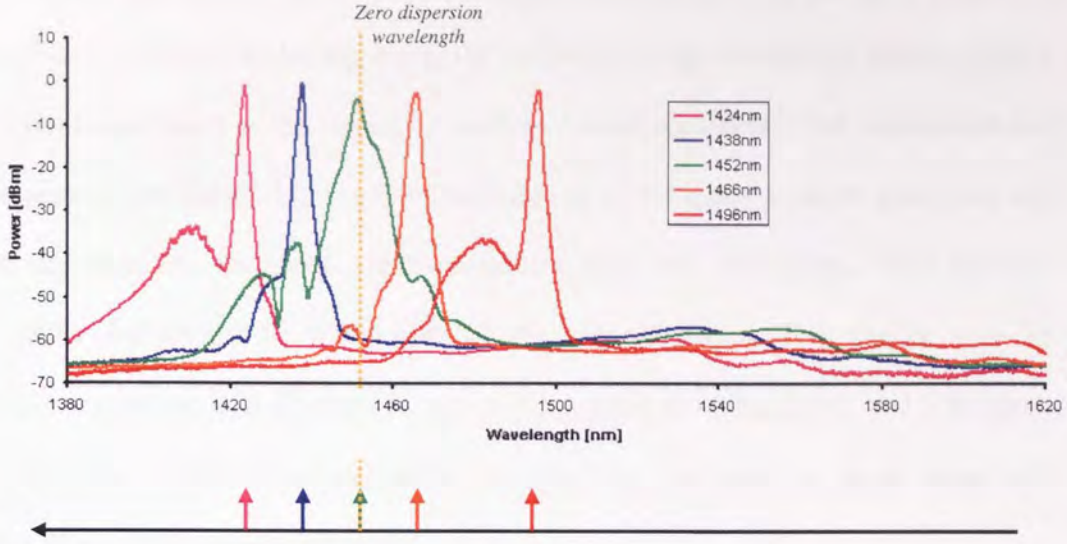

Figure 5.8 Individual pump wavelengths after 25km TW-RS

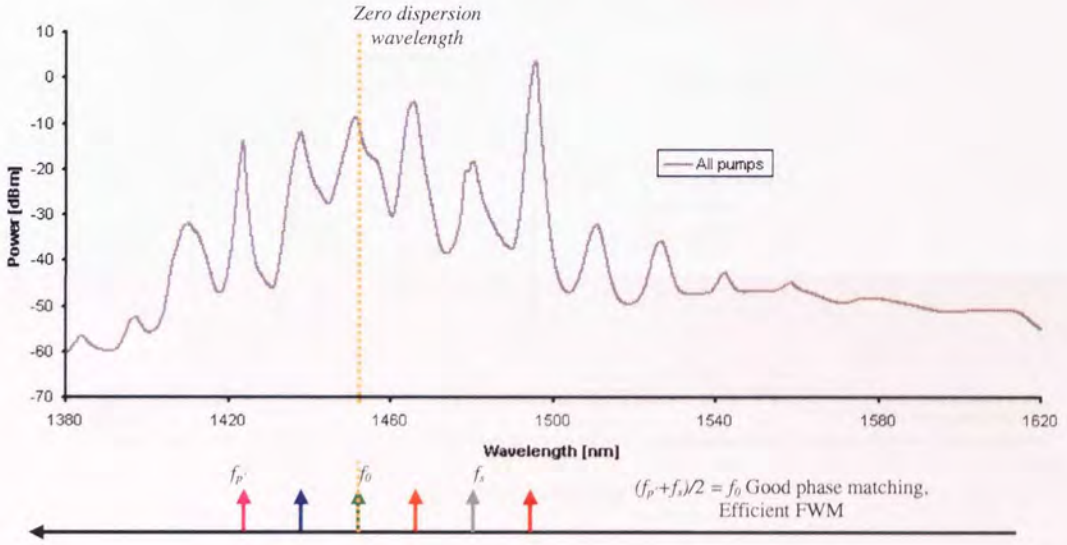

Figure 5.9 All pump wavelengths together after 25km TW-RS

In figure 5.9 many new wavelengths have been created as result of multiple degenerate and non-degenerate FWM processes. The degenerate processes arise mainly due to low dispersion in the pump band and 1452nm pump falling at around the same wavelength as the zero dispersion wavelength. The ZDW for this fibre was verified by measurement and is reinforced by the observation of spectral broadening of the 1452nm pump in figure 5.8 due to various non-linear effects that were discussed in

chapter 4. The products formed from mixing in Fig. 5.9 are more prevalent then those in Fig. 5.7 because by having the ZDW within the pump wavelength region we now have pumps acting as the 'signal' as well as spontaneous noise. The wavelength and frequency denoted by f_s in Fig 5.9 illustrates one of the many products generated, and in this case one generated where previously there was only noise, other products actually fall within the wavelength of the original pumps. This can be seen by exploring various combinations of pumps propagated down the LEAF and TW fibres, a selection of these combinations are provided over the next few pages along with depiction of the products generated.

Starting with pump combinations in TW

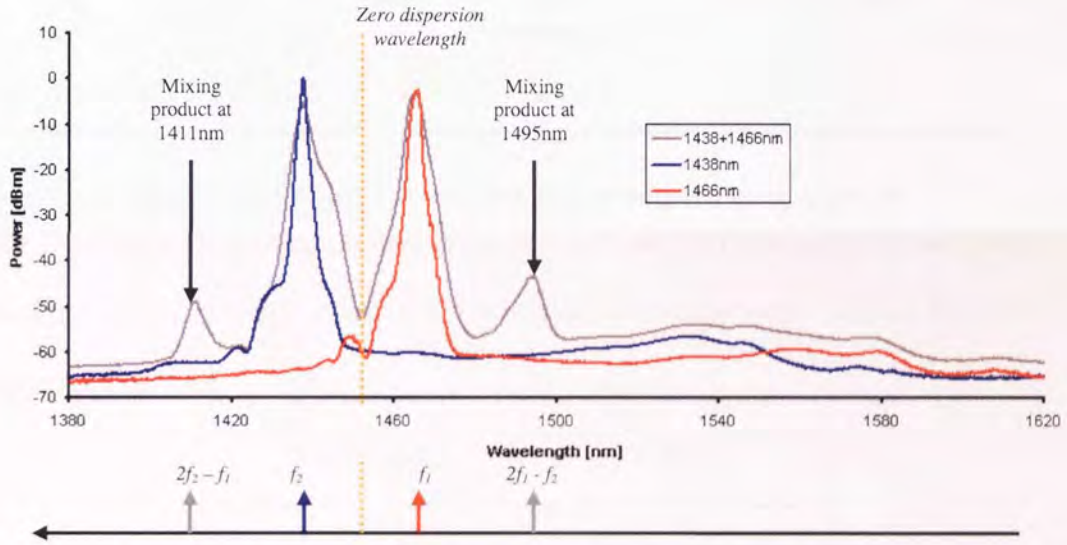

Figure 5.10 1438 and 1466nm pumps after propagation through TW-RS

Here in figure 5.10 we can see the production of two extra wavelength peaks as the result of partially degenerate FWM whereby two photons from the same pump have been mixed with one from the other to create components as illustrated. Even though the ZDW is not at either of the pump frequencies it is close to both of them (approximately central between both pumps) and the dispersion slope is shallow

enough, allowing a certain degree of mixing efficiency to be obtained. If this hypothesis is correct, then, when the pumps are moved away from the ZDW in a symmetric fashion the efficiency should reduce and hence the product magnitude. This can be seen occurring in Fig. 5.11 below.

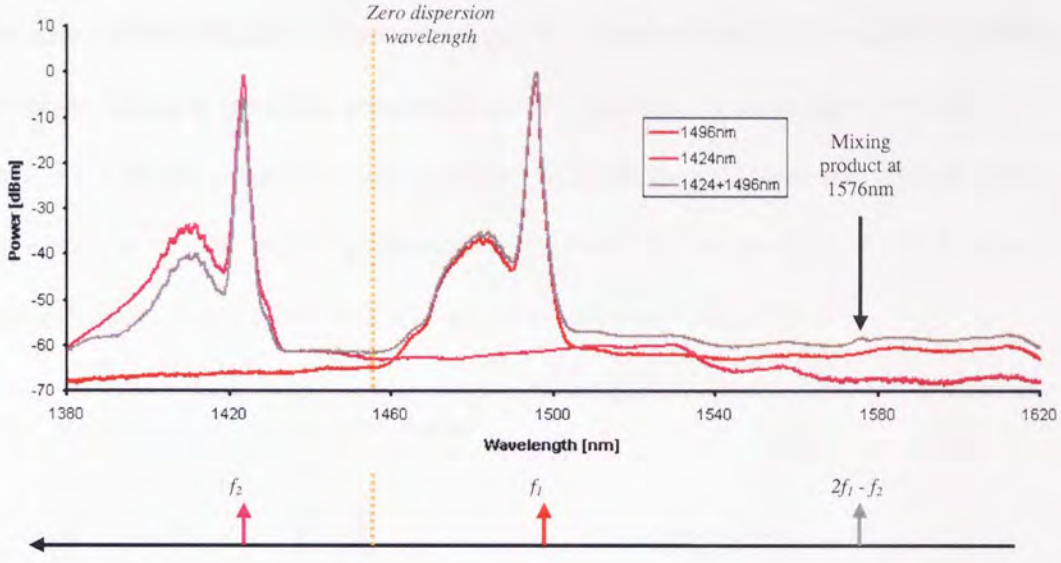

Figure 5.11 1424 and 1496nm pumps after propagation through TW-RS

The location of the mixing product in figures 5.10 and 5.11 can easily be verified by working in the frequency domain. If we convert to an equivalent vacuum frequency our pumps become:

Wavelength	Frequency
[nm]	[THz]
1424	210.67
1438	208.62
1452	206.61
1466	204.64
1496	200.53

From Fig. 5.10 we have f_1 = 204.64 THz and f_2 = 208.62 THz,

Then $2f_2 - f_1$ = 212.6 THz => 1411nm and $2f_1 - f_2$ = 200.66 THz => 1495nm.

From Fig. 5.11 we have f_1 = 200.53 THz and f_2 = 210.67 THz,

Then $2f_1 - f_2$ = 200.66 THz => 1576nm.

The magnitude of the product in Fig. 5.11 is vastly smaller than those in 5.10 due to greatly reduced efficiency. Referring back to what was previously stated regarding products falling at the same wavelength as other pumps, it can be seen from Fig. 5.10 that the 1495nm product would coincide, to some degree, with the spectra of the 1496nm pump. The next figures aim to demonstrate the products formed from a strongly degenerate mixing case where a pump is centred on the ZDW.

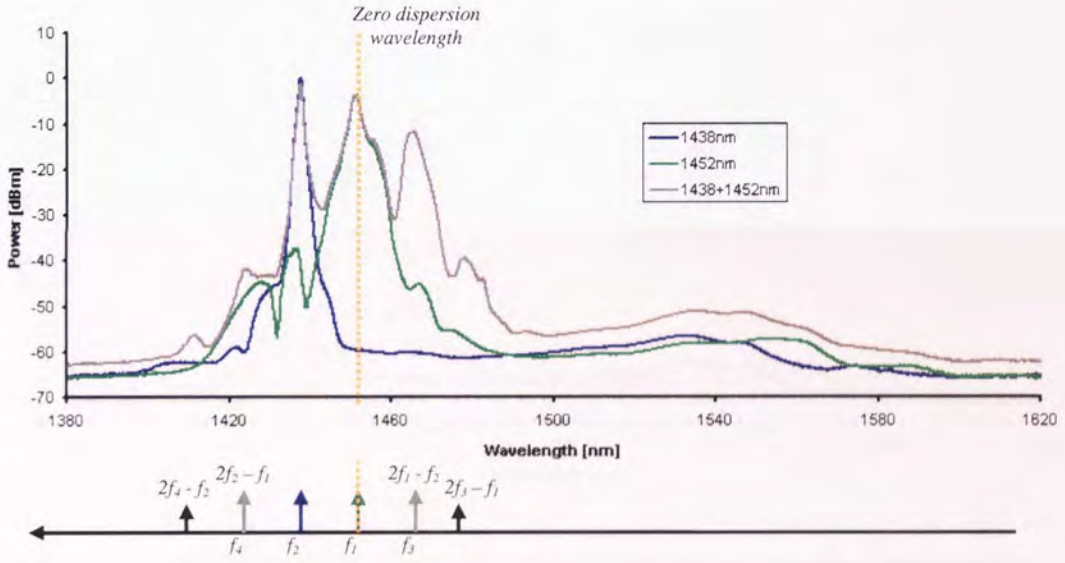

Figure 5.12 1438 and 1452nm pumps after propagation through TW-RS

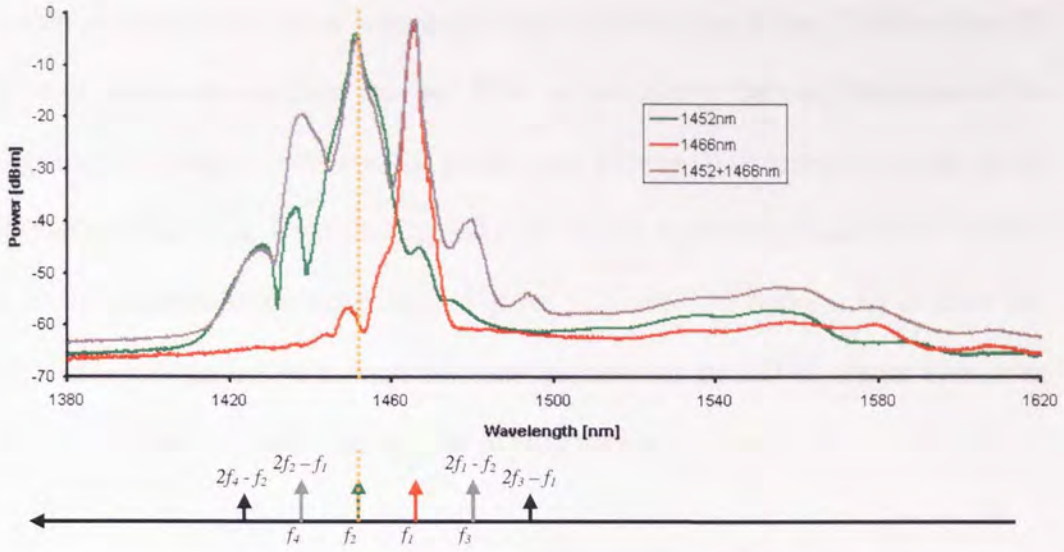

Figure 5.13 1452 and 1466nm pumps after propagation through TW-RS

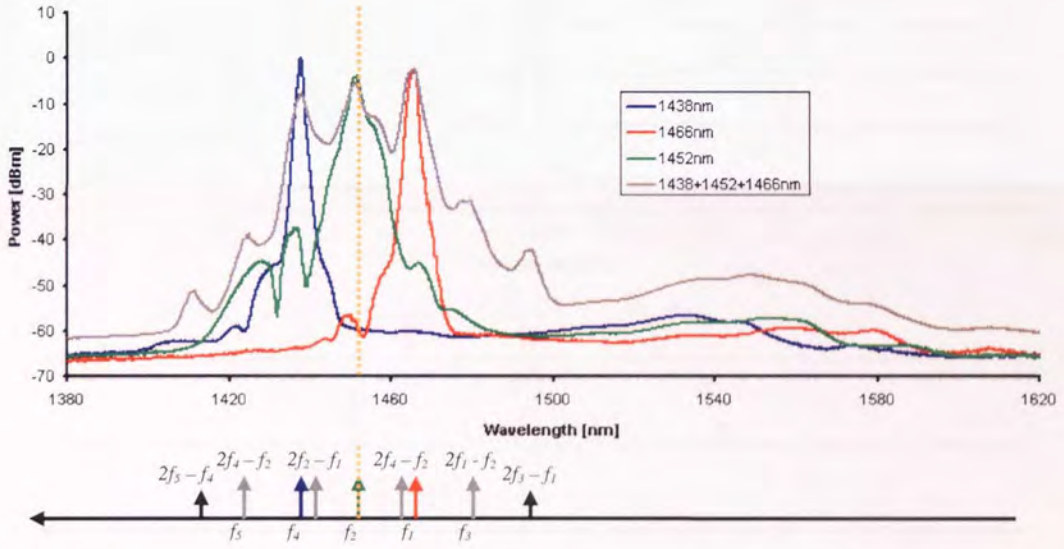

Figure 5.14 1452 and 1466nm pumps after propagation through TW-RS

It must be noted that in the above examples, especially Fig. 5.14, the calculated products are not exhaustive i.e. there are many other combinations that have been omitted for clarity. Figs. 5.12 and 5.13 demonstrate that by having a pump at the ZDW the products formed are of considerable amplitude and also coincide with the spectral location of other WDM Raman pumps.

The examples obtained from using TW-RS as the mixing medium generally produce notable products in the pump wavelength band, partially due to the ZDW position. If LEAF is used as the medium then the ZDW is moved to ~1500nm. This reduces the magnitude of products formed in the pump band. Mixing still occurs around the pump wavelengths due to the low local dispersion value, but it primarily leads to the creation of strong products in the signal band. Figures 5.15 and 5.16 below, aim to show the effect of pump spacing with respect to other pumps and the ZDW. Traces have been offset with respect to each other in order to enhance visual clarity.

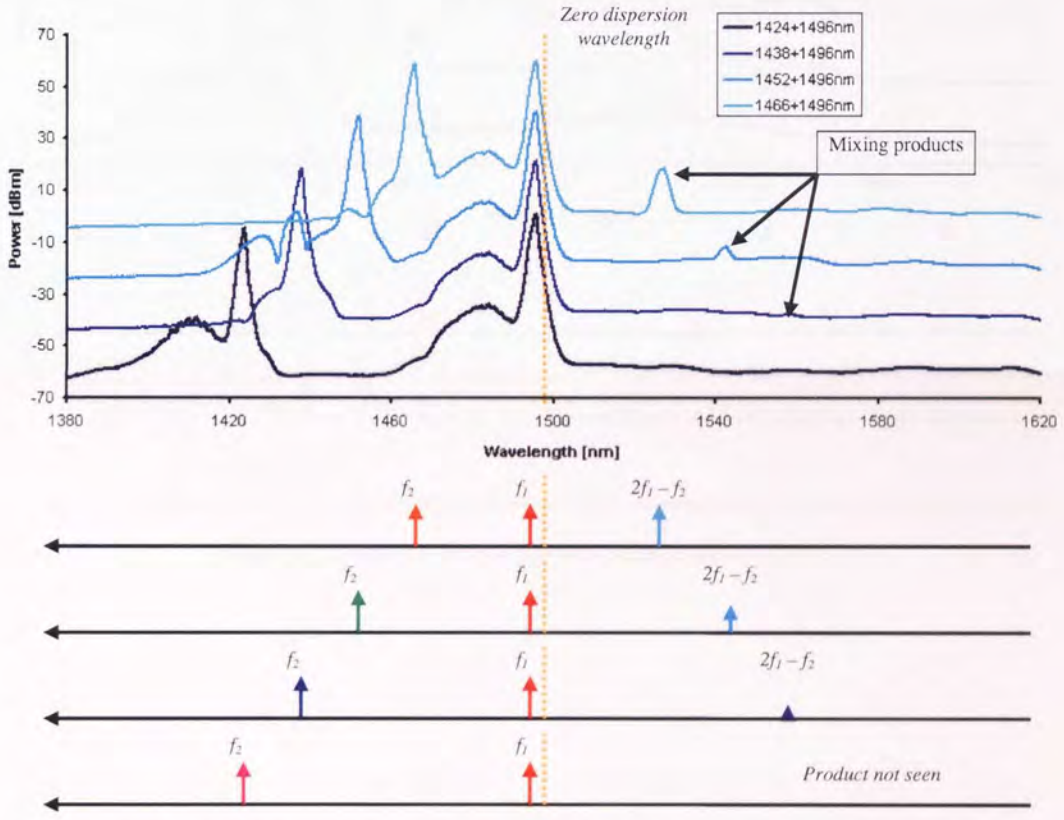

Figure 5.15 Effect of pump spacing from ZDW and 1496nm pump point in LEAF

As observed in the TW-RS case the mixing efficiency between any pump pair increases as the offset between pumps decreases and as the pumps approach the ZDW, i.e. the mixing efficiency is not only dependent on the relative dispersion values

between pumps but also on the absolute dispersion value involved. In the LEAF case, as previously mentioned, the mixing products in the pump wavelength range are greatly reduced in comparison to those in the TW case. This is attributable to the different dispersion characteristics, as shown in figure 5.17 and, to some degree, the core area.

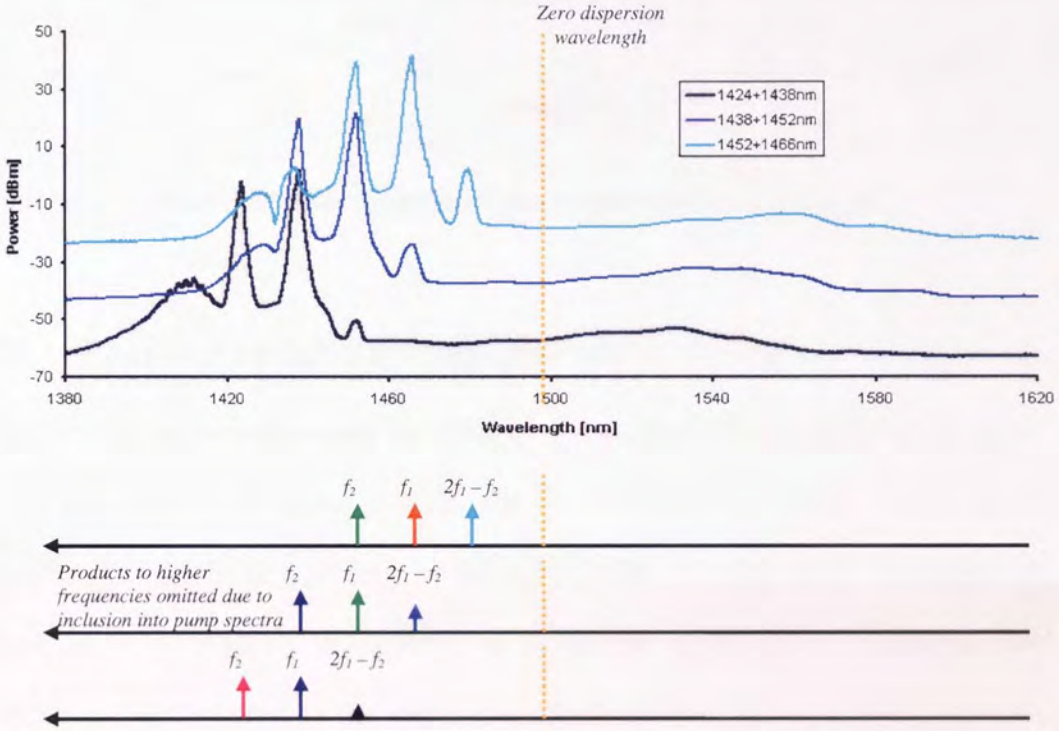

Figure 5.16 Mixing between pump pairs towards ZDW

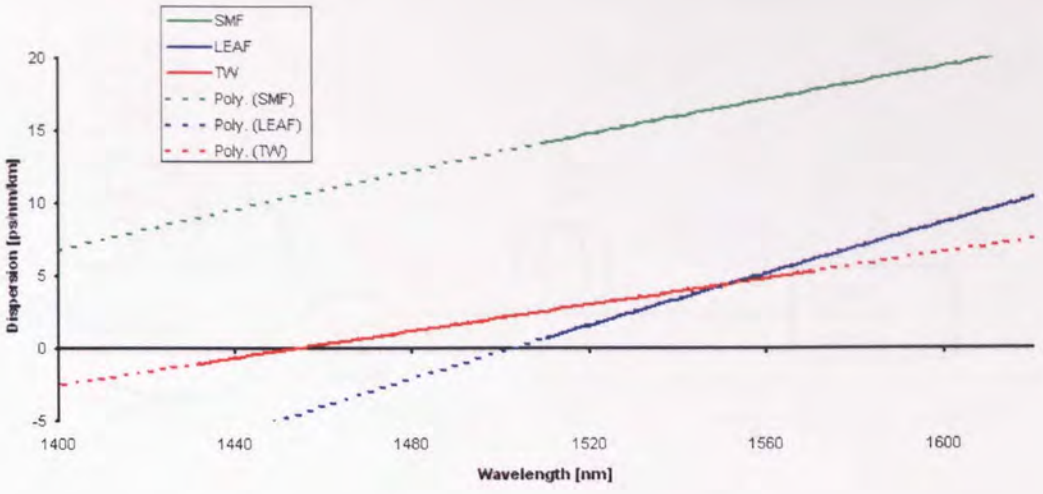

Figure 5.17 Fibre dispersions (solid - measured, dashed - linear fit)

5.4 Four-wave mixing between pumps and signals

Attention is now turned towards the effect of signals mixing with pumps and the effect of mixing products on signal performance. As established in section 5.3 the use of LEAF can create mixing products in the signal band, especially when the pump and signal are co-propagating. In 5.3 there was no discrete signal applied at the input with the pumps light, whereas in this section the effects on and from an inserted signal are explored. As an introduction, the transfer of pump spectral shape to the signal is first looked at. This phenomenon has been well documented and is an important aspect to consider when analysing and modelling FWM effect involving Raman, see also [54, 57]. A simple experiment to investigate this effect is shown in figure 5.18.

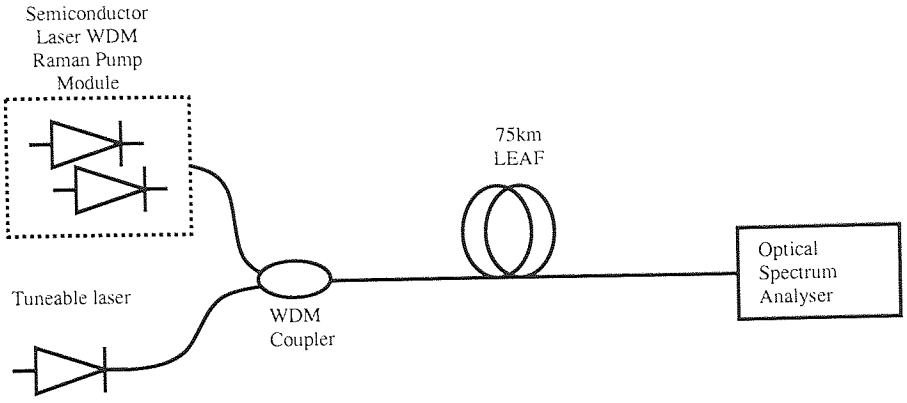

Figure 5.18 Experimental set-up for co-propagating FWM investigations

In this experiment ~350mW Raman pump light at 1452nm was coupled via a dedicated WDM with the output of an External Cavity Tuneable Laser (ECL), the wavelength of the ECL was set to the wavelength that provided the most efficient FWM – this case ~1552nm. It is worth restating that the maximum efficiency for FWM in this type of experiment, i.e. in the presence of Raman amplification, occurs when the signal and the pump reside at equal spacing on either side of the ZDW and the spacing between the pump and signal is equivalent to the Raman shift as mixed components in the signal region also receive maximum gain. The output power of the ECL into the fibre was ~1dBm, the resulting spectra were observed on the OSA with a Resolution Band Width (RBW) of 0.07nm. The measured result is shown in Figure 5.19.

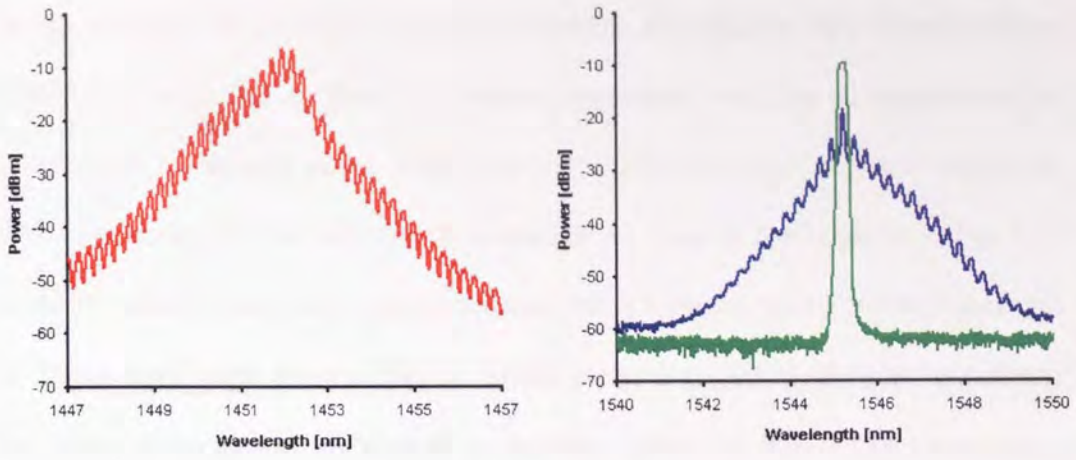

Figure 5.19 Pump modes onto signal (green - I/P signal, blue - O/P signal)

Looking at Fig. 5.19 two principle characteristics can be observed; one being the imposition of a mirror image (with the ZDW as the symmetry axis) of the general pump shape onto the signal and the other being the impression of pump modes onto the signal. To confirm that these modes on the signal are actually from those of the pump, the previous results can be converted into the frequency domain, reversed and offset in order to be overlaid as done in figure 5.20 below. Here the matching of the mode spacing can be clearly seen.

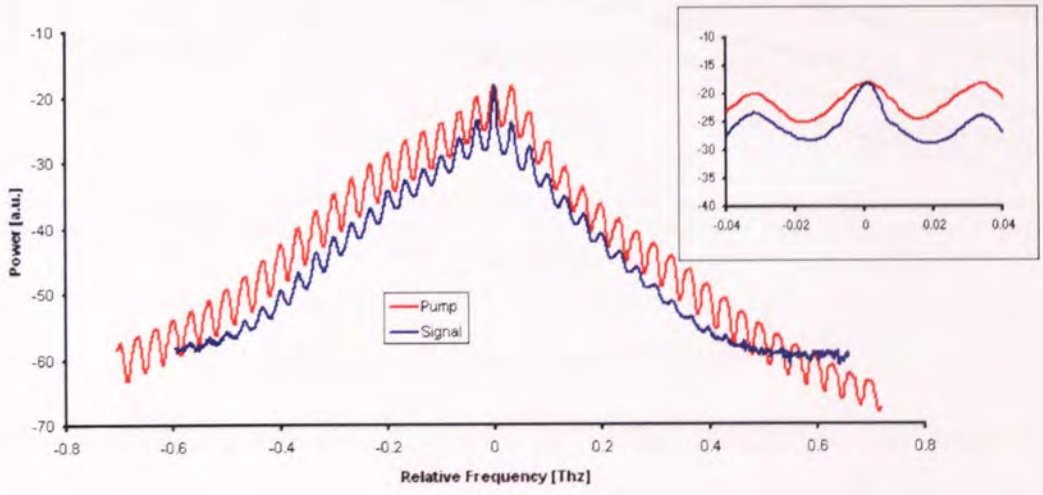

Figure 5.20 Overlay of signal and pump spectra in the frequency domain

With the pump modes mixing with the signal the effect on OSNR can clearly be seen in Fig. 5.19, and the outcome is a drastic reduction. Investigation into this reduction of OSNR is now looked at. There are several experiments that can be implemented to characterise the mixing effect, each requiring a different signal source requirement. The experimental layout each time is in essence the same as that depicted in Fig. 5.18 with the tuneable laser diode being implemented or replaced with a WDM signal grid or Broad Band Light Source (BBLS). These alternative sources allow us to examine the effect of the mixing phenomena on multiple signals, as in a WDM transmission system, and on non-coherent light – essentially representing noise that may build up over a system. Initially results from the ECL will be examined to provide a flavour of the severity and bandwidth of the mixing region under investigation. The following results use a similar set-up from Figure 5.18, but, this time the laser was swept through the mixing region, and the OSA was set to 0.2nm RBW.

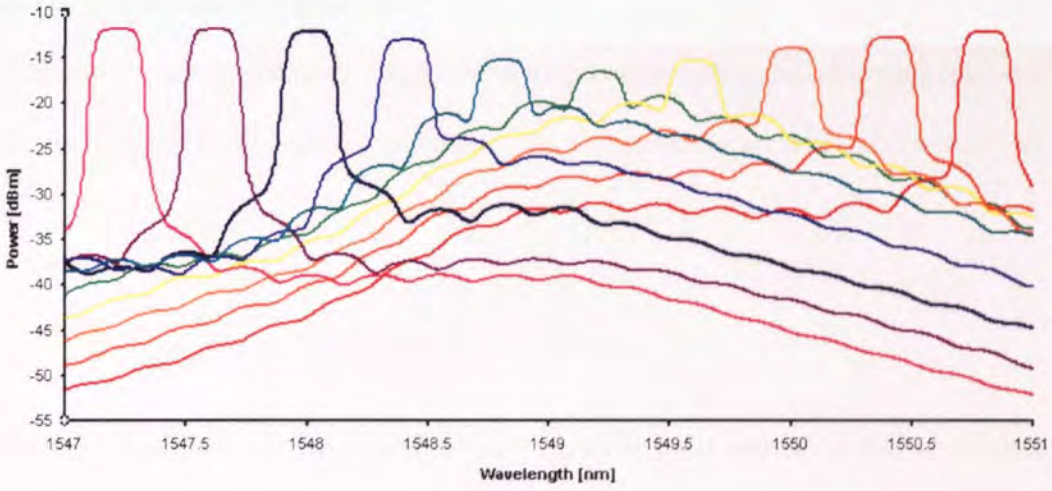

Figure 5.21 ECL swept through FWM region

From this result it is possible to get a feeling for the bandwidth and the degree of OSNR degradation; in fact the sweep range used does not fully escape the FWM region. In the range that is shown, the OSNR has reduced from ~22dB(pink trace) to

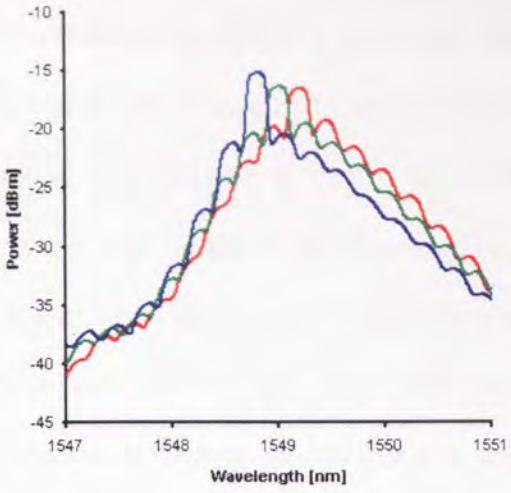

Figure 5.22 Adjacent channels in FWM region

~5dB(light green trace). The degree of reduction is dependent on the FWM efficiency, as seen previously, but also on the signal power – this is where the Raman gain spectra should be considered. It is worth remembering that in the above example the peak gain is at about 1552.5nm, this helps explain why the channels towards longer wavelengths have lower OSNR performance than those on the other side of the FWM region at shorter wavelengths. It is also interesting to look at whether the signal power has been redistributed locally as the peak power has reduced. To do this, adjacent channels can be integrated and compared to see if they contain similar total powers. This can be done to the channels in Figure 5.22.

By taking the output file of the OSA, converting to mW, summing adjacent points and then multiplying by the spectral separation the area under each curve can be evaluated i.e.

$$\left[\sum_{r=2}^{n-1}\frac{P_1}{2}+P_r+\frac{P_n}{2}\right]\Delta\lambda$$

Where P_n represents the power at each measurement point and $\Delta\lambda$ is the wavelength step between measurement points. For the three traces shown we obtain the values 0.0152mW.nm, 0.0157mW.nm and 0.0161mW.nm. The proximity of these values to each other provides some confidence that the signal power has been re-distributed locally; the small differences can be attributed, to some degree, to the variation of the Raman gain and the limited measurement window used.

The reduction in OSNR is worse still when multiple channels are present; figure 5.23 shows the input and output spectrum of a 50GHz ITU grid applied to our experimental set-up, OSA RBW = 0.06nm. The ~25dB OSNR of the best channels has been cut to around 4dB for the worst affected. This maybe attributed, in part, to the degree of superposition of the mixed components raising the noise floor. The channels applied here were CW but, even with modulated data applied, the OSNR reduction renders those wavelengths in the FWM region useless for meaningful transmission.

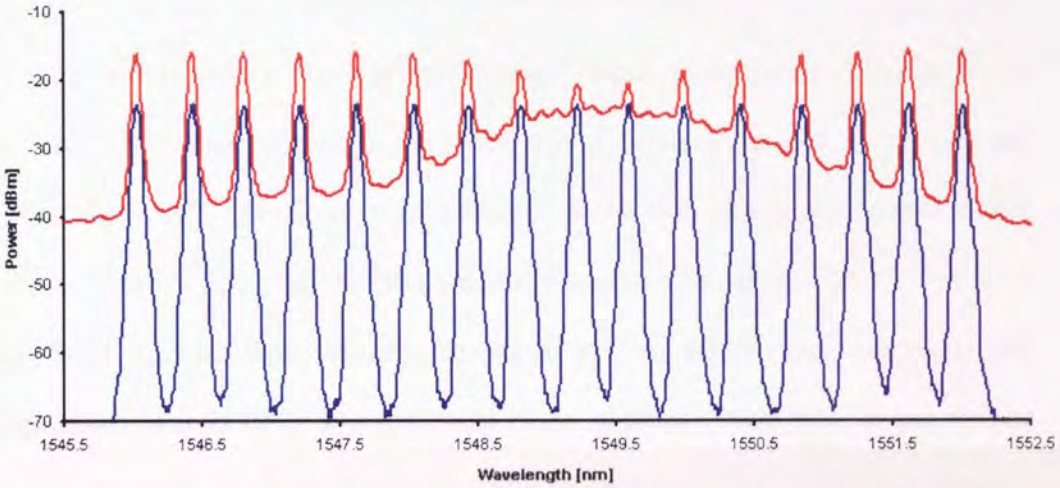

Figure 5.23 Effect on 50 GHz grid

As previously mentioned, the OSNR is attacked from two sides:

1. The coherent signal power is reduced
2. The noise floor is increased

It is therefore interesting to look at the effect when an incoherent BBLS is used as a 'signal' source instead of the ECL or WDM grid. In figure 5.24 the BBLS used was a C-band EDFA set to a total output power of 13.3dBm, also shown is the maximum held gain trace from a stepped ECL with output power of 4dBm moved in 0.25nm steps.

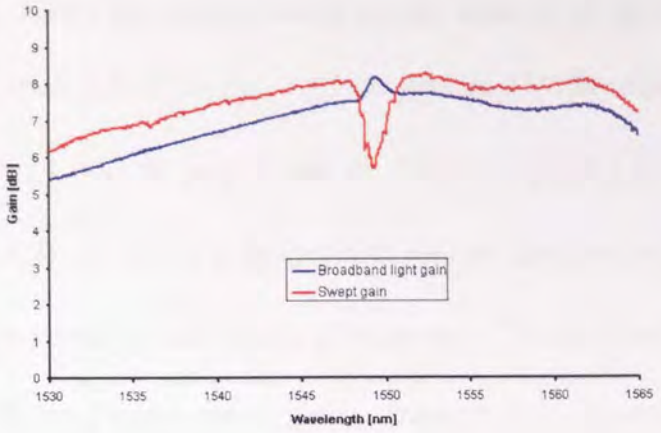

Figure 5.24 Swept gain vs. BBLS gain

The pump power in each case was kept constant. What can be observed in Fig. 5.24 is the striking difference in gain, in the FWM region, between the ECL swept case and the BBLS. The ECL gain drops as expected due to the reduction of peak power as seen in Figs. 5.21 and 5.23, but the BBLS actually receives an enhancement to the gain. This build up has been mainly attributed to two phenomena, resonant gain enhancement due to RIN [58] and Pump-Noise induced FWM [59]. It can also be understood by considering the way in which the coherent ECL laser light power is redistributed as seen in Figs. 5.21 and 5.22 and the way the resultant noise floor rises when many laser wavelengths are present as in figure 5.23. In essence the incoherent noise floor rises and the coherent 'signals' drop down around the wavelength of peak mixing efficiency.

5.5 Mitigation of FWM between pumps and signals

Several papers have linked the pump's spectral width to the severity of the FWM region / ASE enhancement [59, 60, 61]. Reference [59] seeks to explain that a wide spectral width will reduce the pump-noise induced FWM effect because the power

spectral density within the spectral width maybe reduced. If the following FWM process is considered $f_p2+f_n2-f_p1\rightarrow f_n1$ the generated FWM power $P(f_n1)$, due to this process, at f_n1 will be proportional to $P(f_p1).P(f_p2).P(f_n2)$ where $P(f_p1)$, $P(f_p2)$ and $P(f_n2)$ are the input pump-power spectral densities at frequencies f_p1, f_p2 and the noise-power spectral density at frequency f_n2, respectively. A wide pump spectral width (the total pump power remains constant) can reduce the value of both $P(f_p1)$ and $P(f_p2)$, therefore reducing the FWM effect. Reference [60] seeks to reduce the FWM by de-correlating the longitudinal pump modes i.e. reducing the coherence, it is the view of this author that the authors of reference [60] have overlooked the fact that they have broadened the pump spectral width, coherence is still reduced, but no reference was made to the increase in spectral width. Spectral width Δf is related to the coherence time t_c by $\Delta f=(\pi t_c)^{-1}$ [41]. Taking on board these mitigation concepts an experiment was devised to explore them and in the case of reference [60] whether the proposed scheme works for the reason stated by the authors, or if it is due to some other factor, such as the spectral bandwidth of the pump laser.

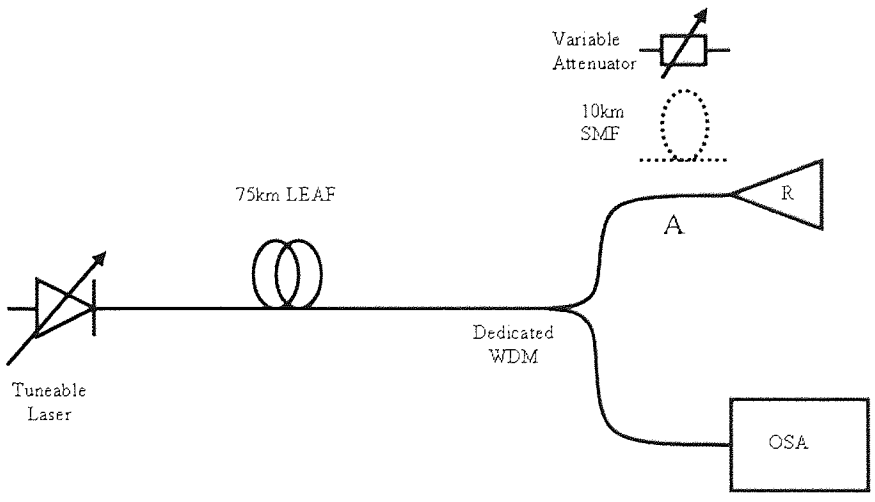

Figure 5.25 Experiment for investigation of FWM mitigation techniques

Figure 5.25 depicts what can generally be considered to be a counter propagating pump configuration. The details of the components used are:

- Tuneable laser: 1510-1610nm range, output power set to 0dBm
- Raman pump: Raman fibre laser at 1455nm with 33dBm maximum output
- WDM: 1400-1500/1500-1600nm Raman WDM

The component point labelled 'A' was either a patch lead, 10km reel of SMF or a variable attenuator (set to a value that provided the same gain in the fibre for the same pump output power). The aim of the experiment was to see if the FWM is reduced because of pump mode de-correlation, spectral broadening because of the SMF element at A or due to natural pump broadening [26] at the higher pump powers required to compensate for pump losses through the SMF. The figure below shows the effect of the mitigation techniques on the pump spectra in Fig. 5.26 and on the signal OSNR (counter propagating to the pump) in Fig 5.27.

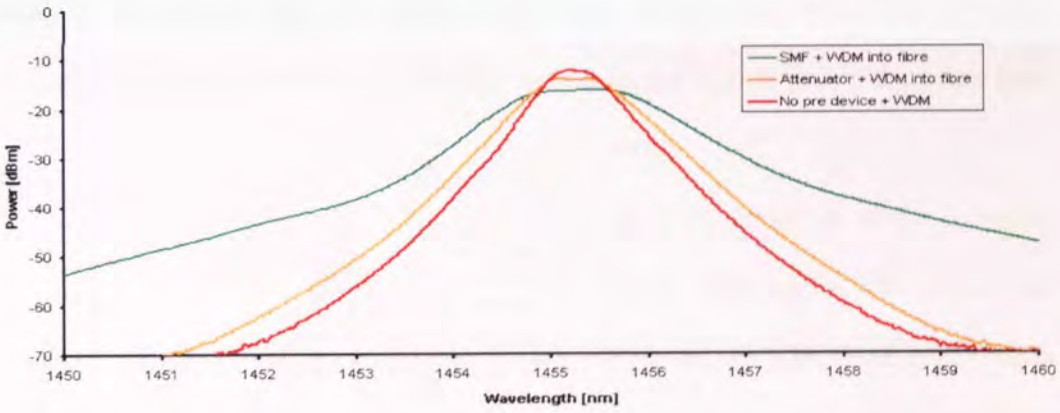

Figure 5.26 1455nm Raman pump after different FWM mitigation techniques

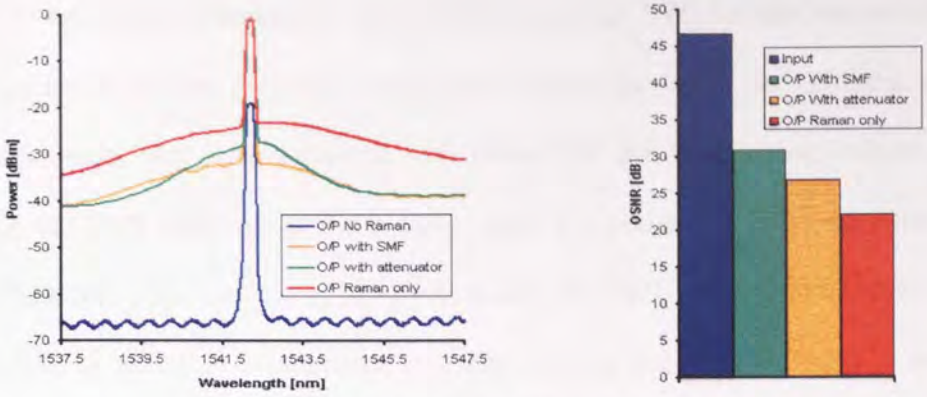

Figure 5.27 Effect on counter propagating signal OSNR

Starting with Fig.5.26 and the pump spectra, the traces represent the spectra for each system variant that provided ~18 dB of gain in the transmission fibre. Pump powers into the fibre (after the WDM) were 995mW 926mW and 964mW for the Raman only, SMF and Attenuator cases respectively, the variation in powers arises from, partially, the wavelength setting of the power meter and the apparent re-distribution of the pump power with respect to wavelength. The spreading of the spectrum in the case of the SMF, as illustrated in Fig 5.26, can be attributed to non-linear effects within the SMF such as modulation instability (see chapter 4) and natural broadening in the pump laser cavity.

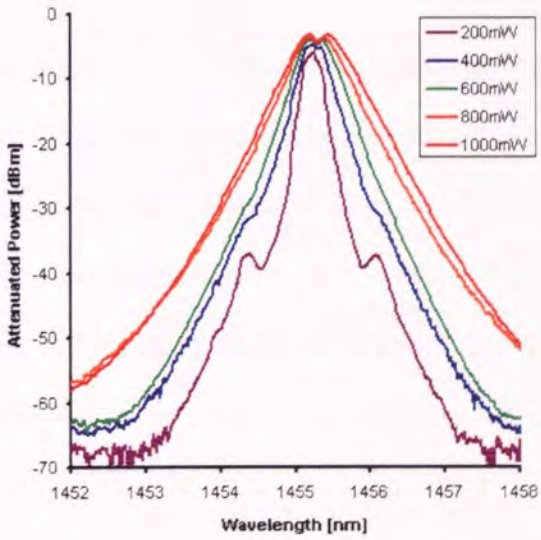

Figure 5.28 Inherent pump broadening

Fig. 5.27 shows the effect on signal OSNR. The signal was a tuneable ECL set at 1542.2nm with 0dBm output, this wavelength was found to be worst affected by the FWM. The blue trace is our signal after propagation through the LEAF span without Raman amplification measured by the OSA set to 0.2nm

RBW and -70dBm sensitivity; the OSNR (in a 1nm BW) for this was 46.6dB. The other traces display the span output with Raman on, under the different schemes; Raman only, with Attenuator and with 10km SMF pre fibre giving OSNRs of 22.1, 26.8 and 31dB respectively. From these values it is possible to relate the improvement with OSNR to the increase in pump line width. The SMF after the pump does improve the OSNR as set-up in reference [60] but possibly not quite in the way described. Reference [60] attributes the performance improvement to pump longitudinal mode de-correlation (reducing the FWM efficiency) due to the pre-fibre dispersion characteristics only. If this was the sole reason then the attenuator would not provide any improvement, but as Fig. 5.27 shows, it does. The results here show that by operating the pump at higher power a natural line width increase is obtained and when attenuated can provide better performance than un-attenuated pump light direct into the fibre for the same gain value. The added broadening in the SMF, due to other effects, serves to increase the line width and further reduce the FWM efficiency by lowering the pump spectral density and therefore also reducing the Rayleigh backscattering of the mixed products, which travelled in the co direction with the pump, which would also impede the signal.

Attention is now turned to further investigating this FWM reduction technique. Staying with the counter propagating pump set-up in Fig. 5.25 experiments were carried out to explore the effect of gain level on the effectiveness of the SMF 'pre' fibre as a FWM reduction technique. Four gain levels were aimed for: 10, 12.5, 15 and 20dB which were referenced by the gain at a wavelength outside of the most affected FWM region, in this case to be 1553nm. The wavelength of tuneable laser was varied in steps of 1nm from 1530 nm to 1553 nm, across the FWM region with an output power into the LEAF fibre of 1dBm for each of the previous gain levels, with and without the 10km

SMF fibre present. The results are provided in the following figures where only a few wavelength steps are displayed in order to maintain clarity.

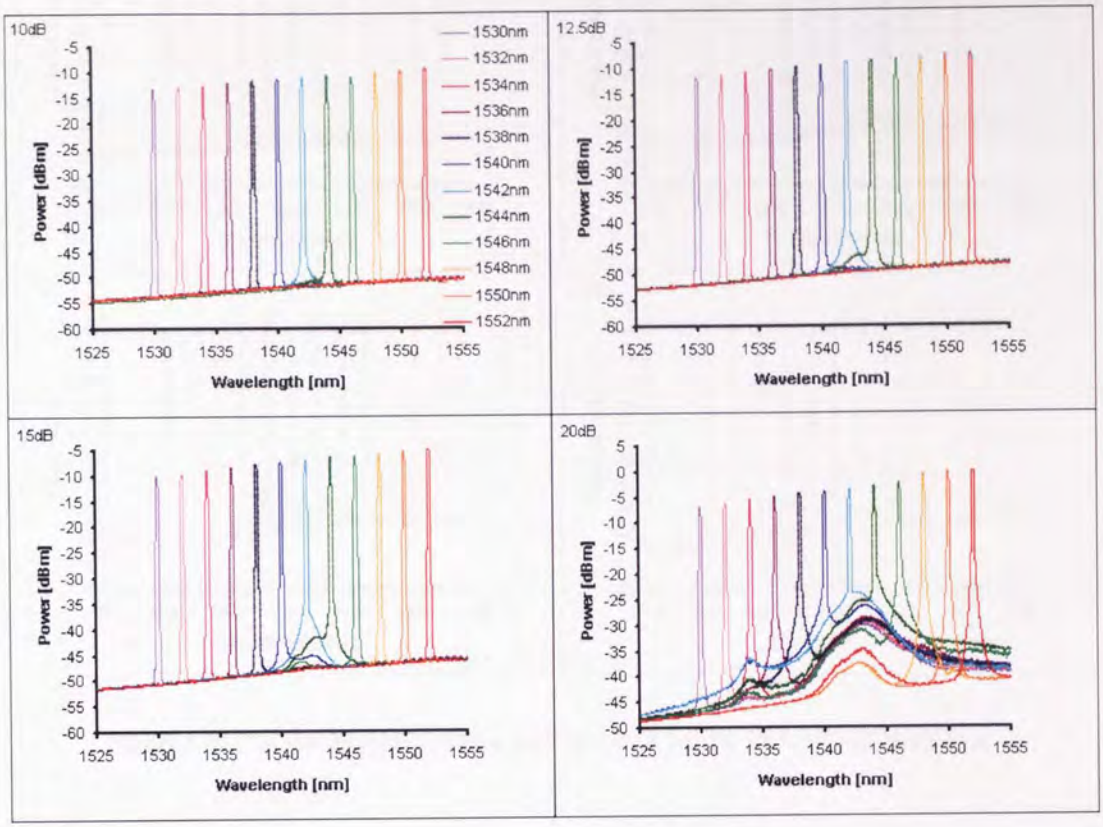

Figure 5.29 Counter pumped spectra with no pre SMF for 10, 12.5, 15 and 20dB gain

In Fig. 5.29 the degradation of OSNR with increasing gain is clearly visible for those channels in the FWM region, which can be considered to be most disrupted between 1533 and 1550nm. Looking at Fig. 5.30, utilising the 10km SMF after the pump unit, the same trend with increasing gain can be observed, but the degree of degradation and the bandwidth of the FWM region has been reduced. The FWM region is this case has been limited mainly to 1536 to 1546nm. These ranges can be seen also in the case of no signal by looking at the spontaneously generated spectrum as illustrated in Fig. 5.32. Fig. 5.31 clarifies the notable improvement the presence of the SMF makes on the OSNR (measured within a 1nm BW). Within the measurements taken here the improvement becomes more prominent with at higher gain levels.

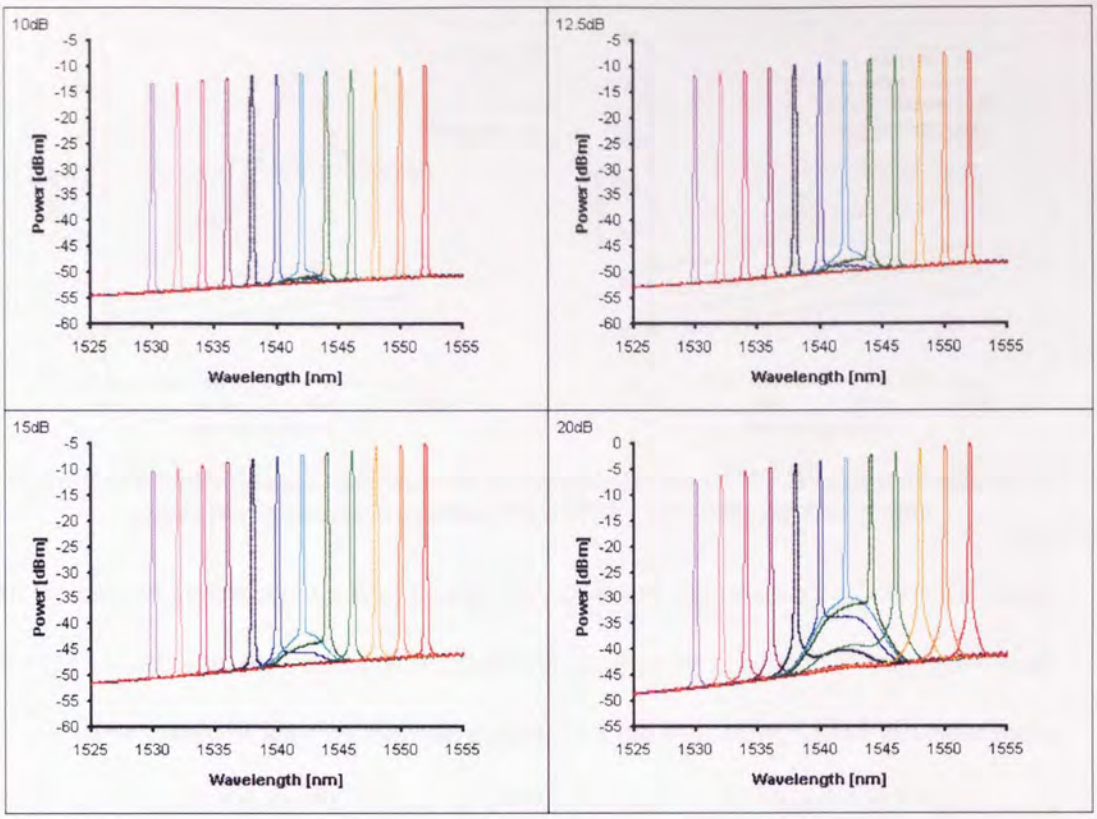

Figure 5.30 Counter pumped spectra with pre SMF for 10, 12.5, 15 and 20dB gain

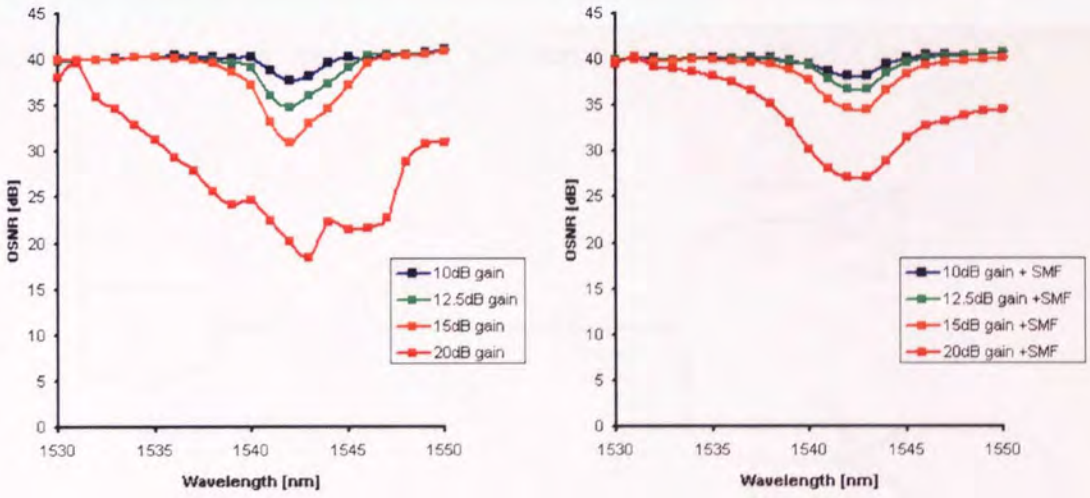

Figure 5.31 OSNR for each gain level and with/without the SMF pre fibre

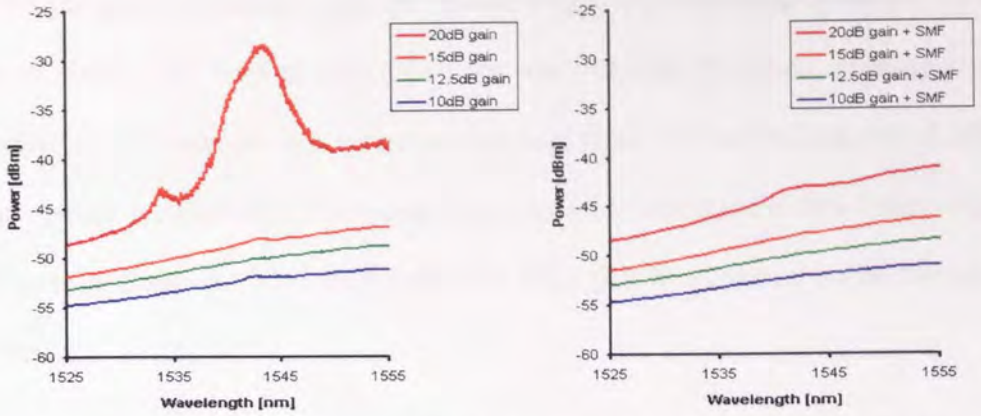

Figure 5.32 Counter pumped spontaneous/FWM spectra for the 10, 12.5, 15 and 20dB gain pump powers used when signal present. No pre SMF – left, With pre SMF – right

In the case of spontaneous/FWM spectra shown above the presence of the SMF makes a huge reduction to the size of the wavelength component generated in the signal band. From these results it appears that the presence of the 10km SMF fibre after the pump laser can indeed reduce the impact of FWM on light in the signal band when using LEAF fibre as the main transmission medium. However, these results refer to the counter propagating pump layout, so the next logical step would be to explore whether such a technique can be applied to the 'Co' propagating pump scenario, see Fig. 5.33.

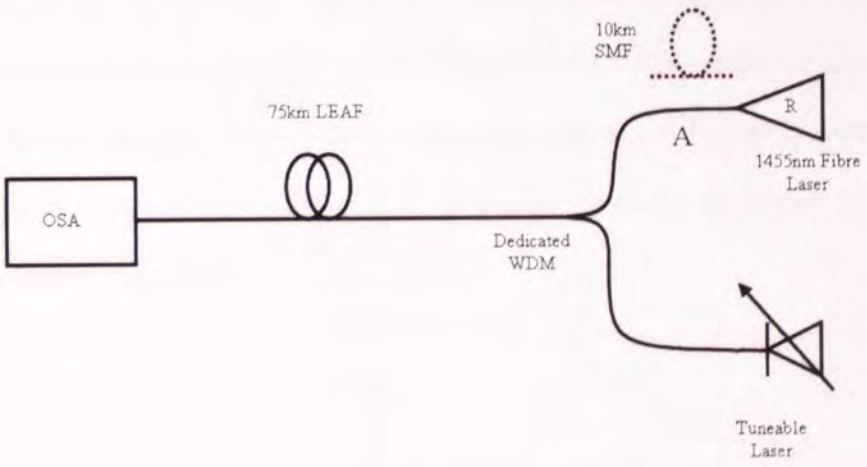

Figure 5.33 Co pump experiment for investigation of SMF pre fibre FWM suppression technique

The following figures present the outcome of sweeping the tuneable laser through the FWM region and the resulting degradation to the OSNR. Also presented are the pump

spectra for each wavelength step. As before, only every other step is shown for the sake of clarity. The level of gain aimed for was ~12.5dB @1553nm, once again the tuneable laser wavelength was varied in 1nm steps from 1530 to 1553nm with a 1dBm output power into the fibre. The pump laser was a 1455nm Raman fibre laser as used in Fig. 5.25. Light was attenuated before the OSA (RBW 0.2nm) to avoid damage to the device.

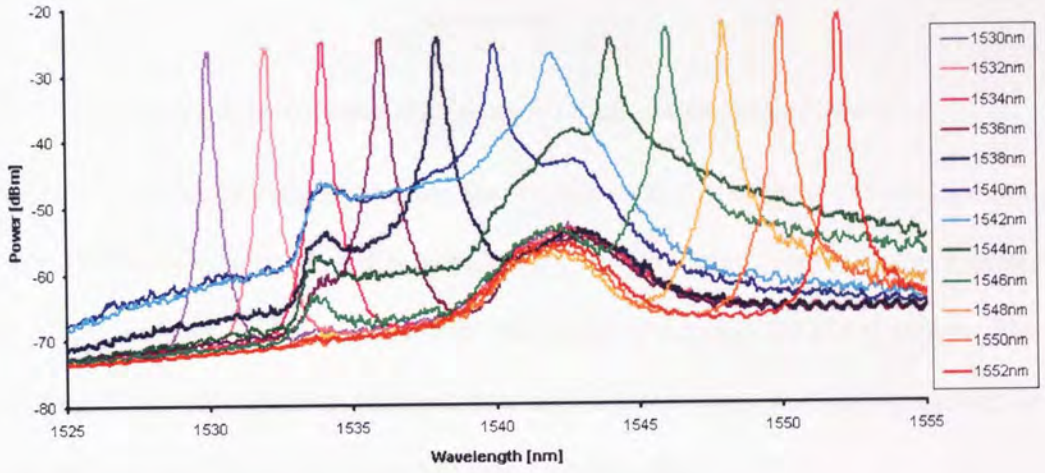

Figure 5.34 Investigation of Co pump in LEAF with no SMF pre fibre

Fig 5.34 shows the resulting output at different wavelengths stepped through the WDM region, after propagation through 75km of LEAF. The effective channels are highly distorted by the mixing with the pump light and this is further illustrated if the above figure is compared with Fig. 5.35 below, which shows the output after 75km with no Raman amplification.

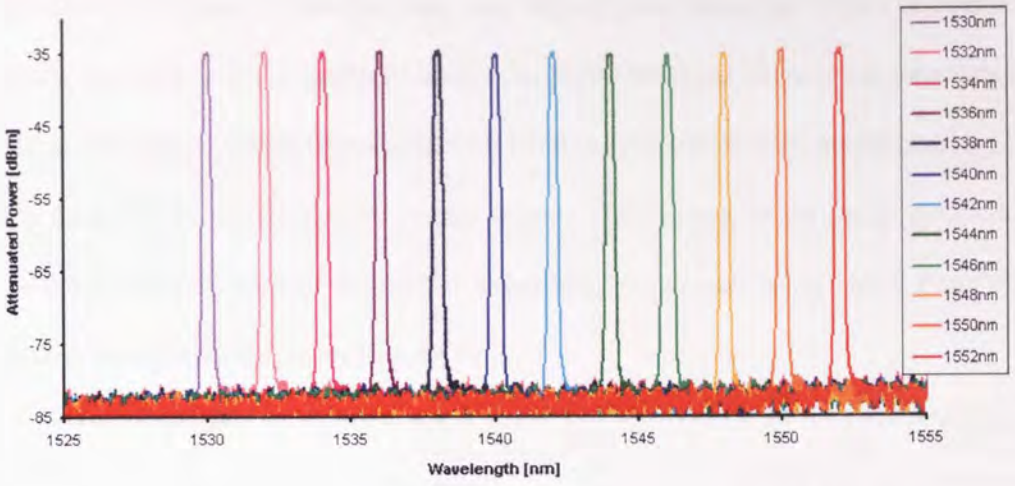

Figure 5.35 Investigation of Co pump in LEAF – output without Raman

It is now possible to fully appreciate the distortion to the original channel spectral shapes. It was also noticed, and is interesting to display here, that the pump spectral shape also changes as the tuneable laser was stepped through the FWM region. The following figures demonstrate this evolution as different mixing products are created in the pump region as result of the applied signal wavelength.

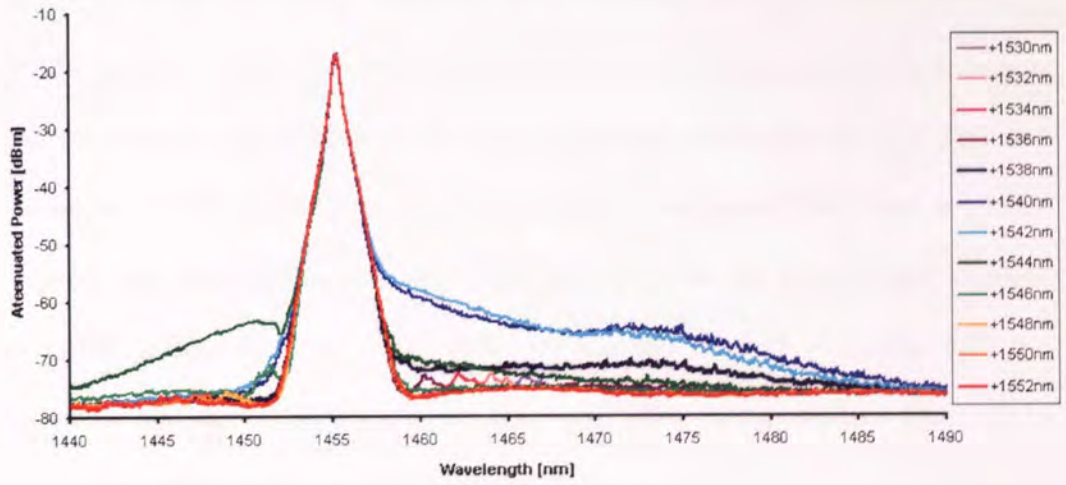

Figure 5.36 Pump spectrum for varying applied signal wavelength as in Fig. 5.34

The movement of the components from the longer wavelength side of the pump to the shorter one was very sensitive to the applied signal wavelength, which can be

appreciated in figure 5.35 as the laser was stepped in 0.2nm steps. These components are not generally a major problem within the pump band but if channels were present next to the pumps, which is possible with band interleaved Raman amplification [53], then their OSNR would also be compromised. This change in the pump noise floor was not previously seen in the similar experiment conducted using Fabry Perot (FP) lasers as the pump source (see Fig. 5.18).

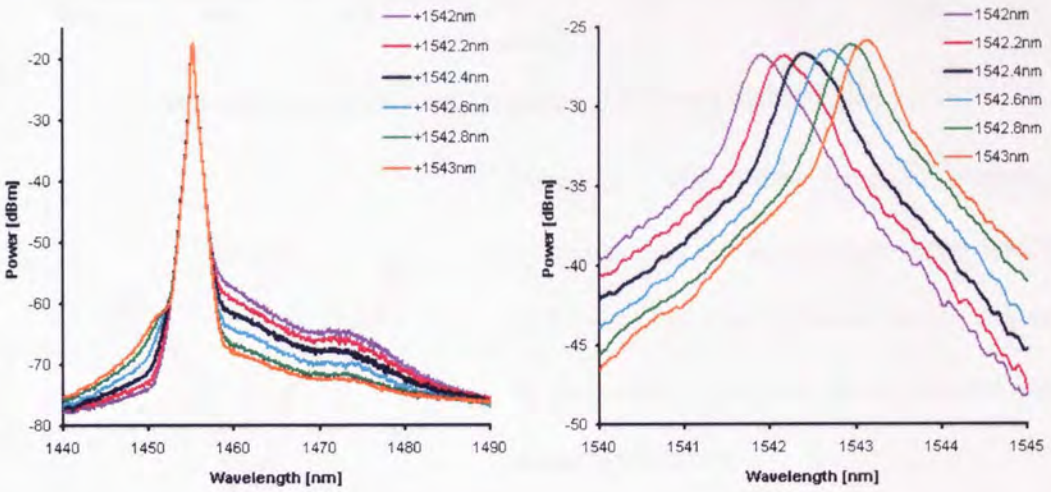

Figure 5.37 Signal stepped in 0.2nm steps with effect on mixing products in pump region

The OSNR of the worst affected channel in the case with Raman amplification on was 4.5dB at 1542nm, versus 46dB at the same wavelength for no Raman case. This is a phenomenal reduction and from the counter pump investigation and it was originally envisaged that the addition of a 10km SMF pre-fibre after the pump would improve this OSNR value. With the 10km SMF reel inserted at point A in Fig. 5.33 the experiment was carried out again to the same gain value used to produce the result in Fig 5.34. The result can be seen below in Fig. 5.38.

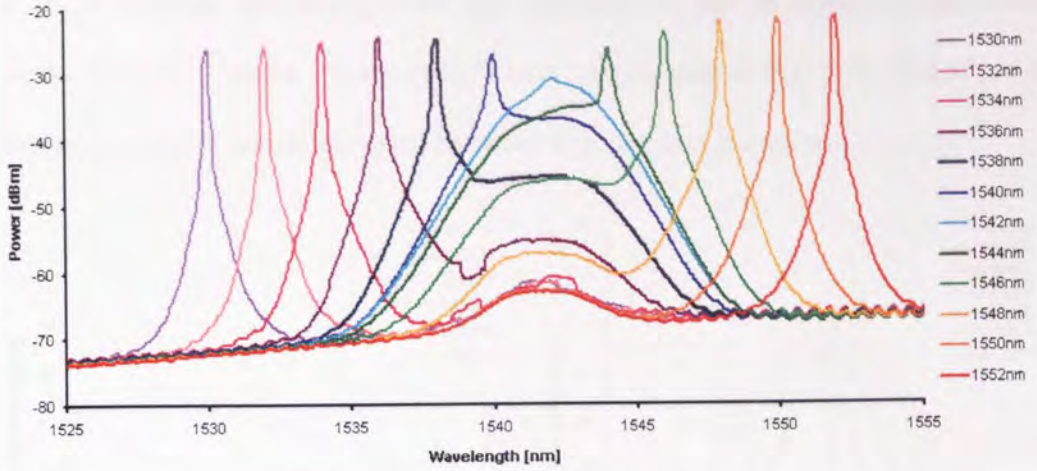

Figure 5.38 Investigation of Co pump in LEAF with SMF pre fibre

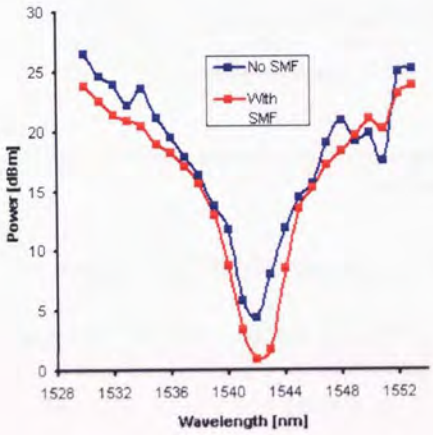

Figure 5.39 OSNR comparison for with/without pre SMF

Here, as with the counter pumping configuration, the wavelength range which is affected has been reduced but the degree of degradation has not been reduced but actually enhanced.

Comparing OSNRs with the standard Raman case we can observe that the addition of the SMF has reduced the OSNR further still to less than 1dB, see Fig 5.39. This throws open the idea that the SMF can de-correlate the pump modes and reduce the FWM efficiency as presented in [60]. In order to provide more insight to this outcome experiments were undertaken to see the result of:

- Having no signal present – spontaneous noise
- Varying pump power/gain
- Swept laser on the pump spectrum

Looking at the spontaneous/no signal case allows us to see how much of the generated bump is four wave mixing between pump and Raman ASE. This result is shown in

Fig. 5.39. Varying the pump power was employed to see its effect on the worst affected channel, 1542nm -shown in light blue with no gain in Fig. 5.40, and to see if there was a point in which the signal becomes engulfed into the noise.

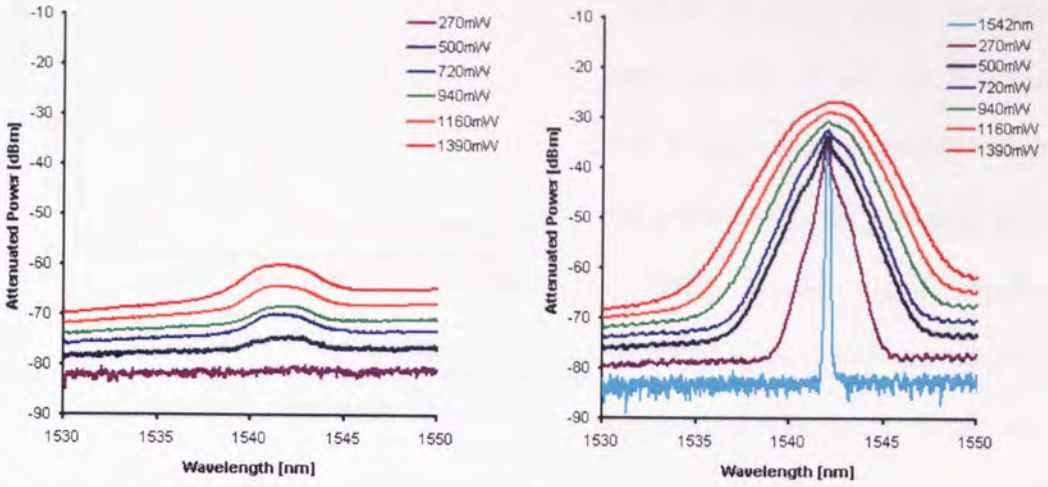

Figure 5.40 Investigation of Co pump in LEAF with SMF pre fibre spontaneous (left) and with increasing pump power (right)

The magnitude of the mixing product formed with ASE present is similar to that produced in the counter pumping regime so the annihilation of the signal at this wavelength is not due purely to a large pump/noise product. Looking to the right of Fig. 5.40 it can be seen that the presence of the signal makes a huge difference to the products' shape. Even with the lowest applied power of 270mW, which gave no noticeable pump/noise product, the signal has been reduced to an OSNR of ~10dB from the reference of ~46dB. Finally the effect on the pump spectrum was investigated. As shown in Fig. 5.41, unlike in the 'Raman only' case, there was no change in the pump spectrum as the laser was swept through the FWM region.

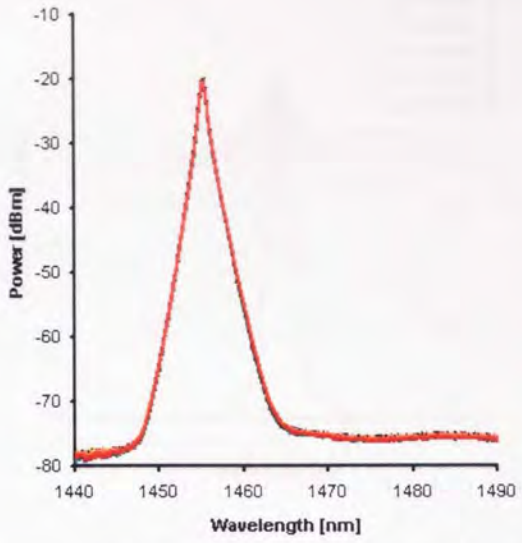

Figure 5.41 Signal stepped in 0.2nm steps with effect on mixing products in pump region with SMF

This may give some grounds for thought, for in the 'Raman only' case there were products appearing back in the pump region but here there are not. It may be possible that products that previously fell in the pump region are somehow now confined to the signal region, intensifying the OSNR degradation. Generally it is unclear as to why the addition of SMF improves performance in the counter regime but degrades signal performance in the co regime, it could possibly be a result of laser coherence and coherence length, which are a function of laser bandwidth. Does a broader pump only improve the performance in the counter pump condition? It was with this question in mind that further ideas were implemented to explore this concept.

To further this work, a broader pump spectrum than the one generated by the SMF was required. It is known that using a fibre with the right dispersion characteristics, a Raman pump spectrum can be broadened before entering the transmission fibre (see chapter 4 and [38]). By using this technique, another pump spectral width could be obtained. The fibre chosen was a 10km reel of TrueWave RS fibre. Using the same Raman fibre laser previously used as the pump source, the output could now be broadened to two different spectral widths/shapes depending on which end of the TW the light was launched into. This is depicted for a pump power of 500mW into the fibre in the following figure 5.42 along with the effect of increasing pump power.

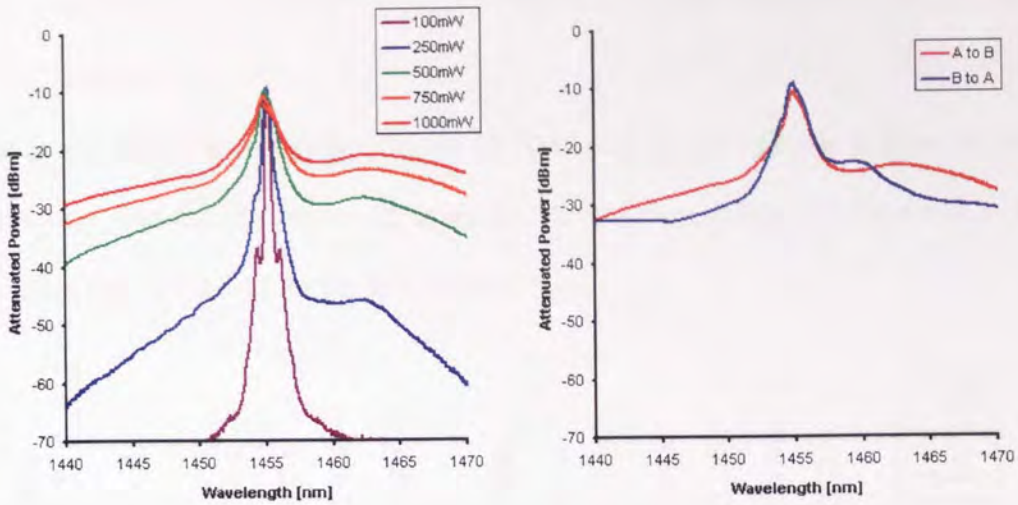

Figure 5.42 Output from 10km TW with increasing I/P power (left) and effect of pumping direction on 500mW I/P power (right)

The TW reel ends were arbitrarily labelled A and B to identify which pumping direction was being used. The fibre was inserted into the same experimental set-up as depicted in Fig. 5.33 at point A instead of the SMF reel, and a series of results were obtained, using the same techniques as in the SMF case, for four experiment variations:

1. No mitigation technique (i.e. Raman only)
2. With 10km SMF
3. With 10km TW-RS A to B direction
4. With 10km TW-RS B to A direction

The signal once again was generated from the tuneable ECL with a 1dBm output, swept from 1535 to 1550nm in 0.5nm steps (results presented here only display 1nm steps to aid clarity) and a gain level of 10dB was aimed for at the wavelength of 1550nm. Pump powers required to achieve this for each of the numbered variations above were:

1. 365mW
2. 700mW

3. 965mW

4. 905mW

The results for the Raman only case and the SMF case are very similar to those shown previously, whereas the new result using the TW is shown in Fig 5.43 for the A to B direction and in Fig 5.44 for the B to A direction.

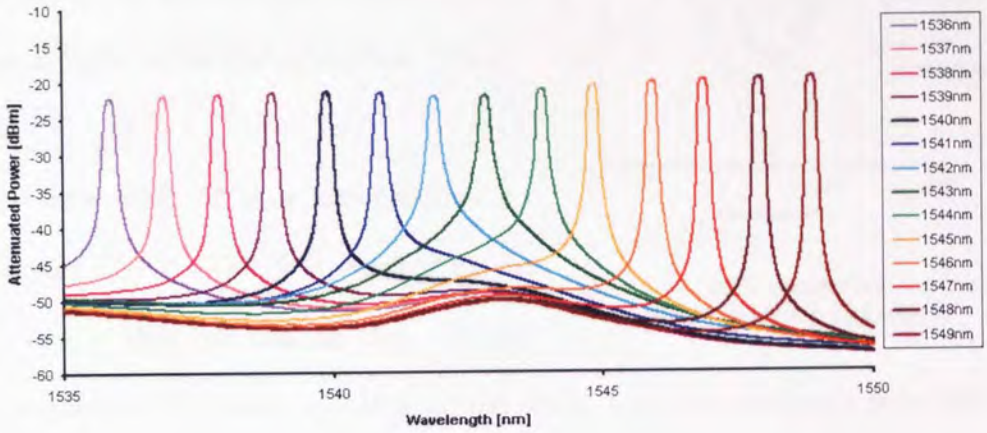

Figure 5.43 Co pump with TW pre fibre, A to B direction

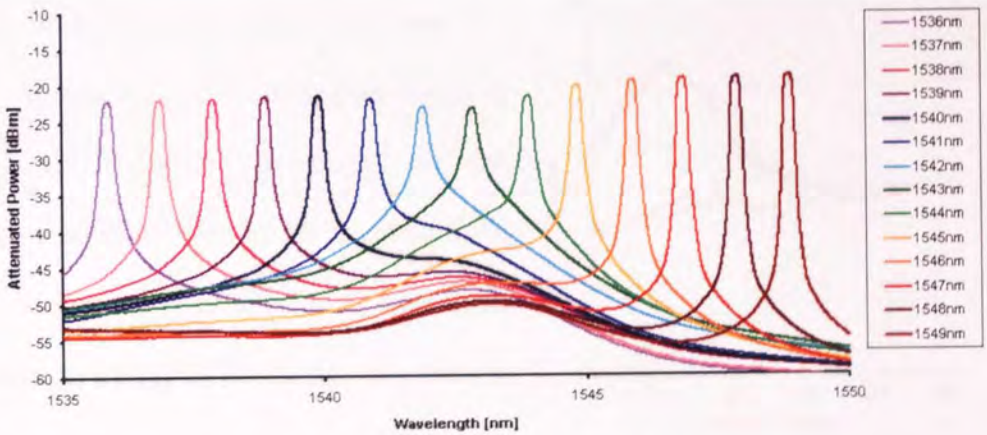

Figure 5.44 Co pump with TW pre fibre, B to A direction

From these two results it is instantly recognisable that the addition has improved the OSNR performance with respect to the SMF and Raman only cases shown previously. It can also be seen that the A to B direction provides a greater improvement than the B to A direction. Fig. 5.45 shows the OSNR comparison for all four variations, for all the

0.5nm steps that were actually measured – the value shown for the SMF and 'Raman only' instances vary slightly from those in Fig. 5.40 due to a lower gain level being utilised. The OSNR towards shorter wavelengths is lower for the TW cases due to the broadened pump light encroaching into the signal wavelengths; using a WDM with a higher extinction ratio could reduce this.

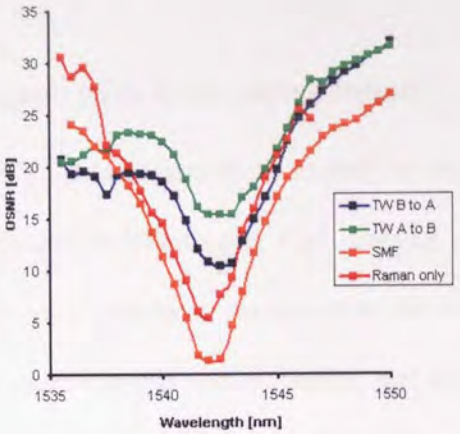

Figure 5.45 OSNR comparison for co pump FWM reduction techniques

This issue aside, if it is assumed that a minimum of 10dB OSNR is required for the recovery of data, we can see that, with the application of TW, some wavelengths that would have not previously been able to operate are now freed. The apparent trade-off is obtained in the wavelength range affected, which for the case of TW is larger than for the SMF and Raman only cases.

This is reflected in the width of the trough in Fig. 5.45. Another illustration of the improvement afforded by the presence of the TW is obtained by using a Broad Band Light Source as the signal, as in Fig. 5.24. Here a C-band EDFA was used with a total output power of ~7dBm. The result without TW and with it, for both directions, is given in Fig. 5.46. As before, a gain level of 10dB was aimed for at 1550nm for all cases, and the result is a massive reduction in the generated ASE peak. Although the co-pump situation has been discussed here, it is

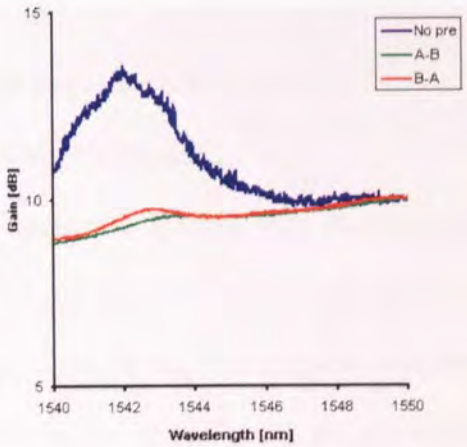

Figure 5.46 Gain comparison with BBLS used as signal source

worth noting that the TW works well in the counter configuration, producing a similar result to the SMF.

5.6 Effect of FWM mitigation techniques with data transmission

This section aims to explore the effect of FWM on data transmission as well as the effect of having a Raman pump on the zero dispersion wavelength, thus creating a more degenerate FWM case. Referring to the previous statement, results presented in this chapter are often categorised as Degenerate and Non-degenerate. Seeing that the lasers used have a non zero bandwidth, no case is purely degenerate and it is felt that these terms should be considered with the term 'partial' and with reference to each other. The motivation behind this section is to explore experimentally the results given in [57]. This reference states several findings, including:

- FWM can be reduced by the use of steep (higher extinction ratio) narrow pumps
- Broad pumps will produce a FWM Region that spans a larger range
- Broad pumps will produce a higher amplitude FWM peak

To investigate these statements a simple experiment was devised with the use of a semiconductor Raman pump module consisting of 10 pumps at 5 wavelengths, as used in Fig 5.3. Out of these 5 wavelengths, 2 were chosen for the investigation: 1452nm and 1496nm. 1452nm was chosen as this could be broadened using the technique discussed in the previous section, and 1496nm as it sits near the ZDW of the LEAF transmission medium, providing the partially degenerate case when propagating through the LEAF. The basic experimental setup is given in Fig 5.47.

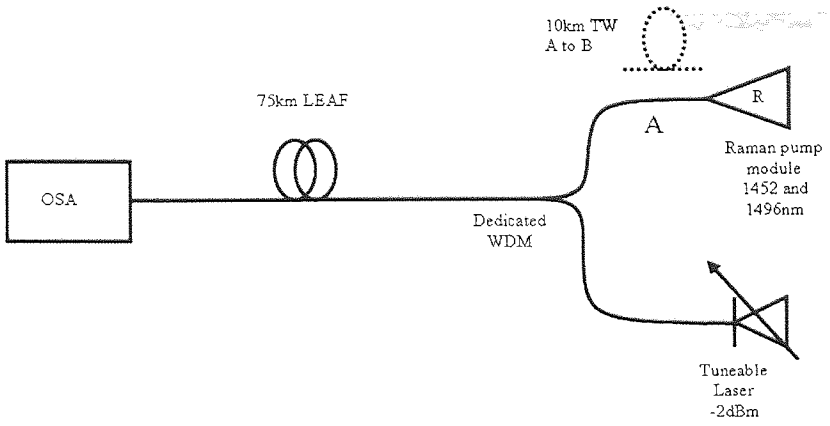

Figure 5.47 Experiment for investigation of degenerate and non-degenerate FWM and pump shape

Four variations of the experiment were undertaken:

1. Non-degenerate Raman only - 1452nm pump only
2. Degenerate Raman only - 1452+1496nm pumps
3. Non-degenerate Raman with TW - 1452nm pump only
4. Degenerate Raman with TW – 1452+1496nm pumps

The use of two pumps gave a gain spectrum that consisted of two peaks, one at ~1562nm and the other at ~1592nm. The gain at both of these peaks was equalised to the value ~5.3dB – limited by the power of the pump diodes and the loss through the TW (2.5 dB at 1455nm). For the 1452nm pump the only change in the operating conditions was the deactivation of the 1496nm pump – the 1452nm pump was run at the same drive current as when both pumps were operating. This leads, of course, to a small drop in the peak gain value and a drop of <1dB in the FWM region. The drop is small because even though the 1496nm pump adds gain at longer wavelengths, it also serves to deplete the 1452nm pump. Looking first at the pump characteristics in Fig. 5.48 it can be seen, on the left, that the addition of the TW fibre has broadened the 1452nm pump while the 1496nm pump is unaffected. The right hand side shows the spectrum from the pump unit for the pump values used for the Raman only case.

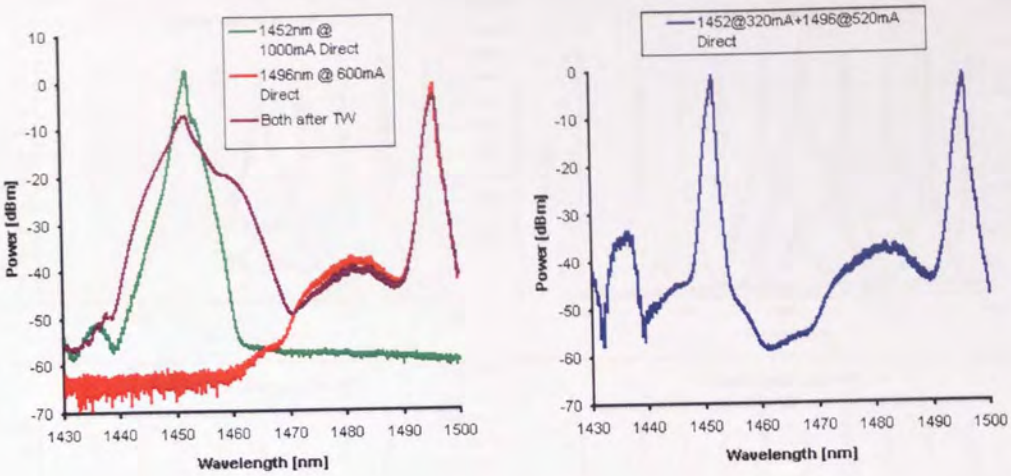

Figure 5.48 Pump spectra for with TW scenario (left) and without TW (right)

Pump powers into the transmission fibre were, for the numbering convention used previously:

1. 165mW (1452nm)
2. 165mW (1452nm) + 187mW (1496nm)
3. 266mW (1452nm)
4. 266mW (1452nm) + 120mW (1496nm)

Moving to the signal region, the tuneable laser wavelength was varied in 2nm steps from 1538 to 1550nm – the region most affected by FWM, for each of the set-up variations. In addition, the laser was set to the wavelength, which gave the lowest OSNR performance where necessary. The results of this can be viewed in Fig. 5.49.

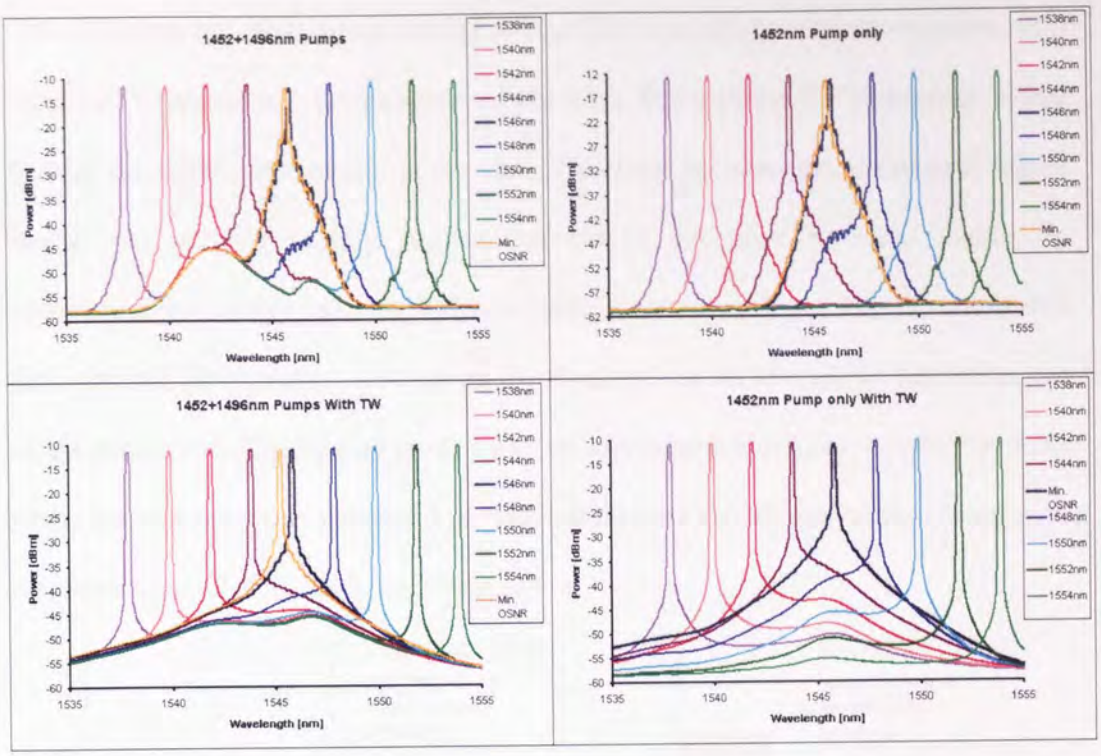

Figure 5.49 Results of wavelength sweep through FWM region under each operating condition

There are several interesting features to note here:

- The dual pump case produces a notably larger noise component in the signal band, which is independent of the wavelength of the signal, generated as a mixing product of the two pumps (refer to Fig. 5.16)
- The OSNR is slightly higher, despite this component, in the dual pump case than in the single pump case
- The signal suffers greatly from pump-signal FWM
- The single pump case has no pump-only mixing component independent of the signal wavelength
- The OSNR is lower in comparison to the dual/degenerate pump case despite there being less power/gain
- The OSNR for the dual/degenerate and the single/non-degenerate case is visibly improved by the addition of the TW reel after the pump unit

The difference in OSNR when looking at Fig. 5.49 is somewhat counter-intuitive, as it would be expected that the presence of the large Pump-Pump FWM product would destroy the OSNR in the dual pump case. This may become true if the peak signal power was reduced slightly further, but maybe explained to some degree by considering that energy from the 1452nm pump is not only mixing with the signal, but also with the other pump, therefore re-distributing it in an alternative fashion to the single pump case. This mixing product can be appreciated in a fuller way in Fig. 5.50, where the spontaneously generated product (no discrete signal) can be seen along with the minimum OSNR found in the FWM region.

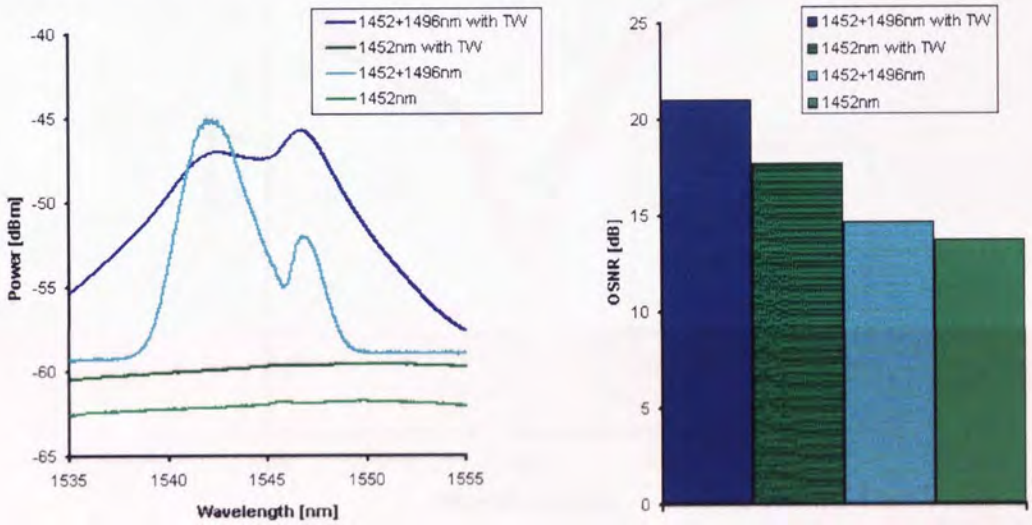

Figure 5.50 No signal mixing product (left) and minimum OSNR (right)

Referring to the left hand plot in Fig. 5.50, the product generated by the dual pump case with the TW present is indeed wider than for the Raman only case, as predicted by [57], however the peak magnitude is not higher than the Raman only case as suggested by [57], and is in fact actually lower. Staying with Fig. 5.50 and looking at the minimum OSNRs, it is seen that, regardless of which pump combination is used in the Raman only case, its OSNR is not better than when the TW reel is present, despite the noise floor being higher in single pump case due to pump-noise FWM.

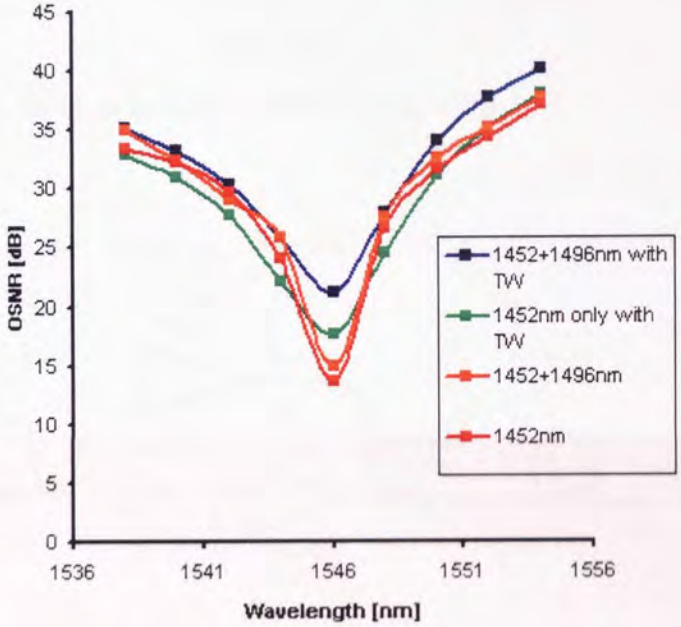

Figure 5.51 OSNR comparison for each experimental variation

Continuing with OSNRs, fig. 5.51 displays the variation across the swept range enabling analysis of the range of wavelengths affected by pump-signal interactions, in addition to the pump-pump interactions shown in Fig 5.50. Here it can be observed that the min. OSNR is improved by the TW for the single and dual pump scenarios, but away from the minimum point the OSNR for the single pump with TW is actually slightly lower over the FWM region when compared to the Raman only single pump variation. This is in agreement with the statement of a wider pump affecting more

channels, but in disagreement with the statement that the wider pump would also more severely degrade the worst affected channel [57]. For the two pump degenerate case the addition of the TW produces an OSNR that is equal and, generally, better than the Raman only case over the FWM region. It now appears that the addition of a TW reel can really improve performance in the FWM region in the co-pump direction where SMF failed; this may be due to the TW disrupting the pump coherence more than the SMF. Up to now, the signal has been a CW source. It is considered important to explore the FWM effect and TW mitigation when the signal is a true signal of modulated data.

The transmission set-up to investigate this is shown in Fig 5.52.

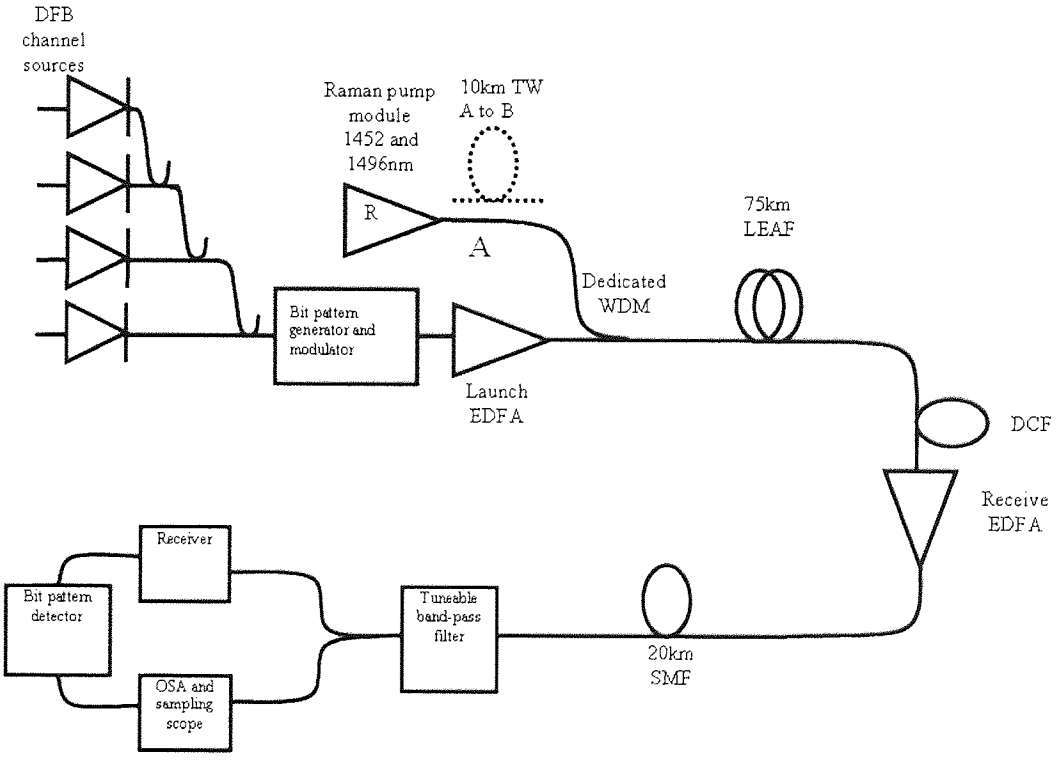

Figure 5.52 Transmission experiment for FWM degradation investigation

Four Distributed Feed Back lasers (DFB) were used as the signal sources and were set to the following wavelengths: 1539.9, 1545.4, 1546.7 and 1549.9nm. The first and the fourth wavelengths are there as reference channels just outside the FWM region, whilst

the other two were chosen to be around the worst affected wavelengths, whether the TW fibre was employed or not. The wavelengths were then coupled together using a 4:1 star coupler, then sent through a RZ transmitter which was fed data at 10Gbit/s from the bit pattern generator, creating pseudo random data with word length of 2^{31} bits. The encoded light was then sent through a launch EDFA, giving a total launch power of ~2.8dB. The data was then coupled with the co-propagating Raman pump into the 75km LEAF span. The span dispersion was compensated by a combination of DCF and 20km SMF trimming fibre. The SMF was placed after the receive EDFA. A tuneable narrow bandpass filter was used to demultiplex the channels, which were then analysed using a sampling scope, OSA and bit pattern detector. The EDFAs were set up so that the system would work without the Raman amplifier, meaning that any degradation in the BER would be due to FWM degrading the OSNR and not due to the signal falling into the noise floor due to loss.

The Raman amp was run in the same combinations as for the experiment in Fig. 5.47, in addition to another combination in which it was completely off. Measurements taken include Gain (measured before the receive EDFA), OSNR and BER for each channel and each system variation. These results are given in Fig. 5.53 and 5.54 below.

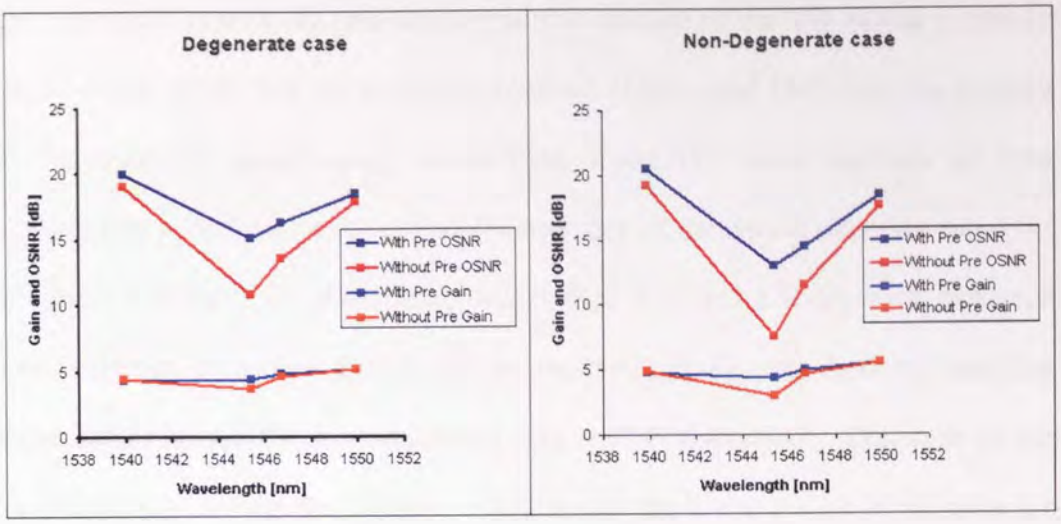

Figure 5.53 OSNRs and gain for Degenerate case (1452+1496nm pumps) and Non-degenerate (1452nm pump only)

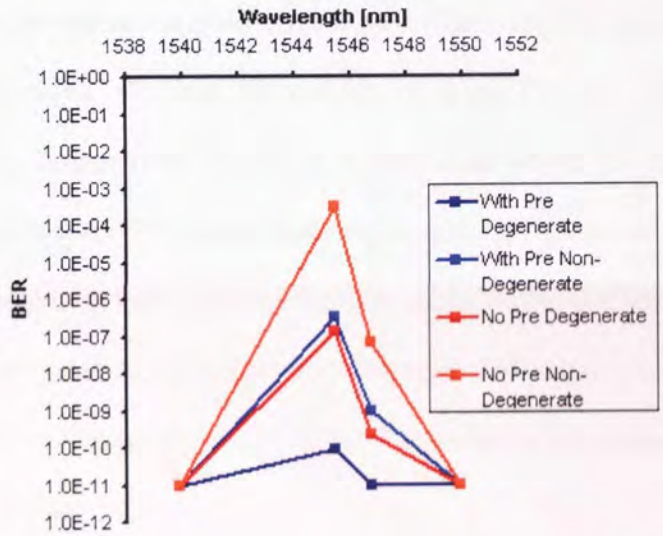

Figure 5.54 BER for each experiment variation

Like in Fig. 5.52, the OSNRs in Fig. 5.53 are lower when only the 1452nm pump is used (the case here referred to as non-degenerate) and there is an improvement in OSNR when the TW is present, especially at the worst affected channels.

Gain is also higher for the worst affected channels when the TW is used, because the in the Raman only (no pre) case the signal channel peak power is reduced by more efficient FWM than when the TW is used. Moving to Fig. 5.54 and focussing on either

the degenerate case or the non-degenerate, the addition of the TW makes a marked improvement on the two worst affected channels (1545.4 and 1546.7nm). In instance of the degenerate pump set-up, the addition of the TW brings channels up from considerably poor error rate to essentially error free (if the typical error free rate limit of 1.0E-9 is utilised). To give further insight, Figs. 5.55 and 5.56 show the measured spectra (before the receive EDFA) and the received eye diagrams from the sampling scope for the no pre/TW experiment and with pre/TW respectively. The noise on the 'ones' can be seen from the increase in thickness of the line at the top of the pulse for the two central channels. Particularly when no TW pre-fibre is applied, the eye for the 1554.4nm is much closed due to this. The 1554.4nm eye opens greatly when the TW is applied for the degenerate and non-degenerate case. These results, along with those in the preceding few pages, reinforce the viability of using TW as a FWM reduction device when using co-pumping Raman in a fibre span where the zero dispersion wavelength falls such that FWM components are seen in the signal band.

As a final note, comparing Figs. 5.55 and 5.56, the pump modes that can be seen in the noise in-between the channels have been reduced/smoothed in the scenario where the TW is utilised, demonstrating the ability of the TW to reduce the correlation between the pump and the signal.

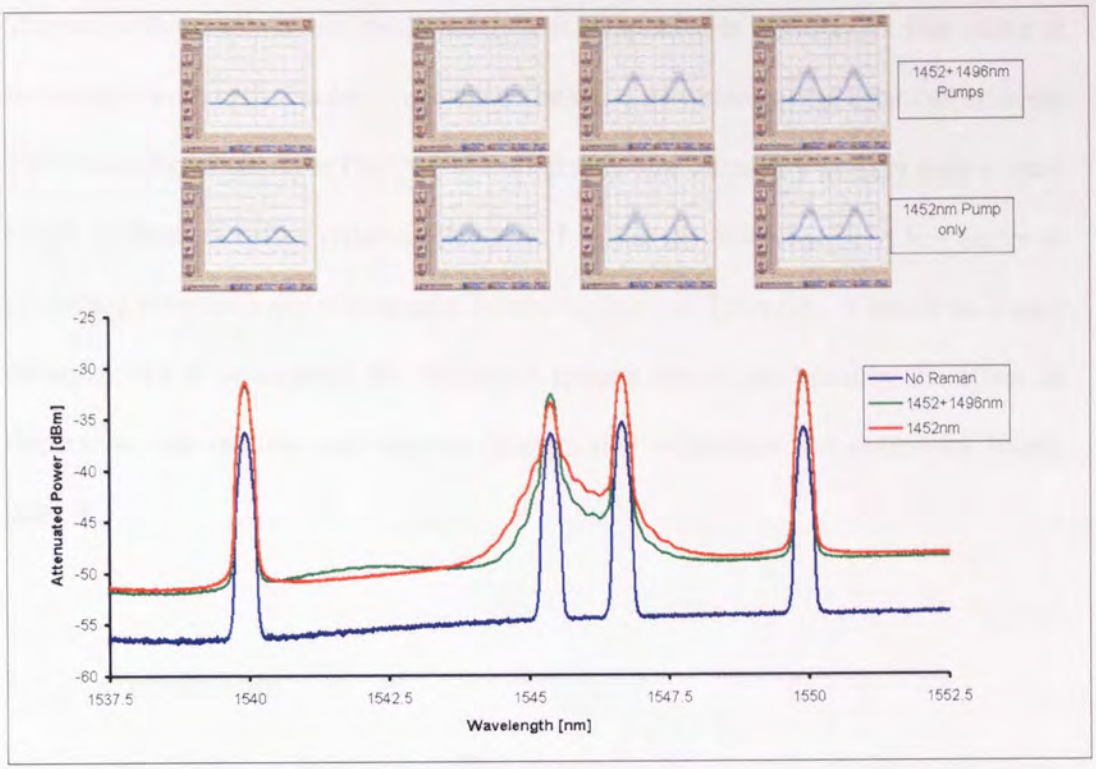

Figure 5.55 Spectra and Eye diagrams for the no pre/TW experiment

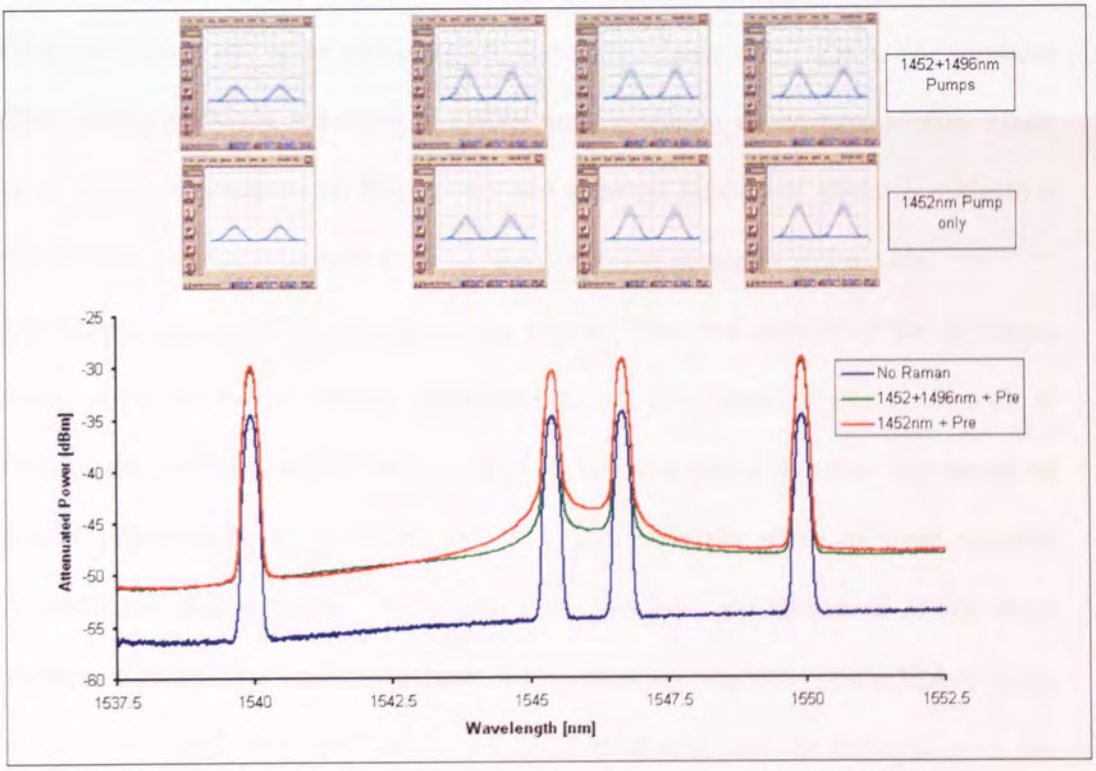

Figure 5.56 Spectra and Eye diagrams for the with pre/TW experiment

The major downside to this additional system component is the inherent loss added at the pump wavelength. Further work would be required to look at the effect of different TW fibre lengths upon the FWM, and it might become necessary to have only a short length of fibre, therefore reducing this loss. It is felt that coherence is a key factor in producing the results and effects seen within this section. Therefore, it would be highly advantageous to understand the mitigation process better and quantify the effect of dispersion, and relative and absolute pump/signal coherence and coherence length upon it.

5.7 Conclusions

Four Wave Mixing in Raman amplified systems is an effect which generates many implications, from pumps mixing with each other generating unwanted components in the signal region and in the pump region, to pumps mixing with signals. The resultant effects are generally a reduction in OSNR and disruption to the gain profile. Much work has been published on this subject and attempts have been made to mitigate it and recover the channel region lost to it, but issues and questions still remain.

This chapter has aimed to give an insight into the form and severity of the problems produced by the various mixing combinations that can occur, as well as to look at some of the possible ways to reduce them. It has also aimed to verify the results of several publications, in particular [57, 60], and highlight some of their possible shortfalls and discrepancies. The results presented here are indicative of the short comings of [60] as the work in question fails to mention, explicitly, the effect of pump broadening which may well be the responsible process and the limitations of the mitigation process portrayed. As a result, a new method of FWM mitigation was

employed in the form of a TW fibre, which can improve the signal performance in the co-pump direction where previous ideas of using SMF were unable to do so.

Chapter 6

Distributed Gain

6.1 Introduction

One of the largest advantages of Raman amplification is the way in which the gain provided can be distributed throughout a certain portion, the effective length of the transmission fibre, as touched upon in chapter 3. This distribution allows an improvement in amplifier noise figure over discrete amplifiers by allowing the signal to recover before its OSNR is depleted by approaching the noise floor and by allowing lower launch powers to be used and thus avoiding various non-linear effects as mentioned in chapter 2.

The area that the gain is given over can be at the end of the span, traditionally referred to as counter-pumping, or at the start of the span as in co-pumping and at both ends by combining co and counter pumping schemes. To enable gain further towards the centre of the span further techniques must by employed such as higher order pumping where a pump laser provides gain to another pump laser and then onto the signal.

This chapter aims to provide an experimental illustration of how a signal evolves along a Raman amplified transmission line when various pumping schemes are employed such as co, counter and bi-directional pumping. It then moves onto how gain can be provided along the entire length of a transmission fibre, effectively producing a quasi-lossless fibre. Application of such a fibre as a data transmission medium is investigated along with the use of co, counter and bi-directional pumping to help generate self-similar parabolic pulses. Finally a brief note is made in reference to RIN noise transfer from pump to signal especially in the co-pumping direction.

6.2 Advantage of distributed gain

The main advantage of distributed gain is the improvement in noise figure over a discrete lumped amplifier. The noise figure of an amplifier is the ratio of the output signal SNR to that of the input signal SNR and can be considered as a measure by how much an amplifier degrades the signal. The improvement in noise figure can be interpreted by using an 'effective' or 'equivalent' noise figure. From [5], this is the noise figure that a fictitious discrete amplifier would need when following an unpumped span to give the same noise performance as a distributed Raman amplifier. Also, the gain of the effective amplifier must be equal to that of the on-off Raman gain case so that it performs as an equivalent pre-amplifier to any following amplifiers. A visual representation, adapted from [5], is given in Fig. 6.1.

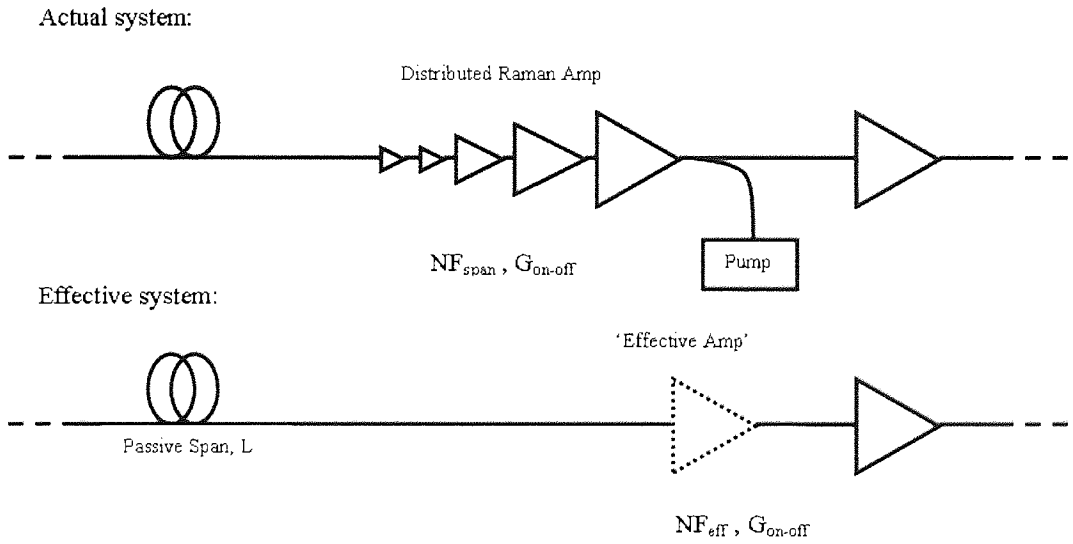

Figure 6.1 Actual and 'Effective' system for Raman counter pumping. Shows the fictitious pre-amplifier with gain $G_{on\text{-}off}$ and noise figure NF_{eff} that follows the unpumped span with length L

For a cascaded chain of amplifiers the total noise figure is given by [5].

$$NF_{total} = NF_1 + \frac{NF_2 - 1}{G_1} + \frac{NF_3 - 1}{G_1 G_2} + \ldots \qquad (6.1)$$

Where NF_i and G_i are the noise figure and net gain (in linear units) for the i^{th} amplifier in the chain. Equation 6.1 shows that the total noise figure is dominated by the noise figure of the first amplifier if its noise figure and gain are sufficiently high. Referring to Fig. 6.1 the effective noise figure can be found by equating the noise figure of the two configurations. From (6.1) the noise figure of the Raman pumped fibre span (NF_{Rspan}) equals

$$\begin{aligned} NF_{Rspan} &= \alpha L + \frac{NF_{eff} - 1}{\frac{1}{\alpha L}} \\ &= \alpha L \times NF_{eff} \end{aligned} \tag{6.2}$$

Where αL is the passive span loss and all quantities are linear units. In dB the noise figure required by the effective amplifier is

$$NF_{eff}(dB) = NF_{Rspan}(dB) - \alpha L_{dB} \tag{6.3}$$

From (6.3) it is seen that NF_{Rspan}(dB) can be less than zero [26], such an amplifier is not physically possible but is indicative of the superior performance achievable from distributed Raman amplification which cannot be attained from placing a discrete amplifier at the end of the span. A basic explanation is that amplification always adds noise to the signal, which degrades the OSNR. In the ideal case the signal travels via a lossless fibre and therefore requires no amplification, in this case the input OSNR is equal to that of the output resulting in a noise figure of one. In the opposing worse case the signal experiences the full loss of the span before receiving amplification. In this case the gain required from the amplifier at the end of the span has increased, to achieve this more pump power is required and therefore more ASE is generated from within the amplifier, at the same time the input power to the amplifier has decreased. This lower input signal power results in the ASE being more successful when competing with the signal for gain. These two mechanisms combine to considerably

reduce the OSNR at the output resulting in a larger NF. If distributed gain is considered as a chain of discrete amplifiers along the fibre, then less gain is required by each amplifier, reducing the ASE generation, and the input signal into the next amp will be greater, reducing the ASE competition. This explains why distributed gain improves performance and why improving a distributed gain technique like Raman by higher order pumping improves the performance further. To further understand how the distributed gain can reduce the signal-spontaneous beat noise it is useful to study the two abstract system configurations in figure 6.2, adapted from [5].

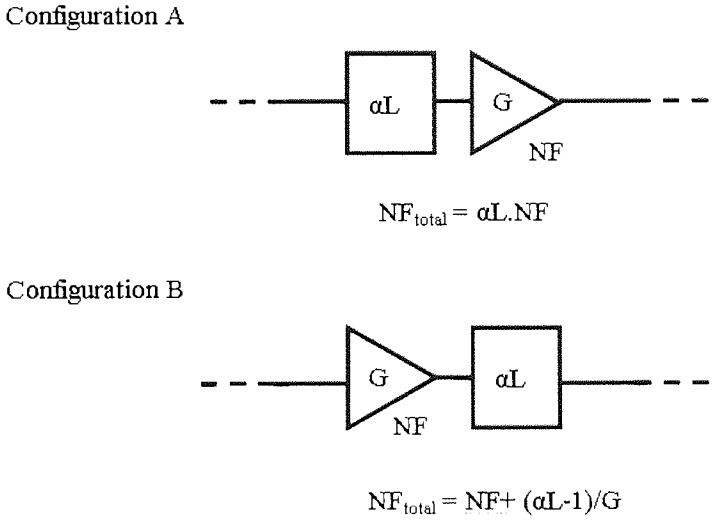

Figure 6.2 Two abstract configurations A and B where a loss element αL is placed either before or after a discrete amplifier. Noise figure expressions are for linear units

Here a loss element (αL), typically a fibre, is inserted before (configuration A) or after (configuration B) an amplifier (G, NF). The total noise figures shown are in linear units. Entering some numbers for illustration, NF = 3dB and G = αL = 20dB, configuration A has a total NF of 23dB and configuration B has 4.8dB. in configuration B the signal and ASE are attenuated equally together but in configuration A only the signal is attenuated therefore resulting in a reduced OSNR.

The effective noise figure is fairly easy to interpret when conventional counter-pumping is employed but is more difficult to comprehend when co-pumping is used, as the gain now occurs at the other end of the span to where the effective amplifier is placed [5]. Considering figure 6.2 it can be seen how moving all the gain to the front of the span would improve the noise figure further especially when the span is pumped to transparency ($G = \alpha L$). However, this noise improvement is not so clear cut, the problem with moving all the gain to the front of the span is that the signal power becomes very large which can quite possibly give rise to other nonlinear effects from chapter 2.

6.3 Experimental Measurements

If the aim from the previous section is to obtain continuous gain distribution then techniques to provide this must be devised as well as methods to verify, experimentally, the result. There have been several studies on the measurement of gain distribution [62, 63, 64, and 65] all feature the same essential component, an OTDR device. Utilising the technique detailed in [62] a system was set-up to measure the gain distribution of a Raman pump/amp for a selection of pump powers for co, counter and co+counter pumping. The system used is illustrated in Fig. 6.3.

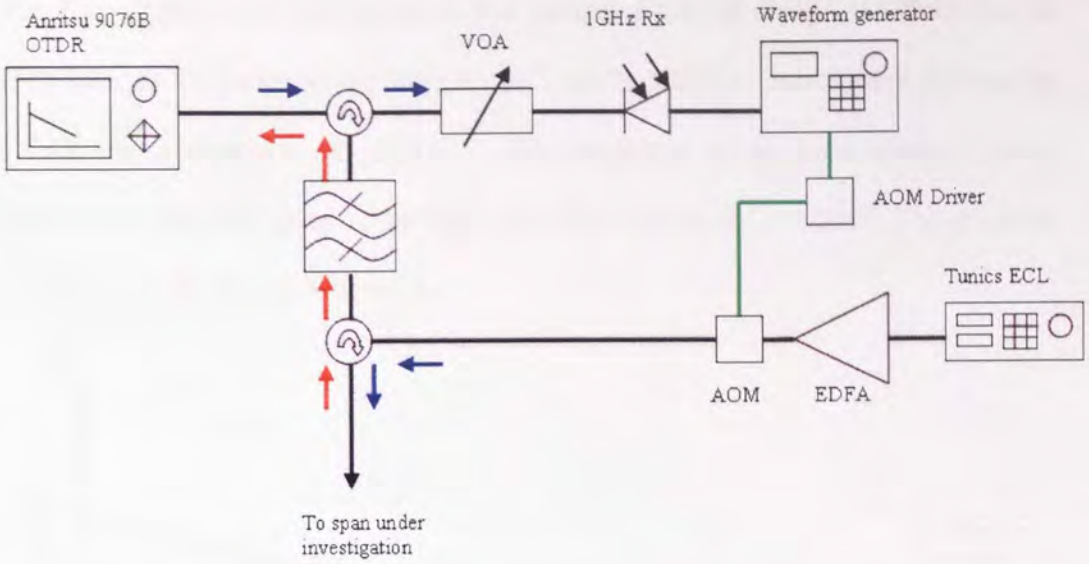

Figure 6.3 System for measurement of distributed Raman gain

In this system the OTDR sends out a measurement pulse which passes through the circulator into the VOA which is there to protect the photo receiver. The photo receiver converts the optical pulse into an electrical one; this pulse is then cleaned up by the waveform generator and fed into the AOM driver which modulates the AOM with the same pulse width and frequency as originally launched from the OTDR. The AOM in turn modulates the EDFA amplified output of the ECL which has gained a broad ASE base, allowing the OTDR to operate. This new OTDR pulse is then moved through another circulator and then into the span under test. The back-scattered pulse is then sent through the circulator and a narrow band-pass filter to remove unwanted Raman ASE. The filtered pulse is then moved back through the first circulator back into the OTDR. An advantage of this configuration is the ability to see the distributed gain for varying signal wavelengths. For high pump powers it was found to be necessary to place an attenuator after the filter in the return path in order to avoid the OTDR giving a return loss error.

The first amplification configuration was counter pumping using a 1455nm Raman fibre laser as the pump source with the ECL set to 1550nm, pulses were rectangular 500nS with a repetition rate of 1KHz. The pump was set to three arbitrary power levels, 120, 240 and 500mW, the fibre span was ~84km of OFS SMF. The resulting OTDR traces are shown in figure 6.4.

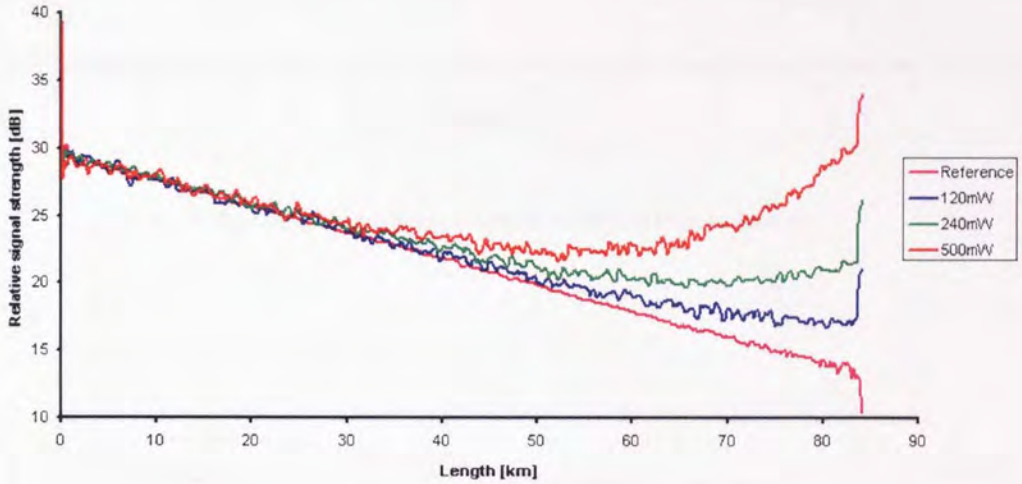

Figure 6.4 Experimental signal evolution with counter pump

The experiment was then repeated using the fibre laser in the co-propagating configuration, the result of which is in Fig. 6.5. The bi directional configuration was then implemented using another 1455nm Raman fibre laser as the counter propagating pump, the pump powers used were equal for the co and counter direction pumps, Fig. 6.6 provides the outcome. The pump powers for these two configurations were set to be the same as those used in the counter result, namely 120, 240 and 500mW.

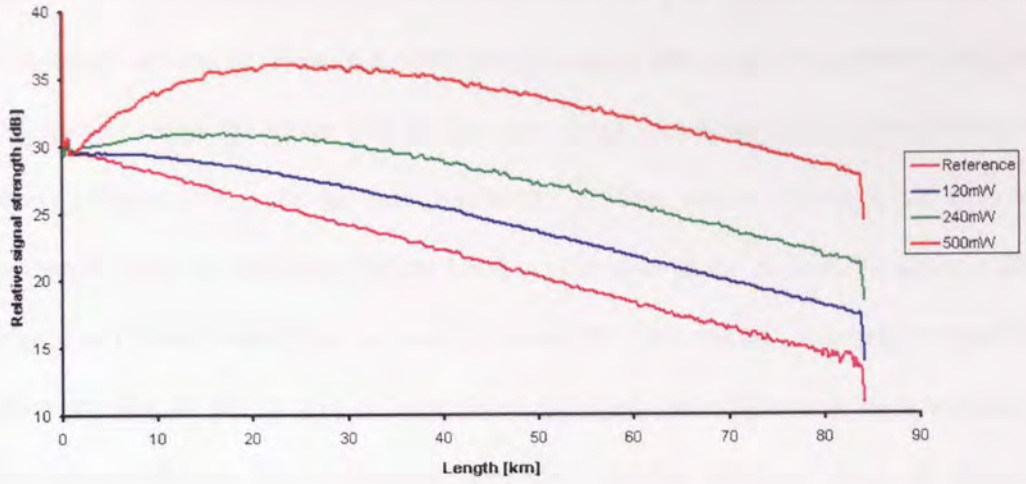

Figure 6.5 Experimental signal evolution with co pump

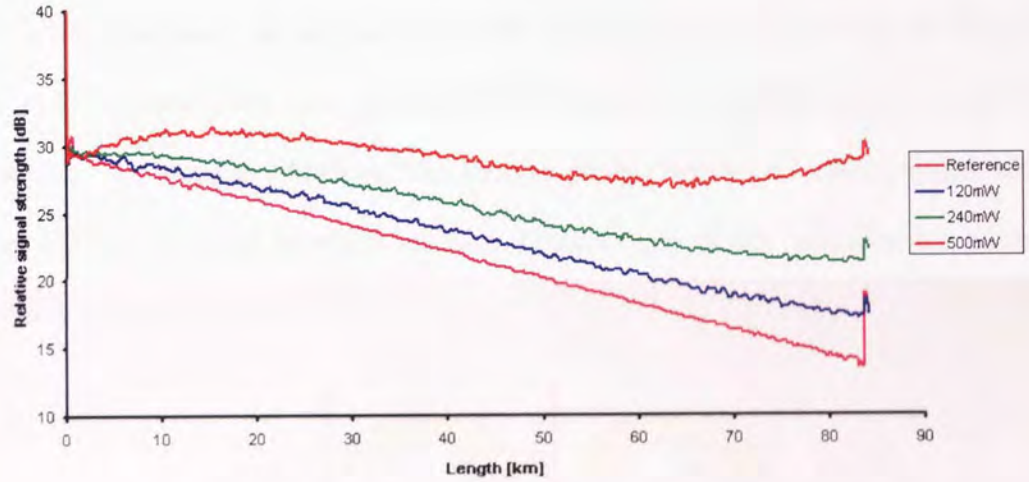

Figure 6.6 Experimental signal evolution with co and counter pump

The experimental results are as typically expected from a Raman amplified span. In the counter pump case the signal strength increases as it approaches the end of the span, with the co pump the signal increases initially away from the start of the span then declines at the rate of the intrinsic fibre loss after about 30km depending on applied pump power. With the bi-directional pump the signal exhibits a combination of the co and counter pump traits. With the bi-direction case (or co and counter pump) the signal can be seen to stay reasonably constant throughout propagation. This clearly illustrates

that bi directional pumping can move us towards the goal of near constant signal as mentioned previously. However, with both pumping directions in operation the gain still fails to reach the centre part of the span tested where the loss gradient from the intrinsic fibre loss can still be seen, around the 30-50km region. The next step is to try and move gain into this area without breaking the span in the middle. To achieve this lengths of Erbium doped fibre have been spliced in to the line and remotely pumped by either the Raman pump [66] or by a dedicated pump laser delivered via a dedicated low loss/low Raman gain coefficient fibre [66]. Another technique is to use what is commonly referred to as higher order Raman pumping [26] where another pump laser of different wavelength, dictated by the Raman shift, is launched together or in the opposite direction to the original pump. For example if gain was required for a signal at ~1550nm then a first order pump would be required at ~1360nm to provide gain to second order pump at ~1455nm. The 1360nm pump could be launched together with the 1455nm or in the opposite direction. The principle of this 'pumping the pump' basically displayed in Fig. 6.7.

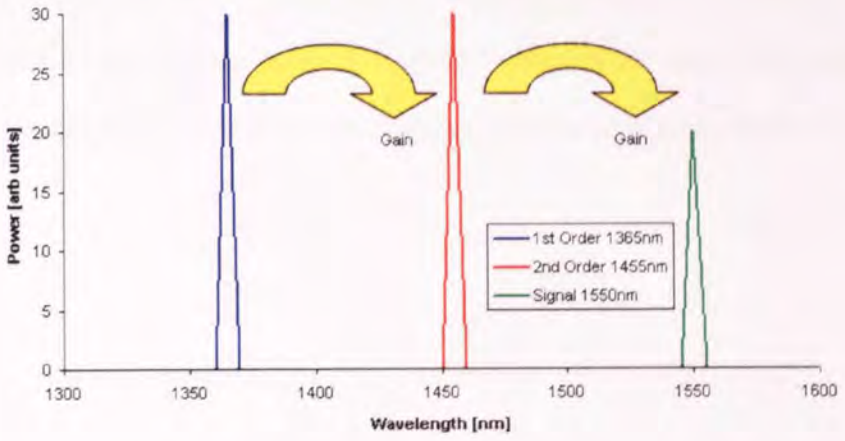

Figure 6.7 Basic illustration of the dual gain transfer in second order pumping

To investigate this, the following pump set-up (Fig. 6.8) was established to look at the effect on a co-pumping configuration using the modified OTDR as before.

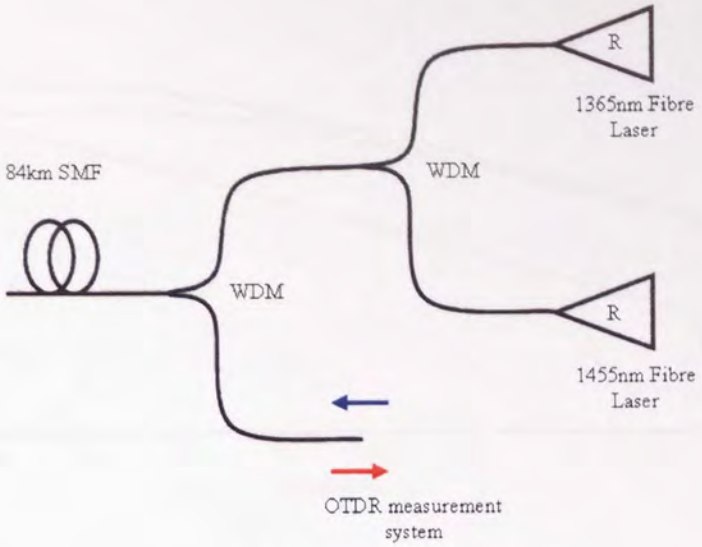

Figure 6.8 Dual order co-pump configuration

A nominal gain value of 8dB was chosen, the 1455nm pump was run by itself to achieve this value and the resulting gain distribution was recorded. Next, the 1365nm pump was employed along with the 1455nm to give the same gain. It was seen that the most noticeable difference in the gain distribution was apparent when the 1455 was set to a minimal value with the 1365nm pump at a much higher value, this allowed the 1455nm pump to act as a 'seed' for the shorter wavelength. By doing this the effectiveness of the 1455nm pump is delayed to later in the span. The comparison between the reference, 1455nm only and the dual pump case is given in Fig. 6.9.

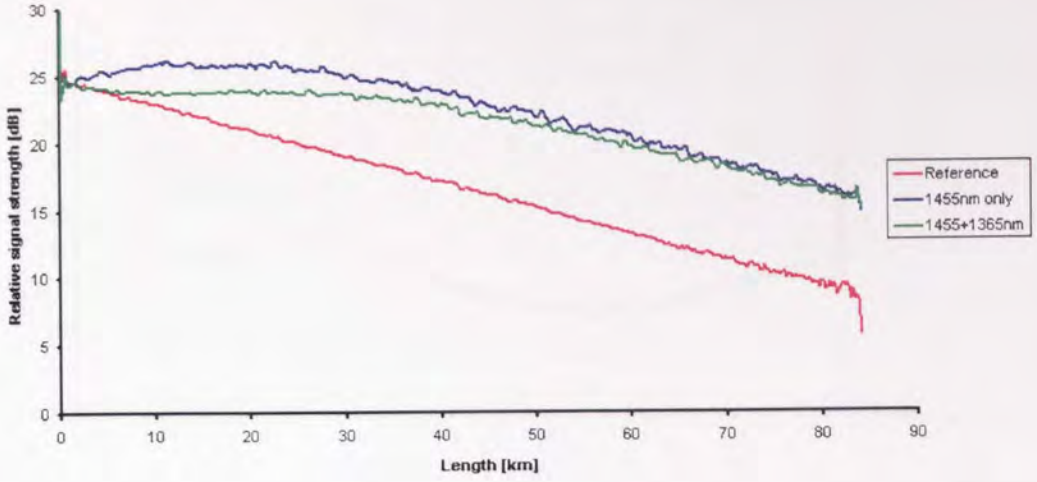

Figure 6.9 Comparison between single and dual order co-propagating pump

For the single order/1455nm only case the pump power was ~240mW and for the dual order/1365+1455nm case the 1365 power was ~500mW with ~20mW from the 1455nm pump. These powers were into the main transmission span. By using second order pumping we can achieve the same gain level as first order but from Fig. 6.9 it can be seen that this gain has been moved further into the span as the green trace does not assume the intrinsic loss slope until later in the span. It is important to note also that the second order scenario does not give rise to a significant increase in signal power over the original launch power. This result is of interest when a large launch power is used, single order pumping here provides a net increase in signal power which may force an already high signal power higher and therefore give rise to detrimental non-linear effects. The dual order case may avoid these non-linear effects by keeping the signal power below the effects threshold. It is also interesting to note that for the first 30-40km of the span the signal power has been kept near constant when the dual order pumping has been used thus moving the goal of constant signal power closer. The next step to attempt would be the application of dual order pumping in the co and counter direction, the result of which is given in Fig. 6.10.

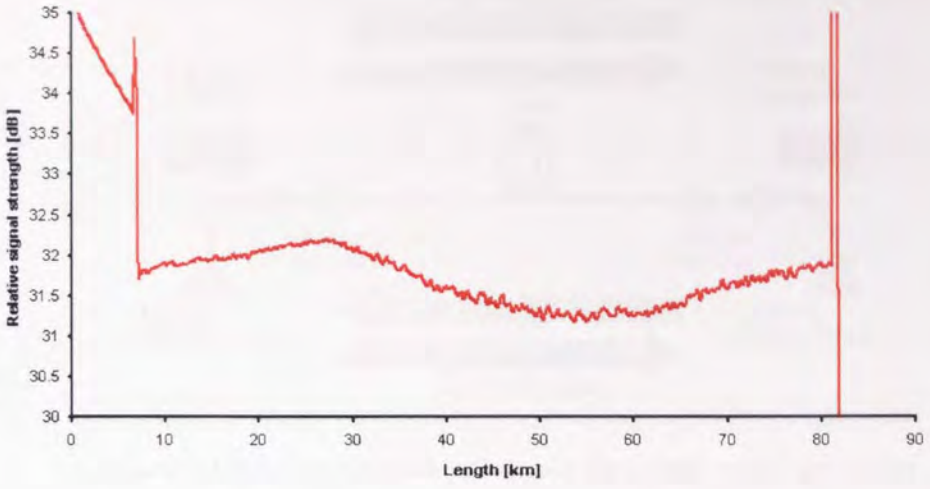

Figure 6.10 Bi direction second order pumping 1550nm signal variation

To improve the clarity of the result across the transmission fibre a 6.7km reel of SMF was placed before the transmission fibre, removing the OTDR 'dead zone' region. Here the total signal variation has been reduced, for the whole span, to just under 1dB.

6.4 Single wavelength pumped quasi-lossless system

The dual order quasi lossless transmission configuration mentioned at the end of the previous section utilised four pump lasers to achieve the published result. It was proposed theoretically by [67] that only two pump lasers, of the same wavelength, may be necessary to provide a similar second order quasi-lossless Raman pumped span as in [68]. This can be achieved by having the pump lasers at the shorter wavelength, say 1365nm, and placing reflective fibre Bragg gratings at either end of the fibre span to be amplified. The system layout and process is best understood by referring to Fig. 6.11 below.

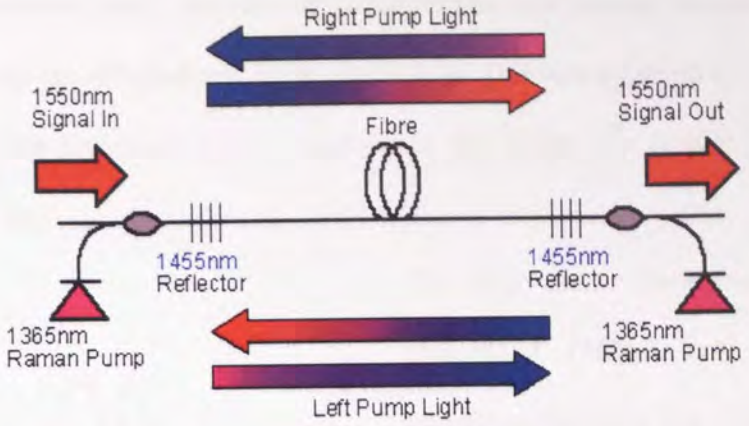

Figure 6.11 Second order quasi-lossless span using single wavelength pumps

The system comprises of seven key components:

- 2 x 1365nm 1.5W Raman fibre lasers
- 2 x 1365/1550nm WDM
- 2 x high reflectivity ~99% narrow band fibre Bragg gratings
- Transmission fibre – arbitrary

Referring to the figure, the 1365nm pump light is coupled into the span via the WDM; it then passes through the FBG into the transmission fibre. As the 1365nm light propagates towards the other end of the fibre span it converts to ~14xxnm via the Raman Stokes shift. This 14xxnm light reaches the grating at the opposite end where the 1455nm component is reflected; this 1455nm component receives gain from the 1365nm pump at that end of the span and grows to a higher power. As the 1455nm light grows it serves to stimulate the gain in the 14xxnm region thus depleting the 1365nm pump and growing larger still to the point where it creates gain around 1550nm. This process is repeated if the other 1365nm pump is considered first and by inspection it is possible to understand the principle of many interactions between the 1365nm discrete pump light, the generated 1455nm pump light and the 1550nm gain/signal.

Initial experiments were carried out to determine the correct choice of grating wavelength and the effectiveness of the built FBGs. This was achieved by pumping the fibre span with the lasers at high power to see where the largest spontaneous components lay.

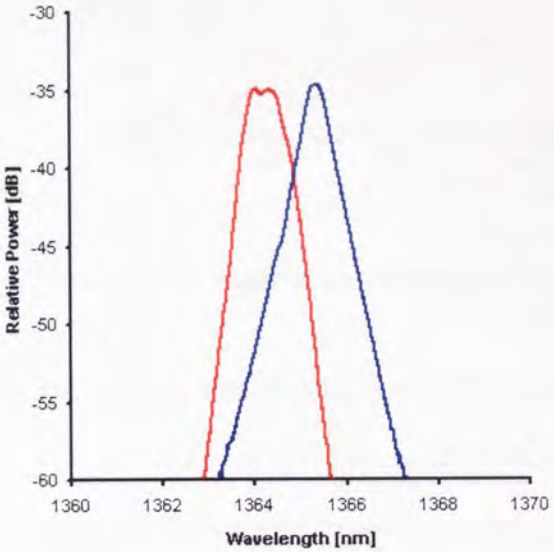

Figure 6.12 Pump laser spectrum for each laser at similar power

The fibre lasers themselves were not exactly at 1365nm but around this number as shown in Fig. 6.12. When the lasers were operated at high powers, say 500mW+ dominant spontaneous peaks formed in the 1400 region, as measured by an OSA at one end of the span, as there was an offset between the two pump lasers there was also an offset between the spontaneous peaks formed from the first Raman shift. These two peaks and there relative offset can be appreciated in figure 6.13. Mid way between these two peaks is approximately 1453.3nm and this was the requested wavelength for two high reflectivity FBGs to be produced.

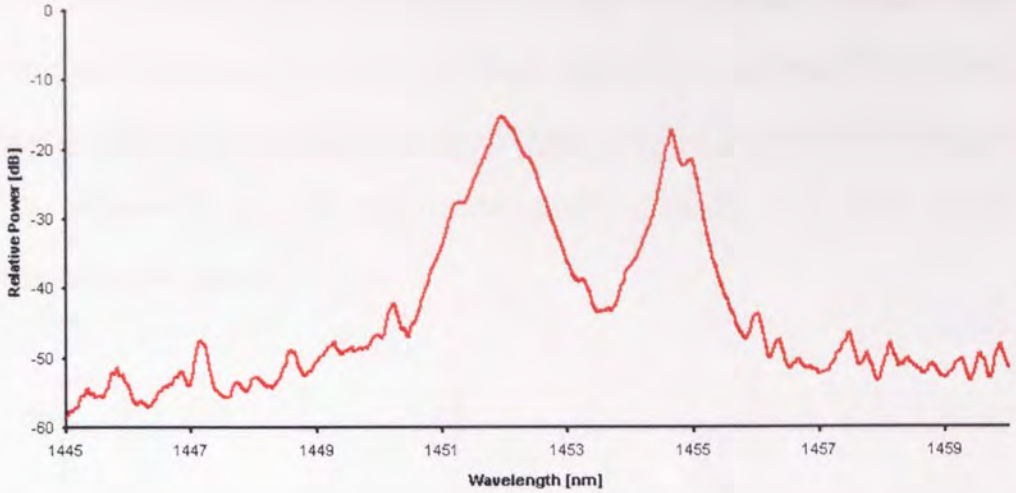

Figure 6.13 Spontaneous spectrum formed from bi directional 1365nm pumping of a 75km SMF span

The gratings produced, by Aston University, were characterised by use of a broadband light source and an OSA, the result of which can be seen in Fig. 6.14 where the relative difference between the transmission and the reflection regions can be evaluated.

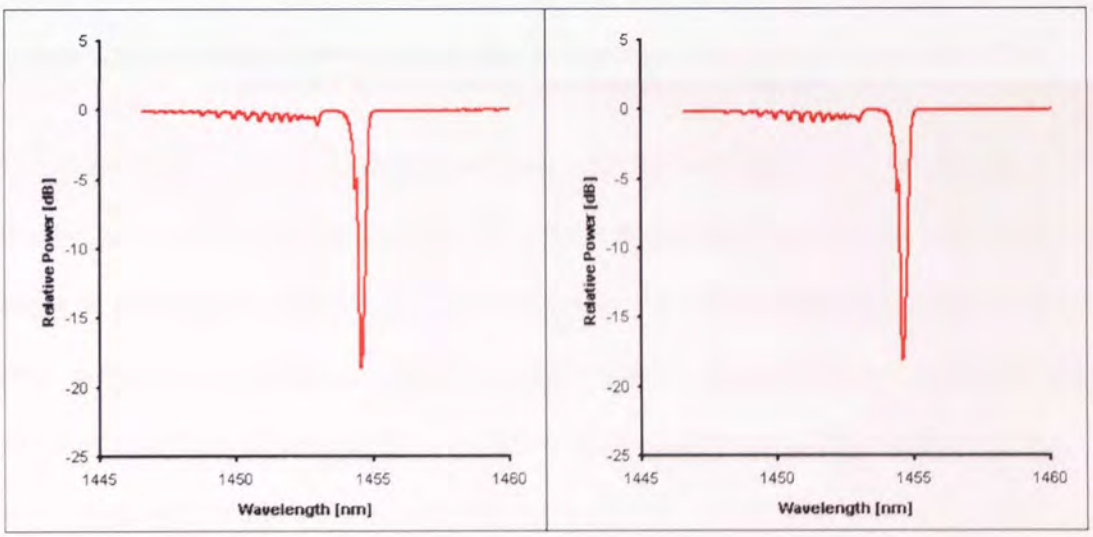

Figure 6.14 Profiles for FBGs used in quasi-lossless system

The produced gratings had a max. reflectivity wavelength of ~1454.6nm. These gratings were then inserted at either end of the transmission fibre, as in Fig. 6.10, and then both pump lasers run again to see if a single dominant spontaneous peak was

formed. The generated single peak, pump wavelength and spontaneous 1500nm light can be viewed in figure 6.15 below. A clearly visible peak has formed at 1455nm along with a spontaneous spectrum around 1550nm, this was the required wavelength and the presence of the ASE indicates that gain/amplification of a signal around 1550nm should be possible.

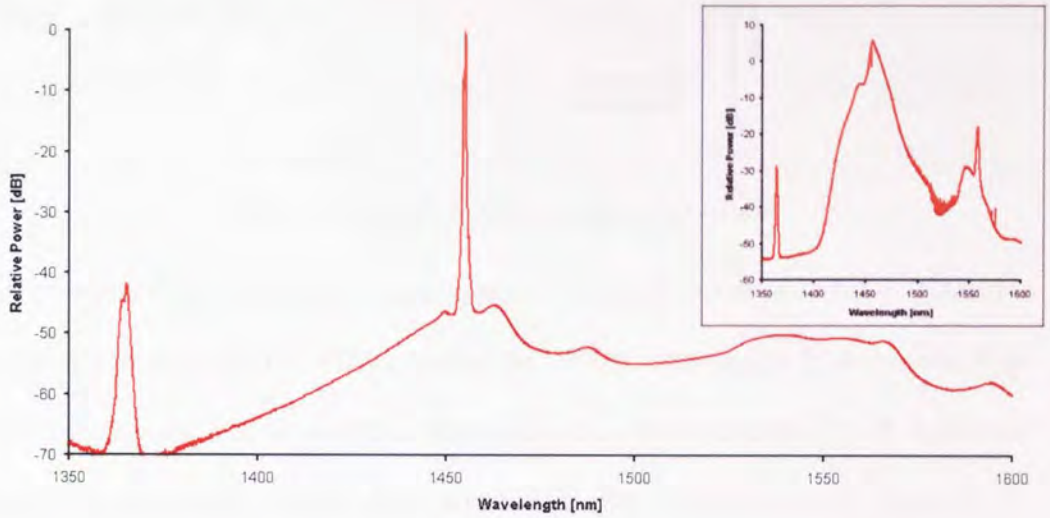

Figure 6.15 Spontaneous spectrum formed from bi directional 1365nm pumping of a 75km SMF span with FBGs at either end and for 25km TW-RS inset

The quasi-lossless system scheme was tested with various fibre types and lengths as was found to work best with standard SMF fibre as it avoided many of the effects that could be generated as detailed in chapters 4 and 5, the effect from using a TrueWave fibre is shown in the inset of Fig. 6.15 where a 25km TW-RS fibre was used with a ZDW of ~1452nm. Clear spectral broadening of the generated 1455nm pump can be seen which will limit the degree of gain provided to the 15xx wavelength region. Three SMF lengths were investigated, 20, 52 and 75km, by using the OTDR system shown previously to study the effect of signal wavelength and by using another OTDR system shown in figure 6.16. This other OTDR configuration produced a less noisy result as there were fewer components involved and worked fine as long as there was minimal net gain.

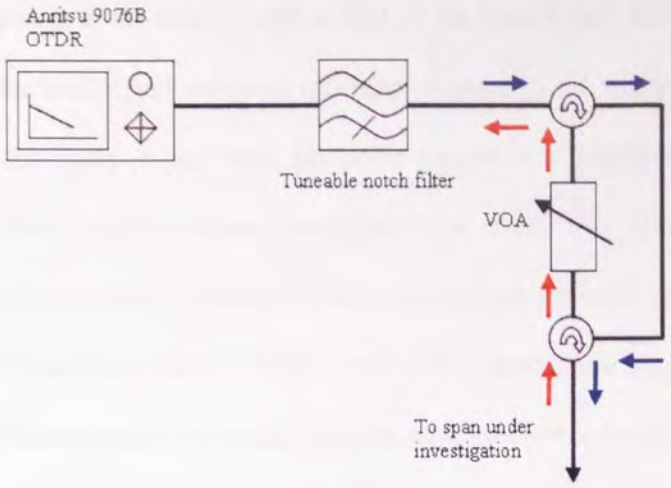

Figure 6.16 Simplified OTDR measurement system

The tuneable filter still allows investigation of signal variation around a narrow wavelength region and the VOA protects the OTDR from overly high powers, it is worth pointing out that a 14xx/15xx WDM was also used before the OTDR system to reduce any generated 1455nm light entering it. The following result, figure 6.17, shows the results for the three different span lengths from using the above OTDR configuration.

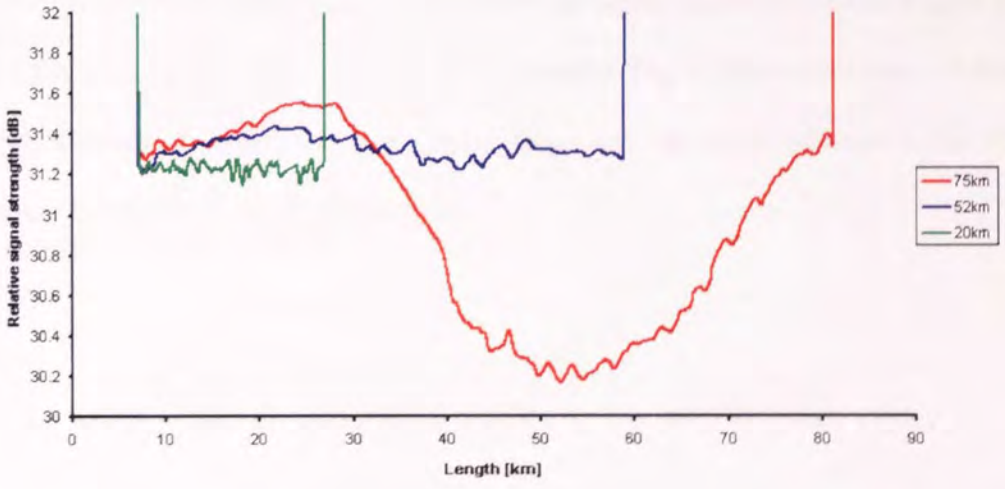

Figure 6.17 Results for three different span lengths using single wavelength quasi-lossless system

Here the same power at the receive end as that of the launch end was aimed for, and for each length the total signal variation was (approximately) 1.4, 0.2 and 0.1dB for the 75, 52 and 20km lengths respectively, the noise present is a limitation of the OTDR when the real time mode without averaging was used, this allowed real time adjustment of the pump lasers. The 1365nm pump powers for each length were 526+ 596mW, 356+ 482mW and 212+ 277mW for the 75, 52 and 20km length again. These variations may in fact actually be smaller but the measurement is limited by noise, also a ~6.7km reel has been placed before the span in the above figure to remove the measurement dead zone. By comparing Fig. 6.17 with Fig. 6.10 we can see that the discrete 1365 and 1455nm pump lasers together produces less signal variation over the same span length. It was considered that the high reflectivity gratings were actually returning too much 1455nm light back into the span and therefore creating a too sudden of gain, whilst when the discrete 1455nm pump is used the power can be reduced to act as seed as discussed previously. It was then decided that lower reflectivity gratings might actually produce a better result. Simulation results do indeed show that different reflectivities may improve the signal variation at some lengths but actually increase it at others, namely shorter lengths. Fig. 6.18 provides some of these simulation results, which enable the reader to see how the signal variation varies with respect to the degree of FBG reflectivity.

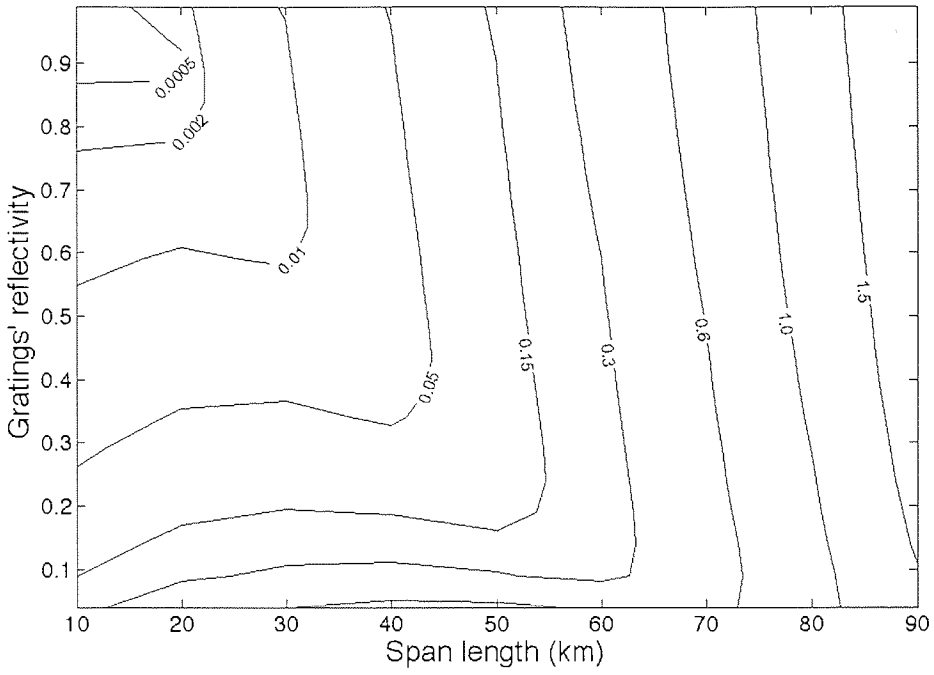

Figure 6.18 Simulation result of signal variation versus span length and grating reflectivity

Experimentally it proved difficult to obtain an acceptable selection of gratings to physically test this concept but a further two were produced with a reflectivity of ~33%. As previously stated and shown by the simulation results, the low reflectivity will benefit at longer lengths and detriment at short lengths. Work revealed that there was insufficient pump power to obtain a quasi-lossless result using the low reflectivity gratings with the 75km span; however they did work to produce a result using the 20 and 52km spans, the result of which is given in Fig. 6.19.

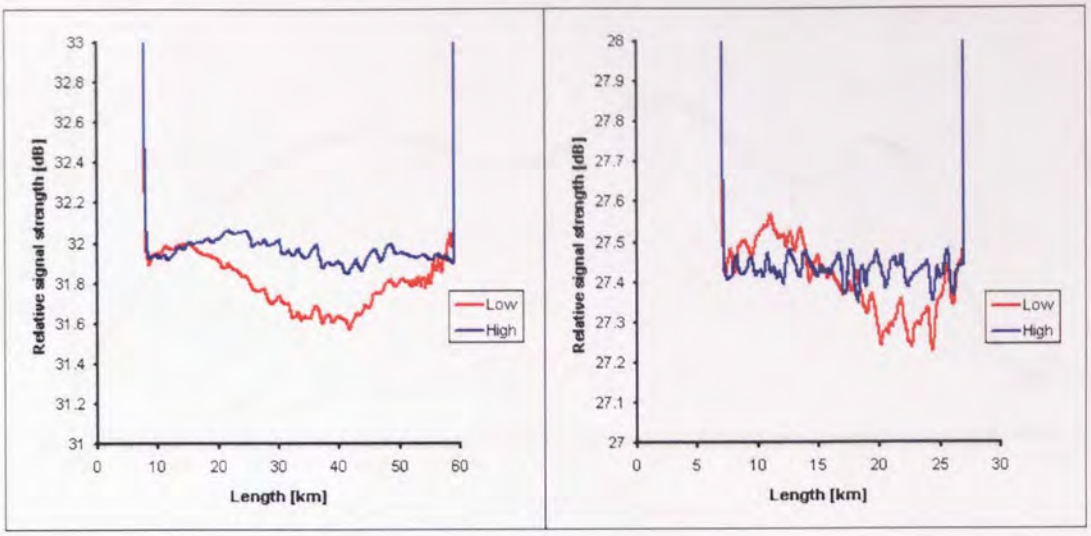

Figure 6.19 Comparisons between the high (~99%) and low (~33%) FBG in 20 and 52km SMF spans

From this result it can clearly be seen that the high reflectivity gratings provide a better result over the lower value gratings. Essential future work would, of course, be to attempt a longer span which would require high power lasers and/or high reflectivity gratings to investigate if the 75km result can be made comparable or better to the result formed by using four discrete pump lasers as used for Fig. 6.10.

6.5 Transmission over quasi-lossless system

As the quasi-lossless system was created to aid signal transmission it is only logical to test such a system with data. Before moving onto data transmission it is important to look at such a schemes ability to be used in today's multi-channel-WDM systems, starting with the amplification bandwidth. The bandwidth was measured by using an EDFA as a broadband light source, 75km of SMF and running the lasers at the level which would produce a near-lossless result for a single channel at 1550nm. The on-off gain is shown in figure 6.20.

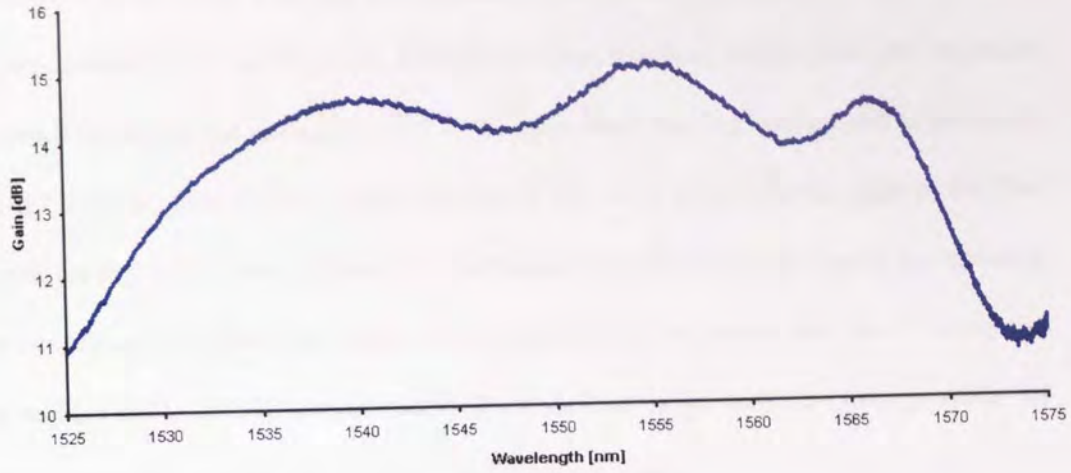

Figure 6.20 Gain spectrum for 75km quasi-lossless system

For a 1.5dB reduction from the peak gain value the bandwidth is ~36nm which reduces to 35nm for a 1.3dB reduction from peak. From experience it is possible to see that this gain spectrum does not look typical for what is essentially a single pump system at 1455nm, namely because of the three peaks instead of the classical two. This can be explained intuitively by considering the first order gain from the 1365nm pump. Refer to Fig. 6.21 to see how the first order gain spreads in the second order gain region.

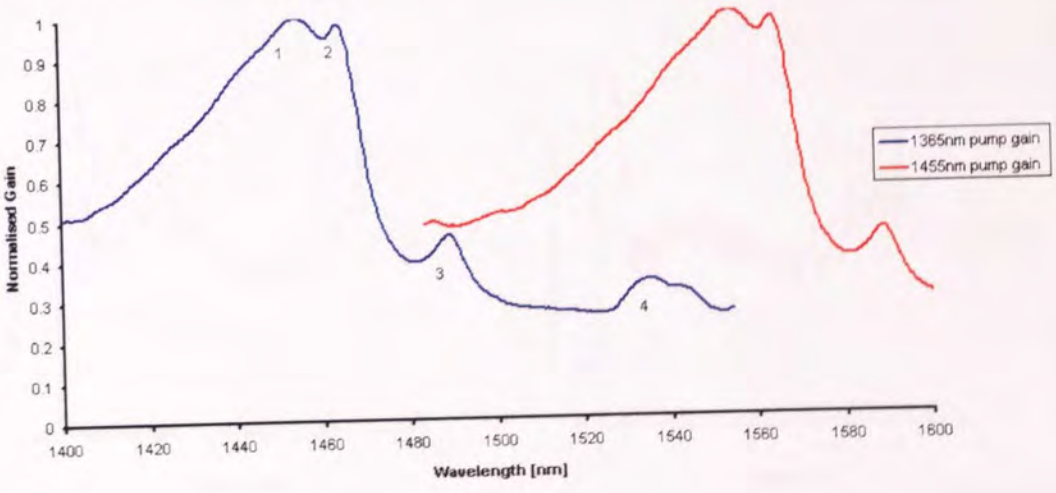

Figure 6.21 Individual gain spectra from 1365 and 1455nm pumps

The first peak in Fig. 6.20 can be attributed to the fourth peak from the 1365nm pump gain denoted by '4' in Fig. 6.21. Though this peak is much smaller than the dominant ones it is substantial enough to add to the gain from the 1455nm/second order pump and create the overall, three peaks, profile in Fig. 6.20. Now with the gain at the first peak (in Fig. 6.20) being noticeably contributed to by the first order pump the question arises, does this affect the longitudinal gain distribution along the fibre? Using the tuneable laser OTDR configuration from before (Fig. 6.3), it was possible to investigate this concept and produce the following result.

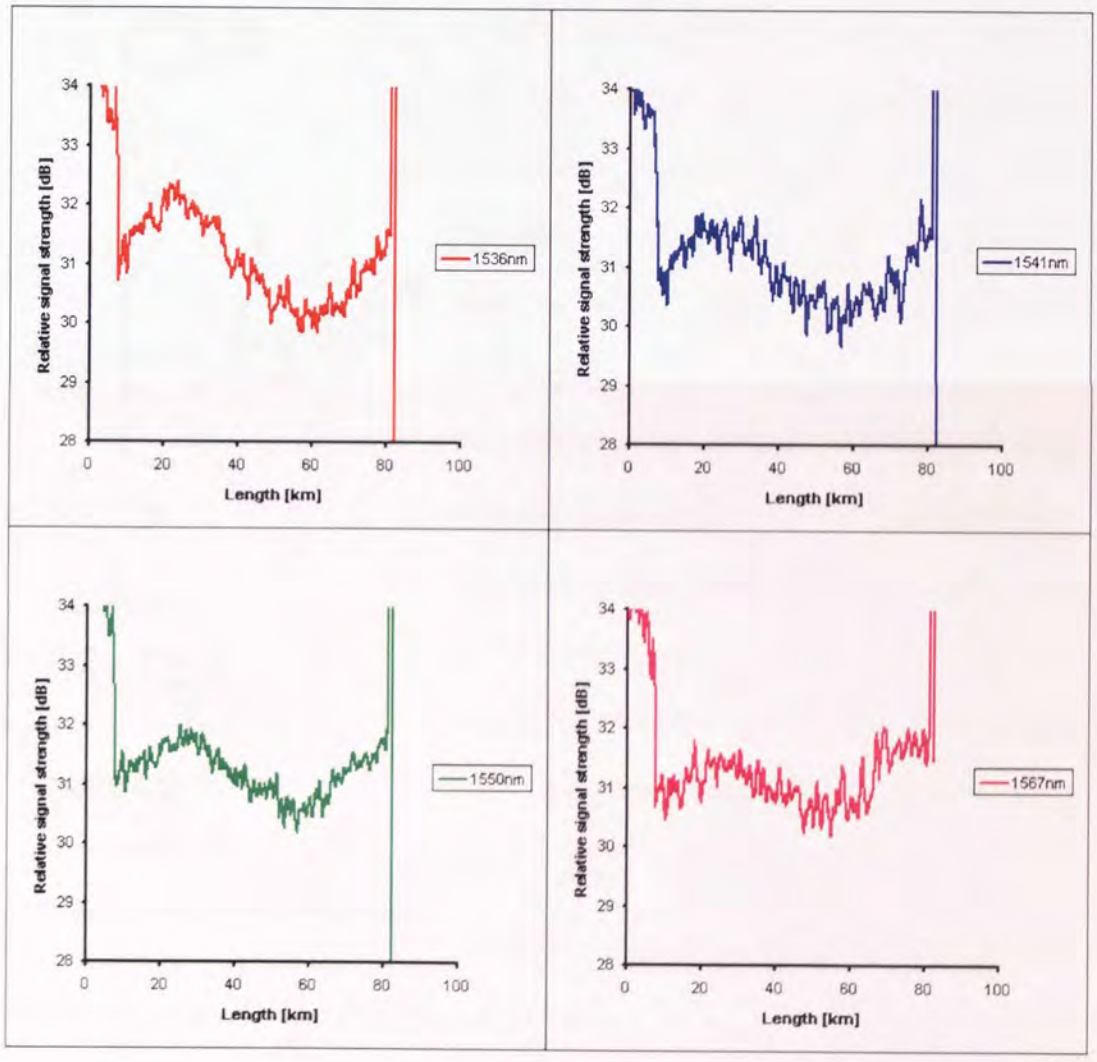

Figure 6.22 Signal variations along a 75km SMF span at different wavelengths

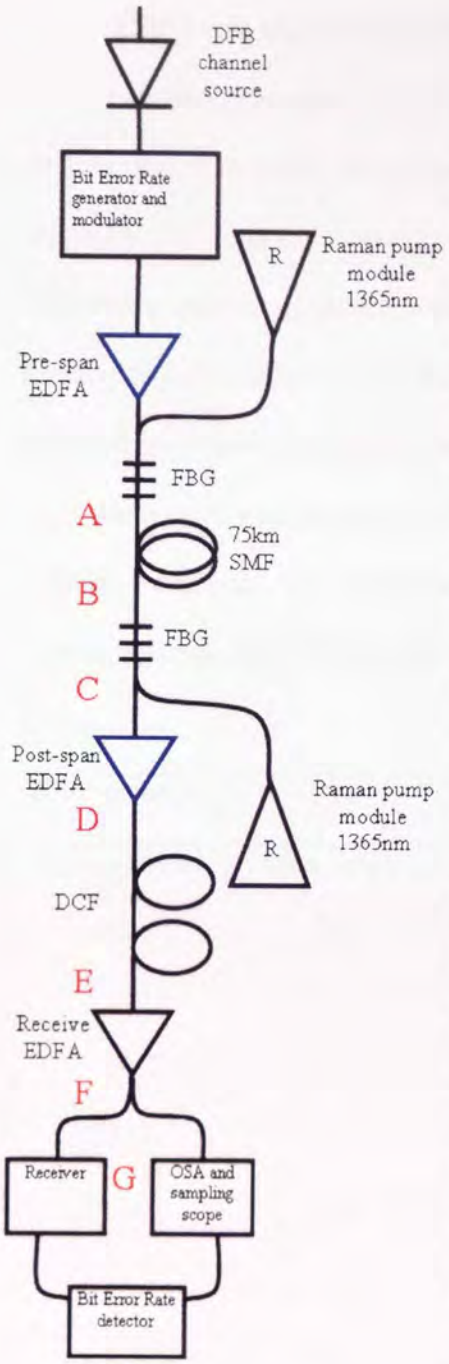

Figure 6.23 QL transmission configuration

Signal variations for 1536, 1541, 1550 and 1567nm are, averaged through the noise, 2, 1.4, 1.3 and 1.1dB respectively. From this it can be seen that there is a change in signal variation with respect to wavelength and it is possible that the larger excursion at 1536nm maybe due to the signal receiving too much gain in the early and latter stages of the span directly from the 1365nm pump as well as that from the 1455nm in such a way that the gain is not ideally distributed. Although it is apparent that there is some variation with respect to signal wavelength the span is still virtually lossless for many wavelengths.

The next aspect to verify was the systems ability to transmit data, it was of course anticipated that the system would indeed be able to transmit data so the following experiments were really devised to evaluate the performance of the 1365nm pump lasers with regard to their Relative Intensity Noise (RIN) and the transfer to the signal – this aspect is looked at more acutely later on. The transmission system was setup into four different configurations:

1. Quasi-lossless system + pre-span EDFA
2. Quasi-lossless system + post-span EDFA

3. EDFA only (no Quasi-lossless system active)

4. EDFA (pre and post with settings from 3) + Quasi-lossless system

These combinations were chosen to determine whether the QL system could replace EDFAs and/or enhance their operation. The EDFA only system was used as a reference. The complete system is shown in Fig. 6.23 where the EDFAs that are to be switched in and out are shown in blue. Peak channel power was measured by use of an OSA with RBW=0.5nm at the points labelled with red letters, when an EDFA was removed pre or post power C has two values, one with the QL system off and one with QL system on. Power at point B was of course measured with the QL system off. The channel wavelength was 1556.75nm and was encoded with a 2^{31}-1 pseudo-random binary sequence at 10.6Gbit/s. Powers and final error rates are given in the following table.

Configuration		1	2	3	4
Measurement point		Peak power dBm	Peak power dBm	Peak power dBm	Peak power dBm
A		-4	-19	-4	-4
B		-18.8	-34	-18.5	-18.5
C	QL off	-21	-36	-20.5	-20.5
	QL on	-6.2	-21	N/A	-4.8
D		-6.2	-4.7	-4.8	-4.8
E		-19.5	-17.6	-17.7	-17.7
F		2.4	2.1	2.1	2.1
G		-3.5	-3.5	-3.5	-3.5
BER		$<1\times10^{-14}$	3×10^{-13}	1×10^{-14}	9.9×10^{-12}

Table 6.1 QL transmission results

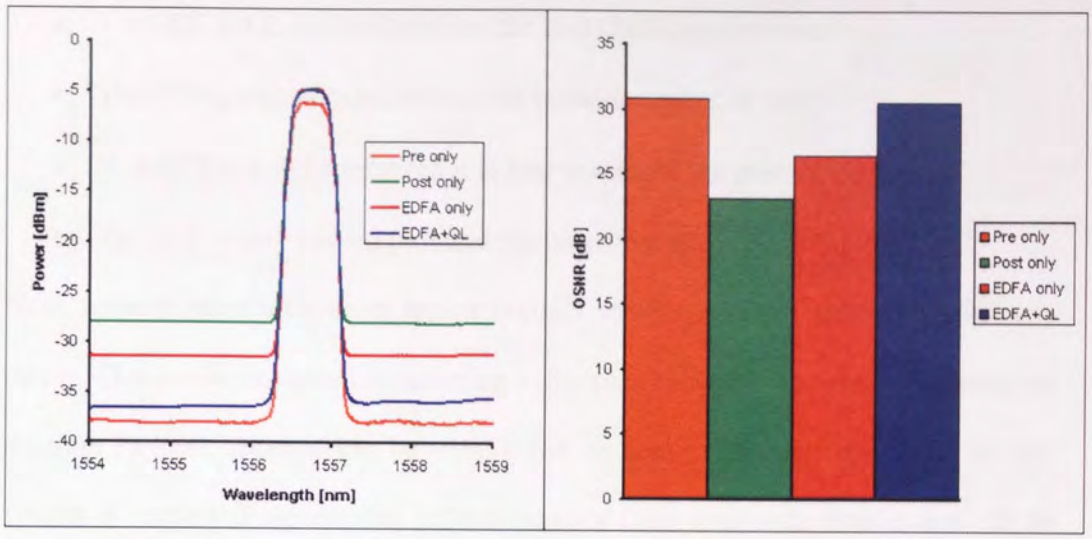

Figure 6.24 OSNR comparison at point D

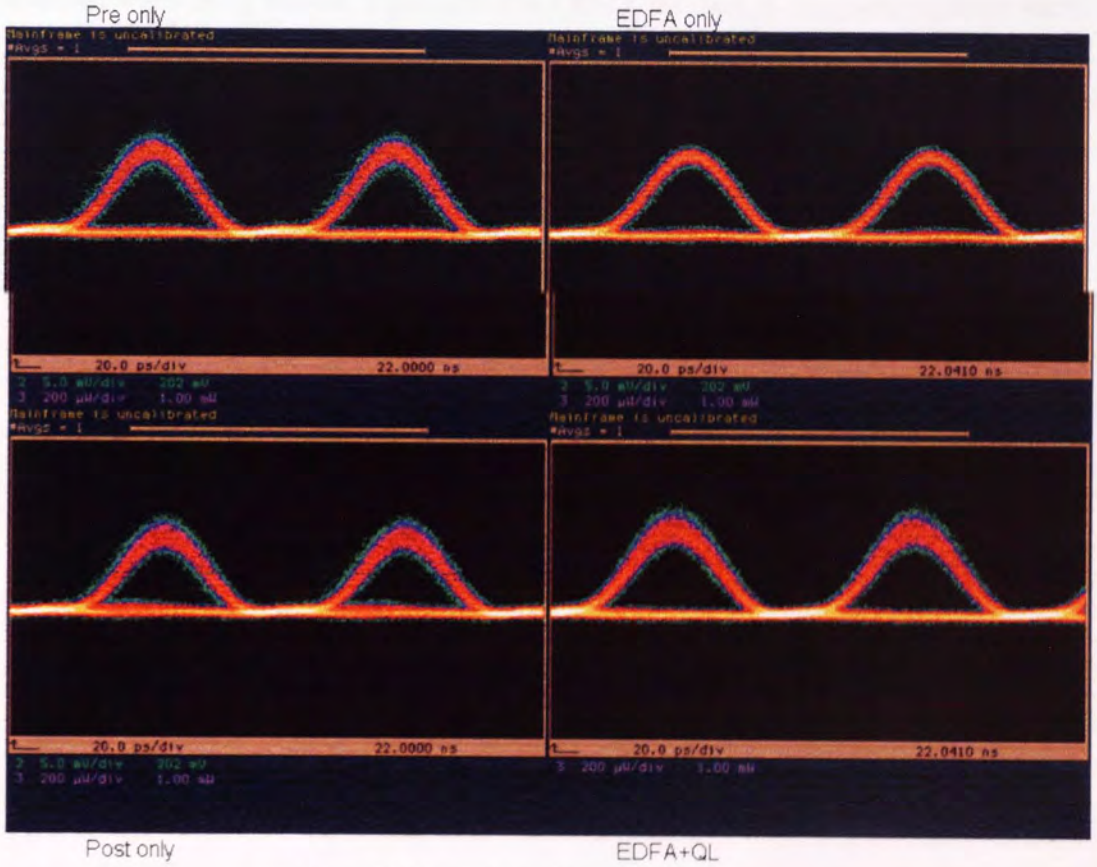

Figure 6.25 Optical eye diagram comparison

From comparing the results in the table and using 6.24 some interesting observations can be made, which include:

- The EDFA+QL system provides the best OSNR performance
- The EDFA+QL system also has the highest number of errors
- If an EDFA is to be removed it is best to remove the post EDFA
- The EDFA only system provides the best error rate

Now, some of these statements appear initially counter-intuitive namely the first two points. This can be explained by referring to figure 6.25 where the temporal optical eye diagram for each scenario can be seen, it can be seen in all cases that when the QL system is employed the eye has suffered closure from amplitude jitter which can be attributed to RIN transfer from the pump lasers to the signal. This is a well-known problem when using Raman, especially when RFLs are used as the pump sources; see [32]. This would also explain why, despite the lower OSNR, the EDFA only system provides the best error rate – it is temporally more stable. It can be briefly concluded that the QL does work but is limited by power fluctuation noise, this degree of noise can be reduced by using a suitable feedback circuit to closely control the drive current of the 1365nm RFLs.

6.6 Relative Intensity Noise RIN

As a final note to this chapter it is worth acknowledging the detrimental effects of RIN transfer from the pump to the signal. All lasers, fibre or solid state, exhibit some intensity fluctuations. Power fluctuations in laser are quantified through a frequency dependant quantity called relative intensity noise [26]. Equation (6.4) is the fundamental RIN definition from [26], given as the fluctuation power in 1Hz of bandwidth relative to the average power squared

$$RIN(f) = \frac{S_{\Delta P}(f) \cdot \Delta f_0 (\equiv 1Hz)}{P_0^2} \tag{6.4}$$

where $S_{\Delta P}$ is the power spectral density of the fluctuation [W^2/Hz], f is the frequency, P_0 is the average power and $\Delta f_0 \equiv 1Hz$ is the bandwidth. If the fluctuation is bandwidth limited to a small bandwidth Δf, over which the spectral density is constant, the RIN definition can be expressed as [26]

$$RIN = \frac{\left\langle \Delta P^2(t) \right\rangle}{P_0^2} \cdot \frac{\Delta f_0}{\Delta f} \tag{6.5}$$

Where $\left\langle \Delta P^2(t) \right\rangle$ is the time averaged mean square fluctuation of the laser. The pump-noise transfer function represents the enhancement in the signal noise at a specific frequency f and is defined as

$$H(f) = \frac{RIN_s(f)}{RIN_p(f)} \tag{6.6}$$

When calculating the above transfer function (equation 6.6) it must be acknowledged that the pump and signal do not travel along the fibre at the same speed due to their differing wavelengths. The difference in speed is dependant on the fibre dispersion and in co-pump propagation there is a walk-off between the signal and pump. Sufficient walk-off or velocity differences between the signal photons and the pump photons subject the signal photons to average pump powers as they propagate along the span length reducing the noise transfer [71]. In the co-direction this walk-off reduces the RIN transfer of relatively high frequency (>20MHz) pump power fluctuations. In the counter pump configuration, the walk-off is mainly due to the opposing velocities of the signal and pump photons, which results in an effective averaging of pump power fluctuations at relatively low frequencies (>2kHz).

Even though all lasers display intensity fluctuations some are worse then others, and in the context of Raman pump sources, it is Raman fibre lasers that are most problematic. A typical RFL may exhibit a RIN value approaching -100dB/Hz whilst

semiconductors achieve a much lower value of ~-115dB/Hz for Fabry Perot and ~-140dB/Hz for high power DFB, FBG stabilised FP lasers do not provide a significant improvement in low frequency noise [72]. For co pumping, where the transfer of noise is far more effective than counter pumping, reference [32] stipulates a RIN value of less than -110dB/Hz is required for a 0.1dB signal Q penalty when the fibre exhibits a dispersion of -15 ps/nm/km at 1500nm, or -118dB/Hz with D = -2 ps/nm/km. If the zero dispersion wavelength lays at the midpoint of the signal and pump wavelengths, the Q penalty would be much greater. From reference [73], the counter pump would require a RIN value of -60dB/Hz to suffer a 0.1dB Q penalty for a fibre with dispersion of -15 ps/nm/km at 1500nm.

The transfer of pump fluctuations onto the signal can be quickly demonstrated using the experimental configuration in Fig. 6.26, where the pump and signal are monitored using a 10GHz photo-diode and an electrical spectrum analyser to see electrically what degree of fluctuations there are and at what frequency they occur.

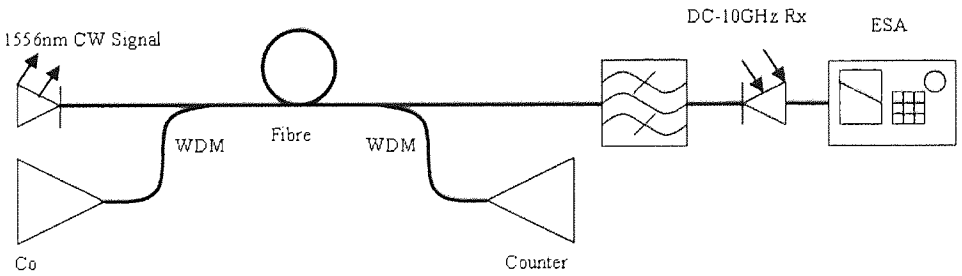

Figure 6.26 Investigation of noise transfer from pump to signal

Before looking at the transfer to the signal it is worth while looking at the measured noise directly from the laser (via 30dB attenuator into the photo-diode) and Fig. 6.27 does just this for increasing power for a 1452nm semiconductor pump module (two cross polarised 1452nm grating stabilised FP lasers) and a 1455nm Raman fibre laser.

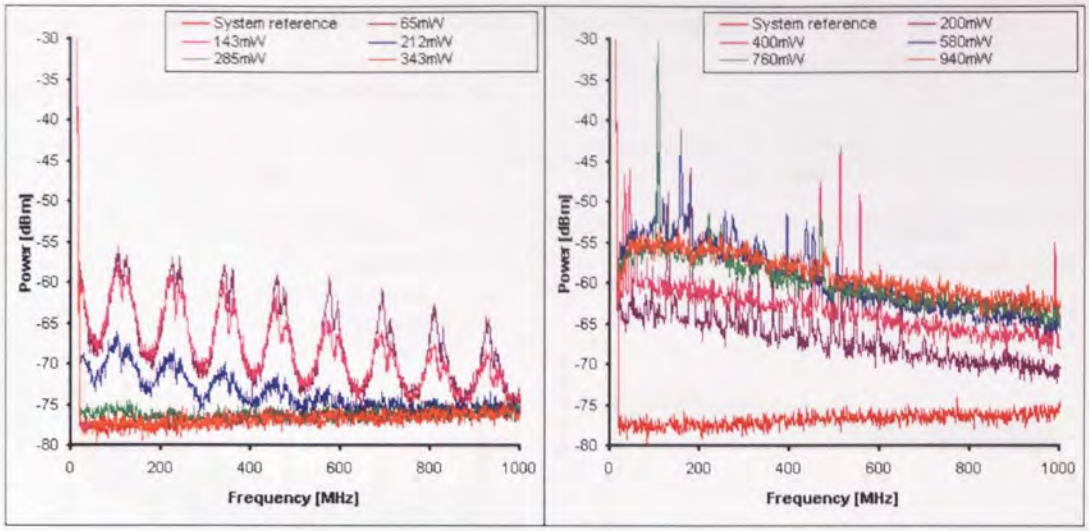

Figure 6.27 Electrically converted measured noise from 1452nm semiconductor laser (left) and a 1455nm Raman fibre laser (right)

Note the ordered modal shape of the semiconductor laser versus the random modes from the RFL. The relative noise peaks in both cases decrease with increasing power but for the semiconductor laser the average noise power tends to the system reference with increasing power indicating that for the lowest noise a semiconductor pump laser is best especially when operated at higher powers.

Moving to the transfer to signal, the set-up from Fig. 6.26 was employed with two fibre types, standard SMF and Corning LEAF fibre, both 20km in length, the pumps were driven to provide the same level of gain (just 4dB) regardless of the fibre type. This meant that the pump was driven at different powers due to the change in the fibre gain co-efficient; this shouldn't be a problem as the aim was to compare the degree of transfer between the fibre types. It was expected that the greater transfer would be apparent in the LEAF case as the dispersion zero wavelength falls approximately between the two pump wavelengths. However, in practice it was not possible to distinguish any noticeable difference in the efficiency of noise transfer. What could be seen clearly (see Fig. 6.28) was that the 'Counter pump + signal' case the noise was much lower, comparable to the inherent 'Signal only' noise, than the 'Co pump +

signal' case which resembled the 'Both pumps no signal' case. This result is in keeping with the theory presented earlier.

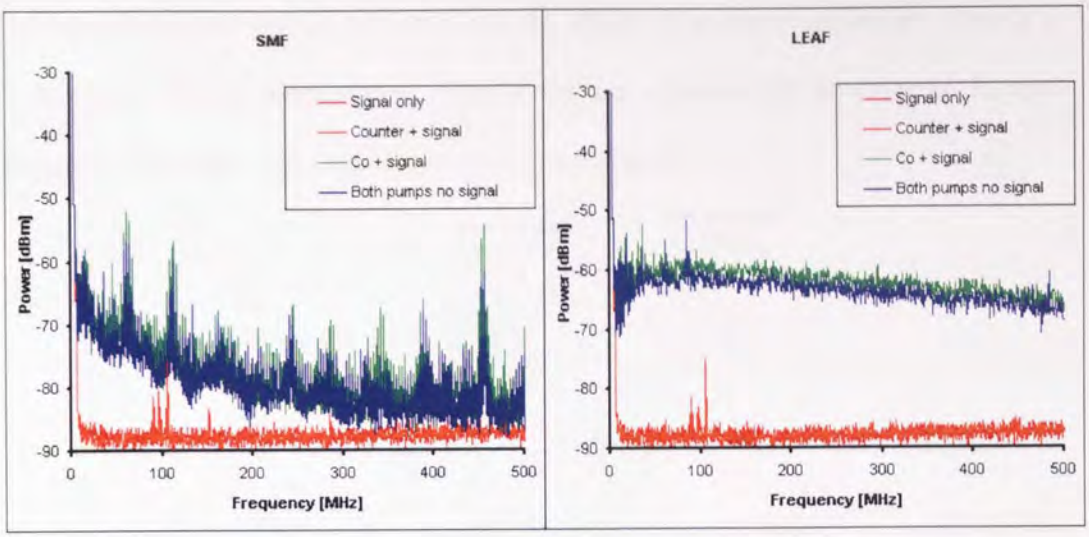

Figure 6.28 Attempt to compare the transfer of noise from pump to signal for two fibre types

6.7 Distributed gain medium for pulse generation

With the possibility of a lossless medium or a medium that offers constant gain, the ability to generate special non-linear pulses arises. These pulses include the well documented and researched optical solitons [11] and the more recently discovered self-similar parabolic pulses. It is the latter of the two pulse types that shall briefly be investigated here in a purely experimental generation approach. If a short pulse propagates down a normal dispersion fibre in the presence of suitable gain it is expected that the pulse will undergo some reshaping from the amplification process [26]. It turns out that the pulse acquires a parabolic shape that is independent of the input pulse shape and power. These pulses are of interest as they possess a linear chirp which leads to efficient compression of the pulse which may then be used for other optical applications, they also represent a particular class of solution to the nonlinear Schrödinger Equation with gain [69, 70]. These pulses have been generated within rare

earth amplifiers and by the use of Raman gain [26] and it is this Raman generation method that is used here.

An experiment was derived to investigate the ability to generate parabolic pulses in a 7.3km reel of TrueWave classic fibre using co, counter and co+counter Raman pumping. The basic experimental set-up is given below.

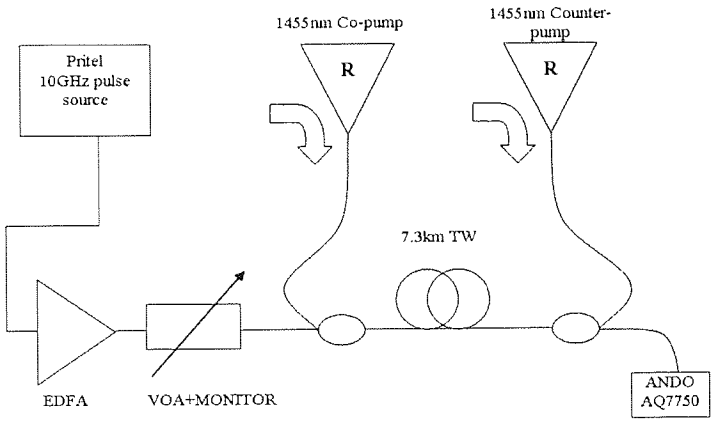

Figure 6.29 Parabolic pulse generation experiment

The experiment comprises of a 10GHz pulse generator by Pritel inc. capable of producing ~2-13ps sech pulses over a wavelength range of ~1530-1570nm, for the first results here a wavelength of 1553nm was chosen. The pulses then passed through an EDFA to increase the launch power and then a VOA with power monitor to allow for setting of powers to the same level for each pumping scenario. The pulses then entered the TW fibre via dedicated WDMs which also coupled in two 1455nm RFL pumps each with a pump power of ~2W max. The fibre possessed a dispersion value of –2ps/nm/km at 1553nm, as given in figure 6.30.

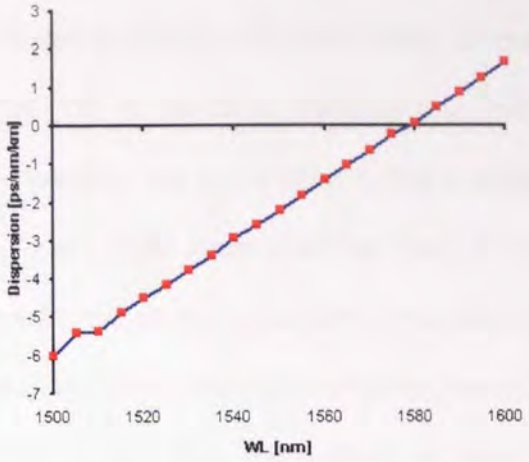

Figure 6.30 TWC dispersion

All pulses were measure using an Ando (now Yokogawa) AQ7750 high speed sampling oscilloscope with a temporal resolution of 800fs. Two arbitrary peak input pulse powers were chosen, 200 and 500mW, and sent through the TWC span with 1300mW pump power in either the co or counter directions or with 650mW in each direction in the co+counter scenario. The temporal results are shown below in Fig. 6.31.

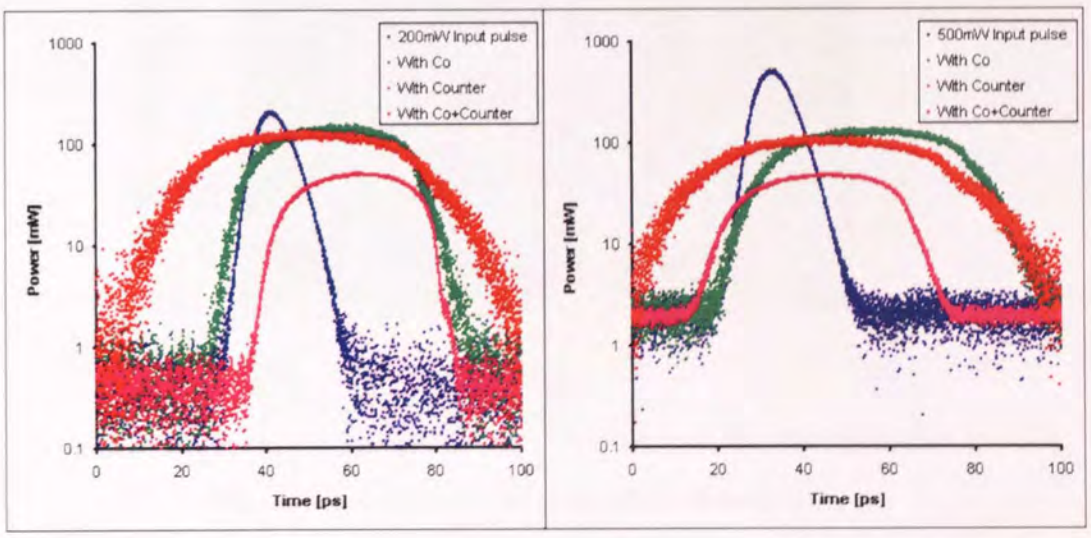

Figure 6.31 Temporal results for parabolic pulse generation

From this figure it can be viewed that the input pulse has evolved into a pulse whose profile resembles a parabolic profile and whose width is determined by the gain distribution in the fibre. The bi directional pumping case enables the largest pulse width to be generated possibly due to the fibre having a higher gain level over its length in comparison to the single pump direction cases. Despite the generation of parabolic style pulses using the shown experiment it was deemed that the EDFA may have been introducing an unknown effect upon the pulse generated and that the launch pulses were excessively large which was leading to discrepancies between the experimental and modelled results. It was suggested that the experiment should be re-constructed without the EDFA.

The system remains the same as in Fig. 6.29 with exception of the EDFA. Using this configuration, a peak pulse amplitude from the Pritel of ~170mW could be obtained into the TWC fibre, see Fig 6.32.

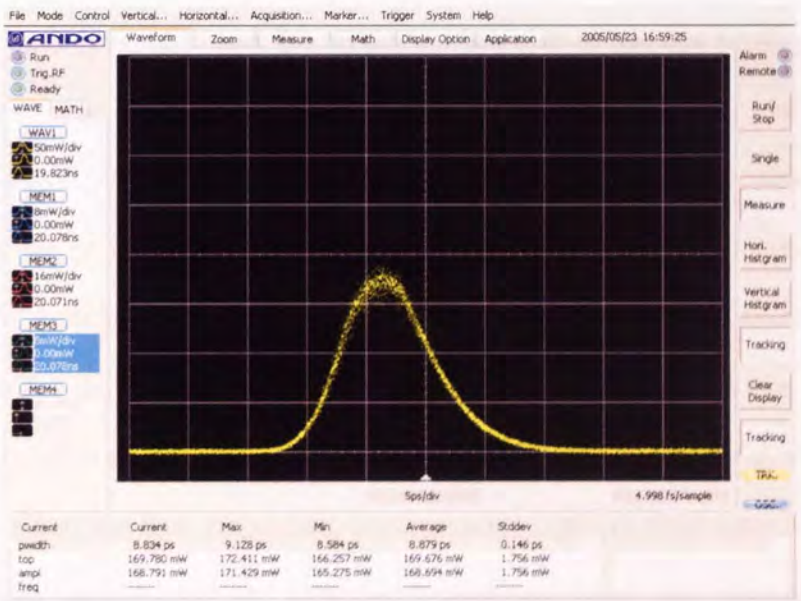

Figure 6.32 Input pulse to TWC fibre without booster EDFA

This pulse then propagated through the TWC fibre, as before, whilst receiving amplification from the two Raman Fibre Lasers. Pump powers used were ~700mW in

the co direction and ~700mW in the counter direction. The generated pulse can be seen in figure 6.33 along with the input pulse, parabolic fit and the associated spectra.

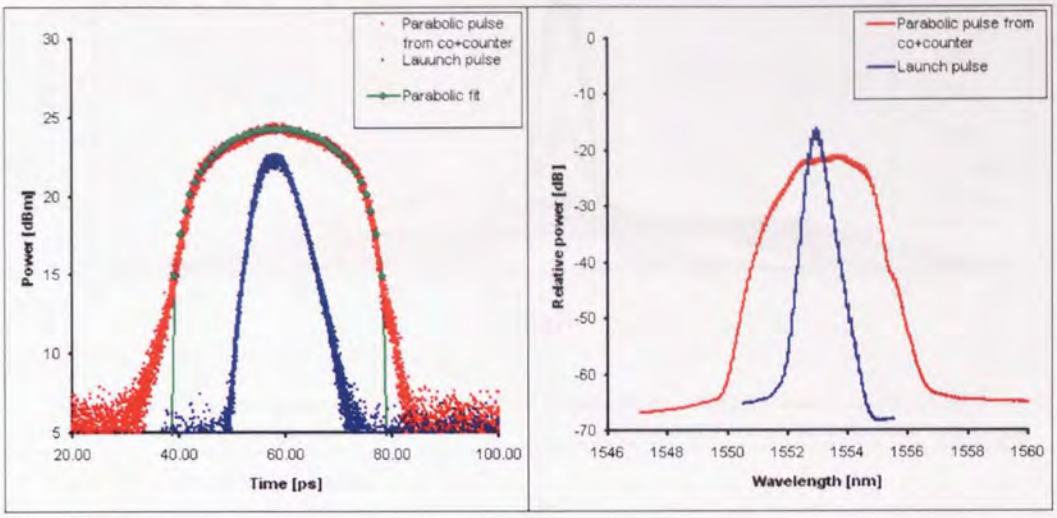

Figure 6.33 Input and output pulses, temporal and spectral results from using no booster EDFA

The input pulse width was ~9ps and the generated pulse was ~30ps. The generated pulse shows a parabolic profile as before, and resembles generated pulses from published work [69]; also note the significant increase in spectral width. The other aspect of parabolic pulses in addition to their shape is their linear chirp characteristics across the pulse. Unfortunately it was not possible to measure this parameter directly, but by the use of various length of SMF (anomalous dispersion at 1553nm) it was possible to compress the generated pulse and compare that compression with compression of the pulse directly from the Pritel pulse source. To do this the pulses were attenuated to an average amplitude of ~15mW in order to avoid the influence of nonlinear effects and then propagated down several lengths of SMF cut with arbitrary lengths. Both pulses, Pritel and parabolic, compressed using this technique. Figure 6.34 shows the compressed parabolic pulse after each fibre length and figure 6.35 provides a comparison between the compressions of the parabolic pulse and the direct Pritel pulse for pulse width (FWHM) and peak amplitude.

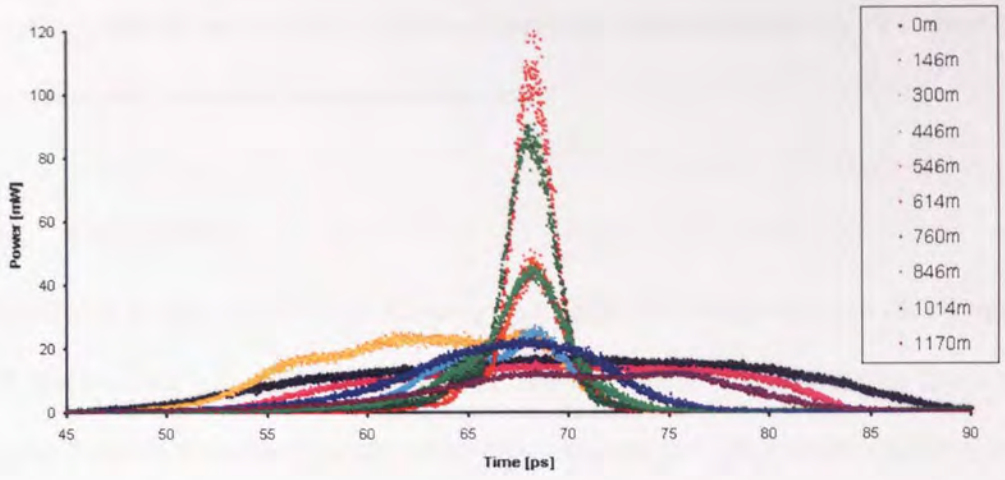

Figure 6.34 Compression of the generated parabolic pulse using various lengths of SMF

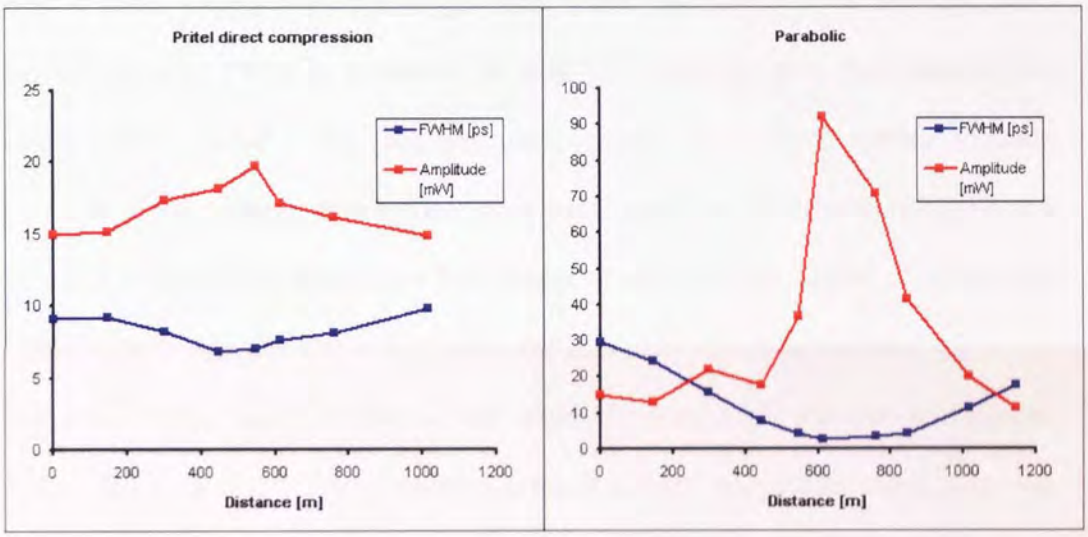

Figure 6.35 Comparison of pulse widths and amplitudes for compression of the direct Pritel pulse and generated parabolic pulse

From the previous two figures it can be seen that the generated pulse compresses considerably from about 30ps to about 3ps however the direct Pritel pulse compressed from about 9ps to only 7ps. This difference in the degree of compression implies that something considerable has occurred to the chirp of the pulse after propagation through the generation media, though of course it is not possible to declare if the new chirp is linear from these results. This ability to compress a pulse by converting it into a parabolic pulse and then compressing is of interest in the field of ultra short pulse

generation and the profile of the generated parabolic pulse would also be of interest to those working in research in optical switching.

6.8 Conclusions

This chapter reviews the fact that Raman gain is distributed with respect to fibre length and confirms this with experimental results. These results also show how the gain can be distributed in the co and counter pump directions and how the distribution along the fibre can be more constant with the aid of bi-directional and second order pumping.

Next a novel second order pumping system which only requires discrete first order pumps and two FBGs is presented. It was seen that the gain provided by this configuration created a line that was quasi-lossless for a signal around 1550nm. However it was pointed out that this system was not quite as effective as using discrete first and second order pumps and the concept of adjusting the degree of reflectivity from the FBGs was introduced to improve the gain variation along the span.

The new systems' gain distribution with respect to wavelength was then investigated and it was seen that the gain covered a much greater wavelength range than was originally expected due to elements of the first order pump featuring at the signal wavelength. This wavelength range was explored to see if the longitudinal gain varied with respect to the signal wavelength and results suggest that a measurable difference occurred. Lastly for the new QL system, its ability to transport data was quickly looked at indicating that a more stable drive circuit would be required for multiple spans. This new system design breeds many questions that only further work can answer and in particularly what is the effect from multipath interference/ double Rayleigh scattering and can such a system allow massive transmission distances to be achieved when using nonlinear concepts such as soliton transmission?

The problematic issue of intensity noise transfer from pump to signal is touched upon and it is displayed that this can be a very noticeable phenomenon in the co propagating pump regime. Finally, transmission is not the only application of distributed gain as the brief work on parabolic pulse generation over a normal dispersion fibre shows.

Chapter 7 Conclusions

The end of the twentieth century saw massive increases in the demand for data transport and research and development in fibre optics, driven by the popularity of the Internet and associated services. This growth lead to the over expansion of many companies, who then suffered when the market collapsed at the beginning of the twenty-first century. After the collapse, many communication providers were interested in improving and optimising existing infrastructure, say by sending faster data rates down existing fibres. Raman amplification can be utilised to increase performance by improving optical signal to noise ratios and by being able to provide gain at other wavelengths for the addition of more channels. Despite the decline of the fibre optics industry, research in Raman amplification has continued to grow as there are many new applications and effects to be studied, of which a handful are explored in this thesis. To recapitulate, the first three chapters aimed to introduce telecoms, fibres and the Raman effect as an amplification technique, whilst chapters 4-6 elaborate further on known processes and bring in multiple original ideas and concepts from research by the author.

Chapter 4 explored the effect of spectral broadening on Raman pump light. Multiple results to illustrate the broadening process were presented. It was seen early on in the work that a range of factors played an important role on the degree of wavelength spread seen, these included: fibre dispersion, length and nonlinearity. A consistent requirement was the need to be near the zero dispersion wavelength but still within the anomalous dispersion region. During investigation of the pump width the resulting gain spectra were observed and as the pump width increased so did that of the gain spectrum along with the spectral distribution. This resulting gain profile was compared to that of when the unbroadened pump was used; the result indicated that a more

uniform distribution of gain had been achieved when a fibre to broaden a pump was used. The chapter then goes on to look at the application to multiple pumps and the use of a much shorter length of fibre with a high nonlinear coefficient as the pump broadening fibre, with the results of both experiments being successful. As stated within the chapter there is still much scope for optimisation of the broadening fibre, to aid this, a firmer understanding of the broadening process is required along with accurate modelling. It would also be of interest for verification of theory and numerical simulations if the observations of the temporal break up of CW light due to modulation instability could be obtained experimentally. Although such an experiment was attempted using an autocorrelator, no meaningful result was obtained. This may be due to the generated pulse train not being a repeating fixed pattern but one with various asymmetric pulses occurring at a varying repetition rate; possibly due to pump power fluctuations. Regardless of the generated pulse shapes and frequency it would be insightful to be able to experimentally visualize such a train.

Chapter 5 investigates a well known process which proves detrimental to Raman amplifiers, the process being four-wave mixing (FWM). Attention is paid to providing a comprehensive graphical illustration of the effect as applied to a multi-pump Raman configuration in order to clearly demonstrate the multitude of new frequencies that can be generated. The remainder of the chapter is dedicated to how FWM affects the channels within the signal band and how these may be mitigated. Several reduction techniques are demonstrated with some interesting and curious properties being recorded, some of which are hard to explain, considered to be a function of coherence, and therefore naturally lend themselves to further investigation. The main point for consideration being how does a fibre placed before a span reduce FWM within that span and what makes that fibre more effective than other types, suggestions are given

but future work is required to obtain a definitive solution. The existing mitigation technique involves a fibre after the pump laser but before the transmission span in a similar way to the configurations used for a different purpose in chapter 4, it is speculated that it maybe possible to obtain a fibre that can perform both the broadening process for the improvement of gain distribution, and for the reduction of FWM equally well. Selection of such a fibre would involve a highly detailed model and possibly large quantities of experimental data.

Chapter 6 turned attention to the distributed nature of Raman gain, it starts out by describing why gain distribution is important in the context of signal to noise performance, followed by experimental illustration of gain variations (with respect to distance) for various pumping configurations, including bi-directional and higher order. This covered the more conventional set-ups, the next step was to present an original configuration utilising a second order style of pumping but by only using one discrete pumping wavelength at 1365nm to eventually provide gain for a 1550nm signal. The 'missing' first order ~1455nm pump wavelength was created within the transmission line by harnessing the Raman effect and using two fibre Bragg gratings at either end of the transmission line. The overall result of this configuration was to create essentially a quasi-lossless or near constant gain fibre span. The outcomes of several initial performance verifying experiments are then given, the result of which points to the need to utilise pump lasers that exhibit much lower amplitude fluctuations or relative intensity noise (RIN). The advantages of distributed gain are not only limited to improving data transmission but such a link could provide the medium for nonlinear pulse generation or propagation, such as solitons or, as in Chapter 6, parabolic pulse generation. This section gives an insight into another large field of study, but here it is meant as a means to demonstrate the usefulness of distributed gain.

Results for the brief experiments performed were certainly encouraging and provides scope for further study including: the effect of pump power, initial pulse power, fibre length and a measurement of generated pulse chirp.

Publications

[1] T. J. Ellingham, L. M. Gleeson, N. J. Doran, "Enhanced Raman amplifier performance using nonlinear pump broadening", *ECOC 2002: Proceedings of the 28th European Conference on Optical Communication*, Copenhagen, Denmark, Tu 4.1.3, 2002 (Sep 2002)

[2] T J Ellingham, J D Ania-Castañón, O Shtyrina, M P Fedoruk and S K Turitsyn, "CW Raman pump broadening using modulational instability", *Nonlinear Guided Waves and Their Applications*, MC42, Toronto, Canada (Mar 2004)

[3] T J Ellingham, A Pustovskikh, J D Ania-Castañón, M P Fedoruk, S Kobtsev and S K Turitsyn, "Raman Amplifier with Increased Flatness Using Modulation Instability", *ECOC 2004: Proceedings of the 30th European Conference on Optical Communication*, Stockholm, Sweden (Sep 2004)

[4] T J Ellingham, J D Ania-Castañón, S K Turitsyn, A Pustovskikh, S Kobtsev and M P Fedoruk, "Dual-pump Raman amplification with increased flatness using modulation instability", *Optics Express* 13 (4), pp. 1079-1084 (Feb 2005)

[5] K Kalli, A G Simpson, Kaiming Zhou, Lin Zhang, D J L Birkin, T Ellingham and I Bennion, "Spectral modification of type IA fibre Bragg gratings by high power near infrared lasers", *Proceedings of SPIE* Volume 5855, 17th International Conference on Optical Fibre Sensors, pp. 896-899 (May 2005)

[6] T J Ellingham, J D Ania-Castañón, S K Turitsyn, A Pustovskikh, S Kobtsev and M P Fedoruk, "Dual-pump Raman amplification with enhanced flatness using modulation instability", *Conference Digest for CLEO Europe 2005*, Munich, Germany, pp. CD7-4-TUE (Jun 2005)

[7] T J Ellingham, M P Fedoruk, O V Shtyrina, J D Ania-Castañón and S K Turitsyn, "Design of a fiber scheme for nonlinear Raman pump broadening through modulation instability", *Conference Digest for CLEO Europe 2005*, Munich, Germany, pp. CJ-1-WED (Jun 2005)

[8] T J Ellingham, J D Ania-Castañón and S K Turitsyn, "Enhanced Raman amplifier gain performance with HNLF broadening", *ECOC 2005: Proceedings of the 31st European Conference on Optical Communications*, Glasgow, United Kingdom, pp. Th3.3.2 (Sep 2005)

[9] T J Ellingham, J D Ania-Castañón, R Ibbotson, X Chen, L Zhang and S K Turitsyn, "Quasi-lossless spans for broadband transmission and data processing", *ECOC 2005: Proceedings of the 31st European Conference on Optical Communications*, Glasgow, United Kingdom, pp. Mo4.2.1 (Sep 2005)

[10] J D Ania-Castañón, T J Ellingham, R Ibbotson, X Chen, L Zhang and S K Turitsyn, "Ultralong Raman fibre lasers as virtually lossless optical media", *Phys. Rev. Lett.* 96 (2), pp. 023902 (Jan 2006)

[11] T J Ellingham, J D Ania-Castañón and S K Turitsyn, "Enhanced Raman amplifier flatness with nonlinear broadening over non-standard transmission fibre", *Opt. Commun.* 257 (1), pp. 176-179 (Jan 2006)

[12] T J Ellingham, J D Ania-Castañón, R Ibbotson, X Chen, L Zhang and S K Turitsyn, "Quasi-Lossless Optical Links for Broad-Band Transmission and Data Processing", *IEEE Photon. Technol. Lett.* 18 (1), pp. 268 - 270 (Jan 2006)

[13] S.V. Smirnova, J.D. Ania-Castanon, T.J. Ellingham, S.M. Kobtseva, S. Kukarina and S.K. Turitsyn, "Optical spectral broadening and supercontinuum generation in telecom applications", *Optical Fiber Technology*, Volume 12, Issue 2, Pages 122-147, (April 2006)

Bibliography

[1] A.G. Bell., "Selenium and the photophone", *The Electrician*, pp. 214-215, 220-221, 1880

[2] J. M. Senior, "Optical fibre communications: principles and practice", Prentice Hall, Second edition, 1992

[3] R.H. Stolen and E. P. Ippen, "Raman gain in glass optical waveguides", *Applied Physics Letters*, Vol. 22, pp. 276-278, 1973

[4] www.marconi.com

[5] J. Bromage, "Raman amplification for fiber communication system", *Journal of lightwave technology*, Vol. 22, No. 1, pp. 79-93, January 2004.

[6] Joseph C. Palais, "Fiber optic communications", fourth ed., Prentice Hall, HJ, 1998

[7] www.sumitomo.co.jp

[8] www.sei.co.jp

[9] L. M. Gleeson, PhD thesis, Electronic Systems Engineering Dept., Essex University, UK

[10] D. Derickson, "Fiber Optic Test and Measurement", Prentice Hall PTR, NJ, 1998

[11] G. P. Agrawal, "Nonlinear fibre optics", Second Edition, Academic Press, London, 1995

[12] E. E. Basch, Optical-Fiber Transmission, Macmillan, 1987

[13] N.J. Smith, N.J. Doran, W. Forysiak and F.M. Knox, "Soliton transmission using periodic dispersion compensation", *Journal of Lightwave Technology*, Vol. 15 No. 10, p 1808, 1997

[14] J.C.D. Brand, "The Discovery of the Raman Effect", *Notes Rec. R. Soc.* Lond. Vol. 43 pp. 1-23 1989

[15] C. V. Raman, "On the molecular scattering of light in water, and the colour of the sea", *Proc. R. Soc.* London, A, 101, pp. 64-80, 1922

[16] C.V. Raman and K.S. Krishnan, "A new type of secondary radiation", *Nature*, London, vol. 121 pp. 501-502, 1928

[17] C.V. Raman and K.S. Krishnan, "A new class of spectra due to secondary radiation", *Indian Journal of Physics*, Vol. 2, pp. 399-419, 1928

[18] R.W. Hellwarth and W.K. Ng, *Proc. IRE* Vol. 50, p2347, 1962

[19] R.H. Stolen, E.P. Ippen and A.R. Tynes, *Applied Physics Letters*, Vol. 20, p62, 1972

[20] R.H. Stolen, E.P. Ippen, *Applied Physics Letters*, Vol. 22, p276, 1973

[21] M.N. Islam, "Raman Amplifiers for Telecommunications 1", Springer-Verlag, NY, 2004

[22] M. N. Islam, "Raman amplifiers for Telecommunications 1", Appendix A2.5, Springer-Verlag, NY, 2004

[23] R. H. Stolen, J. P. Gordon, W. J. Tomlinson and H. A. Haus, "Raman response function of Silica-core fibres", *JOSA B*, Vol. 6, pp. 1159-1166, 1989

[24] R. H. Stolen, "Issues in Raman gain measurements", *in Technical Digest of Symposium Optical Fibre Measurements, NIST Special Publication 953 (National Institute of Standards and Technology)*, Gaithersburg, MD, pp. 139-142, 2000

[25] S.T Davey, D.L. Williams, B. J. Ainslie, W. J. M. Rothwell, and B Wakefield, "Optical gain spectrum of GeO_2-SiO_2, Raman fibre amplifiers," *Proc. Inst. Elect. Eng.*, Vol. 136, pp. 301-306, 1989

[26] C. Headley, G. P. Agrawal, "Raman Amplification in fibre optic communication systems", Elsevier Academic Press, 2005

[27] Y. Emori, *Electronic Letters*, 35, pp. 1355-1356, 1999

[28] L.F. Molenauer, A. R. Grant, and, P. V. Mamyshev, "Time-division multiplexing of pump wavelengths to achieve ultrabroadband, flat, backward-pumped Raman gain", *Optics letters*, Vol. 27, pp. 592-594, 2002.

[29] J. W. Nicholson, J. Fini, J.-C. Bouteiller, J. Bromage, and K. Brar, "A swept-wavelength Raman pump with 69 MHz repetition rate", *OFC 2003*

[30] courtesy of Dr. Juan-Diego Ania-Castanon of the Photonics Research Group, Aston University, UK, 2003

[31] K. Rottwitt, A.J. Stentz, "Optical Fibre Telecommunications", Vol.IVA, Academic Press, San Diego, Chapter 5, CA, 2002

[32] C. R. S. Fludger, V. Handerek and R. J. Mears, "Pump to signal RIN transfer in Raman fiber amplifiers", *Journal of lightwave technology*, Vol. 19, No. 8, pp. 1140-1148, 2001

[33] S, B. Papernyi, V. J. Karpov, and W. R. L. Clements, "Third order cascaded Raman amplification", *OFC 2002*, Anaheim, CA, March 2002, Post deadline paper FB4, 2002

[34] Haxell, I. Robinson, N. Akhtar, A. Ding, M. Haigh, R, "2410 km all-optical network field trial with 10 Gb/s DWDM transmission", *Optical Fiber Conference OFC 2000*, Post deadline PD41-1, 2000

[35] Y. Emori, K. Tanaka, S. Namiki, "100nm bandwidth flat-gain Raman amplifiers pumped and gain-equalised by 12-wavelength-channel WDM laser diode unit", *Electronic Letters*, pp. 1355-1356, 1999

[36] L. F. Mollenauer, A. R. Grant, P. V. Mamyshev, "Time-division multiplexing of pump wavelengths to achieve ultrabroadband, flat, backward-pumped Raman gain", *Optics Letters*, pp. 592-594, 2002

[37] D Vakhshoori, M. Azimi, P. Chen, B. Han, M. Jiang, K. J. Knopp, C. C. Lu, Y. Shen, G. Vander Rhodes, S. Vote, P. O. Whang, X. Zhu, "Raman Amplification using High-Power Incoherent Semiconductor Pump Sources", *OFC 2003*, Post deadline PD47, 2003

[38] T. J. Ellingham, L. M. Gleeson, N. J. Doran, "Enhanced Raman amplifier performance using nonlinear pump broadening", *Proceedings ECOC 2002*, Copenhagen, Denmark, Tu 4.1.3, 2002

[39] M. Karlsson, "Modulational instability in lossy optical fibers", *Journal of the Optical Society of America B*, 12 (11), pp. 2071- 2077, 1995

[40] D. Anderson, L. Helczynski-Wolf, M. Lisak and V. Semenov, "Features of modulational instability of partially coherent light : Importance of the incoherence spectrum", *Phys. Rev.* E, 025601, 2004

[41] A. Mussot, E. Lantz, H. Maillotte, T. Sylvestre, and S. Pitois, "Spectral broadening of a partially coherent CW laser beam in single-mode optical fibers", *Optics Express*, Vol. 12, No. 13, p2838, 2004

[42] A.K. Abeeluck and C. Headley, "Continuous-wave pumping in the anomalous- and normal-dispersion regimes of nonlinear fibers for supercontinuum generation", *Optics Letters*, vol.30, No.1, pp. 61-63, 2005

[43] T. J. Ellingham, J.-D. Ania-Castañón, O. Shtyrina, M. P. Fedoruk and S. K. Turitsyn, "CW Raman pump broadening using modulational instability", *Nonlinear Guided Waves and Their Applications conference*, MC42, Toronto, Canada, 2004

[44] T. Sylvestre, A. Mussot, E. Lantz and H. Mailotte, "Continuum generation in continuous-wave-pumped dispersion-shifted fibers", *CLEO 2005*, paper CD-664, 2005

[45] T. J. Ellingham, A. Pustovskikh, J.-D. Ania-Castañón, M. P. Fedoruk, S. Kobtsev and S. K. Turitsyn, "Raman Amplifier with Increased Flatness Using Modulation Instability", *Proceedings of the 30th European Conference on Optical Communication (ECOC 2004)*, Stockholm, Sweden, Sep 2004

[46] T. J. Ellingham, J.-D. Ania-Castañón, S. K. Turitsyn, A. Pustovskikh, S. Kobtsev and M. P. Fedoruk, "Dual-pump Raman amplification with increased flatness using modulation instability", *Optics Express*, 13 (4), pp. 1079-1084, Feb. 2005

[47] T. J. Ellingham, J.-D. Ania-Castañón, S. K. Turitsyn, A. Pustovskikh, S. Kobtsev and M. P. Fedoruk, "Dual-pump Raman amplification with enhanced flatness using modulation instability", *Conference Digest for CLEO Europe 2005*, Munich, Germany, pp. CD7-4-TUE, June 2005

[48] S. Namiki, Y. Emori, "Ultrabroad-band Raman amplifiers pumped and gain-equalized by wavelength-division-multiplexed high-power laser diodes", *IEEE J. Sel. Top. Quantum Electron.* Vol. 7, No. 3, 2001

[49] T. J. Ellingham, J.-D. Ania-Castañón and S. K. Turitsyn, "Enhanced Raman amplifier flatness with nonlinear broadening over non-standard transmission fibre", *Optics Communications*, 257 (1), pp. 176-179, Jan 2006

[50] D.A. Chestnut, J.R. Taylor, "Gain flattened fiber Raman amplifiers with nonlinearity-broadened pumps", *Optics letters*, No.28 2294-2296, 2003

[51] S. Martin-Lopez, M, Gonzalez-Herraez, P. Corredera, M.L. Hernanz and A. Carrasco, "Gain flattening of fiber Raman amplifiers using non-linear pump spectral broadening", *Optics communications*, 242, pp. 463-469, 2004

[52] T. Zhang, X. Zhang, "Distributed fibre Raman amplifiers with incoherent pumping", *IEEE Photonics Technology Letters*, Vol. 17, No.6, June 2005

[53] T. Tanaka, K. Torii, M. Yuki, H. Nakamoto, T. Naito and I. Yokota, "200-nm Bandwidth WDM transmission around 1.55μm using distributed Raman amplifier", *Proceedings ECOC 2002*, Copenhagen, Denmark, Post deadline PD4.6, 2002

[54] T.-T. Kung, C.-T. Chang, J.-C. Dung and S. Chi, "FWM mixing between pump and signal in a Distributed Raman Amplifier", *Journal of Lightwave Technology*, vol.21, no.5 pp. 1164-1170, 2003

[55] S. Song, C. T. Allen, K. R. Demarest and R. Hui, "Intensity-dependant phase matching effects on four-wave mixing in optical fibres", *Journal of Lightwave Technology*, Vol.17, No. 11, 1999

[56] W. S. Wong, C.-J. Chen, M.-C. Ho and H. K. Lee, "Phase-Matched Four-Wave Mixing between pumps and signal in a co-pumped Raman amplifier", *Photonics Technology Letters*, Vol. 15 No. 2, 2003

[57] J.-C. Bouteiller, L. Leng and C. Headley, "Pump-Pump Four-Wave Mixing in distributed Raman amplified systems", *Journal of Lightwave Technology*, Vol.22, No.3, 2004

[58] G. Bolognini, S. Feralli and F. Di Pasquale, "Resonant gain enhancement induced by pump RIN transfer in distributed Raman amplifiers", *OFC 2003*, pp. 434-435, ThB6, 2003

[59] X. Zhou, M. Birk, and S. Woodward, "Pump-noise induced FWM effect and its reduction in a distributed Raman fiber amplifier", *Photonics Technology Letters*, Vol. 14, No.12, pp. 1686-1688, 2002

[60] S. Sugliani, G. Sacchi, G. Bolognini, S. Faralli, F. Di Pasquale, "Suppression of penalties induced by parametric nonlinear interaction in counter-pumped distributed Raman amplifiers", *ECOC 2003*, Rimini, Italy, paper Tu3.2.6, 2003

[61] F. Di Pasquale, F. Meli, "Effective reduction of pump-signal Four-wave-Mixing interaction in co-pumped distributed Raman amplifiers", *ECOC 2003*, Rimini, Italy, paper Tu4.7.3, 2003

[62] Wuilpart M., Ravet G., Megret P., Blondel M., "Distributed measurement of Raman gain spectrum in concatenations of optical fibres with OTDR", *Electronics Letters*, Vol.39, Issue 1, pp. 88-89, 2003

[63] G. Vilela de Faria, J.P. Von Der Weid, "Tuneable OTDR in Raman-amplified optical transmissions", *LEOS 2004*, Volume: 2 pp. 683 – 684, 2004

[64] Toge, K. Hogari, K. Horiguchi, T. "Technique for measuring longitudinal distribution of Raman gain characteristics in optical fibers", *Journal of Lightwave Technology*, Vol.21, Issue: 12, pp. 3349 – 3354, 2003

[65] C.J.S. de Matos, J.R. Taylor, "Optical time-domain reflectometry of discrete fiber Raman amplifiers", *Photonics Technology Letters*, Vol. 15, Issue: 8, 2003

[66] L. Eskildsen, P. B. Hansen, S. G. Grubb and V. L. da Silva, "Remote postamplifiers in repeaterless transmission systems", *Electronics Letters*, Vol. 31, No. 14, 1995

[67] J.D. Ania-Castañón, "Quasi lossless transmission using second-order Raman amplification and fibre Bragg gratings", *Optics Express*, Vol. 12, pp. 4372-4377, 2004

[68] J.-C. Bouteiller, K. Brar, C. Headley, "Quasi-constant signal power transmission", *Proceedings ECOC 2002*, Copenhagen, Denmark, Paper S3.04, 2002

[69] C. Finot, G. Millot, C. Billet and J. M. Dudley, "Experimental generation of parabolic pulses via Raman amplification in optical fibre", *Optics Express*, Vol. 11, No. 13, pp. 1574-1552, 2003

[70] S. Boscolo, S. K. Turitsyn, V. Yu, J. H. B. Nijhof, "Self-Similar Parabolic Optical Solitary Waves", Theoretical and Mathematical Physics, No. 133, pp. 1647-1656, 2002

[71] M. D. Mermelstein, K. Brar and C. Headley, "RIN transfer measurement and modelling in dual-order Raman fiber amplifiers", *Journal of lightwave technology*, Vol. 21, No. 6, pp. 1518-1523, 2003

[72] Maiorov, M. Komissarov, A. Kudryashov, I. Lunev, A. Connolly, J. Garbuzov, D., "Spectral and noise characteristics of Fabry-perot and DFB 14xx nm InGaAs/InP pump lasers for Raman and Er-doped fiber amplifiers", *OFC 2003*, vol.1, p400 – 401, 2003

[73] C. R. S. Fludger, V. Handerek and R. J. Mears, Correction to "Pump to signal transfer in Raman fiber amplifiers", *Journal of lightwave technology*, Vol. 20, No. 2, p316, 2002